University of Sheffield

Investigating Neurophysiological Dysfunction in *C9ORF72* Patient-derived Striatal and Lower Motor Neurons

Manpreet Singh Atwal

Sheffield Institute for Translational Neuroscience

A thesis submitted for the degree of
Doctor of Philosophy (PhD)

March 2025

Acknowledgements

Firstly, I would like to express my deepest gratitude to my primary supervisor, Dr Matthew Livesey for your constant support, guidance and belief in me as a scientist throughout this journey. I am genuinely grateful for the opportunity to have worked on these very exciting projects, being able to learn from you and to share your enthusiasm and commitment has really driven me to achieve things at times I did not think possible. Thank you.

I would also like to thank Dr Cleide Dos Santos Souza for her insightful advice, in addition to her help training me in cell culture and general good scientific practice upon my arrival to SITraN. A special thanks to my friend Nikita who made work more enjoyable with our chats/ coffee trips – I appreciated these times more than you know.

To my wonderful girlfriend, turned fiancé, turned wife, Jaipreet, who has been my biggest supporter throughout my journey, I simply could not have done this without you. To have married you during my PhD has been the biggest blessing. Thank you for everything especially in these last few months where I have been tucked away writing!

A special thanks to my amazing family especially Mum and Dad for their unconditional love and constant support throughout my journey, and whom without I would not be in the position I am in today, I am forever grateful; I hope I have made you all proud.

Lastly, I would like to dedicate this thesis entirely to my Bibi Ji.
You always knew I could do it. This here is my gift to you; I hope I have made you proud.

Abstract

Frontotemporal dementia and related amyotrophic lateral sclerosis (FTD/ALS) are fatal neurodegenerative diseases that sit on opposite ends of a clinical disease spectrum typically characterised by progressive degeneration of cortical and motor neurons. However, it is becoming increasingly evident that FTD/ALS pathologically impacts other brain regions. Recently, the striatum, a crucial integrative hub within the brain, has been shown to have a major role in cognitive functions impacted in FTD/ALS, displays classical TDP-43 pathology and neuronal atrophy. Altered neuronal excitability is a hallmark feature of neurodegenerative disease and contributes to disease onset and progression. Here, I have investigated whether electrophysiological function relating to intrinsic excitability and responsiveness to major ionotropic receptors are pathologically relevant in FTD/ALS. To this end, enriched cultures of induced pluripotent stem cell-derived striatal medium spiny neurons (MSNs) and lower motor neurons (LMNs) harbouring *C9ORF72* repeat expansion mutations, the most common genetic impairment within the FTD/ALS spectrum, were generated. Using whole-cell patch-clamp electrophysiology my data provides novel evidence of reduced excitability in C9 MSNs, driven by deficits in AP waveform components and delayed outwardly-rectifying K^+ (I_k) channel dysfunction. Pharmacological targeting of big conductance Ca^{2+}-activated potassium (BK) channels and voltage-gated K^+ channels (K_v3) restored I_K channel function and rescued AP waveform deficits, but not intrinsic hypoexcitability, suggesting an interplay between ion channel dysfunction and structural AIS abnormalities. In contrast, C9 LMNs displayed stable excitability under basal and acute KCl stress conditions but exhibited increased excitability upon chronic KCl depolarising stress, implicating homeostatic plasticity mechanisms. Furthermore, C9 LMNs showed potentiated excitatory and inhibitory neurotransmission, with a shift toward NMDAr-mediated signalling, highlighting potential excitotoxic vulnerability. These data implicate complex, regionally specific pathophysiological impairments in C9FTD/ALS that varies between neuronal populations, which has significant implications for future therapeutic strategies.

Table of Contents

List of Abbreviations

Abbreviation	Full name
[18F] FDG-PET	18F-fluoro-2-deoxyglucose positron emission tomography
A	Ampere
aCSF	Artificial cerebrospinal fluid
AD	Alzheimer's Disease
AHP	Afterhyperpolarisation
AIS	Axon initial segment
ALS	Amyotrophic lateral sclerosis
AMPA	α-amino-3-hydroxy-5-methyl-4-isoxazolepropionic acid
AMPAr	α-amino-3-hydroxy-5-methyl-4-isoxazolepropionic acid receptor
ANOVA	Analysis of variance
AP	Alanine-proline
AP	Action potential
APV	D(-)-2-Amino-7-phosphonoheptanoic acid
BDNF	Brain-derived neurotrophic factor
BK	Big conductance calcium-activated potassium
bvFTD	Behavioural variant FTD
C9ORF72	Chromosome 9 open reading frame 72
Ca^{2+}	Calcium
ChAT	Choline Acetyltransferase
Cl-	Chloride
CNQX	Cyano-7-nitroquinoxaline-2,3-dione
CNS	Central nervous system
CNTF	Ciliary neurotrophic factor
CREB	cAMP response element-binding protein
CSF	Cerebrospinal fluid
DARPP32	Dopamine- and cAMP-regulated phosphoprotein 32 kDa
DIV	Days *in vitro*
DKK1	Dickkopf related protein 1
DMSO	Dimethyl sulfoxide
DNA	Deoxyribonucleic acid
DPR	Dipeptide-repeat proteins
EMG	Electromyography
fALS	Familial ALS
fFTD	Familial FTD
FTD	Frontotemporal dementia
FTD/ALS	FTD and ALS
FUS	Fused in sarcoma
GA	Glycine-alanine
GABA	Gamma-aminobutyric acid
$GABA_AR$	Gamma-aminobutyric acid A receptor

GP	Glycine-proline
GR	Glycine-arginine
GRN	Progranulin
GΩ	Giga-ohms
HBSS	Hanks' Balanced Salt Solution
HD	Huntington's Disease
HEPES	4-(2-hydroxyethyl)-1-piperazineethanesulfonic acid
hESC	Human embryonic stem cells
I	Current
I-O	Current stimulus input-action potential output
ICC	Immunocytochemistry
IGF-1	Insulin-like growth factor-1
I_K	Delayed outwardly rectifying K^+ channels
IMS	Industrial methylated spirit
iPSC	Induced pluripotent stem cell
K^+	Potassium
Klf4	Kruppel-like factor 4
K_v	Voltage-gated K^+ channels
LCD	Low-complexity domain
LJP	Liquid junction potential
LLPS	Liquid-liquid phase separation
LMN	Lower motor neuron
LTD	Long-term depression
LTP	Long-term potentiation
MAP2	Microtubule-associated protein 2
MAPT	Microtubule-associated protein tau
MEA	Multi-electrode array
MEG	Magnetencephalography
mEPSCs	Miniature excitatory postsynaptic currents
Mg^{2+}	Magnesium
MN	Motor neuron
MND	Motor neuron disease
MNP	MN progenitor
MRI	Magnetic resonance imaging
ms	Millisecond
MSA	Multiple system atrophy
MSN	Medium spiny neuron
mV	Millivolts
Na^+	Sodium
Na_v	Voltage-gated Na^+ channels
NCT	Nucleocytoplasmic transport
nfvPPA	Progressive non-fluent aphasia

NLS	Nuclear localisation signal
NMDA	N-methyl-D-aspartic acid or N-methyl-D-aspartate
NMDAr	N-methyl-D-aspartic acid or N-methyl-D-aspartate receptor
NMJ	Neuromuscular junction
NPC	Neural progenitor cell
pA	Picoampere
PBS	Phosphate buffered saline
pF	Picofarad
PR	Proline-arginine
PTX	Picrotoxin
PUR	Purmorphamine
RA	Retinoic acid
RAN	Repeat-associated non-ATG
R_{in}	Input resistance
RMP	Resting membrane potential
RNA	Ribonucleic acid
ROCK	Rho-associated protein kinase
ROS	Reactive oxygen species
R_s	Series resistance
sALS	Sporadic ALS
SCNT	Somatic cell nuclear transfer
SD	Semantic dementia
SEM	Standard error of the mean
SHH	Sonic hedgehog
SICI	Short-interval intercortical inhibition
SK	Small conductance calcium-activated potassium
SMI-32	Monoclonal antibody to neurofilament protein
SOD1	Cu/Zn superoxide dismutase 1
SOX2	SRY-related HMG-Box Gene 2
SRSF1	Serine/arginine-rich splicing factor 1
SV2	Synaptic vesicle-associated protein 2
TADRBP	Transactive response DNA binding protein 43 kDa
TDP-43	Transactive response DNA binding protein 43 kDa
TEA	Tetraethylammonium
TMS	Transcranial magnetic stimulation
TTX	Tetrodotoxin
TUJ1	β-III-tubulin
UMN	Upper motor neuron
V	Voltage
VPA	Valproic acid
WCC	Whole-cell capacitance

List of Tables

List of Figures

Declaration

I, the author, confirm that the Thesis is my own work. I am aware of the University's Guidance on the Use of Unfair Means (www.sheffield.ac.uk/ssid/unfair-means). This work has not previously been presented for an award at this, or any other, university.

Publications

PASNICEANU, I. S., **ATWAL, M. S**., SOUZA, C. D. S., FERRAIUOLO, L. & LIVESEY, M. R. 2021. Emerging Mechanisms Underpinning Neurophysiological Impairments in C9ORF72 Repeat Expansion-Mediated Amyotrophic Lateral Sclerosis/Frontotemporal Dementia. *Front Cell Neurosci,* 15**,** 784833.

Chapter 1: Introduction

Motor neuron disease (MND) is an umbrella term used to describe a collection of progressive neurological disorders characterised by the degeneration of motor neurons. The dysfunction and death of these neurons causes the loss of voluntary muscle control. MNDs can affect both children (spinal muscular atrophy) and adults with the different diseases classified according to the disease being inherited or sporadic; and the site of degeneration, either at the upper motor neurons (UMN), lower motor neurons (LMNs) or both. The clinical variants that make up MND consists of progressive muscular atrophy that affects the LMNs only, progressive bulbar palsy cause by injury to either the LMNs or UMNs, primary lateral sclerosis that primarily affects the UMNs and amyotrophic lateral sclerosis (ALS) caused by death of both UMNs and LMNs (Taylor et al., 2016). A large majority of MND patients suffer from ALS (~70%) and patients that do present with the other forms of MND typically develop features of ALS with disease progression, including forms that genetically overlap with Frontotemporal dementia (FTD) (Shaw, 2005, van Es et al., 2017).

1.1 Amyotrophic Lateral Sclerosis

ALS, also referred to as MND in the UK, is a fatal neurodegenerative disease characterised by the progressive degeneration of both UMN in the motor cortex and LMNs located in the brainstem and spinal cord. Motor neuron dysfunction and death results in patients suffering from muscular atrophy, progressive paralysis and invariably death, usually from respiratory failure 3-5 years after diagnosis (Brown and Al-Chalabi, 2017). These neurons that control voluntary muscular movement are all affected by the disease but interestingly, motor neurons innervating the eye or sphincter muscles are usually spared until disease end stage, if at all (Gordon, 2013). The term ALS was coined by the neurologist, Jean-Martin Charcot, who first described the disease in in 1869. In the post-mortem examination of patients with motor impairments he observed muscle wasting (amyotrophy) and damage to the lateral corticospinal tracts of the spinal cord which involves the death of motor neurons (lateral sclerosis) (Gordon, 2013). Today, ALS is the third most common

neurodegenerative disorder with a global prevalence of 6-9 per 100,000 persons (Longinetti and Fang, 2019, Brown et al., 2021). Geographical variations of ALS cases do exist, in the UK alone, this figure stands at 5.69 per 100,000 persons (Burchardt et al., 2022). The lifetime risk of developing ALS is approximately 1 in 350 with an estimate incidence of 2.1-4.4 new cases per 100,000 population per year (Chio et al., 2013, Ryan et al., 2019, Xu et al., 2020). These numbers are likely to increase in the future with an aging population demographic and improved clinical diagnosis. Although cases of early onset have been reported, ALS is primarily an age-related disorder that most commonly occurs between the ages of 50 to 70. In cases of sporadic ALS (sALS) the average age of symptomatic onset is 58-63 whereas familial ALS (fALS) tends to occur at an earlier age between 47-52 (Logroscino et al., 2010, Chio et al., 2013). The disease is more prevalent in males than females by a factor of 1.6 times (Shaw, 2005). All races and ethnic backgrounds are affected by disease, with a slight predisposition in the Caucasian population (Arthur et al., 2016).

1.11 Diagnosis and Clinical Management of ALS

There is no definitive singular clinical test that can provide a diagnosis of ALS. Instead, in the clinic ALS is diagnosed by the exclusion of ALS mimic disorders. The diagnostic toolkit used by clinicians involves blood tests, magnetic resonance imaging (MRI) of the brain and spinal cord to exclude other disorders and neurophysiological assessment (van Es et al., 2017). This involves electromyography (EMG) and electrophysiological nerve conduction studies to exclude similar ALS mimics but also to support ALS diagnosis that are based primarily on clinical assessment made using the Gold Coast criteria (Shefner et al., 2020).

Despite an ever-growing number of pharmacological compounds entering clinical trial (Petrov et al., 2017), there is currently no cure for ALS. At present, therapeutic strategies focus on providing symptomatic management or modest disease-modifying treatments. The provision of supportive care and pharmacological treatment of symptoms from multi-disciplinary health teams can improve quality of life and survival time of patients (Mead et al., 2023). Alternatively, there are three currently approved disease-modifying treatments available to patients. Riluzole, first approved back in

1995 has shown to improve life expectancy by approximately 3 months (Rowland and Shneider, 2001). The mechanism of action by which this drug works is complex and has only recently been deduced. Riluzole therapy functions, at least in part, by reducing glutamate release into the synaptic cleft by inhibiting voltage-gated sodium channel (Na_v) currents and thereby targeting glutamate-mediated excitotoxicity (Wang et al., 2004, Hollingworth et al., 2024) (reviewed in section 1.67). Edaravone, an antioxidant agent approved in the US and a select number of countries, has been shown to somewhat slow disease progression in selective patients (Hardiman and van den Berg, 2017). Tofersen, an antisense oligonucleotide therapy targeting the Cu/Zn superoxide dismutase 1 (SOD1) gene in fALS cases was recently approved in the US (Miller et al., 2022, Ludolph and Wiesenfarth, 2025). The therapy works by binding to SOD1 mRNA and facilitates its degradation therefore reducing synthesis of the SOD1 protein, though its clinical efficacy remains debated (Miller et al., 2022).

1.12 Clinical Features of Amyotrophic Lateral Sclerosis

Heterogeneity in the clinical manifestations of ALS exist based upon the regions of the body at which symptoms first appear, which appear to be localised at initial presentation before becoming widespread. The most common form, limb-onset ALS which accounts for ~66% of cases begins with weakness in the upper or lower limbs. Bulbar-onset ALS (~33%) is characterised by dysfunction of LMNs in the brainstem that ultimately lead to symptoms related to the bulbar musculature (dysarthria, dysphagia) (van Es et al., 2017).

Previously ALS has been regarded as a disease primarily of the motor system, however, since the early 2000s there has been a growing appreciation for cognitive and behavioural impairments as cardinal ALS features. In fact, 51% of ALS patients experience cognitive decline, with 15% meeting the diagnostic criteria for FTD. Similarly, up to 36% of FTD patients present with motor symptoms (Lomen-Hoerth et al., 2003, Ringholz et al., 2005). Today it is now widely accepted that both FTD and ALS (FTD/ALS) sit on opposite ends of a continuous disease spectrum with overlapping features at the clinical level but also at the genetic and pathological level (Van Langenhove et al., 2012) (see section 1.3- 1.4).

1.2 Frontotemporal Dementia

FTD describes a heterogeneous group of neurogenerative diseases that are characterised by progressive neuronal atrophy, primarily in the cerebral cortex of the frontal and temporal lobes, which manifests as impairments in executive function, behaviour and language (Deleon and Miller, 2018). First described by Arnold Pick in 1892, FTD is the second most common dementia after Alzheimer's Disease (AD), though the most common form of dementia in individuals under the age of 65 and is more common in men (Ratnavalli et al., 2002). The estimated incidence of disease is approximately 1.6-4.1 cases per 100,000 population per year (Onyike and Diehl-Schmid, 2013, Coyle-Gilchrist et al., 2016).

1.21 Clinical Features of Frontotemporal Dementia

FTD can be divided into three main clinical syndromes based upon the clinical presentation of patients. These include the behavioural variant (bvFTD), semantic dementia (SD) and progressive non-fluent aphasia (nfvPPA). The latter syndromes can be classified as language impairments specifically relating to a loss of object and word comprehension (SD), and impaired speech with agrammatism (nfvPPA). BvFTD is the most common of all subtypes, comprising ~70% of all FTD cases (Sosa-Ortiz et al., 2012) and most frequently associated with ALS, with about 40% of bvFTD patients developing neuromuscular dysfunction (Lomen-Hoerth et al., 2002, Lipton et al., 2004). Patients often present with progressive behavioural abnormalities relating to disinhibition, loss of empathy, apathy, dietary changes and stereotyped or compulsive behaviours. These manifestations are also complemented by a loss of social decorum with a lack of insight into their condition (Rascovsky et al., 2011, Deleon and Miller, 2018). Neuronal loss within the frontotemporal cortex as well as other brain regions including the striatum underlie the symptoms listed above (Seeley et al., 2008, Olney et al., 2017).

1.22 Diagnosis and Clinical Management of FTD

Diagnosis of FTD can be difficult owing to the complex nature of the disease and associated symptoms tending to overlap between clinical syndromes including ALS (see section 1.12). An extra layer of complexity is added due to the clinical and pathological presentation of patients overlapping with AD (Mendez et al., 2007). At present, diagnosis relies upon a combination of different clinical assessments (Antonioni et al., 2023). Firstly, histopathological evidence via biopsy or post-mortem and genetic testing to confirm the presence or absence of pathogenic mutations especially for familial FTD (fFTD) cases that are predominantly inherited in an autosomal dominant manner. Secondly, neuroimaging which entails MRI and 18F-fluoro-2-deoxyglucose positron emission tomography ([18F] FDG-PET) scans to determine regions of neuropathology and hypometabolism. Importantly, the loci of neuronal atrophy specifically corresponds to certain FTD syndromes. BvFTD is characterised by the bilateral atrophy of the frontotemporal lobes amongst other brain regions including basal ganglia networks (Filippi et al., 2017) relating also to the striatum (Seeley et al., 2008, Olney et al., 2017). Lastly, neuropsychological tests are paramount for the clinical diagnosis of FTD (Antonioni et al., 2023). BvFTD patients are evaluated using criteria developed by the International Behavioural Variant FTD Criteria Consortium in 2011 (Rascovsky et al., 2011) which recognises cardinal disease features relating to cognitive impairment and executive dysfunction. According to these criteria a combination of all these diagnostic factors is required for definitive FTD diagnosis.

From the time of symptomatic onset, the mean survival time is between 3 to 17 years (Olney et al., 2017, Devenney et al., 2019). Currently, there is no disease-modifying therapy for FTD. Disease management focuses on the provision of supportive care which entails occupational or speech and language therapy. Symptomatic treatments can also be provided in the form of antidepressants and antipsychotics. Together, both aim to improve cognitive and behavioural symptoms that impair patient quality of life (Antonioni et al., 2023).

1.3 Genetic causes of ALS and FTD

ALS and FTD are predominantly sporadic disorders, and for the most part due to unknown causes, but genetic mutations do arise spontaneously or appear hereditary in nature. Despite this, sporadic and familial cases share common pathological hallmarks of disease that would indicate a convergence in pathological mechanisms. Study into the genetic foundations of disease has provided invaluable insight into the molecular mechanisms that underlie neuronal dysfunction and death in ALS/FTD. The genetic landscape of both diseases mirrors the clinically diverse elements of ALS/FTD and gives rise to a variety of pathophysiological disease features.

1.31 Sporadic and familial ALS

ALS, like many other neurodegenerative disorders, is a multifaceted disease with a defined monogenic cause in up to 20% of patients, but in the main the disease is determined by a complex interaction between genetic and environmental risk factors (Mead et al., 2023). Patients tend to be categorised into two groups with respect to disease aetiology. The majority of ALS cases (90-95%) are sporadic (sALS), defined as patients with no prior family history of disease. The remaining 5-10% are classified as familial cases (fALS) usually with a highly penetrant autosomal dominant mode of inheritance from a related family member. Identified genetic mutations are believed to associated with around 70% of fALS and 11% of sporadic cases. Both sALS and fALS are phenotypically indistinguishable from each other (Renton et al., 2014).

Based upon twin studies (Al-Chalabi et al., 2010) and population-based pedigree studies (Ryan et al., 2019, Trabjerg et al., 2020) there is an ever-growing appreciation of a genetic component in sALS cases. Hereditability in sALS has been estimated to be in the region of 40-50% (Ryan et al., 2019, Trabjerg et al., 2020). Also, an increased risk of disease in the first-degree relatives of sALS patients has been shown (Hanby et al., 2011). A recent ALS patient cohort study determined 21% of patients had a pathogenic mutation, of which 93% were classified as sALS cases (Shepheard et al., 2021), emphasising the value of routine genetic screens for all ALS patients. Indeed, a combination of genetic and cumulative lifetime exposures to environmental factors are perhaps key in disease aetiology. Besides age and male sex being associated with

increased risk of ALS (Alonso et al., 2009), military service (Kasarskis et al., 2009), cigarette smoking (Armon, 2009), exposure to heavy metals and industrial chemicals have been identified as potential risk factors (Al-Chalabi and Hardiman, 2013). Furthermore, strong evidence for an association between ALS development and physical activity including high impact sports, such as football, has been shown in recent times (Wicks et al., 2007, Harwood et al., 2009).

1.32 Sporadic and familial FTD

FTD describes a group of highly heritable neurodegenerative disorders, with approximately 40% of cases associated with a family history of disease (fFTD) (Fenoglio et al., 2018). Like fALS, this occurs primarily via an autosomal dominant mode of transmission. Within the variants, transmission is principally familial in the behavioural variant whilst a greater number of individuals diagnosed with SD and nfvPPA are sporadic (sFTD) (Greaves and Rohrer, 2019). Considerable genetic heterogeneity exists with over 50 FTD-associated genes described (Sirkis et al., 2019), including mutations in microtubule-associated protein tau (*MAPT)* and progranulin (*GRN*). The former accounting for 30% of fFTD and about 4% of sFTD cases (Stanford et al., 2004, van Swieten and Spillantini, 2007), the latter making up between 5-20% of fFTD and sFTD (Cruts et al., 2006).

On the other hand, the remaining cases are regarded as sFTD. Apart from age and a male predisposition for bvFTD, other lifestyle and environmental factors have been postulated as contributing factors towards sFTD. These include autoimmune disorders and traumatic brain injury and the subsequent neuroinflammation that ensues (McKee et al., 2013, Antonioni et al., 2023).

More than 50 pathogenic mutations have been identified for ALS and FTD (Boylan, 2015, Sirkis et al., 2019). Extensive characterisation of a select number of these mutations have been critical for the progression of the field from disease modelling to understanding of disease pathogenesis. SOD1 was the first ALS-causative mutation to be discovered in 1993 (Rosen et al., 1993), mutations in transactive response DNA binding protein 43kDa (*TARDBP*) and fused in sarcoma (*FUS*) and the proteins they

encode represent a pathological hallmark in a significant proportion of ALS/FTD patients (Sreedharan et al., 2008, Kwiatkowski et al., 2009, Vance et al., 2009) and lastly, the chromosome 9 open reading frame 72 (*C9ORF72*) repeat expansion mutation. The most common genetic cause of both ALS and FTD (DeJesus-Hernandez et al., 2011, Renton et al., 2011) and the mutation upon which my thesis is based on. Collectively, neuropathology associated with mutations in these four genes account for a large proportion of FTD/ALS cases, in the European population alone mutations in these genes are responsible for up to 70% of fALS cases (Chio et al., 2014).

1.33 SOD1

SOD1 is an abundant and ubiquitously expressed cytoplasmic antioxidant enzyme, that functions to catalyse the conversion of superoxide radicals into oxygen and hydrogen peroxide. This function protects the cell from oxidative damage. More than 200 ALS-causing mutations have been discovered in the SOD1 gene which occur across the entire length of the protein, the majority of which are missense mutations (Saini and Chawla, 2024). Despite extensive study over the last 30 years, the pathomechanisms by which SOD1 mutations leads to disease is not completely understood. Mutants tend to retain partial or full enzymatic activity, with no correlation between disease intensity and reduced SOD1 function (Cleveland et al., 1995, Reaume et al., 1996). Initial suggestions of a loss-of-function mechanism leading to reduced protection against oxidative stress (Rosen et al., 1993) have now propagated towards a gain of toxic function in many of the SOD1 mutants. Furthermore, this mechanism of action is supported by the FDA-approval of tofersen for use in the US which works to reduce SOD1 concentration (Miller et al., 2020). Mutations in the SOD1 gene interfere with correct protein folding of the enzyme, inducing protein misfolding and in turn, formation of SOD1-containing proteinaceous intracellular aggregates. These aggregates confer neurotoxicity via several means, including excitotoxicity (Howland et al., 2002, Joyce et al., 2011), mitochondrial dysfunction (Liu et al., 2004, Pickles et al., 2016) and oxidative stress (Joyce et al., 2011). SOD1-ALS accounts for up to 2% of all ALS cases, 20% of fALS cases and approximately 2% of all sALS (Saini and Chawla, 2024). Patients characterised by SOD1 mutations tend to present with

distinct clinicopathological features that differ from the wider subset of ALS cases. SOD1-ALS patients are less likely to suffer from decline in cognitive function and feature SOD1 inclusions not observed in the vast majority of sALS, and even more so in other fALS cases (Turner et al., 2008, Wicks et al., 2009). Also, these patients lack typical transactive response DNA binding protein 43kDa (TDP-43) pathological inclusions that characterise almost all ALS cases (Ling et al., 2013). The transgenic $SOD1^{G93A}$ ALS mouse model was the first animal model of ALS (Gurney et al., 1994), and the most studied. The transgenic overexpression of SOD1 recaptures many ALS disease features including neurodegeneration and motor phenotypes that eventually leads to death. Yet, whilst it has aided our understanding of disease pathomechanisms, there have been several failures in the translation of findings into successful clinical therapies in non-SOD1 ALS cases. This supports the clinical and pathology-related differences of the SOD1 mutation. Nevertheless, these models have shown limited responses to approved riluzole (Gurney et al., 1998) and edaravone therapies (Ito et al., 2008), and the pre-clinical $SOD1^{G93A}$ overexpression model was significant for the progression of tofersen towards clinical trials (Smith et al., 2006).

1.34 TDP-43

Encoded by the *TARDBP* gene, TDP-43 is a ubiquitously expressed DNA-RNA binding protein (Figure 1.1A). Predominantly localised in the nucleus, the protein can shuttle between the nucleus and cytoplasm where it can exert its multifunctional role in stress granule dynamics and RNA metabolism especially splicing regulation, stability, trafficking and biogenesis (Buratti and Baralle, 2001, Tziortzouda et al., 2021). The nuclear loss and cytoplasmic mislocalisation of TDP-43 leads to the aberrant accumulation and aggregation of TDP-43 into intracellular inclusions (Arai et al., 2006, Neumann et al., 2006). Cytoplasmic inclusions are a pathological hallmark in 97% of ALS and 45% of FTD cases (Ling et al., 2013). This common feature further emphasises the link between the two diseases. More than 50 *TARDBP* patient mutations have been discovered that account for 5% of fALS cases and 1% of sALS cases, and together with the presence of TDP-43 pathology in most sporadic and *C9ORF72* related cases, highlights the importance of TDP-43 pathology in the convergence of disease onset and progression across the FTD/ALS spectrum

(Lattante et al., 2013, Chio et al., 2020). The concurrent pathological accumulation of cytoplasmic TDP-43 with its depletion from the nucleus would suggest a dual gain-of-function and loss-of-function disease mechanism. TDP-43 loss-of-function leads to the cryptic splicing of many genes that culminates in the downregulated expression of many proteins including Stathmin-2 (Klim et al., 2019). Indeed, multiple experimental evidence from patient models (Highley et al., 2014), drosophila (Diaper et al., 2013, Solomon et al., 2018) and mice models (Walker et al., 2015a, White et al., 2018) have independently confirmed the importance of enhanced cytoplasmic and reduced nuclear levels of TDP-43 in disease pathogenesis. This stresses the importance in the tight regulation of TDP-43 expression and localisation in TDP-43 proteinopathies.

1.35 FUS

A year after mutations in *TARDBP* were discovered to cause ALS, FTD/ALS-causing mutations were discovered in the gene of another DNA/RNA-binding protein, *FUS,* in 2009 (Kwiatkowski et al., 2009, Vance et al., 2009) (Figure 1.1B). Analogous to TDP-43, FUS is a nucleocytoplasmic protein with multiple roles in RNA processing ranging from transcription and RNA splicing to microRNA biogenesis amongst stress granule formation (Butti and Patten, 2018). To date, over 50 FUS mutations have been identified and accountable for up to 10% of fALS and <1% of sALS cases and 3% of all FTD cases (Seelaar et al., 2010, Gelon et al., 2022). Neuropathologically FUS cases display abnormal cytoplasmic inclusions positive for FUS. Similar to SOD1-ALS and SOD1 inclusions, proteinaceous aggregates composed of FUS are negative for TDP-43 (Gelon et al., 2022). Mutations in the *FUS* gene whilst pathologically distinct from TDP-43 proteinopathies do provide further evidence of a shared spectrum of genetics and pathology between FTD/ALS. Although, the pathomechanism by which FUS can trigger disease onset is unknown, the discovery of the genetic mutation does implicate a role of RNA biology in disease pathogenesis.

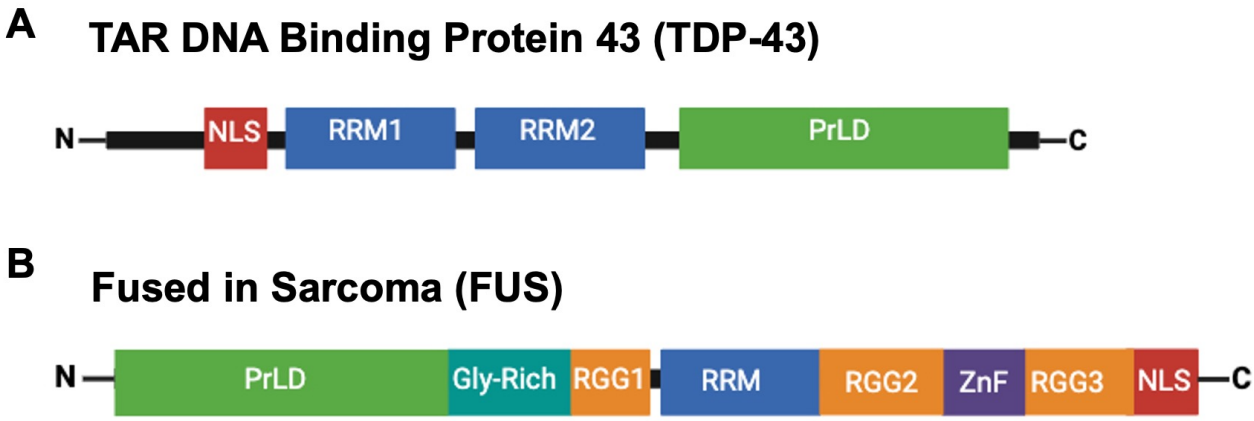

Figure 1.1. Protein domain structure of TDP-43 and FUS. Both proteins contain similar structural domains that corresponds to their similar functions in stress granule dynamics, RNA processing and metabolism. Notably, there are some structural differences. **(A)** The TDP-43 protein contains a nuclear localisation signal (NLS), RNA-recognition motifs (RRM1 and RRM2) important for RNA-binding and a low complexity prion-like domain (PrLD) where most FTD/ALS-linked mutations in TDP-43 can be found. **(B)** The FUS protein contains a PrLD that overlaps with a glycine-rich and arginine-glycine-rich region of which there are three (RGG), a RRM, zinc-finger motif (ZnF) and a NLS where the majority of FTD/ALS-linked mutations in FUS are described. Figure created in BioRender.

1.36 C9ORF72

A groundbreaking discovery was made back in 2011 in the field of FTD/ALS, where a GGGGCC (G_4C_2) hexanucleotide repeat expansion mutation was identified in intron 1 of the *C9ORF72* gene (C9) (DeJesus-Hernandez et al., 2011, Renton et al., 2011). The mutation is the most common genetic cause of FTD/ALS (C9FTD/ALS) accounting for 40% of fALS and 7% of sALS cases, 25% fFTD and 6% sFTD (Majounie et al., 2012). Of all FTD syndromes, the C9 mutation is most prominent amongst bvFTD patients accounting for up to 90% of cases (Majounie et al., 2012). Typically, 30 of these G_4C_2 repeats are considered to represent a pathogenic threshold for disease. Meanwhile, C9FTD/ALS patients tend to present with a repeat length in the hundreds if not thousands (Taylor et al., 2016). The *C9ORF72* mutation epitomises the idea that pure forms of ALS and FTD not only overlap but sit on opposite ends of a clinical disease spectrum. Clinically, C9 individuals have a higher prevalence of both cognitive and motor impairments. The mutation accounts for a sizeable proportion of sporadic and familial FTD/ALS cases with almost all cases of C9 characterised by hallmark TDP-43 pathology (Hardiman et al., 2017). Three mutually inclusive mechanisms have been proposed to mediate C9 neurodegeneration: loss of C9ORF72 protein function (haploinsufficiency) resulting from reduced protein expression; toxic gain-of-function of RNA repeats, leading to formation of RNA foci and/or generation of dipeptide-repeat proteins (DPR) species via repeat-associated non-ATG (RAN) translation (Donnelly et al., 2013, Mori et al., 2013b, Mizielinska et al., 2014, Waite et al., 2014) (Figure 1.2). The relative contribution of each mechanism is still debated today and whilst evidence points towards gain-of-toxicity mechanisms at the heart of this mutation (Haeusler et al., 2016), its likely pathogenicity arises due to a culmination of all three mechanisms. These pathomechanisms are explored further in section 1.4.

1.4 C9ORF72-related Pathomechanisms

The pathological signature of C9-related ALS cases is shared with that of the vast majority of ALS patients, including the degeneration of UMN and LMNs of the motor cortex and spinal cord, Bunina bodies and, ubiquitinated cytoplasmic TDP-43 deposits within neurons and glia. However, specific to C9ALS is the addition of p62-positive

inclusions caused by toxic DPR species (Cooper-Knock et al., 2012). Nonetheless, manifestation of these TDP-43 deposits in both C9-FTD/ALS indicates both ailments converge on a shared disease pathway that give rise to ALS-specific and/or FTD-specific symptoms, and this is indeed the case (Hsiung et al., 2012). Evidence of pathology extends beyond the frontotemporal and motor cortices typically associated with FTD/ALS and is apparent in regions of the basal ganglia including the striatum, hippocampus and amygdala (Murray et al., 2011, Hsiung et al., 2012, Mackenzie et al., 2013), with atrophy also observed in the thalamus and cerebellum (Mahoney et al., 2012, Irwin et al., 2013).

Specific to the C9 mutation is the formation of RNA foci from sense or antisense RNA transcripts mainly in neurons and to a lesser extent glial cells (Lagier-Tourenne et al., 2013, Mizielinska et al., 2013). Foci are spread across the central nervous system (CNS) from motor neurons in the spinal cord to neurons in the motor and frontal cortex, cerebellum and hippocampus (Lagier-Tourenne et al., 2013, Mizielinska et al., 2013, DeJesus-Hernandez et al., 2017). Sense foci are more prevalent across the CNS in comparison to antisense transcripts (Balendra and Isaacs, 2018).

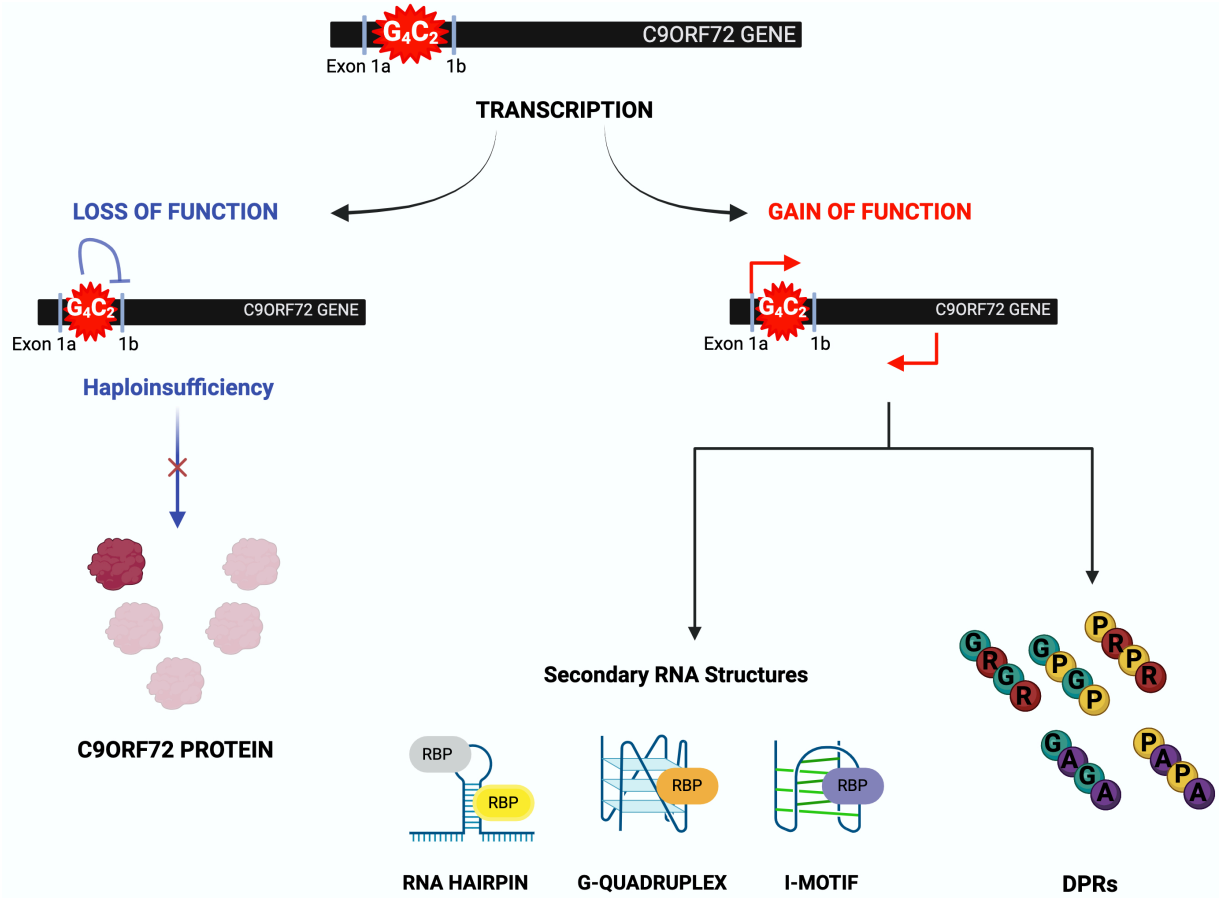

Figure 1.2. Three proposed pathomechanisms of the C9ORF72 G_4C_2 hexanucleotide repeat expansion mutation. C9ORF72 haploinsufficiency whereby there is reduced expression and ultimately a loss-of-function of the C9ORF72 protein. Two gain-of-function mechanisms have also been proposed relating to bidirectional transcription of the repeat expansion leading to the formation of various secondary RNA structures that can form RNA foci that can sequester RNA-binding proteins (RBPs). Alternatively, a second gain-of-function mechanism relates to the RAN translation of the repeat expansion to produce 5 toxically distinct dipeptide repeat proteins (DPRs) (GR, GP, PR, GA, PA). Figure created in BioRender.

Non-canonical translation of these sense (G_4C_2 repeats) and antisense RNA transcripts (C_4G_2 repeats) leads to the production of star-shaped p62-positive, TDP-43 negative DPR inclusions. These are conventionally localised within the cytoplasm or neuronal neurites and to a lesser degree in the nucleus (Al-Sarraj et al., 2011, Mackenzie et al., 2013). RAN translation of the repeat expansion in all reading frames leads to the production of five DPR species. Non-canonical translation of sense RNA transcripts that occurs in the absence of the ATG start codon (RAN translation) produces two DPR species: glycine-arginine (GR) and glycine-alanine (GA). RAN translation of antisense transcripts produces proline-arginine (PR) and alanine-proline (AP) with glycine-proline (GP) produced from sense and antisense transcripts (Ash et al., 2013, Mori et al., 2013a) (Figure 1.2). The toxic effects of DPR expression have been widely reported in various animal and cell models (discussed in section 1.43) but clinicopathological studies have raised questions regarding the significance of DPR pathology in disease. DPR accumulation does not differ in regional distribution between FTD/ALS cases (Davidson et al., 2014). Also, inclusions are detected in non-typically associated ALS brain regions like the hippocampus and cerebellum in conjunction with typical ALS brain regions such as the frontal and motor cortices (Cooper-Knock et al., 2012, Troakes et al., 2012, Mann et al., 2013). Although, detection within spinal motor neurons remains ambiguous, cytoplasmic TDP-43 aggregation is a prominent feature here (Gomez-Deza et al., 2015, Davidson et al., 2016). The sites of neurodegeneration within the CNS and clinicals symptoms converge with TDP-43 pathology in FTD/ALS independent of DPR pathology (Mann, 2015, Davidson et al., 2016). However, notable exceptions have been reported in C9-patients with neuroanatomical correlation between poly-GR, degenerative brain regions and TDP-43 pathology (Saberi et al., 2018, Sakae et al., 2018). Quaegebeur et al observed association between poly-GR concentration and clinical parameters of severity highlighting a neurotoxic role of these species in C9FTD patients (Quaegebeur et al., 2020). Importantly, post-mortem studies represent pathology at disease end stage and with DPR pathology likely to be an initiating stressor that precedes TDP-43 pathology and disease onset (Baborie et al., 2015, Vatsavayai et al., 2016, Solomon et al., 2018), this perhaps explains the close correlation with neuronal atrophy. Regardless, further work is required to elucidate the cryptic role of DPR in disease aetiology.

1.41 C9ORF72 Haploinsufficiency

The C9ORF72 protein represents a ubiquitously expressed protein with physiological function implicated in autophagy, inflammation, stress granule dynamics, homeostatic mitochondrial function and even synapse physiology (Smeyers et al., 2021, Bauer et al., 2022, Sellier et al., 2024). The repeat expansion mutation has been shown to reduce C9ORF72 expression at both the mRNA and protein level in C9FTD/ALS patient-derived motor neurons (Shi et al., 2018) and C9 post-mortem patients (Fratta et al., 2013, Waite et al., 2014, Rizzu et al., 2016) (Figure 1.2). Collectively, these studies are indicative of C9ORF72 haploinsufficiency playing a prominent role in neurodegeneration. Loss of C9ORF72 was sufficient to induce defects in the autophagy-related protein clearance pathways, relating specifically to lysosomal accumulation and morphology, reduced endocytosis and dysregulated autophagosome formation (Farg et al., 2014, Webster et al., 2016, Sellier et al., 2024). C9ORF72 expression is highest in myeloid cells, including microglia (Masrori et al., 2025), consistent with this, all C9ORF72 knockout mouse develop pro-inflammatory and autoimmune-like disease phenotypes, suggesting C9ORF72 has a vital role in immune regulation (Atanasio et al., 2016, Burberry et al., 2016, Sudria-Lopez et al., 2016). Furthermore, C9ORF72 haploinsufficiency has been associated with enhanced synaptic pruning by overactive microglia (Lall et al., 2021). The neuron specific functions of C9ORF72 are however, less obvious. In this regard, recent studies have shown protein interaction with synapsin that aids in the regulation of neurotransmission at excitatory synapses via modulation of synaptic vesicle pools (Bauer et al., 2022). C9ORF72 deficiency has also been associated with synaptic level dysfunction by way of reduced number of excitatory synapses, depletion of synapsin levels and impaired excitatory transmission (Bauer et al., 2022). Also, haploinsufficiency has been associated with changes in synaptic plasticity and glutamate receptor dyshomeostasis in mice and iPSC-derived motor neurons (Sattler et al., 2023). Loss of C9ORF72 protein function and the downstream neurophysiological consequences are explored in greater detail throughout section 1.6. Crucially, unlike C9ORF72 loss-of-function *Caenorhabditis elegans* and zebrafish models that display motor neuron degeneration and motor deficits (Ciura et al., 2013, Therrien et al., 2013), murine models generally lack neuronal loss, and the motor or behavioural phenotypes associated with FTD/ALS (Koppers et al., 2015, Burberry et

al., 2016, Sudria-Lopez et al., 2016), in contrast to toxic gain-of-function models. Thus, haploinsufficiency alone is perhaps insufficient to trigger neurodegeneration in FTD/ALS but instead contributes synergistically to disease alongside toxic formation of RNA foci and DPRs (Zhu et al., 2020). Indeed, recent evidence points towards a synergistic mechanism between haploinsufficiency and gain-of-function mechanisms that exacerbates pathophysiological phenotypes and can enhance vulnerability to glutamate-mediated excitotoxicity (Sattler et al., 2023).

1.42 Toxic Gain-of-function of RNA Foci

Transcription of the G_4C_2 repeat expansion in the sense and antisense direction leads to the formation of abnormal RNA secondary structures such as G-quadruplexes, hairpins and i-motifs (Figure 1.2) (Haeusler et al., 2014, Su et al., 2014). Such structures give rise to the formation of RNA foci that can sequester and thus lead to the depletion of specific RNA-binding proteins involved in splicing, transcription and translational regulation (Balendra and Isaacs, 2018) (Figure 1.2). RNA foci have been identified to interact and co-localise with serine/arginine-rich splicing factor 1 (SRSF1) (Hautbergue et al., 2017) and most frequently with heterogeneous nuclear ribonucleoproteins (hnRNPs) but not TDP-43 or FUS (Sareen et al., 2013, Cooper-Knock et al., 2014). Accumulation of RNA foci are a hallmark feature of C9-related biology that is routinely used to verify and validate C9 disease models.

Evidence of RNA repeat mediated toxicity has been shown in primary neurons (Wen et al 2014), *Drosophila* (Xu et al., 2013, Zhang et al., 2015) and zebrafish models (Swinnen et al., 2018). However, the relative contributions of RNA and DPR-mediated toxicity towards downstream pathology in these models and beyond is unclear. To address this, Mizielinska and colleagues using *Drosophila* models expressed stop codons in each reading frame of the G_4C_2 repeat to prevent expression of the DPRs from the repeat sequence (Mizielinska et al., 2014). Thus, enabling them to study the potential toxic effects of each gain-of-function mechanism independently. Neurotoxicity observed from DPR expression was crucially not observed from sole expression of RNA foci (Mizielinska et al., 2014). Similar to reports from another group using a different *Drosophila* model of disease (Tran et al., 2015). Solomon and

colleagues reported it was the toxicity of DPR species and not G_4C_2 related RNA-accumulation that triggered TDP-43 pathology and resulting disease onset and progression (Solomon et al., 2018). Consequently, the formation of RNA foci is likely to be a toxic mechanism that does contribute to disease but is not the main driver of C9 disease pathogenesis.

1.43 DPR-mediated Toxicity

Arginine-rich DPRs have been widely reported to be the most toxic of all DPR species in zebrafish (Swaminathan et al., 2018) and in several *in vitro* cell models including primary neuronal cultures and induced pluripotent stem cell (iPSC)-derived neurons (Wen et al., 2014, Yamakawa et al., 2015, Mizielinska et al., 2017). The neurotoxic potential of arginine-rich DPRs has been shown extensively to lead to retinal degeneration, reduced survival and locomotor phenotype in *Drosophila* models (Mizielinska et al., 2014, Wen et al., 2014, Baldwin et al., 2016, Freibaum and Taylor, 2017). Poly-GA has also been shown to be moderately toxic in yeast (Jovicic et al., 2015), primary neurons (Zhang et al., 2014) and in the fruitfly (Mizielinska et al., 2014). The remaining DPRs, poly-PA and poly-GP do not appear to exert any toxic effects (Freibaum et al., 2015, Lee et al., 2017b). Cell-cell transmission of all DPR species has been reported and suggested to underlie expression patterns in post-mortem CNS (Westergard et al., 2016). Murine models of disease have provided vital insight into the study of FTD/ALS biology. However, their use in the study of the repeat expansion mutation has been somewhat limited. Various C9ORF72 gain-of-function mouse models have been characterised and whilst molecular phenotypes are generally well replicated these models fail to consistently recapitulate all aspects of disease relating to neuronal loss and motor or cognitive disease phenotypes (Balendra and Isaacs, 2018). FTD/ALS model systems are discussed further in section 1.8.

The exact contribution of DPRs to pathogenicity is still unclear, but several downstream mechanisms including nucleocytoplasmic transport (NCT) (Freibaum et al., 2015, Zhang et al., 2015, Solomon et al., 2018), impaired protein homeostasis (Smeele et al., 2024), DNA damage (Farg et al., 2017), stress granule dynamics (Dafinca et al., 2016, Chew et al., 2019) and mitochondrial dysfunction (Lopez-

Gonzalez et al., 2016) have been implicated whose dysfunction could lead to neurodegeneration. In particular, the arginine-rich DPR species have been shown to impair liquid-liquid phase separation and consequently interfere with nucleoli and stress granule dynamics via their interactions with low-complexity domain (LCD) containing proteins (Lee et al., 2016, Lin et al., 2016). Impairment in the dynamics of these membraneless organelles can lead to deficits in RNA metabolism, processing and NCT (Kwon et al., 2014, Tao et al., 2015, Lee et al., 2016, Boeynaems et al., 2017, Zhang et al., 2018). Interestingly, numerous mutations have been identified in the LCD of many RNA-binding proteins including TDP-43 and FUS and this alone is sufficient to alter phase separation dynamics (Lagier-Tourenne et al., 2010, Molliex et al., 2015). GR and PR DPRs have also been shown to share interactions with TDP-43 positive stress granules or RNA granules which could drive the fibrillisation and aggregation of TDP-43 (Molliex et al., 2015). Furthermore, high concentrations of these DPR species and their derivative G_4C_2 repeat expansion can undergo LLPS that is adequate to induce phase transition of other RNA-binding proteins (Boeynaems et al., 2017, Fay et al., 2017, Jain and Vale, 2017). However, DPR research has largely been investigated in *in vivo* models that express a shortened repeat expansion length. This may not accurately recapture molecular disease mechanisms in a large proportion of patients with longer repeat lengths in the range of over 1000 repeats (West et al., 2020, Sharpe et al., 2021). Nevertheless, cumulative evidence from these model systems would suggest DPRs are key triggers of disease progression via several pathological mechanisms.

1.5 Pathological Mechanisms of FTD/ALS

FTD/ALS represent multifaceted diseases with several cellular functions hypothesised to become dysregulated in disease onset and progression. Significant progress has been made in understanding the molecular and genetic basis of disease, yet how specific mutations drive neuronal dysfunction via downstream pathomechanisms and the precise interactions between these secondary pathways to drive disease progression is unclear. Associated pathological mechanisms include mitochondrial dysfunction, deficits in NCT, impaired protein homeostasis and non-cell autonomous mechanisms.

1.51 Oxidative Stress

Oxidative stress arises from an imbalance between the production of reactive oxygen species (ROS) and the ability of antioxidant defence systems to detoxify the reactive species (Pizzino et al., 2017). ROS can lead to oxidative damage of biological molecules such as proteins, lipids and nucleic acids that can directly or indirectly via interaction with other pathological mechanisms contribute towards motor neuron injury in ALS pathophysiology (Barber and Shaw, 2010, Pollari et al., 2014). Aberrant levels of ROS and oxidative damage have previously been reported in ALS patient spinal cord and motor cortex (Shaw et al., 1995, Ferrante et al., 1997). These have also been reported in patient cerebrospinal fluid (CSF) and serum samples of ALS patients (Zarei et al., 2015). In fact, mutations in the SOD1 gene lead to oxidative stress related cytotoxicity (Bonafede and Mariotti, 2017). Moreover, oxidative stress has been shown to induce hallmark accumulation and aggregation of phosphorylated TDP-43 deposits that can lead to downstream mitochondrial dysfunction (Cohen et al., 2015, Goh et al., 2018, Zuo et al., 2021). Westergard et al demonstrated oxidative stress was sufficient to induce upregulation of DPR translation in *C9ORF72* cell culture models (Westergard et al., 2019). Crosstalk between motor neurons and surrounding glial cells like astrocytes is a well-known phenomenon. With this, astrocytic glutamate release was evident in response to oxidative stress that could amplify excitotoxic injury in motor neurons (Kazama et al., 2020).

1.52 Mitochondrial Dysfunction

The mitochondrion is a membrane-bound organelle that functions as the energy powerhouse of the cell vital for a number of cellular processes. Deficits in mitochondrial function have been implicated in multiple studies and therefore impairments are well-established disease phenotypes. Studies in patient spinal motor neurons and *in vitro* and *in vivo* model systems have identified altered ATP production and mitochondria-dependent apoptosis, ROS imbalances, disrupted axonal transport of mitochondria and perturbed calcium buffering (Cozzolino and Carri, 2012, Debska-Vielhaber et al., 2021, Jhanji et al., 2021, Mehta et al., 2021). Motor neurons are associated with a high metabolic demand and are vulnerable to calcium overloading due to their involvement in Ca^{2+}-dependent process and low buffering capacity

(Menzies et al., 2002). This was shown in C9FTD/ALS patient-derived motor neurons which displayed decreased mitochondrial buffering capacity of Ca^{2+} (Dafinca et al., 2020).

1.53 Deficits in Nucleocytoplasmic Transport

The transport of proteins across the nuclear membrane is crucial in ensuring their correct localisation to retain proper protein function and maintain cellular homeostasis. The importance of correct NCT is best illustrated by experiments studying nucleocytoplasmic shuttling of TDP-43 (Atwal et al., 2025). Expression of TDP-43 with a dysfunctional nuclear localisation signal (NLS) in transgenic mice models and primary neuronal cultures resulted in hallmark nuclear depletion and cytoplasmic mislocalisation and aggregation of TDP-43 (Winton et al., 2008, Igaz et al., 2011, Walker et al., 2015a). This was adequate in causing motor neuron degeneration and locomotor phenotypes in transgenic mouse models, with inhibited expression of the mutated TDP-43 gene sufficient in preventing further exacerbation of disease phenotypes (Walker et al., 2015a). Deficits in NCT and the nuclear pore complex have been identified in several ALS model systems relevant to TDP-43 proteinopathy (Nishimura et al., 2010, Atwal et al., 2025) and C9FTD/ALS (Zhang et al., 2015, Boeynaems et al., 2016, Jovicic et al., 2015, Freibaum et al., 2015, Lee et al., 2016). Indeed, components of the transport machinery and pore complex were positive modifiers of C9-related neurodegeneration from genetic modifier screens in yeast and *Drosophila* models of *C9ORF72* (Zhang et al., 2015, Jovicic et al., 2015, Boeynaems et al., 2016). Moreover, DPR-induced stress granule formation was shown to perturb NCT via abnormal recruitment of NCT factors which led to neurodegeneration (Boeynaems et al., 2017). Aberrant sequestration of NCT factors was also observed in stress granule independent, cytoplasmic TDP-43 liquid droplets (Gasset-Rosa et al., 2019). Comparable NCT perturbations were also observed in models of TDP-43 proteinopathy, with cytoplasmic TDP-43 capable of inducing cytoplasmic mislocalisation of NCT-related karyopherin proteins in C9FTD/ALS *Drosophila* models, a phenotype recaptured in post-mortem frontal cortex of C9FTD and FTD-TDP cases (Chou et al., 2018, Solomon et al., 2018, Atwal et al., 2025). Solomon et al reported a vicious feedback cycle between DPR-mediated TDP-43 and

karyopherin abnormalities that trigger C9-related neurodegeneration (Solomon et al., 2018). A source of potential therapeutic intervention lies with inhibition of SRSF1-dependent nuclear export of pathological RNA repeat transcripts and subsequent DPR translation (Hautbergue et al., 2017, Castelli et al., 2021).

1.54 Astrocyte Mediated Toxicity and Neuroinflammation

Neurodegenerative disorders like FTD/ALS were previously believed to be a disease of the neuronal system but various studies have now established a non-cell autonomous contribution in disease toxicity. Several groups have reported ALS astrocytes are selectively toxic to wild-type (WT) motor neurons in *in vitro* co-cultures including astrocytes derived from C9 patients (Di Giorgio et al., 2007, Nagai et al., 2007, Meyer et al., 2014, Gatto et al., 2021). In alignment with this, co-cultured astrocytes have been shown to release a range of toxic factors (Di Giorgio et al., 2007, Nagai et al., 2007, Varcianna et al., 2019), pro-inflammatory molecules (Haidet-Phillips et al., 2011) and DPR species (Marchi et al., 2022) that are neurotoxic and induce motor neuron death *in vitro.* This corresponds with histological and imaging studies of neuroinflammation in the CNS of ALS patients (Appel et al., 2021).

1.6 Neurophysiological Impairments in FTD/ALS

Physiological neuronal function is governed by the general excitability of the neuron which refers to its ability to generate voltage output in the form of action potentials (APs). This neuronal activity is underpinned by a myriad of complex factors like synaptic physiology and intrinsic excitability, which is reliant upon the functional expression of ion channels connected to AP generation. Today, perturbations in neurophysiology are regarded as pathogenic hallmarks of FTD/ALS (Pasniceanu et al., 2021) that can present at various loci within the neuronal circuitry of the CNS (Figure 1.3). These perturbations are core contributors to disease that are prominent throughout disease prior to symptomatic onset, during the prodromal phase through to the end stage of disease. At this final stage, a systematic loss-of-function arises from neuronal dysfunction and in turn, a combination of loss at the single cell and

network level. Throughout disease pathogenesis perturbations tend to transition from gain-of-function excitotoxic mechanisms towards loss-of-function impairments in neurotransmission. Understanding the primary sources of electrophysiological dysfunction and the mechanistic link between these and downstream pathways in C9FTD/ALS is important in our understanding of disease pathophysiology. These primary origins could extend at least 15 years prior to symptomatic onset as observed in non-symptomatic C9FTD/ALS patients prior to neurodegeneration (Benussi et al., 2016, Geevasinga et al., 2016). Thus, the efficacious window for therapeutic intervention could be as early as this in the disease course. The literature to date has primarily focused on cortical and motor neurons, characteristic sites of disease in C9 and other FTD/ALS genetic backgrounds, using human patients and a variety of physiological models and techniques.

1.61 Cortical Neuron Dysfunction in C9FTD/ALS

A defining feature of FTD/ALS occurs in the form of neuronal atrophy within specific regions of the cortex. Preceding the degeneration of cortical neurons is neurophysiological dysfunction within the cortex and this has been well documented in sporadic and familial disease cases including those with the *C9ORF72* repeat expansion (Williams et al., 2013, Benussi et al., 2016, Geevasinga et al., 2016, Schanz et al., 2016, Nasseroleslami et al., 2019).

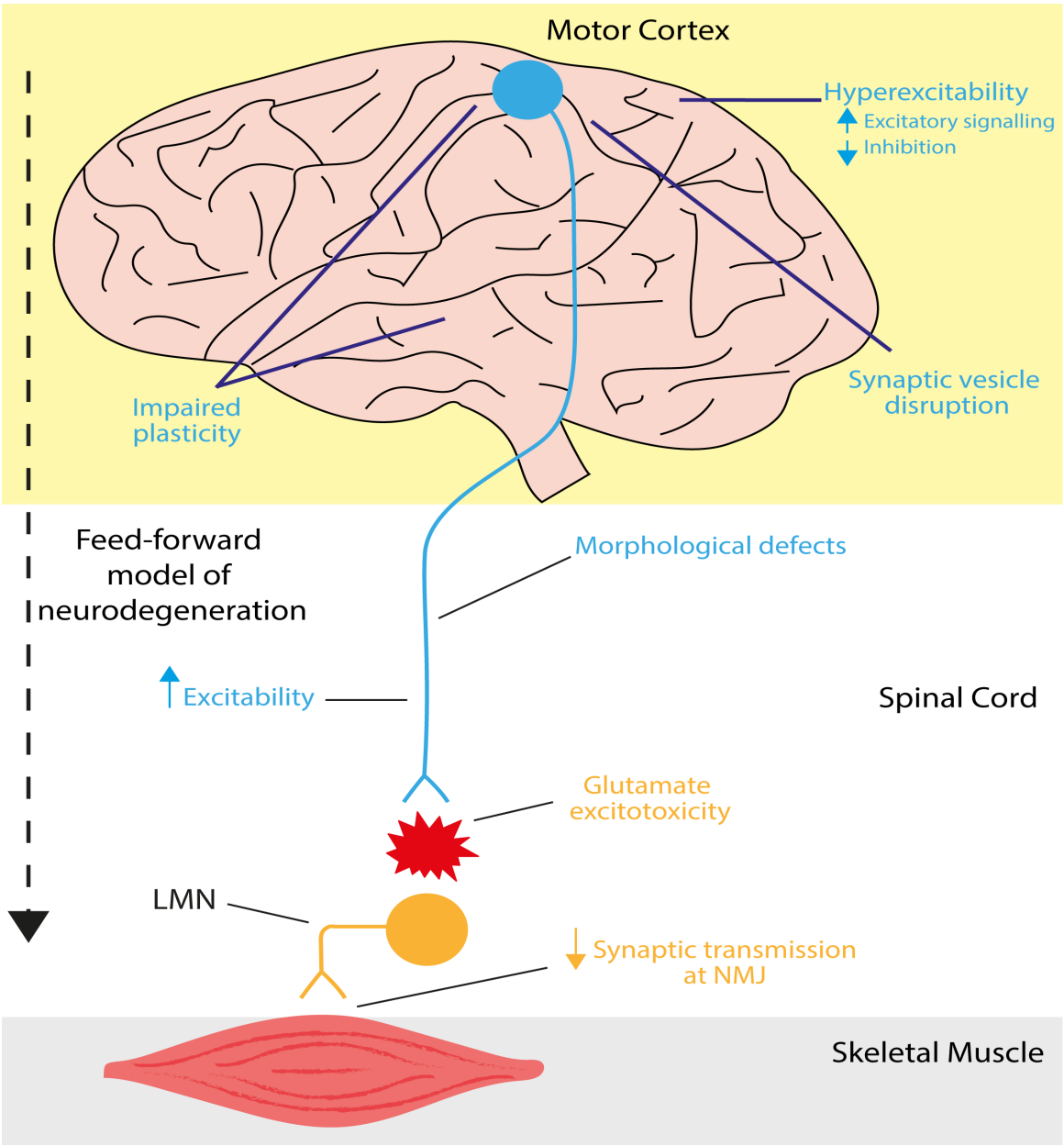

Figure 1.3. Mechanisms of neurophysiological dysfunction in cortical and lower motor neurons that contribute towards C9ORF72 disease progression. Upper motor neurons (blue) originate in the motor cortex and extend projections via the corticospinal tract onto the brainstem and spinal cord. In humans, these corticospinal neurons form a monosynaptic connection with lower motor neurons (orange), that in turn, innervate and relay motor inputs to the effector muscles. This constitutes the motor circuitry in humans. Electrophysiological impairments arise at multiple levels of the CNS circuitry. Cortical abnormalities include hyperexcitability resulting from excessive excitatory signalling or reduced inhibition, disrupted synaptic vesicle dynamics and impairments in synaptic plasticity that also affects cortico-hippocampal circuits. Loss of dendritic architecture and synaptic loss are also observed in upper motor neurons. In a feedforward model of lower motor neuron degeneration, cortical dysfunction precedes and exacerbates motor neuron injury that is driven, at least in part, by glutamate-mediated excitotoxicity. Figure taken, with permission, from (Pasniceanu et al., 2021).

Cortical network dysfunction has been shown to occur early in FTD (Lindau et al., 2003, Nishida et al., 2011) and ALS following examination of patients in resting state magnetoencephalography (MEG) (Proudfoot et al., 2017, Govaarts et al., 2022, Trubshaw et al., 2024) and transcranial magnetic stimulation (TMS) studies (Vucic et al., 2013, Eisen et al., 2017, van den Bos et al., 2019) with longitudinal decline in function observed (Metzger et al., 2024). Indeed, thinning in the motor cortex correlated with disease progression in temporal areas in addition to behavioural and cognitive impairments from MRI studies in FTD/ALS (Verstraete et al., 2012, Mezzapesa et al., 2013, Agosta et al., 2016, Consonni et al., 2018). Analogous to other neurological diseases (Bae and Kim, 2017), early synaptic perturbations are likely to underlie loss of cortical synapses that is proportional to the level of cognitive decline observed in FTD/ALS patients including those characterised by the C9ORF72 mutation (Genc et al., 2017, Henstridge et al., 2018). Eisen and colleagues proposed a staged progression in disease pathology with their feed-forward model for neurodegeneration whereby early cortical dysfunction is proceeded by LMN dysfunction and death (Eisen et al., 1992). Summarised in Figure 1.3. These studies provide evidence for the importance of cortical dysfunction in the early initiating events of FTD/ALS pathophysiology.

1.62 Synaptic Dysregulation in C9FTD/ALS

Synaptic dysfunction has been reported to occur in FTD/ALS patients pre- and post-symptomatic onset including those characterised by the repeat expansion mutation which aligns with a role of the C9ORF72 protein at the synapse (section 1.41). Synaptic dysfunction is an all-encompassing term that relates to alterations in synapse morphology, electrophysiological activity and dysregulated expression of synaptic proteins. Cortical post-mortem tissue of C9 patients revealed distinct transcriptomic profiles relevant to key components of synaptic signalling pathway (Prudencio et al., 2015). Modulation in the expression of a key number of synaptic proteins has been shown extensively in studies within the cortex of C9 post-mortem patients and from a variety of animal and cellular models including C9 patient-derived cortical neurons (Choi et al., 2019, Xiao et al., 2019, Barschke et al., 2020, Jensen et al., 2020, Barbier et al., 2021, Bauer et al., 2022, Laszlo et al., 2022). Reduced levels of synaptic

proteins were also observed in FTD patients prior to symptomatic onset (Goetzl et al., 2016). Deficits in calcium homeostasis and vesicle release were revealed in primary cortical and C9 patient-derived cortical neuronal cultures that showed mechanistic overlap with motor neurons (Jensen et al., 2020). Meanwhile, a study utilising patch-clamp and multi-electrode array (MEA) techniques in cortical neurons derived from C9 iPSC patient lines demonstrated an increase in neuronal network activity attributable to an increase in synaptic density (Perkins et al., 2021). The same study also showed reductions in the ready-releasable pool of synaptic vesicles and impaired synaptic transmission (Perkins et al., 2021). A decreased frequency in the miniature excitatory postsynaptic currents (mEPSCs) of DPR-expressing transgenic mice was shown to coincide with synaptic loss in the prefrontal cortex (Choi et al., 2019). A similar reduction in synaptic function was observed in the thalamus of pre-symptomatic repeat expansion carriers and in the post-mortem cortical regions of bvFTD and C9 patients that was associated with their cognitive decline (Henstridge et al., 2018, Malpetti et al., 2021, Salmon et al., 2021). In addition, primary hippocampal neurons modelling either C9ORF72 haploinsufficiency (Ho et al., 2019) or toxic gain-of-function mechanisms (Huber et al., 2022a) demonstrated decreased spine density and in both models, reduced dendritic branching. In parallel, Lall and colleagues demonstrated a non-cell autonomous component to these phenotypes in addition to cognitive deficits in a C9ORF72 knockout mouse model (Lall et al., 2021). Recently, C9ORF72 haploinsufficiency was associated with a decline in excitatory synapses within primary rat hippocampal cultures (Bauer et al., 2022). Dysregulated synaptic structure, function and protein levels is now a well-documented phenotype that contributes towards neurophysiological impairments in FTD/ALS.

1.63 Neuronal and Network Level Plasticity

The ability of neurons within the nervous system to moderate responses to internal or external stimuli is crucial in the maintenance of correct neuronal and network function. Modulation of neuronal signalling and their ability to remain ‘plastic’ occurs via structural or functional changes at the level of the synapse. A common feature in the early stages of neurodegenerative diseases are functional impairments in neuronal plasticity which represents a state of dysregulated cellular homeostasis that could

drive subsequent neuronal dysfunction and loss (Milnerwood and Raymond, 2010, Starr and Sattler, 2018, Styr and Slutsky, 2018). A TMS study revealed functional impairments in LTP-like network plasticity in pre-symptomatic patients characterised by the C9 mutation and the study proposed such changes could occur at least 15 years before symptomatic onset (Benussi et al., 2016). This is not only suggestive of early cortical dysfunction that may occur at the synapse but could be one of the earliest disease phenotypes observed in FTD/ALS. Similarly, a decrease in the spontaneous neuronal activity of TDP-43 mutant MNs differentiated from knock-in iPSCs was accompanied by synaptic abnormalities prior to any observable TDP-43 pathology or viability (Lepine et al., 2024). Thus, neuronal dysfunction may not only precede TDP-43 pathology but may also occur downstream of TDP-43 pathology as shown by reduced excitatory synaptic transmission and subsequent asynchronous network activity in a mature iPSC-derived neuronal model (Keuss et al., 2024). These deficits were shown to be induced via TDP-43 mediated loss of the UNC13a protein that could be rescued via antisense oligonucleotide therapy targeting the UNC13a cryptic exon (Keuss et al., 2024). Moreover, impaired synaptic potentiation of mEPSCs was established in C9 iPSC-derived cortical neurons that could be rescued in gene-edited isogenic lines corrected for the repeat expansion mutation (Perkins et al., 2021). Impairments in synaptic plasticity are observed in *Drosophila* disease models overexpressing the C9 repeat expansion or FUS mutants (Perry et al., 2017, Sahadevan et al., 2021). Related phenotypes have been extensively shown in various SOD1, FUS and TDP-43 transgenic mice or TDP-43, MAPT and GRN knockout mice (Spalloni et al., 2011, Petkau et al., 2012, Biundo et al., 2018, Koza et al., 2019, Wu et al., 2019, Ho et al., 2021, Handley et al., 2022). In addition, dysregulated gene expression within molecular pathways essential in synaptic plasticity have been shown in C9 patient-derived cortical neurons and C9 patient post-mortem cortex (Prudencio et al., 2015, Dafinca et al., 2016, Perkins et al., 2021). Murine models of C9ORF72 haploinsufficiency suggest a role of the C9ORF72 protein in synaptic function (Ho et al., 2019, Ho et al., 2020). Complete ablation of the C9ORF72 protein was sufficient in reducing long-term potentiation (LTP) and long-term depression (LTD) in cortico-hippocampal circuits (Ho et al., 2020).

Dysregulation in plastic mechanisms that underpin neuronal homeostasis potentially reflects an internal state whereby neuronal function is incorrectly or ineffectively

modulated in response to stressful stimuli. The subsequent failure to adapt to these stimuli could ultimately be the start of a catastrophic pathogenic cascade in FTD/ALS that inevitability leads to neuronal atrophy and death.

1.64 Cortical Hyperexcitability

Hyperexcitability of the cortex refers to the propensity of cortical neurons to fire increased APs in response to stimuli and is believed to be pathologically implicated in motor neuron dysfunction in FTD/ALS, with cortical circuits key regulators of UMN (layer V cortical projection neuron) function within the corticospinal tract. With this, increased cortical excitability is sufficient to drive excitotoxic damage in FTD/ALS patient motor neurons (Khademullah et al., 2020). Such pathology is becoming an increasingly recognised and relevant neurophysiological phenotype observed in both fALS and sALS clinical cases (Geevasinga et al., 2021, Timmins et al., 2023, Xie et al., 2023). The level of cortical hyperexcitability has been shown to correlate with the intensity of cognitive dysfunction and disease prognosis (Shibuya et al., 2016, Agarwal et al., 2021, Higashihara et al., 2021). The maintenance of physiological cortical activity is governed by the delicate balance between excitatory and inhibitory transmission. TMS studies have been crucial in developing a neurophysiological profile of FTD/ALS patients, often characterised by increased intracortical facilitation (excitatory function) and reduced short-interval intercortical inhibition (SICI) (inhibitory function), hence hallmark cortical hyperexcitability (Rossini et al., 2015).

Consistent amongst TMS ALS patient studies is a loss-of-function in the inhibitory function of cortical GABA-ergic interneurons (potentially related to reduced SICI) (Vucic et al., 2008, Geevasinga et al., 2016, Agarwal et al., 2021) including C9 patients (Wainger and Cudkowicz, 2015, Schanz et al., 2016, Nasseroleslami et al., 2019), that proceeds with insidious onset (Menon et al., 2020) prior to symptom onset and LMN degeneration (Menon et al., 2015, Geevasinga et al., 2016). Reductions in SICI suggests possible dysfunction or neurodegeneration of the inhibitory network function of cortical GABAergic interneurons that is sufficient to induce or augment cortical hyperexcitability. Histological studies in animal models of ALS (Nieto-Gonzalez et al., 2011, Khademullah et al., 2020) and in post-mortem cortices of FTD/ALS patients

(Nihei et al., 1993, Ferrer, 1999, Petri et al., 2003) including C9FTD/ALS patients (Lin et al., 2021) revealed a reduction in cortical GABA-ergic interneurons that correlates with a study by Foerster and colleagues whereby decreased GABA levels were detected in ALS patient motor cortex (Foerster et al., 2012).

Currently, the extent of interneuron dysfunction within C9FTD/ALS models remains understudied with our knowledge of such dysfunction derived predominantly from SOD1 or TDP-43 murine models of disease. Embryonic cortical interneuron cultures from SOD1^{G93A} mice (Clark et al., 2018) and pre-symptomatic SOD1^{G93A} parvalbumin-positive GABAergic interneurons (Khademullah et al., 2020), showed attenuations in excitability that later evolved into a hyperexcitable phenotype following symptomatic progression in the same SOD1^{G93A} model (Kim et al., 2017). Of note, the translational value of cortico-motor phenotypes from ALS rodent models should be carefully considered as the mono-synaptic corticospinal tract circuitry is an anatomical exclusive feature of primates, and not rodents (Lemon, 2008). Nonetheless, Khademullah et al were able to pharmacologically rescue disinhibition-induced hyperexcitability in the SOD1^{G93A} model by increasing parvalbumin interneuron activity that was effective in delaying motor deficits and prolonging survival (Khademullah et al., 2020). This along with data from a mutant SOD1 zebrafish study which revealed interneuron dysfunction occurs before motor neuron degeneration (McGown et al., 2013), would imply enhanced interneuron function could reduce hyperexcitability and be neuroprotective to motor neurons. Loss of parvalbumin-positive GABAergic interneurons was suggested to contribute to cortical hyperexcitability-induced cognitive impairments in a TDP-43^{Q331K} FTD/ALS knock-in model (White et al., 2018). Interestingly, in a TDP-43^{A315T} mouse model, intricate interaction between different interneuron populations was shown with hyperexcitability of somatostatin interneurons sufficient to induce hypoexcitability in parvalbumin interneurons (Zhang et al., 2016). It was this, and not any changes in excitatory transmission that resulted in hyperexcitability within this model. Also, defects in inhibitory synapses were noted in a *tau* and *FUS* mouse model (Shimojo et al., 2020, Sahadevan et al., 2021, Scekic-Zahirovic et al., 2021) and reduced inhibitory signalling within the cortex of a C9 female mouse model that resulted in increased motor cortex output (Amalyan et al., 2022).

Alternatively, amplified activity of excitatory cortical neurons could also contribute towards abnormalities in the cortical excitability of FTD/ALS patients. Date from C9 iPSC cortical neurons indicated an increased in excitatory function that was associated with an increase in synaptic density (Perkins et al., 2021). Both pre-symptomatic TDP-43^{Q331K} and SOD1^{G93A} mice displayed amplified excitatory synaptic transmission within the cortical neurons of the motor cortex (Fogarty et al., 2015, Fogarty et al., 2016). Together these studies suggest increased excitatory function could underlie hyperexcitable phenotypes observed early within FTD/ALS patient cortex. Towards the latter disease stages these gain-of-function mechanisms are likely to be transient and shift towards loss-of-function with reduced synaptic function and synapse loss as observed in symptomatic TDP-43^{A315T} mice (Handley et al., 2017). Of note, these pathophysiological changes are likely to mirror the progression from onset of symptomatic disease to symptomatic onset and disease end stage. Even so, transcriptional dysregulation of synapse associated protein could explain these early increases in synaptic density (Prudencio et al., 2015, Perkins et al., 2021). In contrast, C9-related pathomechanisms have been directly linked with synapse loss in various C9 models of disease. Synaptic loss within the prefrontal cortex of DPR-expressing transgenic mice was detected (Choi et al., 2019) whilst arginine-rich DPR knock-in mouse models recapture cortical hyperexcitability, loss of synaptic proteins and age-dependent spinal motor neuron loss (Milioto et al., 2024). Also, a reduction in synaptic density has been shown in models of C9ORF72 haploinsufficiency (Ho et al., 2019, Xiao et al., 2019). Plus, in a microglial specific C9ORF72 knockout mouse model, enhanced cortical synaptic pruning and decreased dendritic branching and cortical synaptic protein levels were pathogenic drivers of cognitive dysfunction (Lall et al., 2021). Altogether, these studies demonstrate the underlying pathophysiology that may underpin synaptic loss observed in bvFTD patients (Malpetti et al., 2023) and C9 patients (Henstridge et al., 2018) and associated cognitive dysfunction.

1.65 Increased excitability and Morphological Defects of Upper Motor Neurons

UMNs of the motor cortex synapse onto LMNs populations of the spinal cord via the corticospinal tract. Hyperexcitable phenotypes within these neurons has been shown and therefore consistent with the feed-forward model of motor neuron degeneration in

ALS, whereby UMN loss is proceeded by LMN death (Marques et al., 2021). In line with this, hyperexcitability of UMNs was observed in TDP-43 mice models of disease that appeared to be driven by reduced inhibitory inputs or intrinsic hyperexcitability, even in the presence of reduced excitatory inputs, that was driven by cytoplasmic TDP-43 mislocalisation (Zhang et al., 2016, Dyer et al., 2021). In rat primary cortical neurons excitatory optogenetic stimulation was shown to induce increased levels of DPR species (Westergard et al., 2019, Catanese et al., 2021). Patch-clamp analysis revealed incubation of acute motor cortex slices with PR DPRs increased the intrinsic excitability of cortical motor neurons (Jo et al., 2022). Cortical hyperexcitability was able to diffuse in an anterograde manner down the mouse corticomotor system to ultimately cause feed-forward LMN degeneration (Reale et al., 2023). In a rodent ALS model, hyperexcitability was shown to replicate typical ALS features such as locomotor phenotypes, motor neuron degeneration and TDP-43 pathology (Haidar, 2021). The ensuing disease phenotypes observed from this rodent model following increased UMN activity are similar to those observed in post-mortem ALS patient tissue (Genc et al., 2017) and other ALS mouse models of disease (Sephton et al., 2014, Fogarty et al., 2017, Handley et al., 2017). Further work is required to study these perturbations in the context of the C9 mutation.

1.66 Lower Motor Neuron Dysfunction

In the human motor circuitry UMNs descend from the motor cortex and form a monosynaptic pathway that innervates the LMNs of the brainstem and spinal cord via the corticospinal tract. These LMNs represent the final components of the circuitry that transmit signals to the skeletal muscle fibres via the neuromuscular junction (NMJ) (Figure 1.3). LMN dysfunction, detected by EMG and nerve conduction studies is a key diagnostic indicator for ALS (Salzinger et al., 2024). Cortical dysfunction precedes that of the lower motor system. Muscle symptoms tend to progress from initial muscular fasciculations and cramps early on in disease towards muscle weakness and atrophy in the latter stages. These symptoms correlate with LMN hyperexcitability early in disease that transitions towards a loss-of-function (hypoexcitability) that culminates in LMN degeneration (Wannop et al., 2021, Salzinger et al., 2024).

1.67 Loss of Synaptic Innervation in the Motor Circuitry

The UMNs and LMNs within the motor circuitry are linked by excitatory glutamatergic synapses. Excessive stimulation at this synapse is thought to lead to the phenomenon of glutamate-mediated excitotoxicity a critical pathogenic driver of motor neuron degeneration in FTD/ALS (Cleveland and Rothstein, 2001). In proportion with upstream cortical hyperexcitability (Geevasinga et al., 2016), downstream synaptic loss in LMNs is observed towards disease end stage. This was observed in extended cultures of C9 iPSC-derived motor neurons that were also accompanied by CREB (cAMP response element-binding protein)-dependent changes in gene expression (Catanese et al., 2021). The presence of excess glutamate within the synaptic cleft likely occurs due to elevated UMN activity although, exactly how this increased excitability within these neurons influences potentially impaired pre-synaptic glutamate release is currently unclear. Further, astrocyte-mediated clearance of synaptic glutamate has been shown to be dysregulated in various ALS models (Rosenblum and Trotti, 2017), thus contributing to elevated synaptic glutamate, but importantly not in C9 iPSC-derived models (Allen et al., 2019, Zhao et al., 2020). During excitatory transmission, glutamate release activates glutamatergic AMPA (α~-amino-3-hydroxy-5-methyl-4 isoxazole propionic acid), and NMDA (N-methyl-D-aspartate) receptors (AMPAr and NMDAr) located on post-synaptic LMNs. The overactivation of these receptors can trigger an overload in the influx of cations like Ca^{2+} thereby resulting in altered excitability and a multitude of Ca^{2+}-induced excitotoxic mechanisms (Van Den Bosch et al., 2006, Pradhan and Bellingham, 2021).

Dysregulated glutamate homeostasis has been reported in several C9 iPSC-derived patient motor neurons studies (Donnelly et al., 2013, Selvaraj et al., 2018, Shi et al., 2018, Bursch et al., 2019), with early work directed towards LMN vulnerability to AMPAr-mediated excitotoxicity (Rothstein et al., 1990, Rothstein et al., 1992, Rothstein, 1995, Cleveland and Rothstein, 2001). Ensuing work in the field has shown upregulated expression of Ca^{2+}-permeable AMPAr through amplified expression of the GluA1 subunit in LMNs derived from C9 patients (Selvaraj et al., 2018, Shi et al., 2018). Using post-mortem samples from patients with the C9 mutation, dysregulated GluA1 expression was selective to LMNs and not patient cortex (Selvaraj et al., 2018, Gregory et al., 2020). These studies highlight regionally specific disease mechanisms

at play in C9-related pathology. C9ORF72 haploinsufficiency has been linked with upregulated GluA1 expression in C9 specific *in vitro* and *in vivo* models (Shi et al., 2018, Xiao et al., 2019). The synergistic interaction between C9ORF72 protein ablation in combination with artificially induced excitotoxicity induced ALS in a rat model (Dong et al., 2021). In knockout murine models of known C9ORF72 protein interactor, Rab39b, evidence for increased GluA1 trafficking and reduced expression of calcium impermeable GluA2-containing AMPAr was shown (Mignogna et al., 2021). Furthermore, deregulated GluA1 expression is apparent in the cortex of sALS patients in addition to neuronal cultures characterised by TDP-43 and FUS mutants (Udagawa et al., 2015, Bursch et al., 2019, Gregory et al., 2020). Also, expression of the calcium impermeable GluA2 subunit was found to be downregulated in a $SOD1^{G93A}$ mouse model and from SOD1 patients (Tortarolo et al., 2006, Gregory et al., 2020). Moreover, GluA2 post-transcriptional defects are reported in sALS patients that have consequently resulted in increased expression of Ca^{2+}-permeable AMPAr (Kawahara et al., 2004, Kawahara and Kwak, 2005, Hideyama et al., 2010).

Multiple lines of evidence have demonstrated elevated CSF levels of glutamate in FTD/ALS patients (Rothstein et al., 1990, Palese et al., 2020) and whilst motor neuron vulnerability to AMPAr-mediated excitotoxicity has been shown in several FTD/ALS models limited data exists for the involvement of NMDAr. However, a recent study has shown upregulation of the NMDAr subunit, GluN1, in a C9 model of iPSC-derived motor neurons (Shi et al., 2018). Dafinca et al reported upregulated expression of Ca^{2+} permeable AMPAr and NMDAr subunits that were common between TDP-43 and C9 patient-derived motor neurons (Dafinca et al., 2020). Most recently in primary C9 hippocampal cultures, dendritic morphological changes were accompanied by a hyperexcitable, glutamate-induced excitotoxicity underlain by enhanced activity of extrasynaptic GluN2B-containing NMDAr (Huber et al., 2022a). The expression of arginine-rich DPRs was interlinked with an NMDAr-dependent excitotoxic mechanism that induced the selective degeneration of *Drosophila* glutamatergic neurons (Xu and Xu, 2018). These data reveal a possible role of NMDAr dysregulation in LMN dysfunction and degeneration.

1.68 Alterations in Lower Motor Neuron Activity

Changes in the neuronal excitability of LMNs from C9 patients is associated with alterations in the intrinsic function of ion channel activity that governs AP generation (Geevasinga et al., 2015). Multiple *in vitro* studies have investigated the physiological mechanisms responsible for neuronal excitability changes that occur throughout the duration of C9 iPSC-derived LMNs cell culture. Electrophysiological investigations of LMN cultures revealed excitability shifts from an initial hyperexcitable state (Wainger et al., 2014, Devlin et al., 2015, Burley et al., 2022, Harley et al., 2023a) to a state of hypoexcitability (Sareen et al., 2013, Zhang et al., 2013, Devlin et al., 2015, Naujock et al., 2016, Guo et al., 2017, Sommer et al., 2022, Harley et al., 2023a). No significant changes in cell viability were reported and prior to dysfunction at the NMJ (Martinez-Silva et al., 2018). Thus, supporting the idea that these excitability changes are an early neurophysiological feature of disease that precedes motor neuron degeneration (Iwai et al., 2016). A similar pattern of excitability changes was also observed in mice models of mutant SOD1 motor neurons (Leroy and Zytnicki, 2015).

The generation of highly enriched neuronal cultures is crucial in the study of the intrinsic excitability of iPSC-derived motor neurons due to the possibility of extrinsic factors impacting motor neuron excitability. With time, iPSC cultures have improved in their enrichment for motor neurons and consistent with this, recent studies have shown no differences in the intrinsic excitability of C9 patient-derived motor neurons (Selvaraj et al., 2018, Zhao et al., 2020). Zhao and colleagues implicated a non-cell autonomous role of C9ORF72 mutant astrocytes that upon co-culture lead to reduced AP output of motor neurons (Zhao et al., 2020). These findings would indicate the presence of astrocytes in the previous studies of enriched motor neuron mixed cultures to be the principal mediators of motor neuron hypoexcitability.

Emerging work in the field is beginning to focus on the potential mechanisms giving rise to these excitability changes. To this end, in $SOD1^{G93A}$ mice Khademullah and colleagues demonstrated selective enhancement of cortical inhibition was adequate to not only reduce cortical hyperexcitability but had a protective impact on spinal motor neurons (Khademullah et al., 2020). This would suggest LMN dysfunction may be driven, at least to some degree, by upstream dysfunction within the (motor) cortex

which feeds into the feed-forward model of degeneration. In the same mouse model, loss-of-function either via degeneration or reduced excitability of inhibitory glycinergic spinal interneurons that was proceeded by locomotor phenotypes and motor neuron degeneration (Allodi et al., 2021, Cavarsan et al., 2023).

LMN hyperexcitability, including through glutamate stimulation, has been shown to drive hallmark TDP-43 pathology (Weskamp et al., 2020) and production of DPR species (Westergard et al., 2019). Together these studies present a potential neuropathophysiological mechanism by which hyperexcitability can induce hallmark pathology that in turn drives further hyperexcitability and degeneration in a toxic positive feedback cycle in C9FTD/ALS.

1.69 The Neuromuscular Junction in ALS

Degeneration of the NMJ and thus the motor unit occurs very early in disease prior to motor neuron loss and symptom onset. This pathology is observed universally across the ALS disease spectrum and supports a pre-synaptic dysfunction of LMNs (Gelon et al., 2022). Dysfunction at the NMJ has been shown in human *in vitro, Drosophila,* murine and zebrafish ALS models with a range of genotypes (Walker et al., 2015a, Cappello and Francolini, 2017, Chand et al., 2018, Butti et al., 2021, Pereira et al., 2021, Massih et al., 2023) including the fast-twitch motor units of SOD1 mice (Cappello and Francolini, 2017). Deficits in function have also been shown in C9 *Drosophila* models overexpressing the repeat expansion in the form of reduced active zone size and neurotransmitter release from pre-synaptic LMNs (Freibaum et al., 2015, Zhang et al., 2015). In agreement, a reduction in the spontaneous post-synaptic activity of C9 iPSC-derived MNs was detected and corresponded with hypoexcitability rather than MN loss (Devlin et al., 2015). Reduced post-synaptic function in LMNs could relate to their diminished ability to generate APs sufficient for acetylcholine release at the NMJ. Tu and colleagues revealed expression of poly-GA, the most abundant DPR, at the NMJ results in deregulated synaptic function (Tu et al., 2023). Furthermore, abnormal vesicular dynamics have been associated with pathophysiological mechanisms in ALS. Such disturbances were shown to precede MN loss in poly-GA transgenic mice and *in vitro* C9 human models which involved loss of synaptic vesicle-

associated protein 2 (SV2) that were also observed in C9 patient-derived cortical neurons (Jensen et al., 2020). In C9 and TDP-43 fly models, Coyne and colleagues reported decreased expression of the molecular chaperone Hsc70-4/HSPA8 at the NMJ that ultimately leads to aberrant synaptic vesicle cycling (Coyne et al., 2017).

1.7 Role of the Striatum in FTD/ALS

An ever-growing amount of evidence has led to FTD/ALS being increasingly recognised as a multifaceted disease with pathology that extends beyond neurons of the cortico-motor and frontotemporal cortical circuits as described in section 1.1 and 1.2. An emerging theme within the field suggests the pathological relevance of extra cortical/motor regions in disease, with a body of research implicating striatal dysfunction in FTD/ALS.

The striatum functions as a central processing centre receiving inputs to and from the cerebral cortices and other basal ganglia structures. The striatum represents a group of subcortical nuclei that can be subdivided into the dorsal and ventral striatum in which the former is composed of the putamen and caudate nucleus and in the latter, the nucleus accumbens. Interestingly, degeneration of the dorsal striatum represents a neuropathological hallmark of Huntington's Disease (HD) patients. This area of the striatum is predominantly involved in motor function (Prager and Plotkin, 2019). However, striatal pathology within FTD/ALS patients is predominantly localised to the ventral striatum that has specific functions in behavioural cognitive functions relating to reward-related behaviour and language (Vatsavayai et al., 2016).

This subcortical brain region performs an integral role in motor control, coordination and execution in conjunction to its key role in higher executive functions relating to decision-making, language processing and behavioural regulation including in a social context (Bede et al., 2016, Ahmed et al., 2021, Kabiljo et al., 2022). The cognitive roles of the striatum overlap with the aberrant cognitive and behavioural phenotypes commonly observed in FTD/ALS patients, implying striatal perturbations may be a contributor factor to such phenotypes (Pauli et al., 2016). Striatal medium spiny neurons (MSNs) form the principal cell type of the striatum, accounting for up to 95%

of the total neuronal population (Prager and Plotkin, 2019). These neurons receive excitatory glutamatergic input from the prefrontal cortex (highly vulnerable in disease) with these neuronal circuitries playing important roles in executive function, motivation, behavioural impulses and inhibition and processing of emotional responses (Alexander et al., 1986, Haber, 2016, Cox and Witten, 2019, Bocchetta et al., 2021). Indeed, glutamate receptor dysfunction within cortical layers of murine models has been coupled with disinhibition and impaired sociability (Gascon et al., 2014, Warmus et al., 2014). In FTD patients, glutamatergic function has been shown to be reduced within the cortex (Ferrer, 1999, Sarac et al., 2008) that would suggest reduced network excitability within cortical circuits. Though, network hyperexcitability in FTD patients has previously been reported (Beagle et al., 2017). Dopaminergic innervation from the substantia nigra to MSNs in the dorsal striatum serves in motor and cognitive control (Murley and Rowe, 2018). Whereas the purpose of dopamine inputs from the prefrontal cortex and ventral tegmental area to the ventral regions via the mesolimbic pathway contributes towards reward reinforcement, learning and motivation-related behaviour (Wise, 2004, Patton et al., 2013, Han et al., 2017). Deficits in these pathways have been associated with a parkinsonism aspect to C9FTD/ALS and could contribute to observed behavioural symptoms (Boeve et al., 2012, Murley and Rowe, 2018, Liu et al., 2022). MSNs also receive GABA-ergic transmission from the axon collaterals of other MSNs or from GABA-ergic interneurons that can modulate MSN activity and may be important for rational and goal-directed behaviours (Wang et al., 2012, Cox and Witten, 2019). MSNs project inhibition to other parts to basal ganglia, which can in turn form a reinforcing feedback loop to the cortex via the thalamus (Haber, 2016, Cox and Witten, 2019, Bocchetta et al., 2021). All of which is consistent with a loss of inhibition observed in FTD/ALS. The afferent and efferent projections to and from the striatum are schematically represented in Figure 1.4.

Neuronal atrophy within the striatum of FTD/ALS patients has been identified in post-mortem patient cases (Kato et al., 1994) and in several neuroimaging studies (Garibotto et al., 2011, Masuda et al., 2016, Radakovic et al., 2018) including C9 patient cases (Bede et al., 2013, Bede et al., 2018, Ahmed et al., 2021). Furthermore, a close association between striatal dysfunction and deficits in frontostriatal networks of FTD/ALS patients was observed that could contribute towards cognitive and behavioural phenotypes in these patients (Bertoux et al., 2015, Bede et al., 2018,

Radakovic et al., 2018, Ahmed et al., 2021). The presence of accumulated TDP-43 deposits within MSNs, the major cell type of the striatum (Prager and Plotkin, 2019), has been identified in FTD/ALS patients (Zhang et al., 2008, Brettschneider et al., 2013) and is markedly pronounced in those harbouring the C9 mutation (Cykowski et al., 2017). Consistent with this, a loss of axon terminals and TDP-43 pathology was evident in the neurites and axon terminals of both FTD/ALS patient cortico-striatal and striatal efferent neurons (Riku et al., 2016, Riku et al., 2017).

Although neuronal atrophy, TDP-43 pathology and network-related dysfunction in cognitive circuits have been identified within the striatum, striatal involvement in FTD/ALS has been potentially overlooked. Even so, functional evidence supporting a role for striatal dysfunction in FTD/ALS remains scarce.

This project will aim to elucidate the involvement of the striatum in FTD/ALS patients.

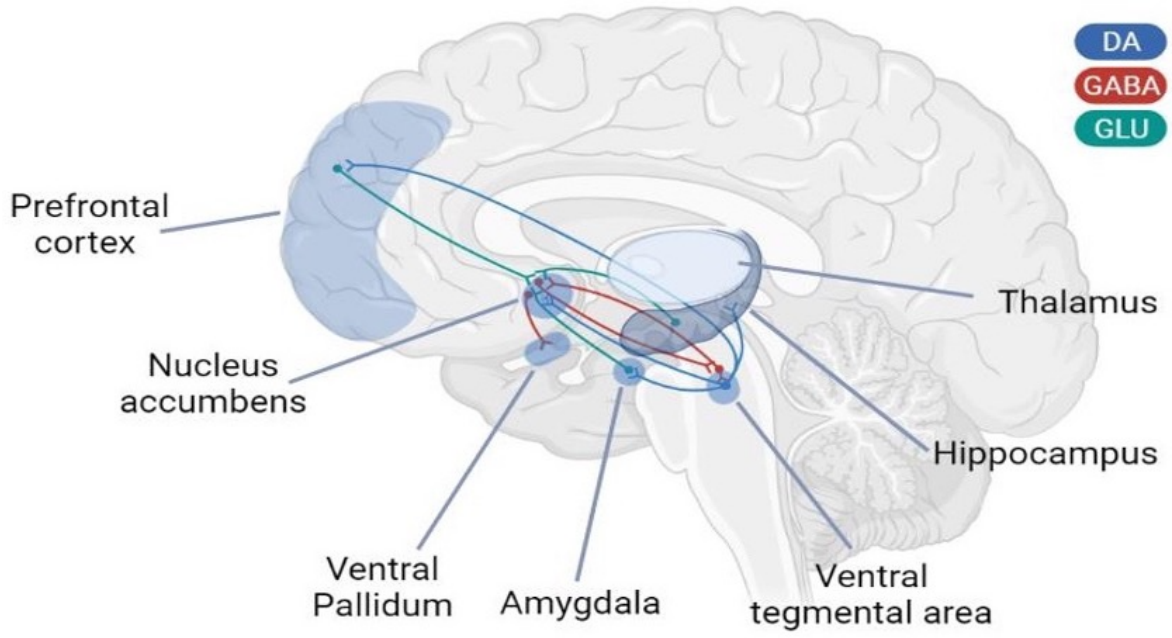

Figure 1.4. Circuit level diagram of striatal input and output projections across different brain regions. Schematic representation of dopaminergic (DA), GABA-ergic (GABA) and glutamatergic (GLU) projections that involve the striatum within larger neural networks. Figure created in BioRender.

1.8 Human Stem Cell Technology

Progress within neurological study and in particular research into neurodegenerative disease pathophysiology and therapeutics have historically been hampered due to an inability to access physiologically relevant human tissue. Consequently, neurodegenerative research has primarily utilised peripheral samples (CSF, urine and blood), human post-mortem material and animal models. However, post-mortem samples are often scarce and predominantly derived from individuals at the end stages of life. Thus, limiting pathological findings specifically to the final phases of disease (Turner et al., 2013). Animal models of disease especially murine and *Drosophila* models have provided invaluable insights into critical aspects of FTD/ALS biology that have been key to progress within the field. Although, these models are generally limited by species differences and their inability to fully recapitulate the full spectrum of disease and therefore recapturing an endogenous cellular disease state (Ferraiuolo and Maragakis, 2021). With the dawn of human stem cell technology, we now have an accessible and renewable source of regionally distinct human-derived neuronal populations. The field of neurodegeneration including FTD/ALS has widely benefited from the ability to study the disease at the cellular level and target therapeutics in a human-specific platforms (Zhao and Moore, 2018). This study involves the use of induced pluripotent stem cells (iPSC) technology to generate two independent region-specific neuronal populations; iPSC-derived striatal medium spiny neurons (Section 2.16) and iPSC-dervied lower motor neurons (Section 2.17).

1.81 Historical Context of Induced Pluripotent Stem Cells

The development of iPSC technology has been built upon the foundation of a series of landmark discoveries within the field of stem cell research. The first scientific breakthrough emerged over half a century ago when the first stem cells were described in mice bone marrow (Till and Mc, 1961). In 1981, mice embryonic stem cells were isolated for the first time that was subsequently followed by the isolation of human embryonic stem cells (hESC) in 1998 (Evans and Kaufman, 1981, Thomson et al., 1998). Discovery of hESC was revolutionary, considering their pluripotency and as an unlimited source of human cells with the potential for therapeutic applications. However, due to technical difficulties and strong ethical concerns related to their

reliance on human embryos the search for alternative approaches to pluripotent stem cell generation was required.

The concept of induced pluripotency whereby differentiated cells could be reverted back into a stem cell fate, offered a potential solution to the challenges posed by embryonic-derived cells. A landmark study by John Gurdon in 1962 provided direct evidence for nuclear reprogramming in somatic cell nuclear transfer (SCNT) experiments using a model of the *Xenopus laevis* frog (Gurdon, 1962). Here, cloned germline-competent organisms were generated from the isolation and transfer of nuclei from terminally differentiated somatic cells into enucleated egg cells. Therefore, demonstrating somatic cell nuclei retained the genetic information required to generate a new organism which was preserved during the differentiation process. This gave rise to the idea of reversible epigenetic mechanisms responsible for the phenotypic diversity of somatic cells. SCNT was further refined in the following decades, which led to the first successful reproductive clone of a mammal in Dolly the sheep (Wilmut et al., 1997).

1.82 The Breakthrough: Induced Pluripotent Stem Cell Technology

The culmination of all these historical advances led to the development of iPSCs, first pioneered by Yamanaka and colleagues in 2006 from adult mice fibroblasts (Takahashi and Yamanaka, 2006) and replicated in adult human fibroblasts in 2007 (Takahashi et al., 2007). The introduction of four transcription factors; Klf4, Sox2, Oct3/4 and c-Myc termed ‘Yamanaka factors’ successfully induced reprogramming of these mature fibroblasts into pluripotent stem cells. For their contributions towards this discovery of iPSCs Yamanaka and Gurdon were co-recipients of the 2012 Nobel Prize in Physiology or Medicine.

The introduction of this non-invasive technology enables researchers to take advantage of iPSC properties of self-renew and potency i.e. the cell’s ability to continuously proliferate and in the latter, differentiate into specialised cell types. iPSCs are reprogrammed from the somatic cells of patients such as skin and blood cells into a pluripotent state, from which they can differentiate into a specific cell lineage via one

of three primary germ layers (Figure 1.5). The power of this *in vitro* human model in disease modelling and therapeutic translation stems from the ability to generate a readily available supply of cell specific populations from any patients including sFTD/sALS cases or those characterised by rare genetic variants. Thus, offering an alternative to animal models of disease. Of note, iPSC reprogramming has been shown to reset the epigenetic signature of derived cells which can lead to a loss of aging-associated phenotypes that are crucial to accurately model age-related FTD/ALS (Cornacchia and Studer, 2017, Cerneckis et al., 2024). Nevertheless, since the first iPSC-derived motor neurons were derived from SOD1 ALS patients (Dimos et al., 2008), iPSC-derived neurons from different regions of the CNS have become routinely used to study FTD/ALS pathophysiology (Ferraiuolo and Maragakis, 2021).

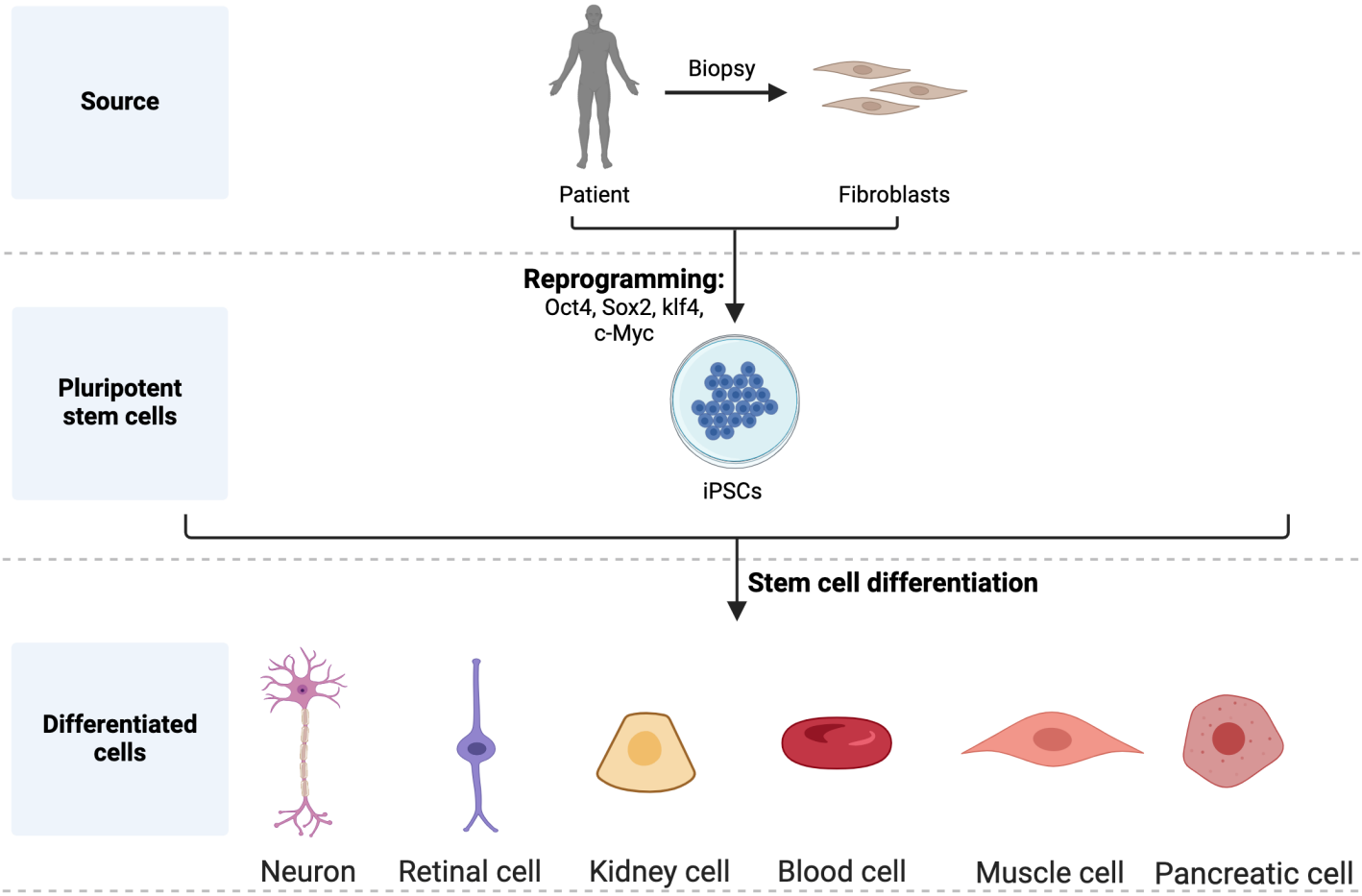

Figure 1.5. Induced pluripotent stem cell technology from human patient to cell-specific in vitro disease models. Somatic cells e.g. fibroblasts are isolated from patients via skin biopsy and are reprogrammed into pluripotent stem cells through viral transduction with the four Yamanaka factors (Oct4, Sox2, klf4 and c-Myc). To drive differentiation of iPSCs towards the desired cell fate, stem cells must be incubated with specific neurotrophic factors in accordance with cellular differentiation protocols. Figure created in BioRender.

1.9 Introduction to patch-clamp electrophysiology

Electrophysiological studies provide critical insight into the function and dysfunction of non-excitable cells in conjunction to electrically active neurons and their networks. The early origins of the study of electrophysiology can be traced back to the 18th century with the pioneering work of Luigi Galvani's who discovered nerve conduction to be governed by electrical excitation (Piccolino, 1998). Since then, the first recording of an action potential (AP) was made by Julius Bernstein. This was followed up in pivotal experiments by Alan Hodgkin and Andrew Huxley in 1952 who described the role of ion channel events that underlie the AP using the voltage-clamp technique, earning them the Nobel Prize in 1963. This technique along with other electrophysiological methods at the time such as sharp microelectrode intracellular recordings suffered from technical limitations that needed to be overcome (Hill and Stephens, 2021). At the time, only macroscopic currents or the membrane potential of the cell could be measured, recordings lacked single ion-channel resolution. This was partly due to the need for low background noise recordings but also leakage currents commonly associated with the techniques at the time. Additionally, precise control of the membrane voltage amongst the internal and external environment was required for the study of ion channel function (Verkhratsky et al., 2006).

These technical challenges were overcome by the development of the patch-clamp technique pioneered by Bert Sakmann and Erwin Neher in 1976, who resolved single channel currents from an electrically isolated frog skeletal muscle (Neher and Sakmann, 1976). A monumental moment for the field of electrophysiology. The foundation for this seminal discovery was built upon earlier work by several groups of electrophysiologists including Neher and Lux (Neher and Lux, 1969), with Neher and Sakmann able to electrically isolate a patch of membrane enabling recordings at the microscopic level (Neher and Sakmann, 1976, Neher et al., 1978). In 1980, the technique was refined by Sigworth and Neher by the discovery of a high resistance seal between the electrode tip and cell membrane, referred to as the gigaohm seal (Sigworth and Neher, 1980). This greatly improved the signal-to-noise ratio not only improving the quality of recordings but also enabling the detection of smaller currents. Further improvements were made to include different recording configurations (Hamill et al., 1981), including the whole-cell configuration which was used in this study.

Briefly, these configurations enable the user to study either single ion channels or the entire ion channel population of a cell, as discussed in detail in Methods section 2.21 Neher and Sakmann were honoured with the Nobel Prize in Physiology and Medicine in 1991 for providing the first measurements of single ion channel currents using the patch-clamp technique, which has since gone on to revolutionise electrophysiological research.

Today, the patch-clamp method has become the gold standard technique in modern electrophysiology that enables researchers to study precise changes in ionic currents through individual ion channels and across whole cell membranes or voltage changes in the cell. The high spatial and temporal resolution of this biophysical technique in conjunction with the various recording configurations has improved our understanding of fundamental cell process ranging from APs to neuronal function and communication. From large giant axons and muscle fibres to human neurons patch-clamp has moved with the times and is routinely used to study the biophysical behaviour of these neurons today. Accordingly, this thesis utilises the patch-clamp technique to study the electrical properties of MSNs and LMNs derived from healthy and disease patients.

1.10 Aims and Hypothesis

Hypothesis 1: In the context of C9ORF72, striatal medium spiny neurons exhibit neurophysiological deficits.

To investigate this, I will generate highly enriched neuronal cultures of human striatal neurons (described in section 2.16) using iPSCs obtained from C9ORF72 patients in alignment with a previously established protocol (Lin et al., 2015). These patients were specifically chosen due to the C9 mutation representing the most common genetic cause of both FTD and ALS. The electrophysiological function of these MSNs will be assessed using patch-clamp electrophysiology (section 2.2), in particular the excitability and excitatory/inhibitory neurotransmission occurring within these cultures at the single cell level will be characterised. This will be used as barometer of neurophysiological function within these neurons in a C9-relevant disease context. As mentioned previously, FTD/ALS is becoming increasingly recognised as a

multifaceted disease with pathology that extends beyond cortical and motor neurons (Nigri et al., 2023). The work here will determine whether neurophysiological impairments as previously reported in FTD/ALS, extends towards medium spiny neurons of the striatum and indeed contribute to disease downstream of the pathogenic mechanisms implicated in C9 disease biology (loss of function, RNA toxicity, dipeptide repeat proteins). Electrophysiological studies can help identify therapeutic disease targets (Wainger et al., 2014, Wainger et al., 2021) and with this, could help distinguish possible therapeutic targets within C9-patient derived striatal neurons.

Hypothesis 2: Different neuronal cell populations display regional differences in electrophysiological dysfunction.

To assess this hypothesis, I will be generating highly enriched lower motor neuron cultures following a protocol previously established by (Du et al., 2015), as described in Methods section 2.17. Motor neurons were derived from the same iPSC-patient lines used to generate striatal MSNs. Importantly, LMN dysfunction is typically associated with ALS pathology and represents a pathological hallmark of disease. Through patch-clamp electrophysiology a physiological profile of iPSC-derived LMNs will be built and the reasons for this are two-fold. Firstly, I wanted to determine whether the neurophysiological profile of iPSC-derived motor neurons generated in this study using the Du et al protocol displayed phenotypic differences to those reported in other iPSC-derived motor neurons studies generated via similar (Burley et al., 2022, Harley et al., 2023a) or alternative protocols (Bilican et al., 2012, Amoroso et al., 2013). Secondly, this will enable me to compare electrophysiological disturbances between iPSC-derived MSNs and iPSC-derived LMNs from the same lines. Thus, allowing me to determine any mutual or regionally specific neurophysiological disturbances in these neurons that belong to different regions of the CNS.

Hypothesis 3: C9 patient-derived LMNs display an impaired homeostatic ability to adapt to neurophysiological challenges that are otherwise managed physiologically in healthy cells.

Importantly, in the third chapter I have considered an important disease modelling question. Typically, in vitro neurons, particularly iPSC-derived MNs, are functionally acting in a basal state, i.e. they receive little input from external sources. However,

MNs in vivo are integrated into networks and receive persistent input that i) drives excitability levels; and ii) drives plasticity in the neurons. Building upon emerging data that plasticity in ALS neurons and circuits is severely impaired, even at an early stage in disease (Benussi et al., 2016), I have investigated the properties of LMNs under specific conditions that cause the emergence of impaired plasticity in the context of C9.

Chapter 2: Material and Methods

This project investigates the electrophysiological perturbations associated with striatal medium spiny neurons and compares these to lower motor neurons derived from the same, healthy or C9 patient induced pluripotent stem cells (iPSCs). The first half of this section will detail how these in vitro human stem cell models were generated. Following this, the use of patch-clamp electrophysiology to study neurophysiological function in *in vitro* neurons will be introduced.

2.1 Cell Culture

2.11 iPSC Cell Lines

In alignment with ethical guidelines, human iPSC lines were either generated internally from the University of Sheffield or purchased from the Cedai-Sinai and Coriell Institute biorepository. Both isogenic lines used in this study have been corrected for the C9ORF72 repeat expansion as indicated on the Cedars-Sinai website (links presented in Table 2.1) and have been utilised in previous publications (Castelli et al., 2021, Saez-Atienzar et al., 2024). The control cell line MIFF1 (Desmarais et al., 2016) was kindly provided by Professor Peter Andrews and Dr Ivana Barbaric (Centre for Stem Cell Biology, The University of Sheffield) and is registered online (https://hpscreg.eu/cell-line/UOSi001-A). All publicly available details of iPSCs, including age and site of disease onset, duration of disease, tissue source, genetic mutation in each patient line, patient sex, ethnic group, patients' age at the time of sample collection and respective repository from which the iPSC cell lines were supplied, are presented in Table 2.1.

2.12 Cell Culture Materials

A list of all cell culture materials including key mediums, neurotrophic factors and cultureware required for the generation of mature iPSC-derived neurons in this study are documented below (Table 2.2).

Table 2.1. iPSC cell line information. The table provides general information on the iPSC cell lines used in this study from which striatal medium spiny neurons and lower motor neurons were derived from. All iPSC lines were produced from skin fibroblasts, except MIFF1 iPSCs that were generated from foetal foreskin fibroblasts.

Cell Line	Clinical Information	Tissue Source	ALS Genotype	Sex	Race	Age at Sampling (years)	Supplier
GM 23338 (Con-1)	Healthy	Fibroblast	-	Male	Caucasian	55	Coriell Institute
MIFF1 (Con-2)	Healthy	Foetal foreskin fibroblasts	-	Male	-	Foetal/ neonatal	University of Sheffield
CS14 (Con-3)	Healthy	Fibroblast	-	Female	Caucasian	30-35	Cedars-Sinai
ALS 28 (C9-1)	Age of onset: 46 Site of onset: left upper extremity	Fibroblast	C9ORF72 expansion (6-8kb) (1000-1333 repeats)	Male	Caucasian	47	Cedars-Sinai
ALS 29 (C9-2)	Age of onset: 46 Site of onset: left upper extremity	Fibroblast	C9ORF72 expansion (6-8kb) (1000-1333 repeats)	Male	Caucasian	47	Cedars-Sinai
ALS 52 (C9-3)	Age of onset: 57 Disease duration: 48 months Site of onset: Left upper extremity	Fibroblast	C9ORF72 expansion (6-8kb) (1000-1333 repeats)	Male	Unknown	49	Cedars-Sinai
Isogenic 29 (C9-2Δ)	Age of onset: 46 Site of onset: left upper extremity	Fibroblast	C9ORF72 Corrected (Isogenic control line of ALS 29)	Male	Caucasian	47	Cedars-Sinai https://biomanufacturing.cedars-sinai.org/product/cs29ials-c9n1-isoxx/
Isogenic 52 (C9-3Δ)	Age of onset: 57 Disease duration: 48 months Site of onset: Left upper extremity	Fibroblast	C9ORF72 Corrected (Isogenic control line of ALS 52)	Male	Caucasian	49	Cedars-Sinai https://biomanufacturing.cedars-sinai.org/product/cs52ials-c9n6-isoxx/

Table 2.2. Cell culture reagents with associated catalogue numbers used for the generation of iPSC-derived MSNs and LMNs. Listed below is the full set of reagents required for this study with information regarding reagent purpose, manufacturer and unique identifier code for each product. Note, 13mm coverslips were used in conjunction with 24-well plates to plate neurons for patch-clamp recordings.

Reagent	Role	Supplier	Catalogue number
DMSO	Freezing cells	Sigma	D2650-100mL
B-27 supplement	Medium	Gibco	11530536
CHIR 99021	Medium	Merck Millipore	SML1046-25MG
Ciliary neurotrophic factor (CNTF)	Medium	Peprotech	450-13
Compound-E	Medium	Tocris	6476
Dickkopf related protein 1 (DKK1)	Medium	Peprotech	120-30
DMH-1	Medium	Merck Millipore	D8946-25MG
Glutamax™	Medium	Gibco	35050061
Human Recombinant Brain derived neurotrophic factor (BDNF)	Medium	Peprotech	AF-450-02
Insulin-like growth factor-1 (IGF-1)	Medium	Peprotech	100-11
KnockOut DMEM/F12	Medium	Gibco	12660012
N-2 supplement	Medium	Gibco	15410294
Neurobasal media	Medium	Gibco	11570556
Penicillin/Streptomycin	Medium	Lonza	DE17-603E
Purmorphamine (PUR)	Medium	Merck Millipore	SML0868-25MG
Retinoic acid (RA)	Medium	StemCell Technologies	72264
SB431542	Medium	Peprotech	3014193
Sonic hedgehog (SHH)	Medium	Peprotech	100-45
Valproic acid (VPA)	Medium	Merck Millipore	PHR1061-1G
Accutase	Passage	Sigma-Aldrich	A6964-100ML
HBSS	Passage	Thermo Fisher Scientific	14170112
Y27632 Rock inhibitor	Passage	Peprotech	1293823
Knockout DMEM	Plate coating	Gibco	10829018
Matrigel	Plate coating	Corning	356230
Poly-L-ornithine	Plate coating	Sigma-Aldrich	P3655-100MG
Corning 6-well plate	iPSC/NPC/MSN/MN plating	Corning	3506
24-well plate	MSN/MN plating	Greiner	662 160
13mm coverslips	MSN /MN plating	Scientific Laboratory Supplies	MIC3336

2.13 iPSC Maintenance

All cell culture products and reagents used in the maintenance and differentiation of iPSC-derived neurons in this study are catalogued in section 2.12. For the maintenance of iPSCs in culture, Matrigel was diluted to 0.1 µg/ml in cold knockout DMEM media and left to coat a 6-well culture plate for one hour at room temperature. The use of Matrigel is vital in supporting cell adhesion to the culture plates in addition to providing a natural extracellular matrix by which cell growth and differentiation are facilitated. iPSCs were plated on 6-well plates and incubated with serum-free mTeSR™-Plus™ medium that was replaced every 48 hours. In accordance with manufacturer instructions, cells were passaged every 4-6 days as clumps using ReLeSR™, a non-enzymatic solution that selectively detaches undifferentiated iPSCs. All iPSCs and iPSC-derived neurons were cultured at 37°C and 5% CO_2.

2.14 iPSC to NPC Differentiation

Differentiation of iPSCs to NPCs was performed from protocols previously established in Du et al., 2015, with adaptations. Once iPSCs lines reached 100% confluency, cells were washed once with PBS to remove any cellular debris or detached cells. A dual-SMAD inhibition protocol, summarised in Table 2.4, was employed to initiate the process of neuralisation by incubating cells with iPSC-NPC day 1-6 differentiation media, which contains CHIR, SB and DMH1. Media was replaced daily. At day 7 of differentiation, cells were cultured in day 7-12 iPSC to NPC differentiation media (Table 2.5) to enhance neuronal differentiation. Media was replaced every 24 hours. Between day 7 to 9 cells were passaged. Passages were performed as followed; cells were first washed with warm HBSS (modified without calcium or magnesium) and then incubated with Accutase at 37°C for 7 minutes to detach adherent cells. Equal volume of cell medium was then added to neutralise Accutase activity before the cell suspension was centrifuged at 200g for 4 minutes. The resulting supernatant was discarded, and the cell pellet resuspended in medium plus Y27632 Rho-associated protein kinase (ROCK) inhibitor (10 µM). Inhibition of these kinases is important in increasing cell proliferation and viability of cell cultures by suppression of cell death pathways. Cells were then replated onto 6-well plates freshly coated with Matrigel and differentiation ensued. The rounded iPSC morphology previously exhibited during the

iPSC stage is no longer observed by 12 days post-differentiation instead, cells display neural rosettes, typically seen at the NPC stage (Appendix 1). Immunostaining done previously by Drs Cleide de Souza/Iris Pasniceanu confirmed the expression of hallmark NPC markers (Pax6 and Nestin) and the absence of key iPSC markers such as Sox2 and Noggin.

Table 2.3. Basal media composition. The basal media serves as an essential nutrient base that helps support cell growth and viability. Supplementation with specific factors enables this base media to be added at different stages of cell maintenance and differentiation.

Component	Concentration	Function
KnockOut DMEM/F12	48% (v/v)	Serum-free media with a formulation optimised for the growth and maintenance of stem cell cultures.
Neurobasal media	48% (v/v)	Serum-free media with a formulation optimised for the growth, maintenance and differentiation of neuronal cell populations.
B-27 supplement	1% (v/v)	Serum-free supplement containing a complex mixture of fatty acids, vitamins, proteins and antioxidant enzymes which helps promote neuronal survival, maturation and differentiation. Aids in neurite growth and neuronal function.
GlutaMax™	1% (v/v)	L-glutamine alternative that is a critical for protein synthesis, energy metabolism whilst improving cell viability and growth for cells in culture.
N-2 supplement	0.5% (v/v)	Serum-free supplement that contains nutrients and hormones to support the growth and survival of neural cell populations.
Penicillin/Streptomycin	1% (v/v)	Antibiotic mixture used to prevent bacterial contamination, vital for ensuring sterile conditions and prolonging viability of neural cell cultures.

Table 2.4. iPSC to NPC media composition (day 1-6). This media consists of basal media supplemented with key factors to stimulate neurogenesis of stem cells.

Component	Concentration	Mechanism/Function
Basal media	Base media	Media base providing essential nutrients and support for cell growth and survival. Supplemented by reagents that promote neural differentiation in stem cells.
CHIR99021	3 μM	GSK3-β inhibitor helps maintain self-renewal and pluripotency of stem cells.
DMH-1	2 μM	Inhibitor of the TGF-β pathway (inhibits neural differentiation) via inhibition of BMP receptors, specifically ALK2. Promotes neurogenesis of stem cells.
SB431542	2 μM	TGF-β pathway inhibitor through inhibition of ALK5/ALK4/ALK7. Inhibits self-renewal and stimulates differentiation of stem cells towards neural lineages.

Table 2.5. iPSC to NPC media composition (day 7-12). The composition of day 7-12 media is identical to the media previously described but with the addition of all-trans retinoic acid (RA) and purmorphamine (PUR). Together, both these factors further stimulate commitment to neural lineages.

Component	Concentration	Mechanism/Function
Basal media	Base media	AS ABOVE.
CHIR99021	1 μM	
DMH-1	2 μM	
SB431542	2 μM	
All-Trans Retinoic acid (RA)	0.1 μM	Vitamin A derivative that functions as a ligand for the retinoic acid receptor. Induces neuronal differentiation in stem cells and progenitors
Purmorphamine (PUR)	0.5 μM	Agonist of the Smo receptor that in turn activates the Hedgehog signalling pathway to enhance commitment to neural lineages.

2.15 NPC Maintenance

NPCs were maintained and expanded in NPC expansion media (Table 2.6). Media was changed every 48 hours. Once cells reached 80-100% confluency, cells were passaged with 10 μM Y27632 ROCK inhibitor and re-plated onto newly coated Matrigel 6-well plates using a 1:2-1:4 ratio. Media changes were always done 24 hours after passage as prolonged incubation with ROCK inhibitor can be toxic to cells. For long-term storage, NPCs were supplemented with 10% DMSO and frozen at –80ºC or in liquid nitrogen until required. New plate downs of NPCs were constantly generated by thawing previously frozen NPCs vials rapidly in a 37°C water bath for approximately 30 seconds. Cells were then plated onto newly coated Matrigel 6-well plates containing NPC expansion media containing 10 μM Y27632 ROCK inhibitor. As described previously, NPCs were incubated for 24 hours at 37°C with 5% CO_2 before media was replaced with fresh NPC expansion media without ROCK inhibitor.

Table 2.6. NPC expansion media composition. At this cell stage the principal components of the media are maintained with the addition of valproic acid (VPA). NPC expansion media is key in the maintenance and proliferation of NPCs.

Component	Concentration	Mechanism/Function
Basal media	Base media	AS ABOVE.
CHIR99021	3 μM	
DMH-1	2 μM	
SB431542	2 μM	
All-Trans Retinoic acid (RA)	0.1 μM	
Purmorphamine (PUR)	0.5 μM	
Valproic acid (VPA)	0.5 μM	Cell-permeable small molecule inhibitor of histone deacetylases that leads to increased histone acetylation. Alters chromatin structure and gene expression including upregulation of neural-specific genes that enhances commitment to neuronal lineage. Maintains NPC populations in a proliferative state during the NPC expansion phase.

2.16 NPC to Striatal Medium Spiny Neuron (MSN) Differentiation

NPCs were differentiated into striatal medium spiny neurons that are GABA-ergic in nature, (Figure 2.1) following protocols previously established by (Lin et al., 2015). NPCs were maintained in NPC expansion media (Table 2.6) until 100% confluency had been reached. At this point, NPC expansion media was aspirated and replaced with GABA1 differentiation media (Table 2.7), for cells aged day 13-24. Media was continually changed every 48 hours. At day 20-21 cells were passaged, cells underwent Accutase treatment to ensure detachment from the plate surface before being counted using the Neubauer Improved haemocytometer (0.1 mm depth, Marienfield). Counts were performed to ensure cells were plated at specific densities. The following equation was used to calculate the exact volume of cells need to achieve a desired cell density:

$$Required\ cell\ suspension\ volume\ (\mu l/well) = \frac{Quantity\ of\ cells\ needed\ per\ well}{cell\ count\ x\ 10000} x1000$$

For patch-clamp recordings, cells were seeded onto 13mm coverslips that had been placed into 24-well plates with the use of sterilised forceps. These coverslips were sterilised in 70% Industrial Methylated Spirit (IMS) for at least an hour and then washed with PBS before transfer into plates. All plates were prepared for culture by coating with poly-ornithine at 1:100 (for glass coverslips) in distilled water overnight at room temperature, to improve cell adhesion. On the day of plating, poly-ornithine was aspirated, and plates were washed three times with PBS followed by Matrigel incubation for an hour. Cells were re-plated onto these freshly coated Matrigel plates in the presence of 10 μM Y27632 ROCK inhibitor. Cells were replated at a density of 120,000 cells per well for patch-clamp analysis. The following day, media supplemented with ROCK inhibitor was removed and replaced with fresh medium to ensure differentiation continued. Media was changed every 48 hours. At day 25 post-iPSC differentiation, medium was switched to GABA2 media (Table 2.8) up until cells reached functional neuronal maturity at day 72. GABA2 media was replaced every 48 hours until day 72. Cells were stained at days 32, 52 and 72 for the expression of key neuronal markers (MAP2 and β3-tubulin) and then labelled with mature markers of GABAergic MSNs (DARPP32 and GABA) to detect for enriched cultures in the later stages of differentiation. Cells were previously characterised by Drs Cleide de Souza/Iris Pasniceanu.

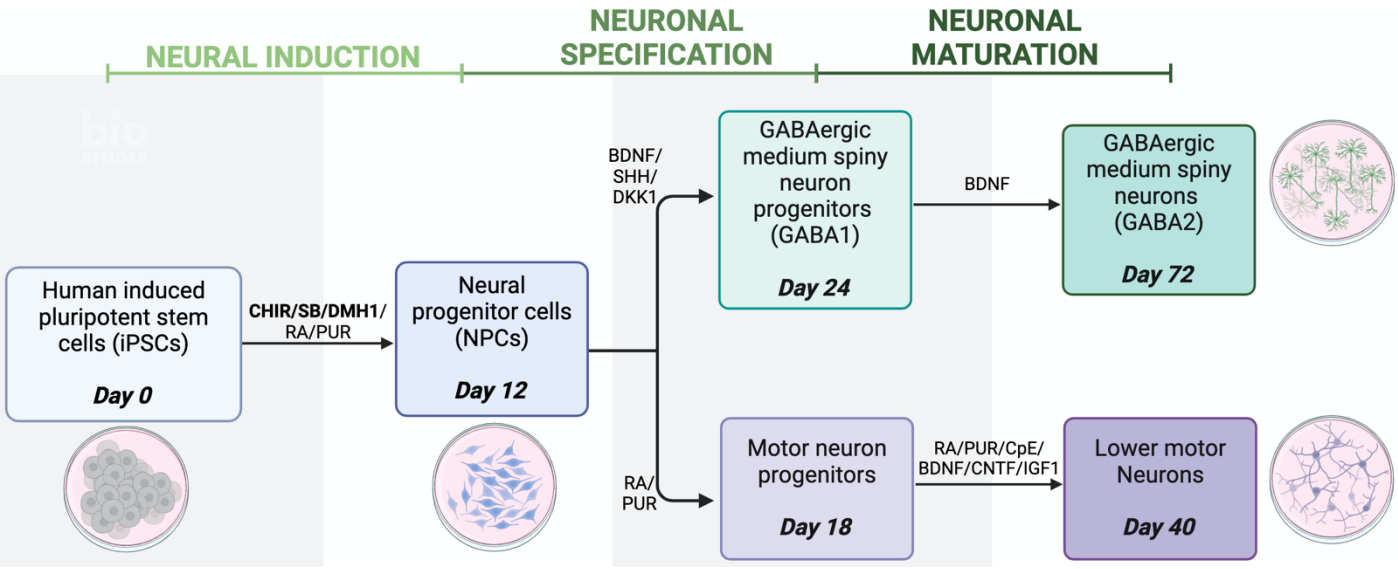

Figure 2.1. *In vitro* differentiation protocol of human iPSC-derived Striatal MSNs and LMNs. The schematic illustrates the multi-step process by which these patient-derived cells are generated, from the iPSC cell stage to full neuronal maturation. Stem cells undergo the process of neuronal induction through dual-SMAD inhibition from days 1-6 with the cocktail of factors highlighted in bold that develop into NPCs. The NPCs are then patterned into either an MSN or LMN cell fate via a precursor stage following treatment with specific morphogens and neurotrophins. Figure created in BioRender.

Table 2.7. GABA1 day 13-24 media composition. Basal media complemented with the factors below were used to steer differentiation of NPCs towards a GABA-ergic neuron cell fate. Listed below are the media constituents along with their respective concentrations and purpose.

Component	Concentration	Mechanism/Function
Basal media	Base media	Media base providing essential nutrients and support for cell growth and survival. Supplemented by reagents to promote differentiation towards GABA-ergic neuronal progenitors.
Brain-derived neurotrophic factor (BDNF)	30 ng/mL	Signalling occurs via TrkB receptors with activation of downstream pathways that promote neuronal survival and maturation. Promotes GABAergic neuronal identity via upregulation of key markers (GAD67 and DARPP-32) (Stroppolo et al., 2001, Willis et al., 2021). Facilitates neurite outgrowth and branching critical for development of GABAergic neurons.
DKK-1	100 ng/mL	Antagonist of Wnt signalling pathway. This pathway functions to promote NPC proliferation. Inhibition of Wnt signalling helps facilitate differentiation of GABAergic neurons. In combination with SHH this increases the success rate of a GABAergic phenotype (Li et al., 2009).
SHH	200 ng/mL	Signalling protein that acts on cells to specify neural cell fates. Upregulates expression of key transcription factors such as Pax6 and Nkx2.1 vital for enhancing specification of NPCs into GABAergic neurons. Integral for the induction of the ventral neural tube, a major source of GABAergic neurons.

Table 2.8. GABA2 day 25-72 media composition. The table below summarises the media components used to provide a nurturing environment for the maturation of striatal medium spiny neurons. Alongside each media component is the respective concentration and purpose of each reagent.

Component	Concentration	Mechanism/Function
Neurobasal media	Base media	Specialised cell culture medium designed to support the long-term growth, maintenance and maturation of neuronal cell cultures. Provides an environment for the growth of enriched neuronal cultures by limiting glial proliferation and provision of essential nutrients such as amino acids and vitamins.
B-27 supplement	2% (v/v)	Serum-free supplement containing antioxidants like vitamin E protecting neurons from oxidative stress thus supporting neuronal survival. Facilitates neuronal maturation through provision of vitamins and hormones to support neuronal metabolism. Promotes development of neurites and synaptic formation.
Penicillin/Streptomycin	1% (v/v)	AS ABOVE.
Brain-derived neurotrophic factor (BDNF)	50 ng/mL	Signalling occurs via TrkB receptors with activation of downstream pathways that promote neuronal survival and maturation. Augments specification of GABAergic neurons via upregulation of key GABAergic markers such as GAD65 and VGAT, that aid in GABA synthesis and transmission essential for mature neuronal function. Facilitates neurite outgrowth and synaptogenesis critical for development of mature GABAergic neurons.

2.17 NPC to Lower Motor Neuron (LMN) Differentiation

NPCs were differentiated into LMNs (Figure 2.1) using protocols adapted from (Du et al., 2015). Once NPCs reached 90-100% confluency, NPC expansion media (Table 2.6) was substituted for motor neuron day 13-18 media (Table 2.9) that was replaced every 48 hours. At day 19 post-iPSC differentiation, motor neuron progenitors were transitioned to motor neuron day 19-28 differentiation media (Table 2.10), also replenished every 48 hours. The progenitors underwent passage at day 20 of the

differentiation protocol. As previously described, this involved soft detachment of cells with Accutase, cells counts using a haemocytometer and re-plated onto plates coated with Matrigel in the presence of 10 μM Y27632 ROCK inhibitor. Cells were replated at a density of 120,000 cells per well for patch-clamp analysis. The next day fresh medium was added, and differentiation resumed. Cells were maintained as per protocol before medium was changed to day 29-40 media (Table 2.11) and replaced every 48 hours until cells reached full maturation at day 40. The same iPSC lines have previously been used to generate motor neurons (Castelli et al., 2021, Zhang et al., 2022). To ensure generation of enriched motor neuron cultures, cells were labelled for expression of mature motor neuron markers (MAP2, NeuN, ChAT, Islet1/2) by Dr. Cleide de Souza.

Table 2.9. Motor neuron day 13-18 media composition. To ensure the necessary conditions to promote motor neuron differentiation, basal media was formulated with the reagents at the concentrations listed below.

Component	Concentration	Mechanism/Function
Basal media	Base media	AS ABOVE.
All-trans retinoic acid (RA)	0.5 μM	Vitamin A derivative that functions as a morphogen that binds to the retinoic acid receptor. These receptors promote specification of motor neuron progenitors via upregulation of key transcription factors like Pax6 and Nkx6.1 that are important for mature motor neuron development. Essential for neural patterning and works in conjunction with the Hedgehog signalling pathway to specifically enhance a motor neuron identity within the cellular population.
Puromorphamine (PUR)	0.1 μM	Smo receptor agonist that activates the Hedgehog signalling pathway, crucial for the ventralisation of neural progenitors and subsequent drive towards motor neuron lineage. Promotes expression of key motor neuron-specific genes, such as Islet1/2 and Olig2, key transcription factors essential for a motor neuron cell fate. Used in combination with RA to increase the efficiency of motor neuron specification.

Table 2.10. Motor neuron day 19-28 media composition. Basal media mixed with the combination of factors below was used to drive differentiation of motor neuron progenitors into young motor neurons. Detailed below is the concentrations and purpose of each factor.

Component	Concentration	Mechanism/Function
Basal media	Base media	AS ABOVE.
All-trans retinoic acid (RA)	0.5 μM	
Puromorphamine (PUR)	0.1 μM	
Compound-E	0.1 μM	Inhibitor of the Notch signalling pathway which is essential for the maintenance of neural progenitors in an undifferentiated and proliferative state. Thus, inhibition of this pathway enables differentiation of neural progenitors. In combination with factors that promote a motor neuron cell fate e.g. agonists of the Hedgehog signalling pathway (RA and PUR), motor neuron specification is enhanced.
Brain-derived neurotrophic factor (BDNF)	10 ng/ml	Signalling occurs via TrkB receptors with activation of downstream pathways that promote neuronal survival and maturation of differentiating motor neurons. Activation of TrkB prevents apoptosis and facilitates neurite outgrowth, promoting motor neurons survival and functional maturation.
Ciliary neurotrophic factor (CNTF)	10 ng/ml	Neurotrophic factor that functions via the CNTF receptor complex and is essential for survival and maintenance of differentiating motor neurons. Prevents motor neuron apoptosis and facilitates neurite outgrowth, promoting motor neurons survival and functional maturation.
Insulin-like growth factor-1 (IGF-1)	10 ng/ml	Neurotrophic factor that activates various signalling pathways including PI3K/AKT and MAPK/ERK pathways via the IFG-1 receptor. These signalling cascades are important for the long-term health of the neuronal population as they support survival, growth and maturation of differentiating motor neurons. Prevents motor neuron apoptosis and facilitates neurite outgrowth, promoting motor neurons survival and functional maturation.

Table 2.11. Motor neuron day 29-40 media composition. The table details the media composition used in the final stages of motor neuron differentiation. The combination of reagents and concentrations listed below provide the necessary environment to support neuronal maturation of motor neurons.

Component	Concentration	Mechanism/Function
Neurobasal media	Base media	AS ABOVE.
B-27 supplement	2% (v/v)	
Penicillin/Streptomycin	1% (v/v)	
Brain-derived neurotrophic factor (BDNF)	10 ng/ml	Signalling occurs via TrkB receptors with activation of downstream pathways that support neuronal survival and maturation of motor neurons. Activation of TrkB increases the expression of motor neuron specific markers such as ChAT, prevents apoptosis and facilitates neurite outgrowth to ensure functional maturation of motor neurons.
Ciliary neurotrophic factor (CNTF)	10 ng/ml	AS ABOVE.
Insulin-like growth factor-1 (IGF-1)	10 ng/ml	

2.18 Motor Neuron D29-40 Media Supplementation

To study homeostatic responses to acute and chronic stressors, day 40 LMNs were cultured in motor neuron D29-40 media (Table 2.11) supplemented with either 15mM NaCl or 15mM KCl. Cells were incubated for either 3 hours (acute) or 7 days (chronic) in culture medium to study their responses to stressors in both the short- and long-term. Full details are specified in Chapter 5 below where the reagents were used.

2.2 Whole-cell Patch-clamp Electrophysiology

To investigate the electrophysiological phenotypes displayed by iPSC-derived neurons generated, patch-clamp technology was employed in the whole-cell configuration as described in detailed below.

2.21 Patch-clamp Configurations

Since the initial design (Neher and Sakmann, 1976), several groups of dedicated electrophysiologists have helped refine the patch-clamp technique. These refinements involved the application of gentle suction to fire-polished, glass micropipettes filled with electrically conducive solution to form high-resistance seals in the gigaohm range (gigaohm seal) between the micropipette tip and cell membrane. The technique was further improved to include different modes of operation (Hamill et al., 1981), including the cell-attached mode (Figure 2.2). Here, the pipette remains sealed to the membrane as described above, without disturbing the integrity of the cell membrane, which remains intact. This configuration allows for the study of single channel currents or summated current from a group of ion channels located within the membrane patch. Also, spontaneous firing activity of the cell can be measured whilst maintaining the intracellular contents of the cell.

Upon application of a short but strong suction (negative pressure) whilst in cell-attached mode, the operator can rupture the membrane patch under the pipette tip and enter the whole-cell patch-clamp configuration (Figure 2.2), as per this study. This creates electrical continuity between the internal pipette solution and intracellular milleu of the cell thus, providing direct electrical access to record from the entire ion channel population of the cell. An example image of a recording taking place in the whole-cell configuration is shown in Figure 2.3. Simultaneously, this electrical connection can be utilised to study the intracellular efficacy of pharmacological compounds on channel function when included in the composition of the internal pipette solution.

My research utilised the whole-cell patch clamp technique in either; the current-clamp configuration to investigate changes in the membrane potential of cells or in voltage-clamp mode to record whole-cell membrane currents. By applying set current pulses to the cell via the pipette, experimenters can record the corresponding voltage responses, usually in the form of action potentials, to current stimulus in current-clamp mode. This is useful for measuring neuronal excitability at either the single cell or network level. Alternatively, in the voltage-clamp configuration, set voltages can be applied through the pipette to fix the membrane potential at a constant value. This, in conjunction with bath-applied pharmacology, enables researchers to influence the driving force for ionic movement across the membrane, with resulting membrane currents from voltage-gated or ligand-gated ion channels recorded. Crucially, the approach allows for detailed examination of neurotransmission and ion channel behaviour.

Other modes of patch-clamp operation include the excised patch techniques of which there are two types. The inside-out patch technique works by retraction of the pipette whilst in the cell-attached configuration to break off a patch of membrane from the cell (Figure 2.2). Doing so, exposes the cytosolic surface of the membrane to the bath solution which is beneficial for studying regulation of channel activity by intracellular ligands. The outside-out patch technique is created by gentle withdrawal of the pipette away from the cell whilst in whole-cell mode. This leads to the formation of a small vesicular structure that remains attached to the pipette tip, with the extracellular side of the membrane remaining exposed to the bath solution (Figure 2.2). Investigators use this configuration to study ion channel properties when sequestered from the cell and subjected to various bath solutions. As highlighted several variations of the patch-clamp technique exist, with each serving a defined purpose. The choice of configuration is dependent on the research hypothesis and conditions of the (intracellular and/or extracellular) experimental environment required to achieve this.

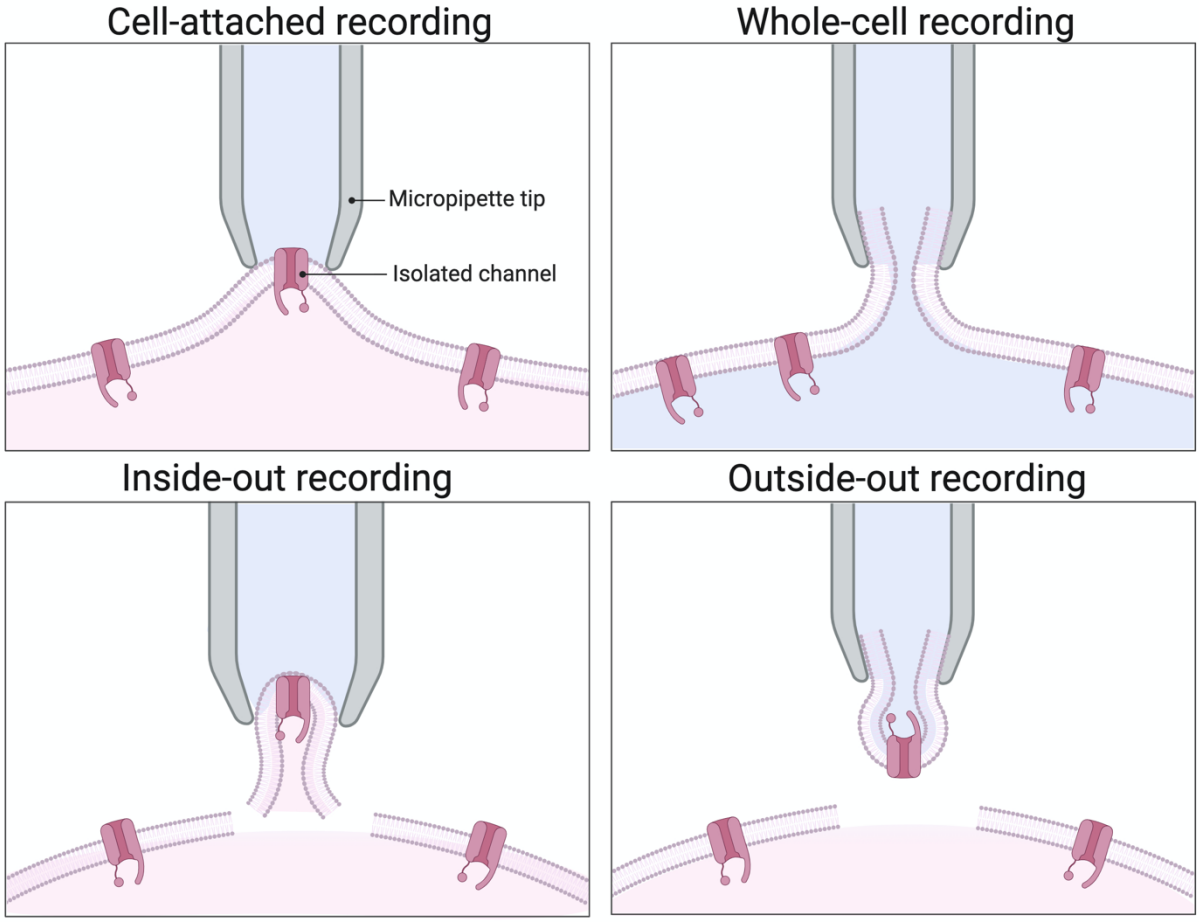

Figure 2.2. Patch-clamp configurations. This schematic represents the different modes of operations patch-clamp users can apply to study the electrophysiological properties of biological material. The 'cell-attached' configuration (*top left*) is established by the movement of the pipette towards the cell membrane and exertion of negative pressure (mild suction) to obtain a high resistance gigaohm seal between the pipette tip and membrane. Inside-out recordings (*bottom left*) are generated by the gentle withdrawal of the patch electrode whilst in cell-attached mode; whereas application of an acute, strong suction opens the membrane, so the K^+-gluconate based internal pipette solution is continuous with the cell cytoplasm, the whole-cell configuration (*top right*). Retraction of the pipette once the membrane has been ruptured results in the outside-out configuration (*bottom right*). All configurations allow the study of either single or small groups of ion channels, except the whole-cell mode, where the entire channel population of the cell is studied. Figure created in BioRender.

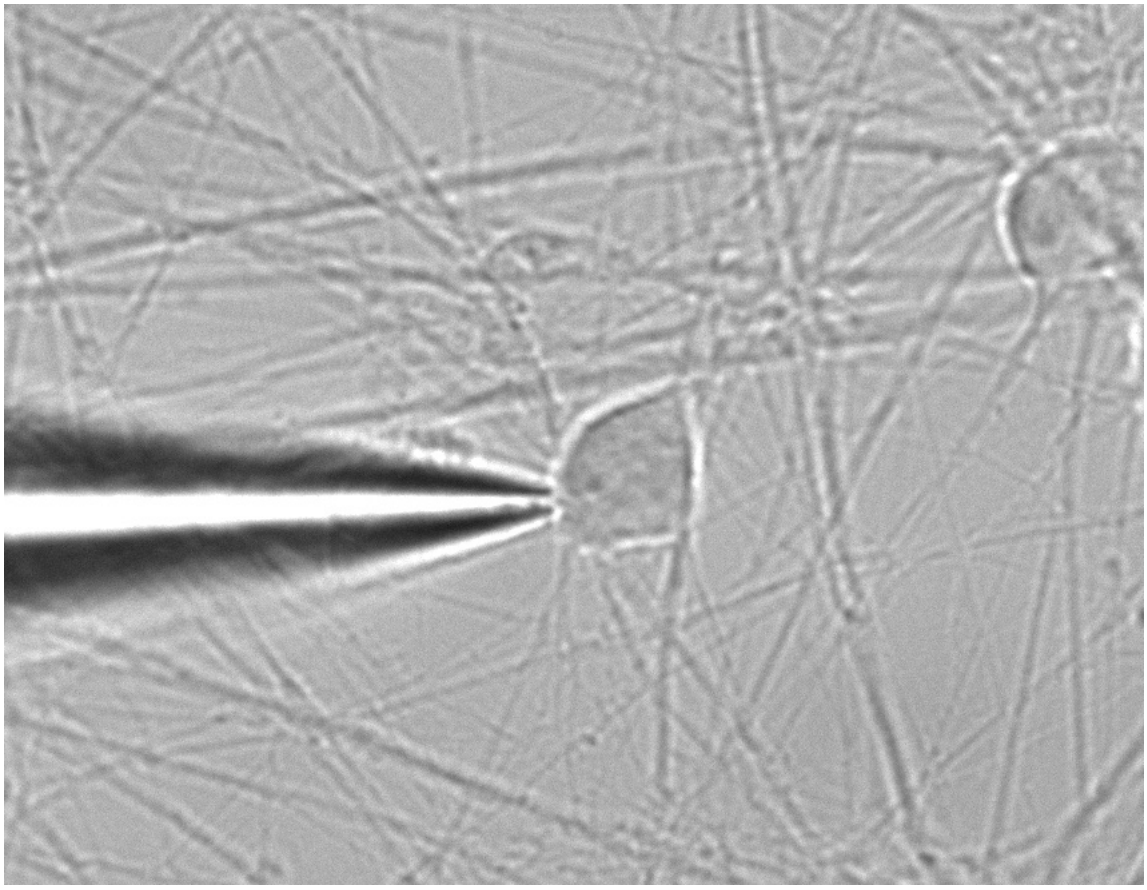

Figure 2.3. iPSC-derived neuron patched in the whole-cell configuration with a glass electrode. The image above is taken from a camera under the microscope in the patch-clamp rig. The neuron was plated onto a glass coverslip that has been placed into the recording chamber constantly perfused with extracellular solution. Successful entry into the whole-cell configuration has been achieved and an image taken live during a patch-clamp recording.

2.22 Electrical Properties of the Cell Membrane

The cell membrane consists of a dense mosaic of phospholipids and proteins that together act as a thin insulating barrier between the electrically conductive interior of the cell and its extracellular environment. The selectively permeable nature of the cell membrane enables it to control the movement of ions and thereby regulate the osmolarity between these environments. Furthermore, this leads to a differential expression of charged particles that in turn establishes significant concentration gradients of key ions such as calcium (Ca^{2+}), chloride (Cl^{-}), sodium (Na^{+}) and potassium (K^{+}) across the membrane. This unequal distribution of charge gives rise to a membrane potential, a difference in the electrical potential between the intracellular and extracellular compartments, typically measured in millivolts (mV) (Figure 2.4). The equilibrium potential of individual ion species can be predicted using the Nernst equation.

Moreover, the phospholipid bilayer is an electrical insulator that separates and stores electrical charge either side of the membrane. This ability enables the membrane to not only have a resistance but also to function as a capacitor, that requires time to charge and discharge, and therefore influences the kinetics and amplitude of any membrane potential changes.

The lipid bilayer of the cell membrane is mostly impermeable to the passage of charged species. However, housed within these lipids are specialised transmembrane proteins consisting of ion channels and transporters, that allows charged ions to traverse the membrane. Each transmembrane protein displays distinct selectivity for specific ions with protein function governed by factors like ligand binding and voltage changes. Essentially, it is this movement of ions between the extracellular space and cytoplasm that underlies the electrical activity measured in neurons and is recorded as current. The flow of current via membrane proteins is determined by the electrochemical driving force (voltage) and the resistance of the membrane to the passage of ionic movement. Ohm's law, a key concept in electrophysiology, describes the relationship between these factors:

$$V = IR$$

where *V* is the voltage (in volts, V), *I* is current (in Amperes, A), and *R* is the resistance (in Ohms, Ω) to current flow. As per the equation, voltage is directly proportional to current flow and inversely proportional to the resistance. Comprehension of the key biophysical properties of the membrane and principles that underlie ion transport, supports scientific understanding of changes in voltage and current that affect, cellular process and signalling pathways involved in homeostatic cell function.

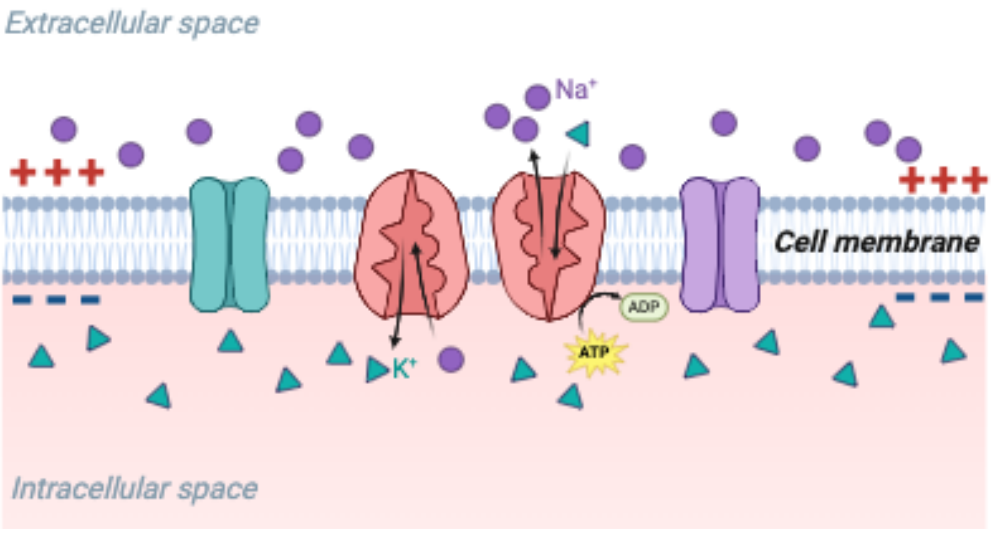

Figure 2.4. Electrical properties of the cell membrane. Schematic representation of the plasma membrane with transmembrane proteins embedded within it. The plasma membrane acts as a diffusion barrier to the passage of ions but does contain specialised transmembrane proteins in the form of ion channels and ion pumps that allow for the transport of specific ions across the membrane. Ultimately, these proteins establish concentration gradients of ions at the membrane creating a voltage difference between the intracellular and extracellular environment. Potassium channel and ions represented in green, sodium channel and ions represented in purple and sodium/potassium pump in orange. Figure created in BioRender.

2.23 Recording Setup

The whole-cell patch clamp configuration was used to record from iPSC-derived neurons using borosilicate glass pipettes of 1.5 mm outer diameter, 0.86 mm inner diameter and 75 mm length (Harvard Apparatus). Patch electrodes were pulled using a Sutter P-97 Horizontal Pipette Puller (Sutter Instruments, Sarasota, FL, USA) and once filled with potassium-gluconate based intracellular solution (Table 2.13) had a final resistance of 4-7 MΩ. An Olympus upright microscope with a x40 immersion lens was used in conjunction with a micromanipulator (Scientifica) to view and position the patch pipette towards the cell (Figure 2.5). iPSC-derived neurons plated onto coverslips were placed in the recording chamber and perfused with a standard extracellular solution (unless stated otherwise), commonly referred to as artificial cerebrospinal fluid (aCSF) solution (Table 2.14), using a gravity-fed perfusion system at room temperature (20-23^{o}C). The use of both internal and external recording solutions was associated with a liquid junction potential (LJP) calculated at +14mV (LJPcalc; Clampex). Holding membrane potential and all reported voltage data were modified accordingly. This phenomenon occurs at the point where two solutions of different ionic concentrations and compositions meet and is caused by unequal rates of diffusion of the different ions across this junction.

Whole-cell patch-clamp recordings were low-pass filtered online at 2 kHz, digitised at 10 kHz via a BNC-2090A (National Instruments, Texas, USA) interface, and acquired using either WinWCP V5.8.2 or WinEDR V4.1.5 Electrophysiology Data Recorder (J. Dempster, University of Strathclyde, UK). Patch-clamp recordings were attained at a range of different holding potentials, as per the experimental requirement, using an Axon Multiclamp 700B amplifier (Molecular Devices, Union City, CA, USA). The key hardware components of the patch-clamp rig are shown in (Figure 2.5). For the study of membrane excitability neurons were held at a holding potential of -74mV (including LJP correction) in the current-clamp configuration with bridge balance and pipette capacitance neutralisation. To investigate neurotransmission and membrane currents neurons were held in the voltage-clamp configuration at a holding potential between -54 to -84mV (including LJP correction) dependent on experimental requirement. Voltage ramp protocols and holding potentials for all experiments are specified fully within their respective chapters and figure legends along with pharmacological

supplementation of aCSF that is also described briefly below. Series resistance (R_s) remained below 25 MΩ during whole-cell recordings, R_s was compensated to 70% for all voltage-clamp experiments. Any recordings greater than 30 MΩ or whereby a change in R_s exceeded 20% were discarded.

2.24 Application of Pharmacological Compounds

Pharmacological agents were applied using a bath-exchange system that employed a 'barrel system' in which aCSF solutions containing differing experimental reagents could be stored independently and systematically applied. As per the experimental requirements, the barrels could be substituted to deliver the appropriate treatment, with the time for complete bath exchange of aCSF being approximately 10 seconds. Onset time of experimental reagents was generally minimised to no longer than 10 seconds except for non-stationary fluctuation analysis and potassium channel modulation experiments involving Tetraethylammonium- chloride (TEA-Cl), NS11021 and AUT1.

For current-clamp recordings the standard extracellular solution was supplemented with cyanquixaline (CNQX, 5 μM), (2*R*)-amino-5-phosphonovaleric acid (D-APV, 50 μM), picrotoxin (PTX, 50 μM) and strychnine (20 μM) to block AMPA, NMDA, $GABA_A$ and Glycinergic mediated synaptic transmission, respectively. TEA-sensitive current was recorded in the presence of external recording solution complemented with Tetrodotoxin (TTX, 300nM), the Na_v channel blocker (Table 2.15). To measure agonist-induced membrane currents, the standard aCSF was supplemented with a cocktail of different pharmacological agents. GABA-evoked currents were measured in the presence of TTX (300nM). Glutamatergic currents were evoked in the presence of PTX (50 μM), strychnine (20 μM) and TTX (300nM). For NMDA current recordings specifically, magnesium free aCSF was additionally supplemented with (50uM) Glycine.

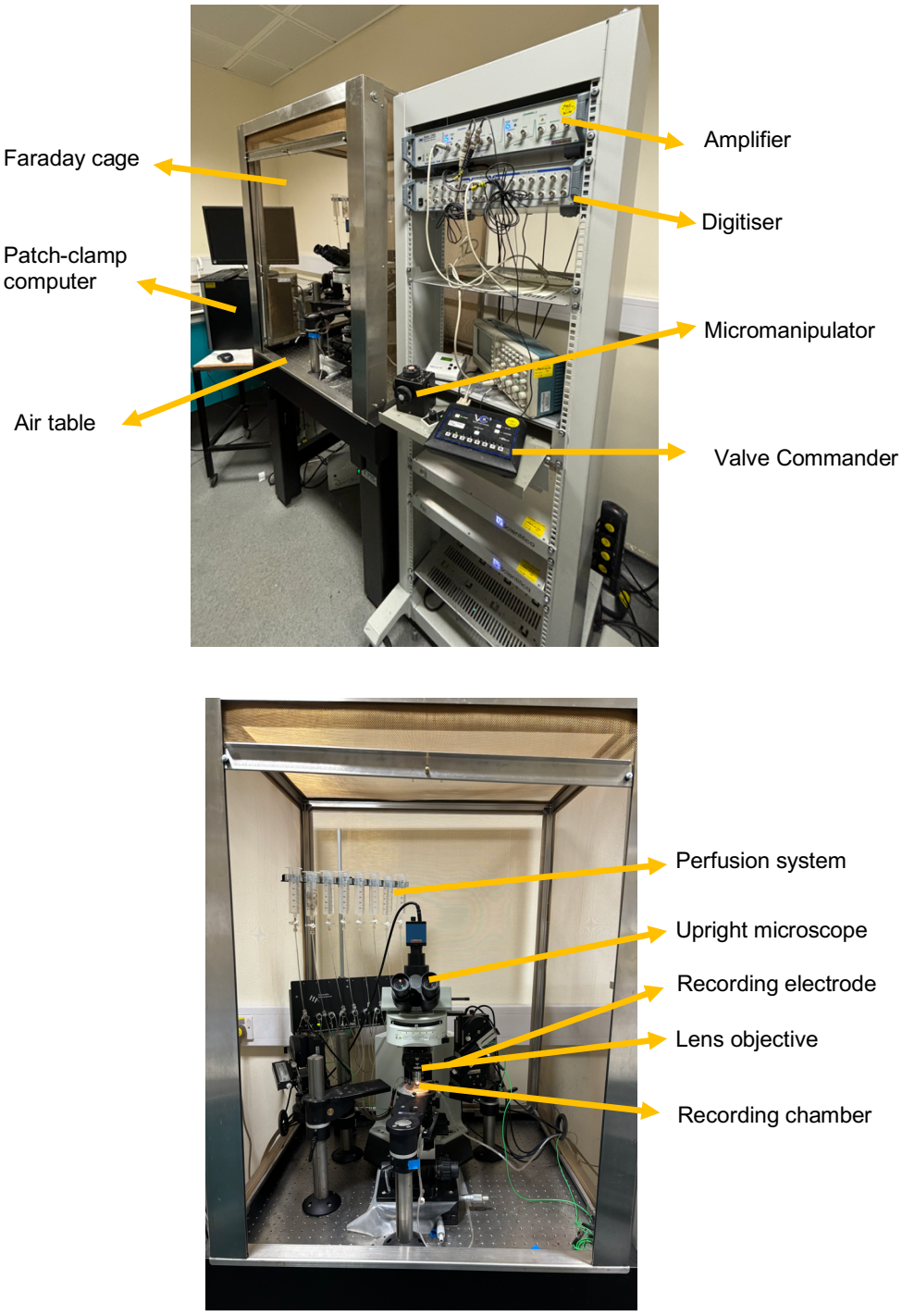

Figure 2.5. Patch-clamp rig setup. The images above are taken from the laboratory and showcase the hardware required for the setup of the patch-clamp rig. The rig setup is enclosed within a Faraday cage shielding the contents of the rig from external electromagnetic interference, doing so minimises noise in any recordings. The anti-vibration air table minimises any vibrations from the surrounding environment that could disturb recordings. The perfusion system, controlled by the valve commander, provides a stable environment for cellular recordings with the supply of extracellular solution to the recording chamber and extraction of solution in a way to maintain laminar flow of solution in the recording chamber where the coverslip is positioned.

The actual patch-clamping is performed with a patch pipette attached to a headstage, the micromanipulator allows for fine movements in three-dimensional space of the recording patch pipette onto the cell, as viewed under the upright microscope. The main amplifier detects miniscule currents flowing across the membrane and amplifies this signal that is then filtered for any unwanted interference, to ensure a strong and clear signal is to be processed and analysed. The digitiser converts the recorded analogue signal into digital, that can then be processed by the computer software and fed back to the operator.

2.25 Patch-clamp Electrophysiology Materials

A list of all electrophysiological materials including key components of the intracellular and extracellular solutions and pharmacological activators or inhibitors of ion channel activity utilised for whole-cell patch-clamp recordings in this work are documented below (Table 2.12).

Table 2.12. Electrophysiology reagents with associated catalogue numbers. The table includes a list of all reagents used for the acquisition of patch-clamp recordings. Included in the information below is the purpose of each reagent, the suppliers from which the reagents were purchased from and their respective catalogue numbers.

Reagent	Role	Supplier	Catalogue Number
Calcium Chloride ($CaCl_2$)	Extracellular solution	Thermo Scientific Solutions	J63122
D-(+)-Glucose	Extracellular solution	Sigma-Aldrich	G5767
HEPES	Extracellular solution	Sigma-Aldrich	H337
Potassium Chloride (KCl)	Extracellular solution/ neuronal media supplement	TCI Chemicals	7447-40-7
Sodium Chloride (NaCl)	Extracellular solution/ neuronal media supplement	Sigma-Aldrich	793566
Magnesium Chloride ($MgCl_2$)	Extracellular/Intracellular solution	SERVA	39772.02
Magnesium-Adenosine triphosphate (Mg-ATP)	Intracellular solution	Sigma-Aldrich	A9187
Potassium-Gluconate	Intracellular solution	Sigma-Aldrich	P1847
Sodium creatine phosphate dibasic tetrahydrate	Intracellular solution	Sigma-Aldrich	27920
Sodium- Guanosine triphosphate	Intracellular solution	Sigma-Aldrich	G8877

(Na-GTP)			
Sodium-HEPES	Intracellular solution	Sigma-Aldrich	H3375
α-amino-3-hydroxy-5-methyl-4-isoxazolepropionic acid (AMPA)	Select pharmacology in Extracellular Solution	APExBIO	B6238
(2*R*)-amino-5-phosphonovaleric acid (APV)	Select pharmacology in Extracellular Solution	Biogems	7908985
AUT1	Select pharmacology in Extracellular Solution	Cayman Chemical	1311136-84-1
Bicuculline Methiodide	Select pharmacology in Extracellular Solution	Sigma-Aldrich	14343
Cyanquixaline (CNQX)	Select pharmacology in Extracellular Solution	Tocris	0190
Gamma-aminobutyric acid (GABA)	Select pharmacology in Extracellular Solution	Sigma-Aldrich	A5835
Glycine	Select pharmacology in Extracellular Solution	Merck	3570
Ifenprodil	Select pharmacology in Extracellular Solution	Tocris	0545
N-methyl-D-aspartate (NMDA)	Select pharmacology in Extracellular Solution	Selleckchem	S7072
NS 11021	Select pharmacology in Extracellular Solution	Tocris	4788
Picrotoxin (PTX)	Select pharmacology in Extracellular Solution	Sigma-Aldrich	P1675
Strychnine Hyrdochloride	Select pharmacology in Extracellular Solution	Sigma-Aldrich	S8753
Tetraethylammonium-chloride (TEA-Cl)	Select pharmacology in Extracellular Solution	Merck	T2265
Tetrodotoxin Citrate	Select pharmacology in Extracellular Solution	LKT Labs	18660-81-6

Table 2.13. Composition of the K-gluconate based intracellular solution. Detailed in the table below is the contents of the intracellular solution used for patch-clamp recordings that have been combined to mimic the ionic contents of the cells. During electrophysiological recordings the intracellular solution is kept continuous with the cell cytoplasm. Before use, the solution was filtered through a 0.3mm syringe filter, snap frozen at -80^{o}C. before being placed at -20^{o}C for long-term storage.

Component	Concentration (mM)	Purpose
K-gluconate	155	Provides a high K^+ concentration that mimics the high physiological [K^+] within the intracellular milleu, vital for sustaining a stable resting membrane potential and in turn cell function. Maintains the osmolarity of the intracellular environment to ensure cell stability during recordings. Limits chloride content within the intracellular environment by acting as a large anion with low membrane permeability. Thus, maintains physiological chloride concentration gradient across the membrane.
$MgCl_2$	2	Vital support for protein function by acting as enzyme co-factors for ATPase enzymes. Aids in the maintenance of solution osmolarity.
Na-HEPES	10	Buffering agent effective at maintaining physiological pH (7.2-7.4) of the intracellular environment that is critical for preserving function of pH sensitive- enzymes and ion channels.
Na-PiCreatine	10	Supports energy metabolism of the cell. Source of ATP for cell by acting as a phosphate donor for ADP. This is crucial for energy dependent cellular processes such as maintaining membrane pumps e.g. Na^+/K^+/ATPases that help regulate ionic gradients.
Mg_2-ATP	2	Direct energy supply for the cell that can be used in energy dependent processes such as synaptic transmission, maintaining ionic gradients and in turn the resting membrane potential.
Na_3-GTP	0.3	Crucial regulator of G-protein activity. GTP is essential for ensuring G-protein signalling pathways are

		conserved including those that involve neurotransmitter receptors.
pH 7.3, 320-330mOsm		

Table 2.14. Standard extracellular solution composition. The components of the extracellular solution with their respective concentrations ensure the recording environment of the neurons studied, closely resembles the physiological extracellular environment. The solution allows for the accurate study of membrane excitability and ionic currents.

Component	Concentration (mM)	Purpose
NaCl	152	Replicates the ionic conditions of the extracellular environment by maintaining high physiological [Na^+] and [Cl^-]. Thus, ensuring a strong driving force for the influx of these ions. Enhances the electrical conductivity of the extracellular milieu, necessary for the measurements of membrane current and potentials.
KCl	2.8	Low K^+ concentrations simulate physiological conditions of the extracellular fluid. Maintains K^+ equilibrium potential which is key for setting a stable resting membrane potential.
HEPES	10	Buffering agent that upholds pH within the physiological range (7.2-7.4). Limited interference in biological reactions due to the compound being a zwitterionic chemically stable, highly soluble and membrane impermeable buffer.
$CaCl_2$	2	Helps support the cell in Ca^{2+} dependent signalling processes e.g. neurotransmitter release. Maintains ionic gradients across the cell membrane.
$MgCl_2$	1.5	Recreates physiological extracellular conditions with respect to Mg^{2+}. Helps to stabilise the cellular environment via regulation of cell metabolism and energy.
Glucose	10	Primary energy source for cells that helps to power essential energy-dependent cell processes. Preserves cell health as cells have access to constant energy source for the duration of patch-clamp experiments.
pH 7.3, 320-330mOsm		

Table 2.15. Tetraethylammonium chloride extracellular solution composition. An amended version of the standard extracellular solution with equimolar replacement of NaCl with 30mM TEA-Cl. This modified extracellular solution is paramount for the isolation and study of I_K channel currents. Constituents of the solution listed below with their respective concentrations and roles.

Component	Concentration (mM)	Purpose
NaCl	122	Maintaining high physiological [Na^+] and [Cl^-] that provides a strong driving force for the influx of these ions especially in initiation of action potentials. Enhances the electrical conductivity of the extracellular milieu, necessary for the measurements of membrane current and potentials.
TEA-Cl	30	Non-selective potassium channel blocker that supresses outward potassium currents. TEA displays distinct selectivity for different potassium channel subfamilies and is effective at targeting K^+ channels that contribute to I_K currents e.g. Kv3 family.
KCl	2.8	Low K^+ concentrations simulate physiological conditions of the extracellular fluid. Maintains K^+ equilibrium potential which is key for setting a stable resting membrane potential.
HEPES	10	Buffering agent that upholds pH within the physiological range (7.2-7.4). Limited interference in biological reactions due to the compound being a zwitterionic chemically stable, highly soluble and membrane impermeable buffer.
$CaCl_2$	2	Helps support the cell in Ca^{2+} dependent signalling processes e.g. neurotransmitter release. Maintains ionic gradients across the cell membrane.
$MgCl_2$	1.5	Recreates physiological extracellular conditions with respect to Mg^{2+}. Helps to stabilise the cellular environment via regulation of cell metabolism and energy.
Glucose	10	Primary energy source for cells that helps to power essential energy-dependent cell processes.

		Preserves cell health as cells have access to constant energy source for the duration of patch-clamp experiments.
pH 7.3, 320-330mOsm		

2.26 Electrophysiological Data Analysis

Electrophysiological analysis of AP frequency was stopped at the point of neuronal accommodation that was observed at unphysiological levels of current stimulation. All physiological datapoints to the point of accommodation were included in analysis. Unless stated otherwise, information collected on AP parameters was done on the first AP fired by the cell, with APs defined as any spikes with a peak equal to or above 0 mV. Current amplitudes were analysed following ample onset time of experimental reagents at the point where membrane currents were in steady state.

2.3 Statistical Analysis

Statistical analysis of data was conducted, and graphs generated using GraphPad Prism 10 (GraphPad Software, Inc., La Jolla, CA). All data reported in this thesis is presented as the mean ± standard error of the mean (SEM). In this study, 'n' refers to the number of experimental replicates (individual cells), and 'N' denotes the number of *de novo* preparations of batches used to generate these replicates. This level of distinction was to ensure any phenotypic variations observed in iPSC-derived material was not attributable to any potential variations between batches. Data distributions were tested for normality using the Shapiro-Wilks normality test. Both paired and unpaired Student's t-test were used to compare datasets between two conditions or cell lines. For statistical comparisons of datasets from three or more groups, a one-way or two-way analysis of variance (ANOVA) with the appropriate post-hoc test was chosen. Where data distributions were not normally distributed, a Kruskal-Wallis test with Dunn's pairwise multiple comparisons was used instead to assess for statistical significance. For all statistical tests done, only a p-value <0.05 was considered significant. Instead, this approach allows for such batch-to-batch variability to be accounted for, thereby enhancing the accuracy of data interpretations after experimental intervention.

Chapter 3: C9-patient Derived Medium Spiny Neurons are Hypoexcitable

3.1. Introduction

Conventionally, ALS is considered to be a disease of the motor system. However, in recent decades there is a growing recognition that ALS sits on a clinical disease spectrum with FTD, with patients characterised by the degeneration of both the cortico-motor system but also within the pre-frontal and anterior-temporal lobes of the cortex. Consequently, the cognitive and behavioural impairments typically associated with FTD overlap with those observed in ALS patients, especially in cases characterised by the C9ORF72 repeat expansion mutation, the most common genetic cause of both FTD/ALS (Mead et al., 2023). Impairments In personality and behaviour range from executive dysfunction, loss of motivation to language complications and apathy (Rascovsky et al., 2011). These functions are not exclusively governed by the frontotemporal regions of the cortex and is known to include a contribution from other extra cortical regions like the striatum (Bocchetta et al., 2021).

The striatum is comprised of a cluster of subcortical nuclei that forms the primary input into the basal ganglia and can be classified into the dorsal (caudate and putamen) and ventral (nucleus accumbens) striatum. The former is involved in sensorimotor function whilst the latter is vital cog in the limbic circuitry that has a significant role in the cognitive processing of emotion and behaviour (Bocchetta et al., 2021). This region is predominantly, 90-95%, composed of inhibitory medium spiny neurons that are GABA-ergic in nature with the remaining cellular population made up of inhibitory interneurons (Cox and Witten, 2019). The striatum is an essential integrative signalling centre, where the execution, inhibition and selection of appropriate behaviours and motor movements are gathered from different brain regions such as the cortex, thalamus and midbrain regions before appropriate regulation and integration by the striatum (Haber, 2016) (Figure 1.4). The dorsal striatum receives dopaminergic inputs from the substantia nigra pars compacta that enables it to mediate cognitive related behaviours including motor control and coordination (Haber, 2016, Bamford and Bamford, 2019, Cox and Witten, 2019). The ventral striatum receives dopaminergic projections from the ventral tegmental area as part of the mesocorticolimbic pathway

that functions in reward processing (Han et al., 2017), decision-making and program behaviours (Patton et al., 2013, Bamford and Bamford, 2019). Excitatory glutamatergic transmission from the cortical regions and thalamus also provides a key input to the striatum (Wilson and Groves, 1981, Paraskevopoulou et al., 2019). Specifically, the glutamatergic corticostriatal projection neurons, a key neurodegenerative substrate in FTD (Bertoux et al., 2015, Bede et al., 2018, Ahmed et al., 2021), originate from different cortical regions such as the motor and premotor cortex onto the dorsal striatum (motor planning, learning and execution), and prefrontal cortex onto the dorsal and ventral striatum (executive function, emotional processing, motivation and decision making) (Kringelbach, 2005, Haber, 2016). The amygdala also innervates the ventral striatum, crucial for emotion-based behaviours (Phelps and LeDoux, 2005). The neuroanatomy of these circuits links the striatum to a broad range of cognitive functions, functions that overlap with the cognitive impairments in FTD/ALS patients. Indeed, striatal dysfunction in FTD patients has been associated with a range of cognitive deficits in apathy and impulsivity (Lansdall et al., 2017, Liu et al., 2023), binge eating (Perry et al., 2014) and long-term memory (Bertoux et al., 2018). Furthermore, there is growing evidence of atrophy within the ventral striatum of bvFTD patients (Garibotto et al., 2011, Halabi et al., 2013, Moller et al., 2015, Landin-Romero et al., 2017, Jakabek et al., 2018, Upadhyay et al., 2024). Thus, implicating a role for striatal dysfunction in cognitive functions impacted in FTD/ALS.

As previously mentioned in Introduction section 1.7, atrophy within FTD/ALS patient striatum including in the ventral regions has been observed in multiple studies (Kato et al., 1994, Riku et al., 2016, Radakovic et al., 2018) including patients harbouring the C9 repeat expansion mutation (Bede et al., 2013, Ahmed et al., 2021). These structural changes within patient striatum correlates with observed deficits in frontostriatal networks that characterise the presymptomatic stages of C9FTD/ALS (Lee et al., 2017a) and are likely contributors to motor and neuropsychological phenotypes observed during symptomatic disease stages (Bertoux et al., 2015, Machts et al., 2015, Ahmed et al., 2021). Of note, these pathophysiological phenotypes along with hallmark TDP-43 pathology have been shown explicitly in FTD/ALS ventral striatum (Bede et al., 2013, Brettschneider et al., 2013, Machts et al., 2015, Bede et al., 2018, Tae et al., 2020, Ahmed et al., 2021). The internal capsule

physically separates the dorsal and ventral striatum. These areas of the striatum are differentially impacted in disease, with dorsal regions afflicted in HD (Prager and Plotkin, 2019) compared with ventral striatum in FTD/ALS (Bertoux et al., 2015). Even so, HD patients are also defined by cognitive impairments during disease, which closely resembles FTD, suggesting spreading to the ventral striatum (Paulsen, 2011).

Neurophysiological disturbances in the cortical and motor neurons are an established feature of FTD/ALS that is prominent throughout the course of disease (reviewed in Introduction section 1.6). Strikingly, neurophysiological excitability represents an attractive therapeutic target in ALS, with Riluzole the only currently licensed ALS treatment in the UK targeting such function. Whilst extra cortical/motor involvement in FTD/ALS is now beginning to emerge, to date, the functional relevance of this involvement with respect to neurophysiology is unknown. To this end, I focus on characterising the electrophysiological features of striatal medium spiny neurons in the context of *C9ORF72 repeat expansion*.

3.2. Aims and Objectives

Based on the growing evidence within the literature of functional deficits within the striatum playing a key role in FTD/ALS, I hypothesise this dysfunction extends to impairments in the excitability of striatal MSNs. This hypothesis is supported by several key findings: the ventral striatum plays a key role in cognitive processes impacted in FTD/ALS (Ahmed et al., 2021), extensive TDP-43 pathology is observed in human post-mortem MSNs (Brettschneider et al., 2013), the principal cell type in the striatum, MRI brain imaging shows substantial atrophy of the ventral striatum and lastly (Bertoux et al., 2015), altered neuronal excitability is pathological hallmark of FTD/ALS (Vucic et al., 2013).

The aim of this chapter was to challenge this hypothesis, done so by investigating the neurophysiological function of iPSC-derived MSNs from patients harbouring the most common genetic cause of both FTD/ALS, the C9ORF72 repeat expansion mutation. To achieve this, highly enriched MSN cultures were generated from healthy and C9-afflicted individuals plus gene-edited isogenic lines whereby the *C9ORF72* repeat expansion had been specifically excised (full description of iPSC lines presented in

Methods section 2.1). The human *in vitro* iPSC model has previously been used to generate and study enriched striatal populations in other diseases of the striatum (Nekrasov et al., 2016, Henkel et al., 2023). The electrophysiological behaviour of these enriched MSN populations was then characterised in high resolution at the single cell level using whole-cell patch-clamp electrophysiology.

3.3. Results

3.31 Generation of iPSC-derived C9-Medium Spiny Neurons

In this study, medium spiny neurons (MSNs) were derived in vitro from iPSCs using a previously established protocol (Lin et al., 2015).The iPSC lines were obtained from two unrelated healthy individuals (Con-1, Con-2), three unrelated individuals carrying the *C9ORF72* repeat expansion mutation (C9-1, C9-2, C9-3), and two gene-edited lines (C9-2Δ and C9-3Δ), created from C9-2 and C9-3 respectively, using CRISPR-Cas9 technology to specifically remove the GGGGCC repeat expansion mutation. The iPSC lines were characterised and described in previous studies (Castelli et al., 2021, Palminha et al., 2022) and background information of these lines is also available in Table 2.1.

MSNs were converted from iPSCs using an established and previously reported *in vitro* protocol (Lin et al., 2015; summarised Figure 3.1A). Full details of the differentiation of MSNs are described in sections 2.1.4-2.1.6. In summary, a dual SMAD inhibition protocol was utilised to efficiently induce neurogenesis to generate Pax6+ and nestin+ neural progenitor cells (NPCs) (Appendix 1). Both Pax6 and Nestin are NPC markers. NPCs were then patterned and differentiated towards GABA-ergic MSNs using BDNF, SHH and DKK-1. Subsequent maturation of MSNs was achieved through BDNF supplementation. Immunocytochemical characterisation was conducted longitudinally at 20, 40, and 60 days *in vitro* (DIV) post NPC generation to assess the efficiency of MSN differentiation. By DIV20, 80-90% of cells across all lines displayed neuronal morphology and were β-III-tubulin (TUJ1) positive, a post-mitotic neuronal marker that remained consistent through to DIV60 (Lee et al., 2005) (Figure 3.1B-C).

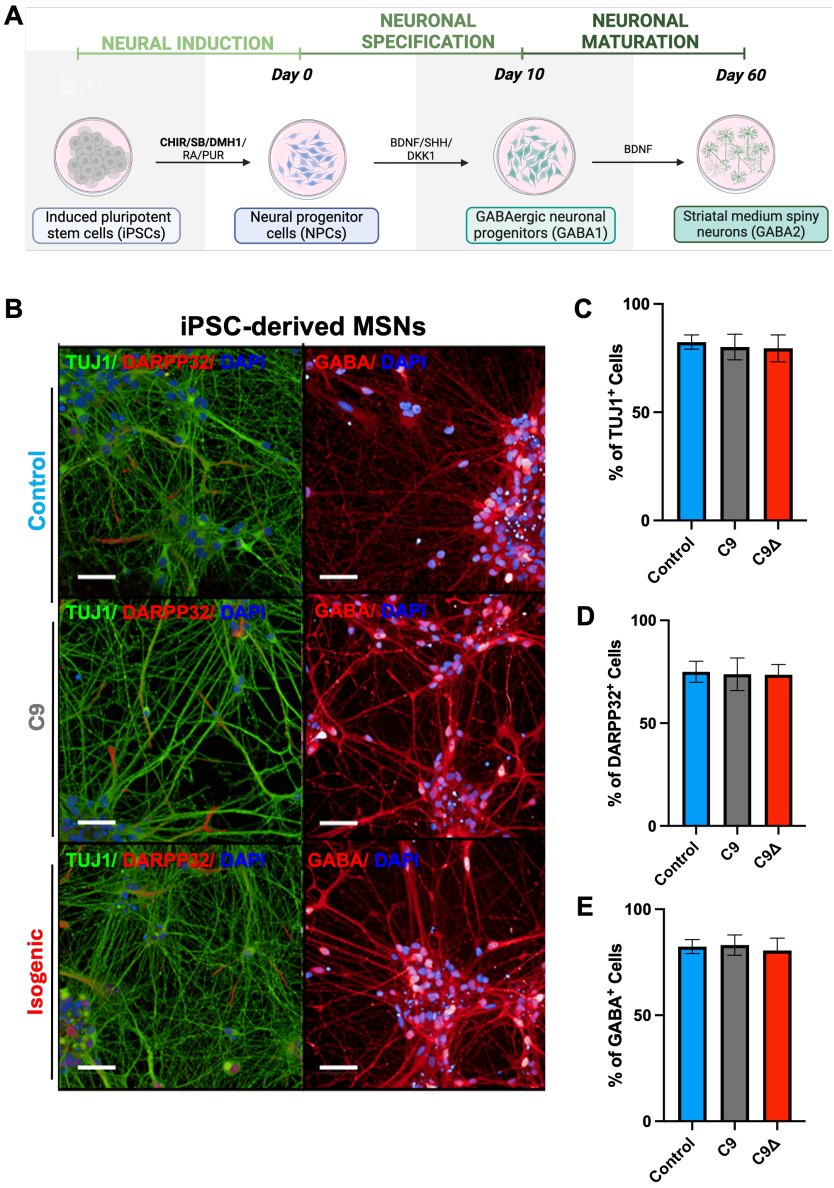

Figure 3.1. *In vitro* differentiation of highly enriched GABA-ergic MSNs from human iPSCs. (A) Fibroblasts were acquired from healthy and C9 patients (Table 2.1) and reprogrammed into iPSCs that underwent a 3-step differentiation process of neural induction, specification and maturation as detailed in the Methods chapter (Sections 2.1.4- 2.1.6). The dual-SMAD inhibition method was used to induce the neuralisation of stem cells. Patterning of NPCs into GABA-ergic MSN progenitors was stimulated by BDNF, DKK-1 and SHH treatment. BDNF application promotes the maturation of progenitors into functionally mature MSNs. Timepoints cited in this thesis represent the time between neural formation of NPCs (Day 0) to mature MSNs (Day 60). Figure created in BioRender. **(B)** Representative images of day 60 control, C9 and C9-isogenic MSNs stained for β-III-tubulin (TUJ1) (green) and either DARRP32 or GABA (red). Nuclei were counterstained with DAPI (blue). Scale bar: 50 µm. **(C-E)** Bar graphs showing the total number of **(C)** TUJ1+, **(D)** DARPP-32+ and **(E)** GABA+ cells expressed as percentage of total number cells counted; Values expressed as mean ± SEM. Highly enriched TUJ1+, DARPP-32+, GABA+ MSN cultures were generated at day 60. Note, images and quantification data were previously generated and taken with permission from Dr. Iris Pasniceanu and Dr Cleide De Souza. Data, β-

III-tubulin: Control MSN: N=3; C9-MSN: N=3; Isogenic MSN: N=3; DARPP-32: Control MSN: N=3; C9-MSN: N=3; Isogenic MSN: N=3; GABA: Control MSN: N=3; C9-MSN: N=3; Isogenic MSN: N=3. No significant differences between each parameter were determined by one-way ANOVA followed by Tukey's multiple comparison test.

Expression of DARPP-32, a mature striatal neuron marker (Blom et al., 2013), became prominent at DIV40 in all lines and was present in approximately 75% of all cells by DIV60 (Figure 3.1B-D), comparable to previously reported efficiencies (Lin et al., 2015). MSNs are inhibitory GABA-ergic neurons, thus positive detection of the neurotransmitter GABA was found in 75-85% of DIV60 TUJ1+ neurons across all lines (Figure 3.1B-E). The high efficiency of neuronal differentiation across all iPSC lines employed was further confirmed by the low expression (<5%) of the progenitor marker Nestin at DIV20 and the negligible presence (<5%) of the astrocytic marker GFAP throughout the culture period (data not shown). Thus, the differentiated cultures from each iPSC line employed were enriched for viable DARPP-32+, GABA+ MSNs.

3.32 Electrophysiological Characterisation of iPSC-derived MSNs

The excitability of neurons determines how effectively they can generate and transmit action potentials, which is the fundamental biophysical correlate that underpins all brain functions, including cognition, behaviour and movement. This neuronal activity is governed by the external influences of excitatory and inhibitory transmission in conjunction to the intrinsic excitability of the neuron, which relates to the internal ability of a neuron to fire APs (Pradhan and Bellingham, 2021). Since striatal performance in FTD/ALS is consistent with a loss-of-function (Bede et al., 2018, Ahmed et al., 2021), I examined whether C9 patient-derived MSNs exhibited any neurophysiological perturbations by performing highly sensitive, whole-cell patch-clamp electrophysiology, allowing for detailed evaluation of MSN excitability at the single cell level.

To assess action potential generation, MSNs at days 20, 40 and 60 post NPC-differentiation were examined in the current-clamp configuration and subjected to a sequential current injection protocol ranging from –20 to +50 pA from a holding potential of –74 mV (LJP corrected). Recordings were conducted in standard

extracellular solution (Table 2.14) containing; AMPAr antagonist, CNQX (5μM), NMDAr antagonist, APV (50μM), $GABA_AR$ antagonist, PTX (50μM) and glycine receptor antagonist, strychnine (20μM) to block synaptic transmission during recordings. This ensured excitability was governed by factors relating to the intrinsic properties of the cell, relating to factors such as the threshold potential, ion channel makeup and distribution.

The voltage response of individual MSNs to depolarization was assessed, initially categorising their evoked activity into three distinct behaviours: multiple action potentials (≥2), single action potential, or no response, with action potentials defined as rapid potential deflections exceeding 0 mV (Figure 3.2A). At day 20, 47% and 42% of Con-1 and Con-2 MSNs respectively, displayed either no response or fired a single AP. From day 40 onwards, MSNs from healthy iPSC lines uniformly generated multiple action potentials (Figure 3.2B), validating the protocol's efficacy in producing functional MSNs that mature over time. Meanwhile, MSNs derived from C9-patient lines failed to display progressive increases in their firing frequency from DIV20 to 60, multiple AP activity was ~50% at day 20 and relatively unchanged at day 60. Instead, C9-MSNs consistently underperformed relative to control lines, with 40-60% firing only a single AP or showing no response (Figure 3.2B). The isogenic C9-3Δ line, however, mirrored the healthy controls and not the C9-3 line, robustly generating multiple APs (Figure 3.2B). The data imply the *C9ORF72* mutation interferes with the intrinsic excitability of MSNs. Representative responses evoked by the protocol highlight a weaker level of action potential generation in DIV40 and 60 C9-MSNs compared to Control and isogenic C9-3Δ MSNs (Figure 3.2C-D). All Con-1 and Con-2 MSNs displayed multiple AP firing at day 40 and 60. These statistics were closely resembled by the isogenic C9-3Δ where 88% at DIV40 and 100% of cells at DIV60 displayed maximal firing activity. This contrasted with C9-3 MSNs, or in fact any of the C9-MSNs, whereby multiple firing activity barely surpassed 50% across these timepoints (Figure 3.2C-D). To illustrate this, sample recordings were obtained for each iPSC line, at each time point and at each level of current-induced depolarization and presented in Figure 3.3. The traces particularly at DIV40 and DIV60 highlight the lack of robust firing elicited by depolarisation in all C9 (C9,1, C9-2, C9-3) versus control (Con-1, Con-2) and isogenic lines (C9-3Δ). These data suggest that the C9 repeat expansion is driving an excitability problem in MSNs.

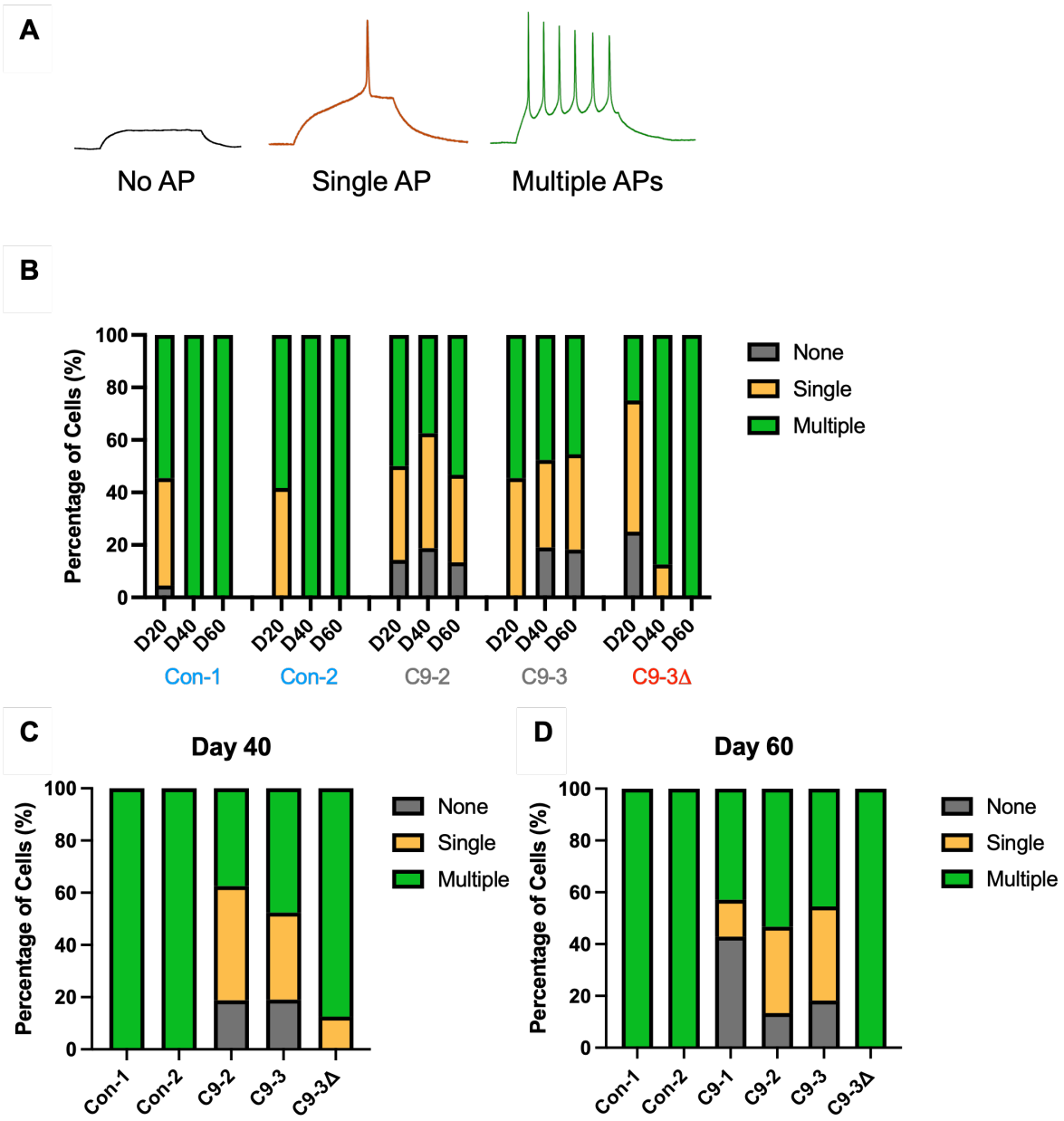

Figure 3.2. Decreased firing capacity in C9 Striatal MSNs. (A) Voltage response of cells following current injections were classified into three separate categories; no response: where voltage responses failed to surpass 0 mV, firing of single APs or multiple APs. **(B)** Percentage of cells displaying each firing category at days 20, 40 and 60 during differentiation of Con-1, Con-2, C9-2, C9-3 and C9-3Δ MSNs. Activity in isogenic C9-3Δ and both control lines, Con-1 and Con-2, increases with time compared to all C9 lines, which show a reduced firing capability throughout the differentiation process. **(C-D)** This reduced level of activity in all C9-MSNs versus healthy control lines and paired isogenic line (C9-3 and C9-3Δ), extends to the firing patterns observed at day 40 **(C)** and 60 **(D),** but not Day 20 (data not shown). Data: Con-1: day 20, n=22, N=7; day 40, n=18, N=3; day 60, n=14, N=6; Con-2: day 20, n=12, N=2; day 40, n=8, N=2; day 60, n=10, N=3; C9-1: day 60, n=14, N=5; C9-2: day 20, n=14, N=3; day 40, n=16, N=3; day 60, n=15, N=7; C9-3: day 20, n=11, N=6; day 40, n=21, N=5; day 60, n=22, N=6;C9-3Δ: day 20, n=4, N=3; day 40, n=8, N=4; day 60, n=18, N=4.

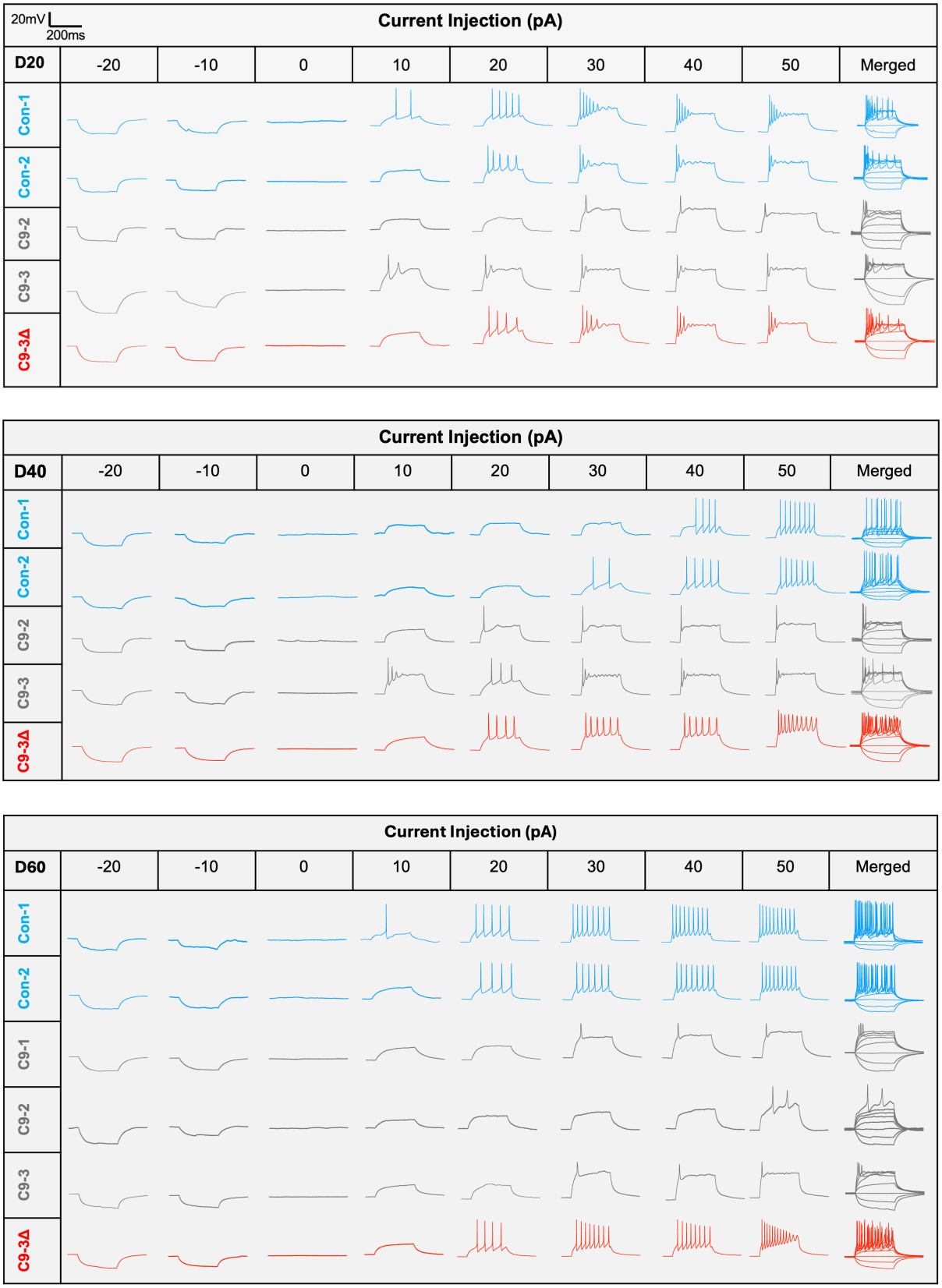

Figure 3.3. C9-MSNs display a loss-of-function phenotype. Matrix schematic of illustrative AP traces recorded in the whole-cell current-clamp configuration from individual cells reveal C9-MSNs exhibit impairments in excitability. Voltage responses are shown from healthy control lines (blue), C9 patients (grey) and a paired isogenic

line C9-3Δ (red) in response to a train of incremental current injections (-20pA to 50pA in 10pA steps) from a LJP corrected resting membrane potential held at -74mV. AP traces were attained from MSNs throughout the differentiation process at day 20, 40 and 60 timepoints.

3.33 C9 Patient-derived MSNs are Hypoexcitable

To further explore whether C9-MSNs do indeed have deficits in AP generation, I recorded the number of APs evoked, if at all, in response to a train of incremental, depolarising current injections (0 to +50pA, 5pA steps, 500ms duration). This allowed for the construction of current stimulus input- action potential output graphs to be plotted for Con-1, Con-2, C9-2, C9-3 and C9-3Δ across days 20,40 and 60 to inspect changes in excitability throughout the differentiation process (Figure 3.4A-E). As control lines matured from DIV20 to 60, data from Con-1 and Con-2 lines revealed a statistically significant increase in the number of APs elicited in response to current stimulation (two-way ANOVA: Con-1: $F(20, 510) = 5.164$, $p<0.0001$; Con-2: $F(30, 375) = 8.315$, $p<0.0001$) (Figure 3.4A-B). In contrast, both C9-2 and C9-3 MSNs displayed abnormal development of their excitability profile illustrated by consistent low levels of AP firing activity throughout these maturation timepoints (two-way ANOVA: C9-2: $F(30, 630) = 1.208$, $p>0.05$; C9-3: $F(30, 765) = 0.732$, $p>0.05$) (Figure 3.4C-D). Once again, the C9-3Δ align closely with the behaviours of control lines and not its C9-3 counterpart in that the firing activity of these isogenic cells in response to current stimulation, significantly increased with time (two-way ANOVA: C9-3Δ: $F(20, 240) = 3.707$, $p<0.0001$ (Figure 3.4E). Full details of statistical tests including the results of Tukey's multiple comparison test are detailed in Appendix 2.

To confirm these findings, I next wanted to analyse and compare the AP activity profiles of all iPSC-lines studied once they reached functional maturity at day 60. Voltage responses of both Con-1 and Con-2 indicate these cell lines are extremely responsive to current stimulation and are almost superimposable in nature, as are the low-level voltage responses of C9-2, C9-3 and the additional C9-1 MSNs (Figure 3.4F).

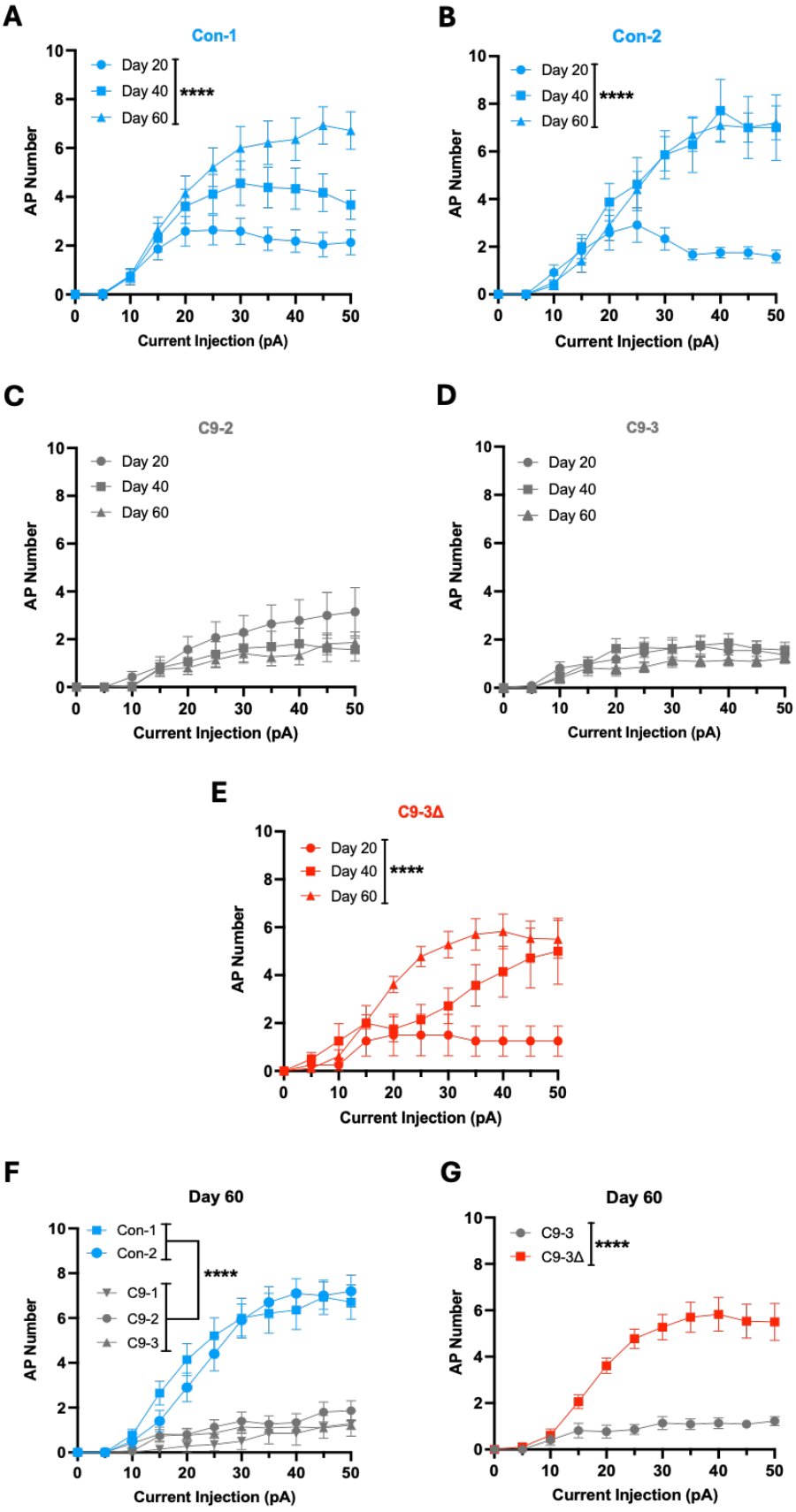
A
Con-1
Day 20
Day 40
Day 60
****
AP Number
Current Injection (pA)
B
Con-2
Day 20
Day 40
Day 60
****
AP Number
Current Injection (pA)
C
C9-2
Day 20
Day 40
Day 60
AP Number
Current Injection (pA)
D
C9-3
Day 20
Day 40
Day 60
AP Number
Current Injection (pA)
E
C9-3Δ
Day 20
Day 40
Day 60
****
AP Number
Current Injection (pA)
F
Day 60
Con-1
Con-2
C9-1
C9-2
C9-3
****
AP Number
Current Injection (pA)
G
Day 60
C9-3
C9-3Δ
****
AP Number
Current Injection (pA)

Figure 3.4. C9-MSNs are hypoexcitable. (A-E) The number of APs evoked following current stimulation stratified by timepoint (day 20, 40 and 60) for (**A)** Con-1, (**B)** Con-2,(**C)** C9-2, (**D)** C9-3 and (**E)** C9-3Δ MSNs demonstrate C9-MSNs become increasingly hypoexcitable as they mature from day 20 to day 60. Both healthy control lines and C9-3Δ MSNs exhibit increased AP discharge with time as opposed to C9-MSNs that show persistent hypoexcitability. **(F-G)** All three C9-MSNs (C9-1, C9-2, C9-3) lines show a reduced capacity to fire APs compared to healthy controls **(F)** and C9-3 vs C9-3Δ MSNs at day 60 **(G)**. All data presented as Mean (±SEM). * $p<0.05$, **** $p<0.0001$ from repeated measures two-way ANOVA followed by Tukey's multiple comparisons test. Data: Con-1: day 20, n=22, N=7; day 40, n=18, N=3; day 60, n=14, N=6; Con-2: day 20, n=12, N=2; day 40, n=8, N=2; day 60, n=10, N=3; C9-1: day 60, n=14, N=5; C9-2: day 20, n=14, N=3; day 40, n=16, N=3; day 60, n=15, N=7; C9-3: day 20, n=11, N=6; day 40, n=21, N=5; day 60, n=22, N=6; C9-3Δ: day 20, n=4, N=3; day 40, n=8, N=4; day 60, n=18, N=4.

Statistical comparison of each individual C9-MSN line with control lines showed significant decreases in AP activity (two-way ANOVA: $F(60, 1050) = 9.489$, $p<0.0001$; Tukey's multiple comparison test results listed in Appendix 3) following exposure to the current stimulus protocol. In addition, differences in the voltage response of day 60 C9-3 versus C9-3Δ were evaluated (Figure 3.4G). The CRISPR-Cas9 gene-edited, C9-3Δ MSN, in which the *C9ORF72* repeat expansion has been specifically excised, demonstrated significantly enhanced excitability compared to its corresponding C9-3 MSN line across almost all current stimuli (two-way ANOVA: $F(15, 525) = 17.12$, $p<0.0001$; Sidak's multiple comparison test results described in Appendix 4). Removal of the repeat expansion in C9-3Δ MSNs is sufficient for rescue of voltage activity in response to current depolarisations. Together, these data provide evidence of a hypoexcitable phenotype in C9 iPSC-derived MSNs.

3.34 Hypoexcitability of C9 MSNs is not Driven by Impairments in Maturation

To ensure the intrinsic hypoexcitability of C9 patient-derived MSNs did not arise from abnormalities in the development of any of the iPSC lines, a maturation profile of patch-clamp recorded neurons was built. This consisted of measuring the intrinsic membrane properties of the neuron. Specifically, the whole-cell capacitance (WCC), resting membrane potential (RMP) and input resistance (R_{in}) were measured to capture a snapshot into a cell's development, health and excitability.

The phospholipid bilayer functions as an electrical insulator that stores electrical charge either side of the membrane. Thus, it functions in the same way as a capacitor. The WCC positively correlates with the surface area of the cell, which helps provide a functional readout for cell size and in turn, membrane integrity. WCC across all lines progressively increased throughout the maturation timepoints in alignment with previous reports by (Gertler et al., 2008, Bicanic et al., 2017) (Figure 3.5A). Although, WCC did not always show statistically significant increases between each successive timepoint, for each iPSC line there was a positive increase overtime. This was seen for Con-1 (Kruskal-Wallis test: $p<0.05$; Dunn's multiple comparison test: day 20 vs day 40: $p=0.0161$), Con-2 (one-way ANOVA: $p<0.05$; Tukey's multiple comparison test: day 20 vs day 60: $p=0.00115$; day 40 vs day 60: $p=0.0358$), C9-2 (one-way ANOVA: $p<0.05$; Tukey's multiple comparison test: day 20 vs day 60: $p=0.0377$; day 40 vs day 60: $p=0.0239$), C9-3 (one-way ANOVA: $p<0.05$; Tukey's multiple comparison test: day 20 vs day 60: $p=0.0045$; day 40 vs day 60: $p=0.0249$) and C9-3Δ (one-way ANOVA: $p<0.05$; Tukey's multiple comparison test: day 20 vs day 40: $p=0.0033$; day 20 vs day 60: $p<0.0001$). The WCC at day 60 was comparable across all iPSC lines including in C9-3 versus C9-3Δ MSNs (unpaired *t-test*: $p=0.356$) (Figure 3.5B). One significant difference was established between Con-1 and Con-2 (Kruskal-Wallis test: $p<0.05$; Dunn's multiple comparison test: $p=0.0254$). The data signify WCC is not afflicted in the development of these iPSC-derived MSNs.

Regulation of the RMP is essential for proper neuronal cell function as deviations from this can influence ionic gradients of key ions such as Na^+, K^+ and Cl^- across the membrane and influence neuronal excitability. RMP was measured in the absence of any current stimulation prior to each recording. Longitudinal analysis of RMP led to the discovery of an enhanced RMP with time for Con-1 (one-way ANOVA: $p<0.05$; Tukey's multiple comparison test: day 20 vs day 60: $p=0.0154$), Con-2 (one-way ANOVA: $p<0.05$; Tukey's multiple comparison test: day 20 vs day 60: $p=0.0002$), C9-3 (one-way ANOVA: $p<0.05$; Tukey's multiple comparison test: day 20 vs day 60: $p=0.0045$; day 40 vs day 60: $p=0.0249$) and C9-3Δ (one-way ANOVA: $p<0.05$; Tukey's multiple comparison test: day 20 vs day 40: $p=0.0033$; day 20 vs day 60: $p<0.0001$) but not C9-2 where this increase was deemed insignificant (one-way ANOVA: $p>0.05$) (Figure 3.5C).

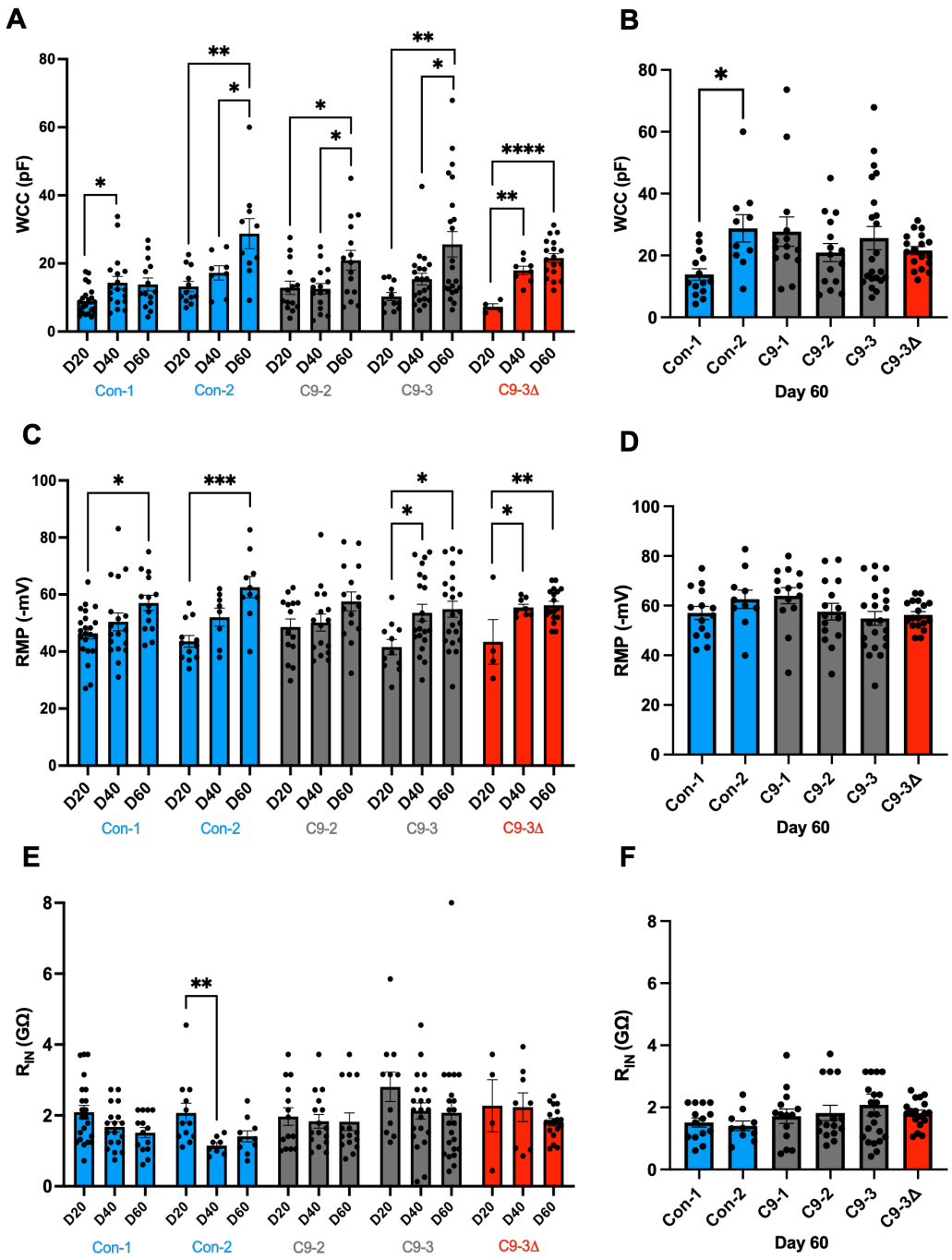

Figure 3.5. Hypoexcitability in C9-MSNs is not due to impairments in maturation. **(A-F)** Intrinsic membrane properties for Con-1, Con-2, C9-2, C9-3 and C9-3Δ at days 20, 40 and 60. Data from day 60 is from Con-1, Con-2, C9-1, C9-2, C9-3 and C9-3Δ. Quantification of the mean **(A-B)** whole cell capacitance (WCC) at days 20,40 and 60 **(A)** and for day 60 specifically **(B)**. Individual cells are represented by individual circles superimposed onto the bar graphs. A trend towards increased WCC with maturation is observed and a similar WCC is seen across all lines at day 60. Quantification of the mean **(C-D)** resting membrane potential (RMP) at days 20,40 and 60 **(C)** and across all lines at day 60 **(D)**. The RMP becomes increasingly hyperpolarised with maturity and is similar across all lines at day 60. Quantification of the average **(E-F)** membrane input resistance (R_{IN}) at all three timepoints **(E)** and specifically at day 60 **(F)** is similar across all stages of maturation. All data presented as Mean (±SEM). * p<0.05, ** p<0.01, *** p<0.001, **** p<0.0001 from one-way ANOVA followed by Tukey's multiple comparisons test or Kruskal-Wallis test followed by Dunn's multiple comparisons test.

Data: Con-1: day 20, n=22, N=7; day 40, n=18, N=3; day 60, n=14, N=6; Con-2: day 20, n=12, N=2; day 40, n=8, N=2; day 60, n=10, N=3; C9-1: day 60, n=14, N=5; C9-2: day 20, n=14, N=3; day 40, n=16, N=3; day 60, n=15, N=7; C9-3: day 20, n=11, N=6; day 40, n=21, N=5; day 60, n=22, N=6; C9-3Δ: day 20, n=4, N=3; day 40, n=8, N=4; day 60, n=18, N=4.

No statistical significance was reported for the neuronal RMP at DIV60 in any of the iPSC lines (one-way ANOVA: $p>0.05$; C9-3 vs C9-3Δ; unpaired *t-test*: $p=0.668$) (Figure 3.5D). The RMP values reported here are in range with previously reported iPSC-derived MSN RMPs (Arber et al., 2015, Stanslowsky et al., 2016). My findings here demonstrate the RMP across all MSNs followed a similar hyperpolarising trend with time and is not related to neuropathological phenotype observed in C9-MSNs. Instead, this provides further evidence of functional maturation throughout the differentiation period.

The resistance encountered by current because of membrane channels and transporters is commonly referred to as the R_{in}. This measurement provides an insight into ion channel expression, membrane integrity and ultimately neuronal excitability. A high R_{in} suggests low ion channel expression or a small membrane surface area (small WCC), indicative of a more excitable cell as small amount of current can cause amplified voltage changes. Contrastingly, a low R_{in} reflects a less excitable neuron with a high density of membrane proteins or a large WCC. The R_{in} was captured prior to any patch-clamp recordings via WinWCP or WinEDR software. For all control, case and isogenic lines the R_{in} was assessed and was relatively consistent from DIV20 to DIV60 (Figure 3.5E) and at DIV60 (Figure 3.5F). The only exception to this was a significant decrease in Con-2 at day 20 to day 40 (Kruskal-Wallis test: $p<0.05$; Dunn's multiple comparison test: $p=0.009$). A low R_{in} is an established feature of mature neurons (Schmidt-Hieber et al., 2004), a feature of the iPSC-derived MSNs I have generated and a feature that is not altered in any MSN cell lines.

Altogether, these results signify alterations in the intrinsic excitability of C9-MSNs are not driven by changes to the sub-threshold, passive membrane properties, which were largely comparable between control, isogenic and case lines. Nor do they indicate this

hypoexcitable, loss-of-function phenotype arises due to impairments in maturity of C9-MSNs.

3.35 Excitatory Glutamatergic and Inhibitory GABA-ergic Transmission are not Impacted in C9 MSNs

The general excitability of neurons within the central nervous system whilst regulated by the intrinsic factors of the neuron previously mentioned, is also governed by the delicate balance between excitatory glutamatergic and inhibitory GABA-ergic transmission. Furthermore, tight regulation of $GABA_AR$ and glutamatergic receptor expression have previously been shown to be vital for mature development of MSNs (Beutler et al., 2011, Wang et al., 2024). Thus, I next wanted to determine whether neurotransmission is altered or whether there are receptor-related deficits in the maturity of patient-derived MSNs.

A functional readout of $GABA_AR$ expression was recorded from DIV40 MSNs in the voltage-clamp configuration, whole-cell membrane currents were induced from bath application of GABA (100μM) from a holding potential of -54mV (LJP corrected). The resting potential was changed to ensure a sufficient driving force for the influx of Cl^-. The response of all MSNs to GABA application was first grouped into two categories: GABA responsive MSNs (Figure 3.6A) or GABA non-responsive, responses were defined as positive deflections above baseline membrane current. GABA-evoked current responses in control and C9-MSNs were blocked by washing on $GABA_AR$ antagonist, bicuculine (Figure 3.6B). Thus, confirming evoked responses resulted from $GABA_AR$ activation. At DIV40, a sizeable proportion of MSNs (13-29%) from Con-1 (13%) and Con-2 (29%) patients failed to respond to GABA stimulation (Figure 3.6C). Conversely, a greater proportion of C9-MSNs did respond to bath-applied GABA with only 7-11% of cells not responding across all patient lines (Figure 3.6C). All C9-1 and C9-2Δ produced GABA-evoked membrane currents (Figure 3.6C). Although differences in percentage response were observed, this did not translate to any differences in the $GABA_AR$ current density calculated for each iPSC line (one-way ANOVA: $p>0.05$), including C9-2 versus its paired isogenic line C9-2Δ (unpaired *t-test*: $p=0.987$) (Figure 3.6D).

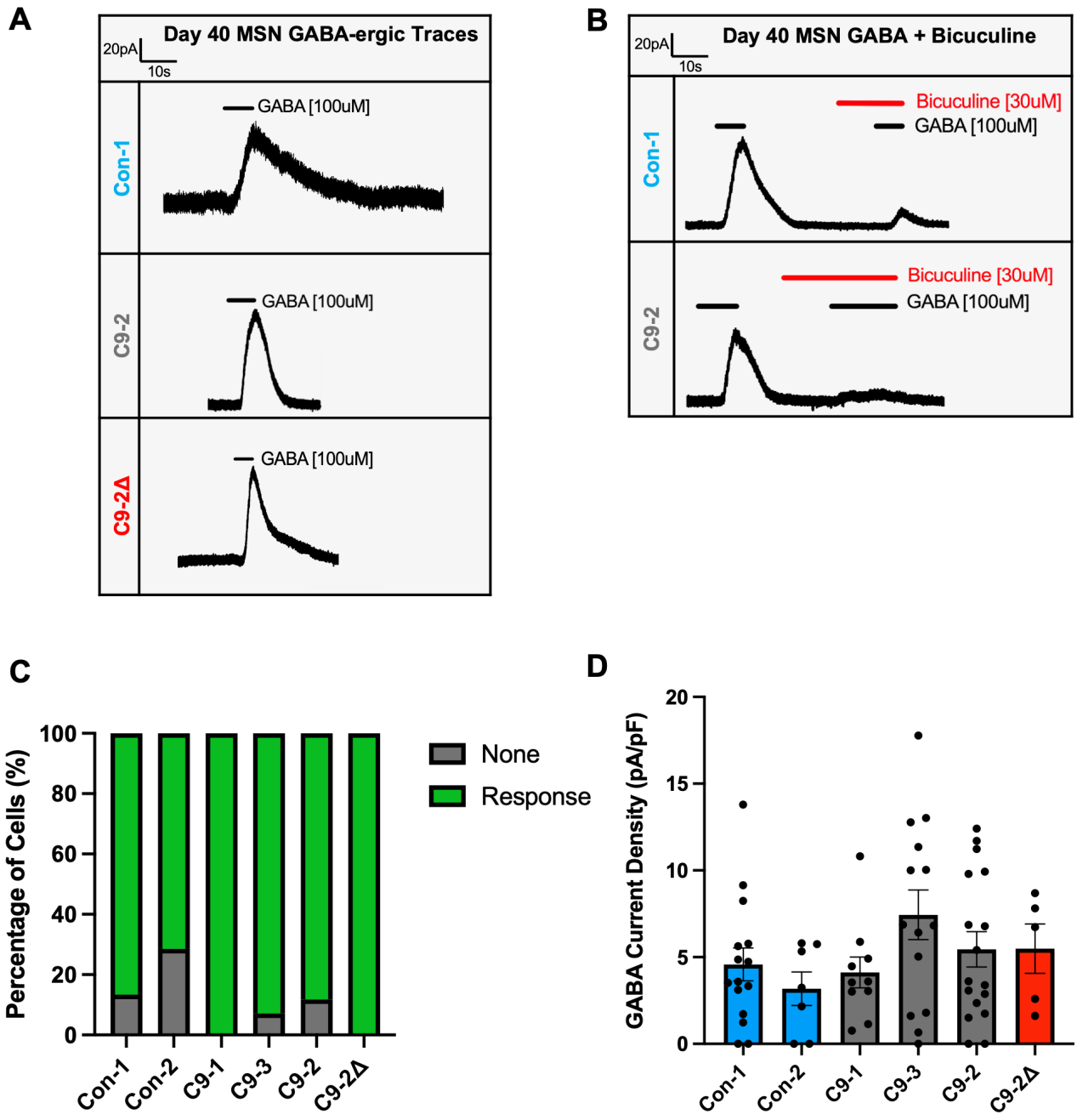

Figure 3.6. GABA-ergic transmission is not impaired in day 40 striatal MSNs. (A-B) Membrane currents were evoked by bath-applied GABA (100μM) **(A)** and blocked by $GABA_AR$ antagonist bicuculine (30μM) **(B)** in the whole-cell voltage-clamp configuration from a LJP corrected holding membrane potential of -54mV. **(C)** Voltage-clamp recordings from individual MSNs were grouped into either GABA-responsive or GABA non-responsive categories, with no significant differences observed between control, isogenic and C9-patient MSNs. **(D)** The mean whole-cell $GABA_AR$ current density was similar across all lineages. Individual cells are represented by individual data points overlaid onto the bar graph. All data presented as Mean (±SEM). Data: Con-1: n=15, N= 4; Con-2: n=7, N=2; C9-1: n=10, N=2; C9-3: n=14, N=3; C9-2: n=17, N=5; C9-2Δ: n=5, N=1. No significant differences between $GABA_AR$ current density

was assessed by one-way ANOVA followed by Sidak's multiple comparisons test and unpaired *t-test* (C9-2 vs C9-2Δ).

Current density was documented by measuring current amplitude to GABA application in relation to membrane capacitance, an electrophysiological indicator of cell size. My findings establish GABA-ergic transmission is not impaired in striatal MSNs.

Next, functional expression of ionotropic glutamatergic receptors, namely AMPAr and NMDAr, was studied in striatal MSNs. Glutamatergic transmission is paramount for homeostatic function of MSNs with the striatum receiving glutamatergic innervation from several brain regions including the frontal cortex and thalamus (Ding et al., 2008, Paraskevopoulou et al., 2019). Thus, whole-cell voltage-clamp recordings were conducted in MSNs from a resting membrane potential held at -74mV (LJP corrected) and membrane currents were induced from bath applied AMPA (50μM) and/or NMDA (100μM, in the presence of glycine, 50μM) (Figure 3.7A). Confirmation of AMPA and NMDA receptor activation was achieved by application of CNQX and APV antagonists respectively, which led to block of receptor mediated currents in control and case lines (Figure 3.7B-C). Voltage-clamp recordings from individual MSNs were grouped into either AMPA-responsive or NMDA-responsive categories with responses defined as negative deflections below baseline membrane current. No meaningful differences were detected between control and C9-patient MSNs, though Con-1 had a large percentage of cells that lacked glutamatergic transmission (Figure 3.7D-E). Mean whole-cell AMPA and NMDA current densities revealed consistent values across all lineages (Kruskal-Wallis test: $p>0.05$) (Figure 3.7F-G). In addition, the AMPA/NMDA ratio was calculated from the same cells where simultaneous application and response to AMPA and NMDA was recorded. The AMPA/NMDA ratio was less than 1 for all lineages which implies a greater proportion of glutamatergic transmission is driven by NMDAr activated currents in DIV40 MSNs. Overall, my results first establish no $GABA_AR$ nor any glutamatergic receptor related dysfunction in striatal MSNs. This would imply dysregulation of these ionotropic receptors does not contribute directly to the hypoexcitable phenotype observed or influences maturation of MSNs. The disturbance in excitability appears to be physiologically selective to altered excitability.

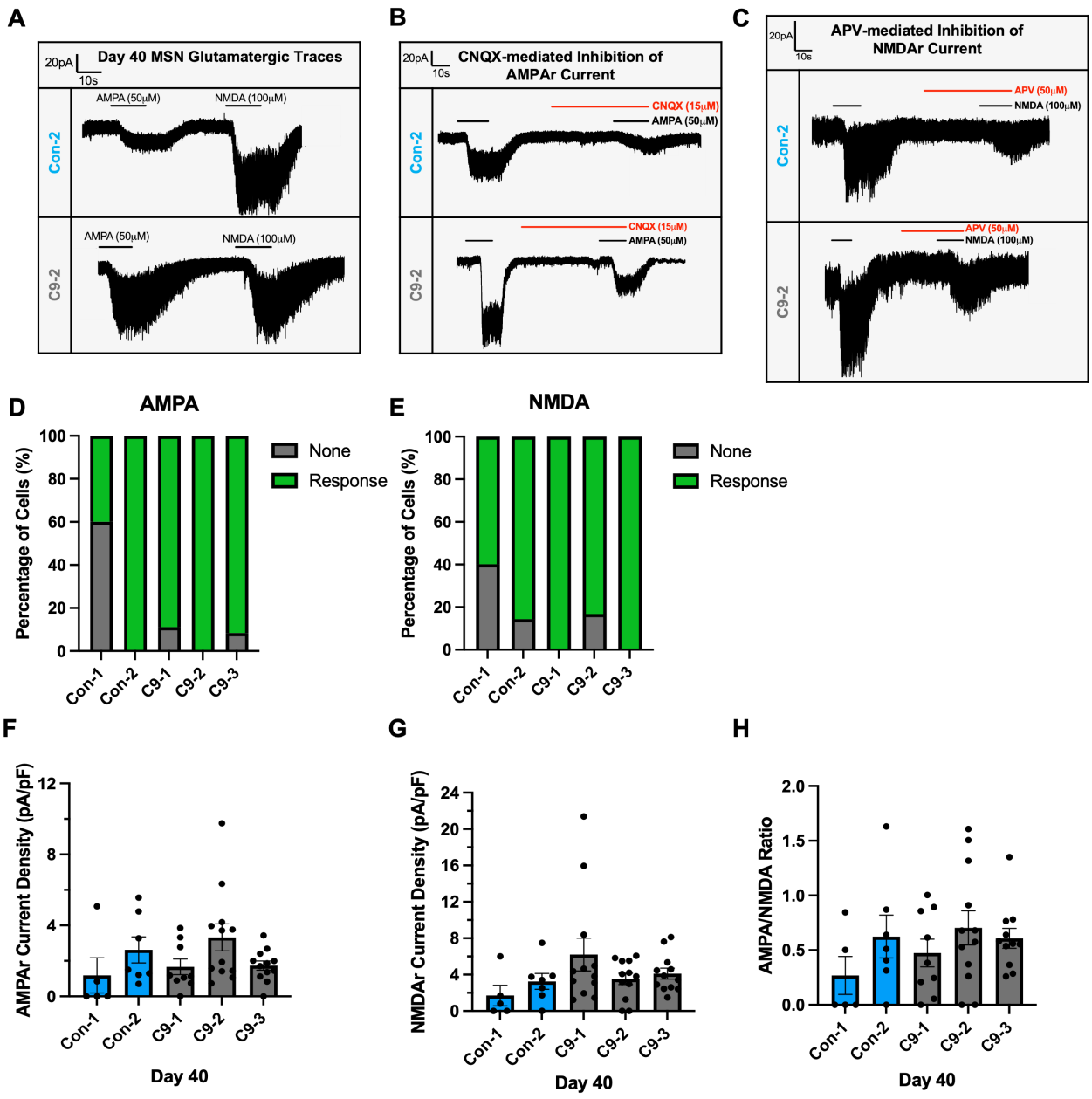

Figure 3.7. Glutamatergic transmission is not impaired in day 40 MSNs. (A-C) Membrane currents were evoked by bath-applied AMPA (50μM) and NMDA (100μM, in the presence of glycine, 50μM) **(A)** and blocked by either AMPAr antagonist CNQX (15μM) **(B)** or NMDAr specific antagonist APV (50μM) **(C)** in the whole-cell voltage-clamp configuration from a LJP corrected holding membrane potential of -74mV. **(D-E)** Voltage-clamp recordings from individual MSNs were grouped into either AMPA-responsive **(D)** or NMDA-responsive **(E)** categories, generally no meaningful differences were observed between control and C9-patient MSNs. Although, Con-1 had a large percentage of cells that lacked glutamatergic transmission. **(F-G)** The mean whole-cell AMPAr **(F)** and NMDAr **(G)** current density was similar across all lineages. **(H)** All day 40 MSNs have an AMPA/NMDA ratio less than 1 indicative of a larger proportion of glutamatergic transmission being driven by NMDAr-mediated currents. Individual cells are represented by individual data points overlaid onto the bar graph. All data presented as Mean (±SEM). Data: Con-1: n=5, N= 3; Con-2: n=7, N=3; C9-1: n=9-12, N=3; C9-2: n=12, N=4; C9-3: n=12, N=2. Statistical insignificance

of AMPAr and NMDAr current densities were determined by Kruskal-Wallis test followed by Dunn's multiple comparisons test.

3.36 The AP Waveform is Disturbed in C9 MSNs

Following the lack of deficits in MSN maturation and sub-threshold properties, subsequent analysis involved studying the evoked APs in greater detail to determine whether phases of the AP, which are a function of ion channel activity, are altered in C9-MSNs. Initially, the minimum current amplitude required to trigger an AP was measured, the rheobase. The exact amount of current required to evoke the first AP provides a useful readout of cell excitability. For analyses of AP parameters, MSNs that did not fire any APs were excluded from the analyses. Longitudinal analysis of the rheobase overtime for each line revealed any changes in the rheobasic current were statistically insignificant (Kruskal-Wallis test: $p>0.05$) (Figure 3.8A). Rheobase values also remained consistent across all lineages at day 40 (Figure 3.9A). At day 60 an increased rheobase value was associated with C9-MSNs (Figure 3.9B), in particular between Con-1 and C9-1 MSNs (Kruskal-Wallis test: $p<0.05$; Dunn's multiple comparison test: $p=0.012$) plus C9-3 and C9-3Δ striatal neurons (unpaired *t-test*: $p=0.0356$). These significant differences, however, were not unanimous across all comparisons between control and C9-derived neurons. Therefore, reduced excitability of C9-MSNs is unlikely to be explained by modifications in rheobase.

The threshold potential of the first evoked AP was then examined various lines across all timepoints. The threshold potential provides critical information on the level of stimulation required to initiate AP responses and is associated with rheobasic data. The AP threshold remained relatively constant with development for all lines (one-way ANOVA: $p>0.05$) but not for Con-2 where AP threshold became hyperpolarised with age (one-way ANOVA: $p<0.05$; Tukey's multiple comparison test: day 20 vs day 40: $p=0.0001$; day 20 vs day 60: $p=0.0001$) (Figure 3.8B). Yet, comparison between lines at day 40 revealed a modest, but significant, depolarisation of the AP threshold in C9-MSNs when assessed against healthy (one-way ANOVA: $p<0.05$; Sidak's multiple comparison test: Con-1 vs C9-3: $p=0.005$; Con-2 vs C9-2: $p=0.01$; Con-2 vs C9-3: $p=0.0006$) or the paired isogenic control (unpaired *t-test*: C9-3 vs C9-3Δ: $p=0.0047$) (Figure 3.9C).

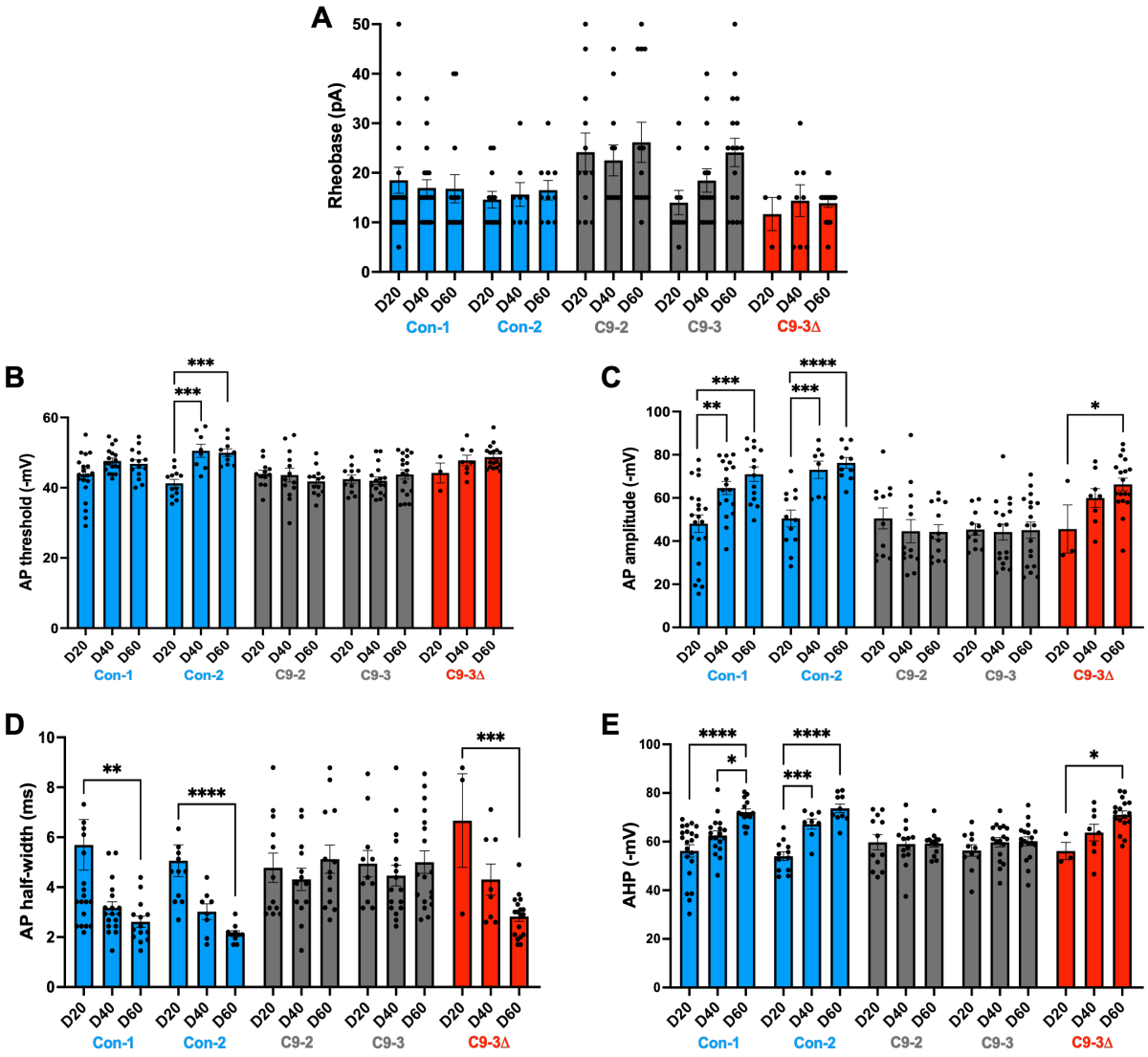

Figure 3.8. Specific AP parameters are modified in C9-MSNs. (A) The minimum current stimulus required to illicit an AP (rheobase) and threshold potential **(B)** showed no significant changes across days 20, 40 and 60 for Con-1, Con-2, C9-2, C9-3 and C9-3Δ. Individual cells are represented by individual circles overlaid onto the bar graphs. **(C)** The AP amplitude increased longitudinally from day 20 to 60 in both control lines (blue) and C9-3Δ but not for any of the patient lines (grey). **(D)** Notably the AP half-width decreased substantially from day 20 to 60 in both control lines and C9-3Δ but not for any of the patient lines. **(E)** Significant hyperpolarisation of the AHP was observed from day 20 to 60 in both control lines and C9-3Δ but not for any of the C9-patient lines. All data presented as Mean (±SEM). * p<0.05, ** p<0.01, *** p<0.001, **** p<0.0001 from one-way ANOVA followed by Tukey's multiple comparisons test or Kruskal-Wallis test followed by Dunn's multiple comparisons test. Data: Con-1: day 20, n=21, N=7; day 40, n=18, N=3; day 60, n=14, N=6; Con-2: day 20, n=12, N=2; day 40, n=8, N=2; day 60, n=10, N=3; C9-2: day 20, n=12, N=3; day 40, n=13, N=3; day 60, n=13, N=7; C9-3: day 20, n=11, N=6; day 40, n=17, N=5; day 60, n=18, N=5; C9-3Δ: day 20, n=3, N=2; day 40, n=8, N=4; day 60, n=18, N=4.

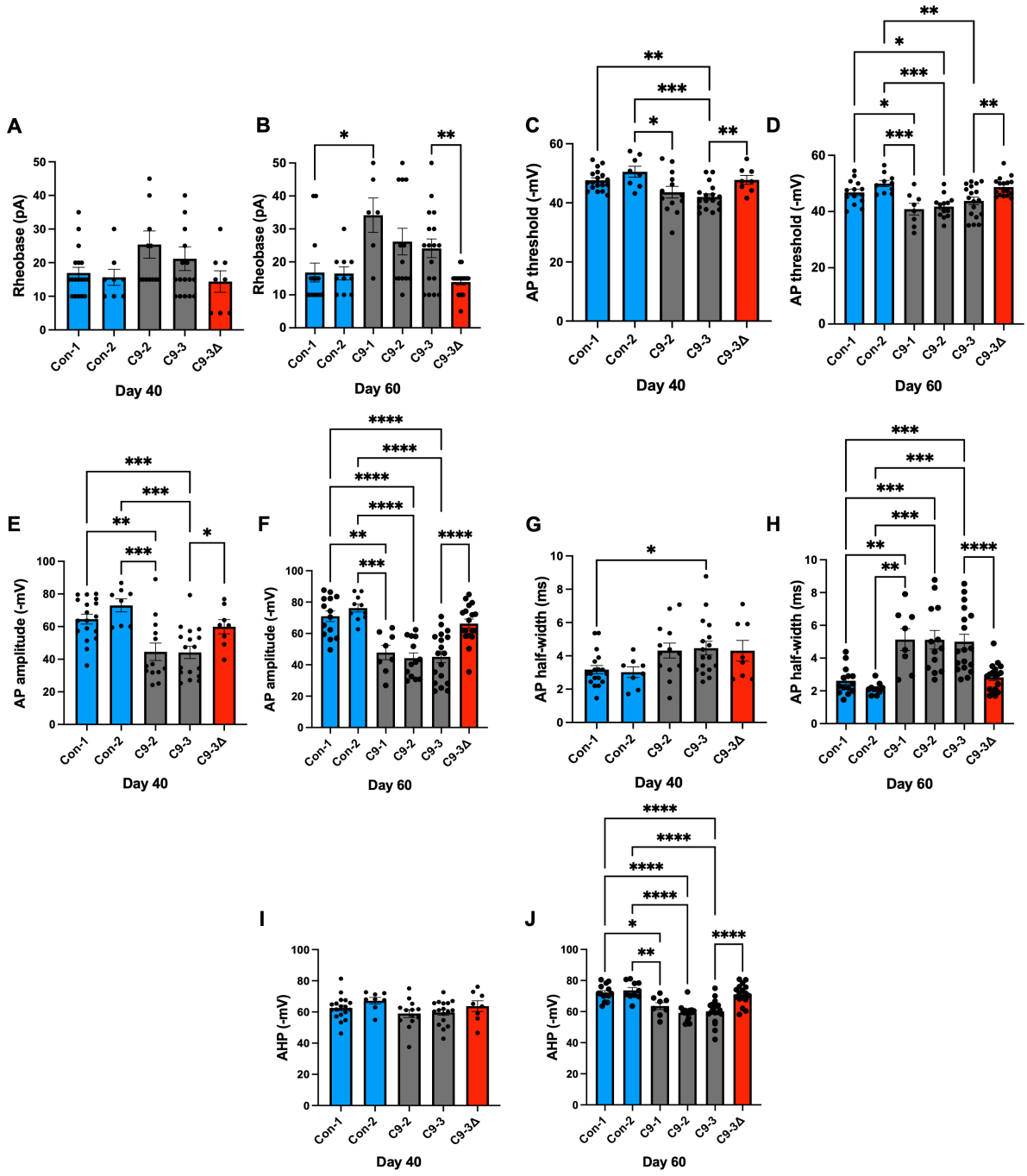

Figure 3.9. Key features that shape the structure of the AP are distorted in C9-patient lines. AP Parameters were measured and compared between lines Con-1, Con-2, C9-1, C9-2, C9-3 and C9-3Δ at days 40 and 60. Individual cells are represented by individual circles overlaid onto the bar graphs. **(A-B)** The recruitment current required to evoke the first AP (rheobase) at days 40 and 60. Measurements of the threshold potential **(C-D),** AP amplitude **(E-F)**, AP duration **(G-H)** and AHP **(I-J)** were recorded for the first AP evoked by current stimulation at days 40 and 60. Note, any trends between healthy control and isogenic lines versus C9-patient lines at day 40 are further pronounced at the day 60 timepoint. All data presented as Mean (±SEM). * p<0.05, ** p<0.01, *** p<0.001, **** p<0.0001 from one-way ANOVA followed by Tukey's multiple comparisons test or Kruskal-Wallis test followed by Dunn's multiple

comparisons test and unpaired *t-test* (C9-3 vs C9-3Δ). Data: Con-1: day 40, n=18, N=3; day 60, n=14, N=6; Con-2: day 40, n=8, N=2; day 60, n=10, N=3; C9-1: day 60, n=8, N=5; C9-2: day 40, n=13, N=3; day 60, n=13, N=7; C9-3: day 40, n=17, N=5; day 60, n=18, N=5; C9-3Δ: day 40, n=8, N=4; day 60, n=18, N=4.

A phenotype further pronounced at day 60 (one-way ANOVA: $p<0.05$; Sidak's multiple comparison test: Con-1 vs C9-1: p=0.023; Con-1 vs C9-2: p=0.029; Con-2 vs C9-1: p=0.0003; Con-2 vs C9-2: p=0.0003; Con-2 vs C9-3: p=0.005) (unpaired *t-test*: C9-3 vs C9-3Δ: p=0.0036) (Figure 3.9D). Depolarisation of the AP threshold aligns with hypoexcitability measured in in C9-MSNs (Figure 3.4) as these cells would therefore require a larger current stimulus to reach threshold and fire APs. Though rheobase data was overall non-significant between control and case lines, there is a clear trend towards a raised rheobasic current in C9-MSNs that aligns closely with the AP threshold data here.

The next phase of the AP to be investigated was the AP amplitude, the voltage difference between the peak of the AP upstroke subtracted by the threshold potential to provide a readout of the membrane excitability. The amplitude of the first evoked AP progressively increased from day 20 to day 60 in both Con-1 (one-way ANOVA: $p<0.05$; Tukey's multiple comparison test: day 20 vs day 40: p=0.0043; day 20 vs day 60: p=0.0002) and Con-2 (one-way ANOVA: $p<0.05$; Tukey's multiple comparison test: day 20 vs day 40: p=0.0005; day 20 vs day 60: $p<0.0001$) (Figure 3.8C), in line with the functional maturation of iPSC-derived neurons (Bullmann et al., 2024). This increase was also observed in the C9-3Δ at day 20 to 60 (one-way ANOVA: $p<0.05$; Tukey's multiple comparison test: p= 0.044) but not in the corresponding C9-paired MSN or in C9-2 (one-way ANOVA: $p<0.05$) (Figure 3.8C). Examination of the AP amplitude across all lines at days 40 and 60 showed a reduction in the C9-MSNs compared to both controls and between the paired C9 and isogenic lines (Figure 3.9E-F). At day 40 statistical comparisons between all lines were significantly different (one-way ANOVA: $p<0.05$; Sidak's multiple comparison test: Con-1 vs C9-2: p=0.0018; Con-1 vs C9-3: p=0.0006; Con-2 vs C9-2: p=0.0003; Con-2 vs C9-3: p=0.0001) (unpaired *t-test*: C9-3 vs C9-3Δ: p=0.0183) (Figure 3.9E). At day 60 these reductions in amplitude were augmented between C9-MSNs and control and isogenic lines (one-way ANOVA: $p<0.05$; Sidak's multiple comparison test: Con-1 vs C9-1: p=0.0011; Con-

1 vs C9-2: p<0.0001; Con-1 vs C9-3: p<0.0001; Con-2 vs C9-1: p=0.0001;Con-2 vs C9-2: p<0.0001; Con-2 vs C9-3: p<0.0001) (unpaired *t-test*: C9-3 vs C9-3Δ: p<0.0001) (Figure 3.9F). Reductions in AP amplitude of C9-MSNs indicate their diminished ability to respond to membrane depolarisations and are thus coherent with a loss of excitability in these neurons.

To next determine whether the duration of APs was affected in these striatal neurons, the AP half-width was quantified. This is defined as the duration of the AP at half its peak amplitude, i.e. the time between the AP upstroke and downstroke. Previous studies have shown the AP duration decreases with maturity (Arama et al., 2015, Bullmann et al., 2024) and longitudinal data from day 20 to 60 in control and isogenic lines correlates with these findings (Figure 3.8D), but interestingly, not in C9-derived MSNs (Kruskal-Wallis test: p<0.05; Dunn's multiple comparison test: Con-1: day 20 vs day 60: p=0.0016; Con-2: day 20 vs day 60: p<0.0001) (one-way ANOVA: p<0.05; Tukey's multiple comparison test: C9-3Δ: day 20 vs day 60: p=0.0007). Furthermore, the half-width does appear prolonged in C9-derived striatal neurons at day 40 especially between Con-1 and C9-3 lines (Sidak's multiple comparison test: p=0.09) (Figure 3.9G). However, statistical comparisons only revealed lengthening of the half-width in C9-3 MSNs against Con-1 (one-way ANOVA: p<0.05; Sidak's multiple comparison test: p=0.04) (Figure 3.9G). Further analysis at day 60 revealed a substantial increase in the AP duration, approximately 200%, in all C9-MSNs when compared with both Con-1 and Con-2 (one-way ANOVA: p<0.05; Sidak's multiple comparison test: Con-1 vs C9-1: p=0.0044; Con-1 vs C9-2: p=0.0008; Con-1 vs C9-3: p=0.0006; Con-2 vs C9-1: p=0.0012; Con-2 vs C9-2: p=0.0002; Con-2 vs C9-3: p=0.0002) (Figure 3.9H). Added comparisons between C9-3 and its corresponding gene-edited isogenic line displayed similar increase in the time interval of C9-3 APs (unpaired *t-test*: C9-3 vs C9-3Δ: p<0.0001) (Figure 3.9H). Collectively, this shows the multiple phases of the AP occur over a longer time in C9-MSNs compared to healthy neurons.

The inactivation phase of the AP where the neuronal membrane potential decreases below the normal RMP is referred to as the afterhyperpolarisation (AHP). To gain insights into the AHP values were recorded from day 20 to 60 striatal neurons. The

AHP became progressively hyperpolarised from day 20 through to day 60 in both Con-1 and Con-2 and a similar trend was apparent in C9-3Δ MSNs (one-way ANOVA: $p<0.05$; Tukey's multiple comparison test: Con-1: day 20 vs day 60: $p<0.0001$; day 40 vs day 60: $p=0.01$; Con-2: day 20 vs day 40: $p=0.0001$; day 20 vs day 60: $p<0.0001$; C9-3Δ: day 20 vs day 60: $p=0.011$) (Figure 3.8E), similar to reports in iPSC-derived MSNs (Arama et al., 2015). For C9-MSNs the AHP stayed relatively consistent over this same time course (one-way ANOVA: $p>0.05$). At day 40 only modest changes in the AHP were recorded between iPSC-derived striatal neurons that under statistical comparisons did not achieve significance (Figure 3.9I). Nonetheless, large variations in the AHP at day 60 (Figure 3.9J) was noted with considerable depolarisation of the AHP in all C9-MSNs when compared to both healthy controls (one-way ANOVA: $p<0.05$; Sidak's multiple comparison test: Con-1 vs C9-1: $p=0.0182$; Con-1 vs C9-2: $p<0.0001$; Con-1 vs C9-3: $p<0.0001$; Con-2 vs C9-1: $p= 0.0074$; Con-2 vs C9-2: $p<0.0001$; Con-2 vs C9-3: $p<0.0001$). The same enlarged differences were true between the C9-3 and C9-3Δ pair (unpaired *t-test*: $p<0.0001$). Similar to phenotypic amplitude and half-width data from C9-MSNs, the AHP phenotype appears at day 40 before coming progressively stronger at day 60. Moreover, these data suggest AP repolarisation could be hindered in C9-MSNs.

3.37 Potassium I_K Channel Function is Reduced in C9 MSNs

Here, I report clear dysfunction in various AP parameters such as threshold, amplitude, duration and AHP of evoked APs in C9-MSNs. Parameters of which are predominantly governed by the ion channel activity of voltage-gated Na^+ (Na_V) and K^+ (K_v) channels. Now, previous data generated in the lab show a lack of deficits in the Na_V channels that underpin the depolarisation phase of the AP (Appendix 5). Consequently, biological correlates that regulate the AP repolarisation phase were studied in greater detail. Thus, work initially focused on the functional expression of delayed outwardly-rectifying K^+ channels (I_k). These relatively slow activating K^+ channels play important roles in regulating membrane excitability. Specifically, these channels contribute to membrane repolarisation and thus, can influence AP duration in conjunction to the AHP phase of the AP (Boettger et al., 2002, Furness et al., 2004, Kshatri et al., 2018).

I_k channel activity was isolated and measured using protocols previously established by (Livesey et al., 2016). In the whole-cell voltage-clamp configuration MSNs were subjected to a 250ms, 100mV depolarising pulse from the holding potential of -70mV (without LJP correction) to +30mV to activate I_k channels (Figure 3.10A). This was initially conducted in the presence of standard extracellular solution (Table 2.14). The protocol was then repeated in the presence of 30mM tetraethylammonium (TEA) (Table 2.15) to block I_k channel activity. TEA-sensitive current was isolated by subtraction of TEA-blocked current from the previous activation current (Figure 3.10B-D). Both extracellular solutions were supplemented with the maximal efficacious concentration of tetrodotoxin (TTX, 300nM) to block Na_V (activation). The average peak amplitude for each MSN was calculated from a triplicate of recordings, with peak current amplitude measured at 300ms post-protocol induction. The ensuing average TEA-sensitive current was normalised to the recorded WCC value for each MSN (current density) as a readout of I_k channel expression (Figure 3.10E). Comparative analysis at DIV40 indicates C9-3 MSNs exhibit significant reduction of I_k current density versus its corresponding gene-edited isogenic line C9-3Δ (unpaired *t-test*: p=0.0026) (Fig 3.10E). A clear reduction in current densities was also observed between Con-1 and C9-3. Nonetheless, the differences from this preliminary dataset were deemed insignificant (Dunn's multiple comparison test: p=0.07) and further work is required to increase the statistical power of these data. The preliminary data here would indicate dysregulated I_k channel expression observed here could, at least in part, contribute to the loss-of-function phenotype in C9-MSNs.

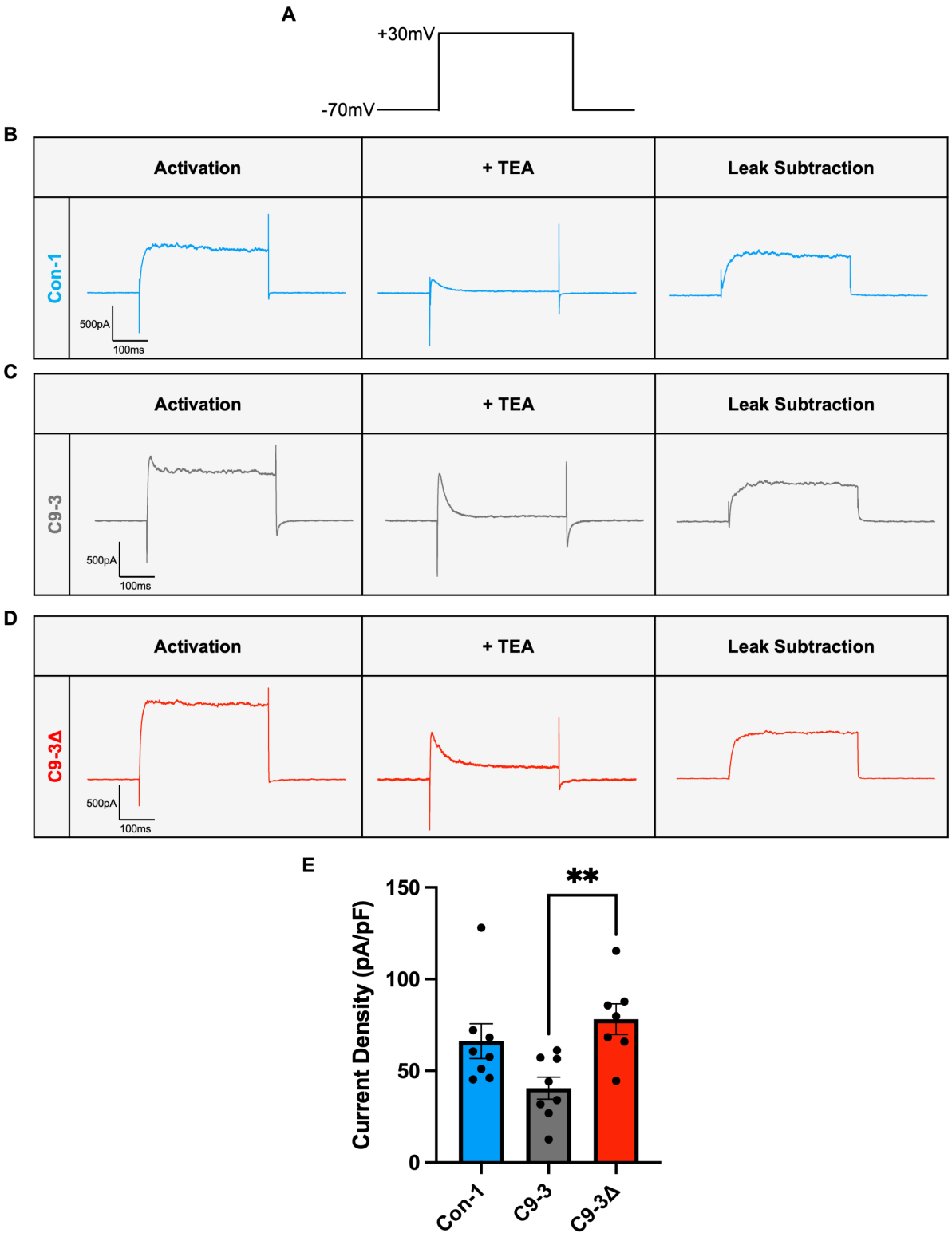

Figure 3.10. Reduced function of delayed outwardly-rectifying K^+ channel (I_k) in C9 MSNs. (A) To isolate I_k channel activity, a 100mV depolarising pulse was applied to activate I_k channels (*activation*). This was then repeated in the presence of TEA (30mM). TEA-sensitive current was determined by subtracting current data of the former by the latter to provide a readout of I_k channel activity (*leak subtraction*). **(B-D)** Exemplar current traces in the absence and presence of TEA along with subtracted

current data for day 40 Con-1 **(B)**, C9-3 **(C)** and C9-3Δ **(D)** MSNs. I_k current amplitudes were measured 300milliseconds after activation. **(E)** Increased I_k channel expression from C9-3 to C9-3Δ MSNs. All data presented as Mean (±SEM). ** p<0.01 from unpaired *t-test* (C9-3 vs C9-3Δ). Data: Con-1: n=8, N= 2; C9-3: n=8, N=2; C9-3Δ: n=7, N=1.

3.38 Pharmacological Gain of K^+ Channel Function Rescues AP Waveform in C9 iPSC-derived MSNs

To determine the precise source(s) of these electrophysiological perturbations in C9-MSNs in particular, excitability and AP parameters, and to what extent these phenotypes could be rescued various pharmacological compounds were washed onto C9-MSNs.

Previously, big conductance calcium-activated potassium (BK) channels have been shown to influence intrinsic membrane excitability, AP duration and AHP all of which are impacted in C9-MSNs (Edwards and Weston, 1995, Wang et al., 2014, Contet et al., 2016). Therefore, it is likely that post-AP threshold activated K+ channels such as these BK channels are impacted rather than sub-threshold channels that govern sub-threshold properties not afflicted in these C9-MSNs. Furthermore, BK channels have been shown to be expressed ubiquitously throughout the CNS (Wanner et al., 1999, Grunnet and Kaufmann, 2004) including in striatal MSNs (Contet et al., 2016). Therefore, making them a promising target to rescue C9-related disease phenotypes. To this end, voltage responses from the same C9-3 MSNs were evoked using the same whole-cell current clamp protocols as previous, first in the presence of standard extracellular solution (Table 2.14) and then subsequently in the presence of BK channel activator, NS11021 (10μM) (Bentzen et al., 2007) (Figure 3.11A-B). The BK activator was washed onto the cells for at least 60 seconds prior to recording. Voltage responses were recorded from the first AP induced from a +30pA current stimulus. Unlike (Layne et al., 2010), NS11021 application had no influence on the AP number evoked from depolarising current inputs, with superimposable voltage output observed in C9-3 MSNs before and after treatment (Figure 3.11C). Also, the rheobasic current (paired *t-test*: p=0.668) and AP duration (paired *t-test*: p=0.375) were unaffected following pharmacological treatment (Figure 3.11D-E).

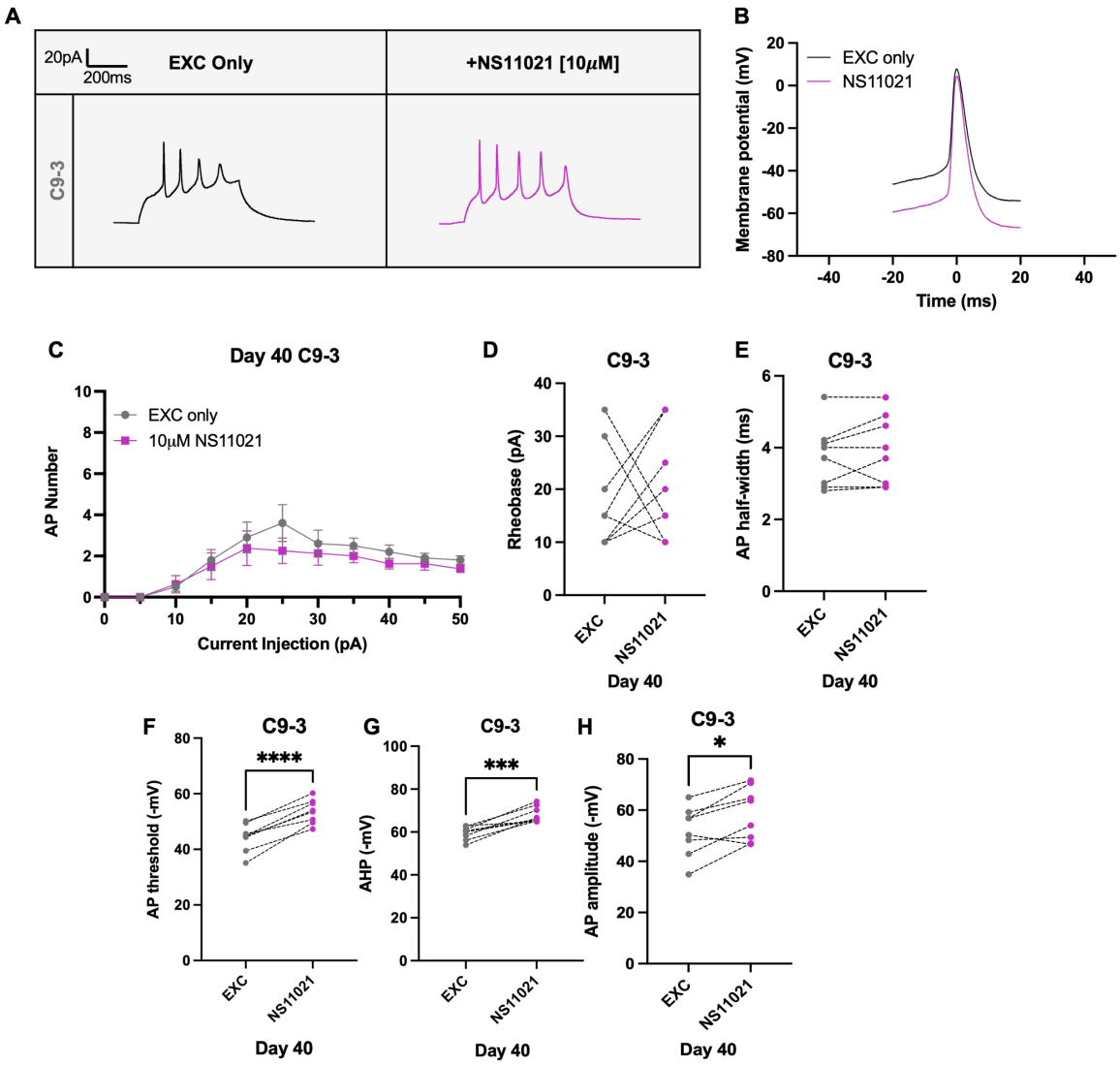

Figure 3.11. BK channel activator NS11021 rescues threshold, AHP and AP amplitude of day 40 C9-MSNs. To rescue hypoexcitability and disease phenotypes associated with the AP parameters 10μM NS11021 was washed onto the C9-3 patient line. **(A-B)** Representative voltage response in full **(A)** or from the first AP evoked **(B)** following 30pA current stimulation in the absence or presence of NS11021. Voltage responses were recorded from the same cell **(C-F)**. NS11021 treatment had no effect on AP numbers evoked from current stimulation **(C)**, rheobase **(D)**, or AP duration **(E)**. **(F)** The AP threshold was significantly hyperpolarised following treatment with the BK channel activator as was the AHP of C9-3 NS11021-treated MSNs **(G)**. The size of the AP was also marginally larger following NS11021 treatment **(H)**. All data presented as Mean (±SEM). * p<0.05, *** p<0.001, **** p<0.0001 from paired *t-test* (EXC vs NS11021 from the same C9-3 MSN). Data: C9-3: n=8, N=4.

Surprisingly, NS11021 application was able to recover the threshold potential of C9-3 treated MSNs towards values previously observed in day 40 control MSNs and above values in C9-3Δ (Figure 3.9C), with hyperpolarisation of the average threshold value from -44mV to -54mV (paired *t-test*: $p<0.0001$) (Figure 3.11F). Interestingly, BK channel activity is not typically associated with the AP threshold (Contet et al., 2016). Hyperpolarisation of the threshold potential thus coincides with amplification of AP amplitude in response to NS11021 exposure when compared to baseline responses (paired *t-test*: $p=0.014$) (Figure 3.11H), with peak membrane potential values similar in evoked APs (data not shown). AP size was shown to be downregulated in C9-MSNs prior (Figure 3.9E), but the data here following BK channels activation show amplitude size is increased in line with control and isogenic D40 MSNs. The AHP in the absence and presence of NS11021, recorded from the same C9-3 cell was found to be markedly altered (Figure 3.11G). In fact, the AHP was found on average, to be 15% more hyperpolarised following treatment with NS11021 (paired *t-test*: $p=0.0005$). Whilst no large alterations in AHP were witnessed in day 40 MSNs (Figure 3.9I), there is a clear depolarisation of AHP at this timepoint of which becomes further pronounced at day 60 (Figure 3.9J). So, this phase of the AP is afflicted in C9-MSNs. These data not only suggest BK channels contribute to the neurophysiological phenotypes in C9-MSNs but that they could be useful targets to correct the deficits in AP waveform in C9-MSNs.

Concurrent with these NS11021 experiments, data from cortical preparations from an *ex-vivo* SOD1 ALS mouse model demonstrated treatment with the K_V3 ($K_V3.1$- 3.2) positive modulator, AUT1 was sufficient for a gain-of-function rescue of network excitability (data not shown). Furthermore, a sister compound, AUT00206 that targets the striatum is current in clinical trials for Schizophrenia (Angelescu et al., 2022, Kaar et al., 2022). Therefore, I washed on the AUT1 compound to rescue electrophysiological dysfunction in C9-MSNs. Like NS11021 experiments, current-clamp recordings were conducted in the absence and then presence of AUT1 (30μM) with the pharmacological agent washed onto the cells for at least 60 seconds prior to the second recording of voltage response (Figure 3.12). Across the train of current injections and especially at 30pA stimulation no differences in the output activity were recorded from either day 40 C9-1 or C9-3 MSNs (Figure 3.12A, C-D).

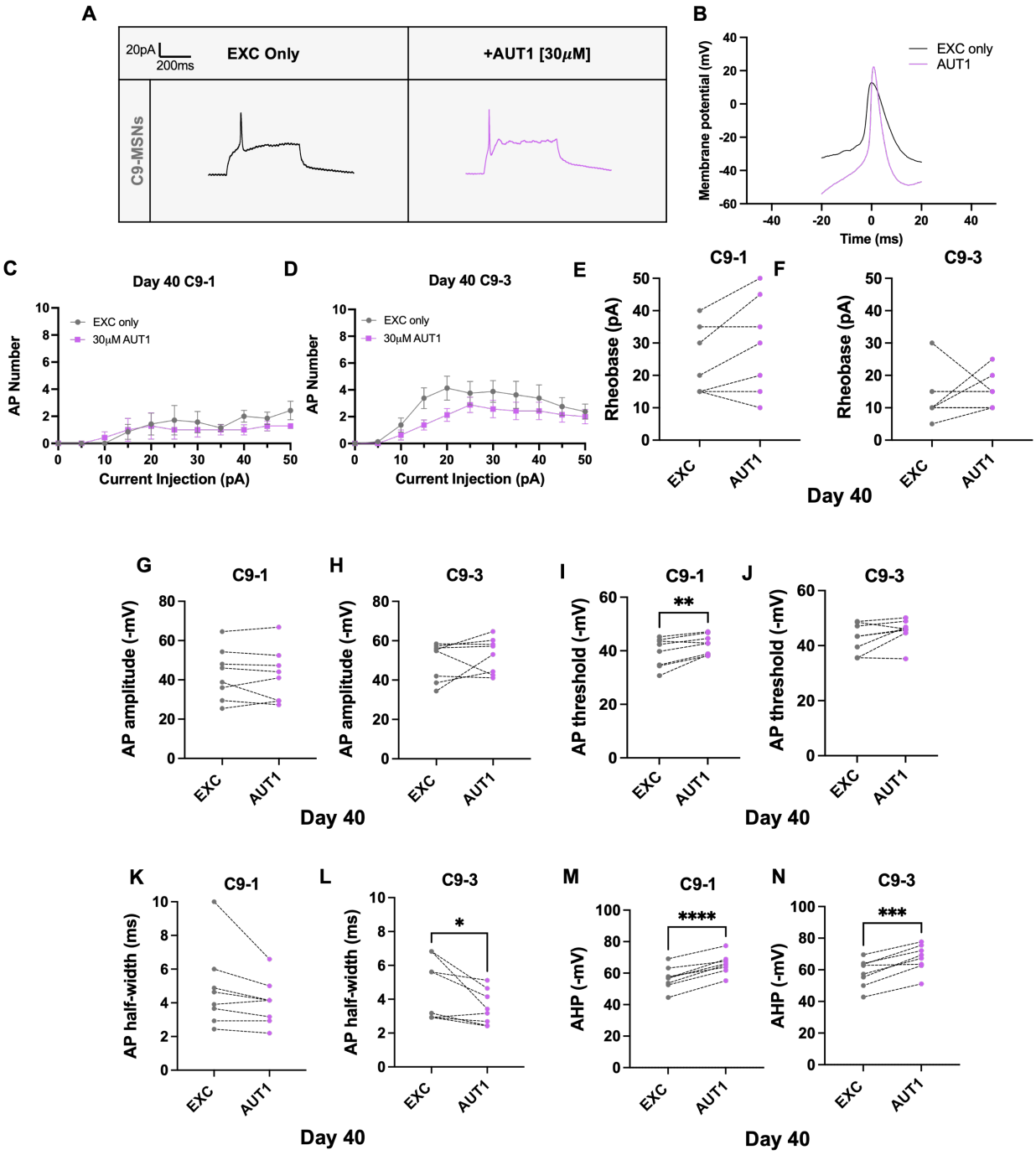

Figure 3.12. K^+ channel modulator AUT1 rescues AHP of day 40 C9-MSNs. To rescue hypoexcitability and disease phenotypes associated with the AP parameters 30μM AUT1 was washed onto C9-patient lines. **(A-B)** Representative voltage response in full **(A)** or from the first AP evoked **(B)** following 30pA current stimulation in the absence or presence of AUT1. Voltage responses were recorded from the same cell **(C-N)**. AUT1 treatment had no effect on AP numbers evoked from current stimulation **(C-D)**, rheobase **(E-F)** or AP amplitude of both C9 lines **(G-H)**. Threshold potential was moderately hyperpolarised in C9-1 but not C9-3 MSNs **(I-J)**. **(K-L)** AUT1 treatment was able to partially rescue AP duration of C9-3 MSNs and significantly hyperpolarised the AHP of both C9-patient lines **(M-N)**. All data presented as Mean (±SEM). * p<0.05, ** p<0.01, *** p<0.001, **** p<0.0001 from paired *t-test* (EXC vs AUT1 from the same C9-1 or C9-3 MSN). Data: C9-1: n=8, N=3; C9-3: n=8, N=4.

Nevertheless, closer examination of the first evoked AP at the stimulation revealed disturbances in AP waveform following AUT1 application (Figure 3.12B). Hence, closer scrutiny of the various AP parameters for both lines (Figure 3.12E-N). AUT1 has been shown to increase AP frequency in mouse cortical slices (Rosato-Siri et al., 2015). Nonetheless, no alterations in the recruitment current (C9-1 and C9-3: paired *t-test*: $p>0.05$) (Figure 3.12 E-F) or amplitude of the AP (C9-1 and C9-3: paired *t-test*: $p>0.05$) was detected in either lineage (Figure 3.12 G-H). This is in disagreement with previous reports from *in-vitro* murine cortical slices that show augmented AP amplitude in response to AUT1 (Rosato-Siri et al., 2015). The AP threshold in C9-1 (paired *t-test*: $p=0.0082$) but not C9-3 MSNs (paired *t-test*: $p=0.089$) did shift towards more negative potentials as a result of AUT1 wash (Figure 3.12 I-J). Though, the average shift in threshold was very modest with a difference of 3mV before and after drug treatment. Interestingly, AP duration was dramatically reduced in both C9-MSNs (Figure 3.12K-L) with a rescue of disease phenotype in C9-3 MSNs (Figure 3.12L) as an effect of AUT1 wash. The average AP duration before and after AUT1 application decreased from 4.6ms to 3.5ms (paired *t-test*: $p=0.036$). This represents a large 24% decrease in AP duration from the same C9-3 MSNs and resembles previous reports by (Rosato-Siri et al., 2015). The average AP duration was similarly attenuated in C9-1 MSNs by 16% from 4.8ms to 4ms after AUT1 wash though statistically insignificant (Figure 3.12K) (paired *t-test*: $p=0.08$). Hyperpolarisation of the AHP was pronounced in both C9-MSNs (C9-1: paired *t-test*: $p<0.0001$; C9-3: paired *t-test*: $p=0.0004$) (Figure 3.12M-N). The average change in AHP for each C9-MSN following AUT1 treatment was 8 to 9mV (Figure 3.12M-N), identical to the efficacy of NS11021 for treated C9-3 MSNs. Crucially, AP duration and AHP that were previously dysfunctional in C9-derived striatal neurons are corrected with AUT1 treatment and fall in synchrony with previous DIV40 data from healthy controls and in the case of C9-3, C9-3Δ (Figure 3.9G, I).

3.4. Discussion

This chapter takes advantage of iPSC technology in generating a supply of striatal MSNs derived from physiologically relevant, C9ORF72 repeat expansion patients. Also, the power of this model is further augmented by the ability to generate, gene-edited isogenic lines specifically corrected for the G_4C_2 repeat expansion. The neurophysiological characteristics of iPSC-derived MSNs derived from C9 patients were then investigated using whole-cell patch-clamp electrophysiology to study whole-cell membrane currents and voltages changes under high resolution at the single-cell level. Using these techniques, I report striatal MSNs derived from multiple C9 patients become progressively hypoexcitable with time that did not arise due to any impairments in maturation. In response to depolarising current pulses a lower number of APs were recorded for all C9 patient MSNs compared to MSNs derived from healthy age-matched controls and a corresponding gene-edited isogenic line. The absence of a hypoexcitable phenotype in the gene-corrected isogenic line (C9-3Δ) strengthens the idea of the repeat expansion driving alterations in excitability. Close examination of the AP waveform provides clear evidence for ion channel dysfunction, with specific impairment of AP duration, threshold, amplitude and AHP all consistent with hypoexcitability in C9 MSNs. These impairments are argued not to coincide with a delayed maturation of C9 MSNs because the passive membrane properties and expression of transmitter-gated ion channels, which undergo maturation in MSNs (Beutler et al., 2011, Wang et al., 2024), are not disturbed in C9 MSNs. Specifically, dysfunction appears attributable, at least in part, to the family of post-threshold delayed outwardly-rectifying potassium channels (I_k), including Ca^{2+}-activated potassium channels, which have roles in regulating membrane repolarisation and influence AP duration and the AHP (Kshatri et al., 2018), parameters that were all impaired in C9 MSNs. Subsequent investigation into I_K channel function revealed downregulated channel function in MSNs generated from patients with the repeat expansion mutation. Lastly, selected pharmacological agents were washed onto C9 MSNs to: i) discern possible molecular mechanisms behind hypoexcitability and related waveform deficits and ii) determine whether such deficits could be alleviated. Amelioration of waveform impairments such as AHP, AP half-width, amplitude and threshold, but not excitability, were observed following pharmacological treatment with BK channel activator, NS11021 and/or K^+ channel modulator, AUT1. Therefore, the

data would suggest the contribution of dysregulated K^+ channel function is a likely contributor towards neurophysiological perturbations in AP waveform. These data are important for the strategy to generate tractable therapeutic targets to rescue such hypoexcitable dysfunction in C9 MSNs.

The electrophysiological data from striatal MSNs here demonstrates the broad scale upon which FTD/ALS impacts different regions of the CNS, that extends beyond areas typically associated with disease, in the cortex and spinal cord. Use of patch-clamp technology in this study provided novel insights into functional impairments that extend beyond the cortex and spinal cord in C9 iPSC-derived MSNs. These new data presents novel functional evidence for an emerging theme within FTD/ALS that implicates a dysfunctional role for the striatum in disease. Existing literature demonstrates frontostriatal dysfunction in FTD/ALS patients (Garibotto et al., 2011, Halabi et al., 2013, Bertoux et al., 2015, Moller et al., 2015, Landin-Romero et al., 2017), that would suggest a loss-of-function mechanism within these networks and aligns with MSN hypoexcitability reported here. The excitability of striatal MSNs is regulated in part by the excitatory glutamatergic inputs received from the cortex and thalamus (Cox and Witten, 2019), and inhibitory GABA-ergic innervations from the axon collaterals of other MSNs or inhibitory interneurons within the striatum (Tunstall et al., 2002, Tepper et al., 2004). Though, the data in this study would suggest MSN responses to glutamatergic (AMPA and NMDA) and GABA inputs are not afflicted in patient lines as observed by a lack of changes in the current density of these receptors expressed in C9 MSNs. In the context of FTD/ALS, the selective loss of excitatory inputs (Bertoux et al., 2015, Radakovic et al., 2018, Ahmed et al., 2021) and inhibitory inputs (Kato et al., 1994, Riku et al., 2016, Radakovic et al., 2018) are likely contributors to excitability changes within MSNs. Concurrent with this, a loss of glutamatergic and GABA-ergic transmission has previously been reported in FTD patients that can arise from a loss of neurons, pre-synaptic release or via a loss-of-function of post-synaptic glutamate receptors (Ferrer, 1999, Bowen et al., 2008, Sarac et al., 2008, Benussi et al., 2017). However, my data would indicate MSN responsiveness to such excitatory or inhibitory transmission are not diminished and therefore not the primary drivers of excitability changes in this model system at least. Instead, this study demonstrates intrinsic hypoexcitability within C9 MSNs, the principal cell type in the striatum. A loss-of-function mechanism in these inhibitory

GABA-ergic projection neurons would lead to a loss of subsequent inhibition at target sites innervated by striatal MSNs. This includes the external globus pallidus and the substantia nigra pars reticula which together comprise part of the striatal output nuclei in conjunction to striatal projections to the prefrontal cortex (Wilhelm et al., 2023). These output nuclei send excitatory projections towards the cortex via the thalamus, the relay station of the brain that is connected to various regions including the prefrontal cortex where thalamo-cortico-thalamic feedback loops are formed (Floresco, 2007, Narboux-Neme et al., 2012, Haber, 2016, Cox and Witten, 2019). Multiple lines of evidence have previously implicated dysfunction in FTD/ALS patient thalamus including presymptomatic cases of C9FTD/ALS (Rohrer et al., 2015, Cash et al., 2018, Murley et al., 2020, Bocchetta et al., 2021). Therefore, I would hypothesise reduced GABA-ergic signalling from C9 MSNs would consequently lead to increased excitation of FTD/ALS patient cortical regions through increased activity of the striatal output nuclei and thalamus as a result of reduced GABA transmission from the striatum. This coincides with cortical hyperexcitability commonly observed in FTD/ALS patients and the cognitive symptoms presented especially during disease onset and progression (Beagle et al., 2017, Agarwal et al., 2021, Higashihara et al., 2021). Ultimately, functional neuronal network deficits have been linked with clinical symptoms in FTD/ALS (Huber et al., 2022b). For instance, connectivity between the ventral striatum and prefrontal cortex form part of the salience network which has an essential role in processing responses to emotional and sensory stimuli (Seeley, 2019). In line with this, behavioural symptoms are reported in C9 patients that relate to dysfunction within the salience network circuitry (Lee et al., 2014). Thus, its plausible C9 MSN loss-of-function observed here could contribute to such network deficits.

Altered excitability within striatal MSNs has also been reported in other neurodegenerative disease such as Huntington's Disease (HD) which unlike FTD/ALS primarily affects the dorsal striatum (Reiner and Deng, 2018, Lim and Surmeier, 2020). Cognitive and psychiatric disturbances form a key feature of HD as the disease progresses (Paulsen, 2011, Blumenstock and Dudanova, 2020), that overlap with FTD phenotypes suggestive of pathological spillover into the ventral striatum. Furthermore, a hypoexcitable phenotype was observed in iPSC-derived MSNs from patients with multiple system atrophy (MSA) (Henkel et al., 2023). However, hyperexcitability within

the ventral striatum of a transgenic AD mouse model and in a motivationally supressed rodent model has been reported (O'Donovan et al., 2019, Fernandez-Perez et al., 2020). Such phenotypic variations in comparison to the findings in this study are likely to be attributable to differences in model system and disease. Nevertheless, these neurophysiological perturbations in the ventral striatum were postulated to play a role in apathy, anhedonia and addictive behaviours observed in AD patients (Fernandez-Perez et al., 2020). Indeed, microglial-induced hypoexcitability of striatal MSNs was sufficient in leading to changed eating habits, aversion and a negative affected state in murine models (Klawonn et al., 2021), which overlap with symptoms from bvFTD patients with dysfunction in ventral corticostriatal circuitries (Le Bouc et al., 2023). Moreover, MSN function has been shown to be important in the sleep-wake cycle (Mahon et al., 2006), that is crucially disturbed in C9-ALS patients (Guillot et al., 2025), which highlights the importance of tightly regulated MSN activity in striatal circuits that mediate key cognitive behaviours.

Investigation into the neuronal mechanisms that underlie reduced excitability in MSNs revealed this neurophysiological phenotype does not arise due to impairments in maturation of C9 MSNs. Analysis of intrinsic membrane properties (WCC, R_{in} and RMP), beyond being representative measures of neuronal development and maturation, demonstrate sub-threshold properties remain unchanged throughout maturation in C9 MSNs in relation to healthy and isogenic control MSNs. These sub-threshold properties are governed largely by basal, sub-threshold level, K^+ channels, including the K_v7 family, which in turn regulate excitability (Brown and Passmore, 2009, Moakley et al., 2019). Interestingly, pharmacological activators of K_v7 ion channels have been shown to reduce C9 patient-derived motor neuron hyperexcitability and improve MN survival (Wainger et al., 2014, Huang et al., 2021b), that have since translated into the clinical trial of the anti-convulsant drug and K_v7 activator, retigabine (Wainger et al., 2021). However, it could be argued that application of this pharmacological agent would be inappropriate in our hypoexcitable model of C9 MSNs, since subthreshold properties that are contributed to by K_v7 are not impacted. This alludes to the possibility of regional specific disease mechanisms at play in disease and thus the need for regionally specific disease therapeutics.

Neuronal function is governed by action potential generation which is comprised of distinct stages that are collectively orchestrated by ion channel activity. Examination of the different action potential phases revealed waveform deficits in evoked APs of C9 MSNs that were all consistent with a hypoexcitable phenotype. These post-threshold properties manifest in several forms, with reduced size and increased AP duration in addition to depolarisation of the AHP and threshold potential required to elicit APs observed in C9 MSNs. Accordingly, these data potentially implicate functional impairment within ion channels that facilitate these aspects of AP activity. The physiological implications of alterations in the AP waveform will likely have a significant impact on neuronal function at the single cell and network level. These are discussed below. In the first, whilst the data here would indicate glutamatergic receptor expression is not downregulated, depolarisation of the AP threshold in hypoexcitable MSNs is likely to reduce the efficacy in which glutamatergic synaptic transmission successfully induces AP transmission. In addition, lower amplitude of evoked APs may reduce the effectiveness of signal propagation and GABA release at pre-synaptic terminals of MSNs, resulting in lower synaptic release efficacy. Interestingly, a study by Henkel and colleagues demonstrated reduced spontaneous neuronal activity in iPSC-derived MSNs from MSA patients that may be linked to downregulation of $GABA_A$ and $GABA_B$ receptors and altered glutamate responsiveness, that differs from the data presented in this study. Nevertheless, disruption in the balance of neuronal excitation and inhibition in the striatum was shown (Henkel et al., 2023), that could contribute towards cognitive dysfunction (Jimenez-Balado and Eich, 2021). The spatial and temporal precision of AP firing is crucial in the functional role of MSN activity and subsequent GABA release properties vital for modulation of cognitive behaviours (Tritsch and Sabatini, 2012). Furthermore, and perhaps more significantly, increases in AP half-width and depolarisation of the AHP observed here in patient MSNs is consistent with impaired high-fidelity signalling associated with MSN function. Altogether, intrinsic hypoexcitability of C9 MSNs is likely to have functional consequences on the amplitude of stimuli required to generate MSN activity but also neurotransmitter release onto target cells.

Data from the laboratory indicate that Na_v expression is unchanged, thus ruling out reduced Na_v expression in driving reduced AP amplitude or depolarisation of AP threshold. In this regard, increased half-width and depolarised AHP is likely to cause

impaired deactivation-reactivation dynamics of Na_v channels, implying a reduced ability for the translation of synaptic inputs into high frequency and correctly timed AP output (Chen et al., 2006). Since, Na_v channel expression was not reduced, I next considered that delayed outwardly-rectifying K^+ channels (I_K), which contribute towards the latter stages of the downward AP repolarisation phase, were disturbed. Further since basal membrane properties were not changed, these data collectively suggest that it is post-threshold K^+ channels that are disturbed in C9 MSNs. Consistent with a loss of function at this part of the waveform, C9 MSNs displayed reduced I_K channel function in comparison to control and corresponding MSNs from isogenic controls. Critically, these data agree with numerous studies. Inhibition of I_K channel function with tetraethylammonium (TEA) leads to a prolongation of AP repolarisation (Stanfield, 1973), not only does this resemble a loss of I_K function but essentially phenocopies the AP waveform deficits in C9 MSNs. TEA leads to the non-specific inhibition of K_v channels, big conductance calcium-activated potassium (BK) channels and delayed rectifier channel currents (Gu et al., 2007), which have been shown to be reduced in sALS patients and SOD1 ALS patient-derived motor neurons (Shibuya et al., 2011, Wainger et al., 2014), are linked to neuronal hyperexcitability in ALS and epilepsy (Kanai et al., 2006, Wainger et al., 2014, Gao et al., 2022). Whilst, I_K channel expression is decreased in both ALS MNs and C9 MSNs, the I_K associated- MSN hypoexcitability observed here contrasts with I_K associated- MN hyperexcitability.

BK channel activity was specifically investigated due to its electrophysiological function closely corresponding with the hypoexcitable phenotypes in C9 MSNs. Firstly, channel function is blocked by TEA. Secondly, this ion channel can influence neuronal excitability in conjunction to AP duration and AHP that are perturbed here (Wang et al., 2014, Bock and Stuart, 2016, Contet et al., 2016). Indeed, BK channel inhibition has been shown to induce deficits in AP structure that closely resemble C9 patient MSNs (Hull et al., 2013, Kohashi and Carlson, 2014, Kimm et al., 2015). Thirdly, the sister subfamily of small conductance calcium-activated potassium (SK) channels, responsible for AHP current, represents a promising therapeutic candidate in ALS (Castelli et al., 2021, Catanese et al., 2021). Lastly, BK channels are notably expressed in MSNs therefore making it a prime candidate to rescue MSN hypoexcitability (Contet et al., 2016). To this effect, BK channel activator NS11021 (Bentzen et al., 2007), was adequate in rescuing waveform deficits (AP threshold,

amplitude and AHP). These data are important because it indicates that the impaired waveform of C9-MSNs can be pharmacologically rescued. However, importantly, the impact of this compound was insufficient in rescuing the hypoexcitable phenotype in C9 MSNs. Whilst prior studies have demonstrated BK channel gain-of-function induced increases in neuronal excitability (Brenner et al., 2005, Montgomery and Meredith, 2012), BK channel modulation has been shown to have diverse impacts on excitability, representing context dependent effects of BK channels on neuronal excitability (Gittis et al., 2010, Hull et al., 2013, Kimm et al., 2015). The functional consequences of modulating ion channel activity is complex, in nigral dopaminergic neurons modulation of BK channel function was cross-regulated and tightly coupled with K_v2 activity (Kimm et al., 2015). This would suggest there are additional mechanisms at play here responsible for reduced excitability in C9 MSNs that may relate to deregulated activity in functionally associated ion channels. This intricate interaction between the functional activity of different ion channels is an important consideration in the potential therapeutic design of ion channel modulators in FTD/ALS.

Similarly, TEA blocks voltage-gated K^+ channel function (Rudy and McBain, 2001), a family of K^+ channels important in the control of spike frequency and repolarisation (Rudy et al., 1999, Gittis et al., 2010). Here, I show using the potassium channel modulator AUT1, which is reported to target K_v3 channels amongst others (Rosato-Siri et al., 2015), constriction of spike width and hyperpolarisation of AHP. However, such data presents a complex enigma as a shortened waveform does not induce any changes in the excitability of C9 MSNs. Previously, both positive and negative modulation of K_v3 function have been shown to be related to either an increase or decrease in spike frequency and repolarisation kinetics, respectively (Rudy et al., 1999, Lau et al., 2000, Porcello et al., 2002, Lien and Jonas, 2003, Johnston et al., 2010), with the latter aligning with observations in C9 MSNs. Also, $K_v3.1$ knockout-mice also demonstrated reduced sleep behaviour (Espinosa et al., 2004) that is a phenotypical feature of FTD/ALS, thus highlighting the potential relevance of this ion channel in disease. Notably, there is limited evidence for K_v3 expression within striatal MSNs (Weiser et al., 1994) which could account for these regionally observed differences. Nevertheless, using NS11021 and AUT1 I show rescue of AP waveform deficits alone is insufficient in rescuing hypoexcitability in C9 MSNs. This points

towards a complex phenotypic mechanism that underlies neurophysiological perturbation with respect to AP waveform deficits and hypoexcitability in iPSC-derived C9 MSNs. Modulation of single K^+ channel activity is inadequate in a complete rescue of electrophysiological function. The most parsimonious explanation for these observations in patient MSNs is likely due to complex K^+ channel dysregulation that specifically impacts multiple subsets of post-threshold I_K channels and/or intricate deregulation of axon initial segment (AIS) function, where a multitude of these I_K channels are expressed.

The AIS located at the proximal region of the axon represents the site of AP initiation. This region located between the soma and proximal axon is a specialised microdomain defined by a complex molecular composition that includes the master scaffolding protein, ankyrin-G and a high density of Na_v and K_v (Huang and Rasband, 2018). The AIS has been shown to have a critical role in the regulation of neuronal excitability. This is characterised by its ability to remain 'plastic' via adjustment of its length or distance from the cell soma accordingly to maintain homeostatic control of neuronal excitability (Grubb and Burrone, 2010, Grubb et al., 2011, Wefelmeyer et al., 2015, Galliano et al., 2021). AIS pathology has been implicated in neurological disorders (Booker et al., 2020, Page et al., 2022), including FTD/ALS (Sohn et al., 2019, Bonnevie et al., 2020, Harley et al., 2023a). In the C9 iPSC-derived MSNs, I would hypothesise AIS disturbances in the form of a reduction in length or increased distance from the soma are critical instigators of MSN hypoexcitability. AIS remodelling in either form is likely to occur in the absence of changes in dendritic arborisation as indicated by a lack of changes in the whole-cell capacitance of C9 MSNs, a proxy for cell size. However, further work should be done to stain for and compare morphological characteristics between control and C9 MSNs. Indeed, the repeat expansion has been shown to induce significant alterations in neuronal branching and dendritic spine morphology in primary hippocampal cultures (Huber et al., 2022a). However, whether such changes in dendritic spine morphology and density would occur in my highly enriched iPSC-derived monocultures remains unknown. This relates to iPSC cultures being morphologically immature relative to primary cultures especially in the absence of astrocytes which are crucial for synaptic expression and maturity (Cerneckis et al., 2024). Interestingly, Lezmy and colleagues demonstrated chronic pharmacological block of I_k channels such as $K_v7.3$ thus mimicking a loss of ion channel function,

triggered a distal relocation of the AIS that resulted in a compensatory reduction in intrinsic excitability (Lezmy et al., 2017). Complex dysregulation of delayed rectifier currents are likely to induce deficits in AP waveform structure that conform with AIS-induced reduction in neuronal excitability. Together these represent core components of a dual mechanism that underlies electrophysiological dysfunction specifically in C9 patient iPSC-derived MSNs.

3.5. Conclusion

In this chapter, novel electrophysiological dysfunction in C9 MSNs is reported. Data generated provide functional evidence of reduced excitability in C9 MSNs and deficits in the AP waveform, especially in features that correspond to the repolarisation phase. The repeat expansion mutation in C9 MSNs is associated with downregulated I_k channel function that are not observed in controls or corresponding isogenic lines. Targeting select, post-threshold, I_k channel (BK and K_v3 potassium channels) function, which contributes directly towards the AP repolarisation phase, was sufficient in rescuing AP waveform deficits, but not excitability. These perturbations are therefore likely to be associated with a combination of structural alterations in the AIS and K^+ channel dysregulation in C9 MSNs. The translational impact of my findings and potential directions for future study are discussed further in Chapter 6.

Chapter 4: Lower Motor Neurons Derived from the Same Patient Lines Display Regionally Specific Enhancements in Neurotransmission

4.1. Introduction

ALS is characterised by the progressive degeneration of both upper and lower motor neurons. Perturbations of these neurons that form part of corticospinal motor circuitry that controls voluntary movements (Figure 1.2), ultimately give rise to progressive muscular atrophy, paralysis and death (Cleveland and Rothstein, 2001). Electrophysiological activity is essential for proper neuronal function, however in ALS, neuronal dysfunction tends to either lead directly to motor symptoms or indirectly by causing neuronal degeneration that leads to downstream symptomology. A prominent clinical symptom observed during symptomatic onset in ALS patients is the presence of muscular fasciculations, which may arise due to increased excitability of LMNs innervating the muscles (Geevasinga et al., 2016, King et al., 2016, Bashford et al., 2019, Menon et al., 2020). Neuronal hyperexcitability is also observed in early SOD1 rodent models (Quinlan et al., 2011, Martin et al., 2013). Indeed, hyperexcitability represents a therapeutic target for current (riluzole) and potential future treatments (Wainger et al., 2021, Hollingworth et al., 2024). The consensus from patient studies is that hyperexcitability within the locomotor circuits precedes hypoexcitability in the lower regions of the circuitry as symptomatic disease progresses (Pasniceanu et al., 2021). In the context of the *C9ORF72* mutation, LMN excitability is complex, with reports of unchanged, hyper- or hypo-excitability in several iPSC-derived LMN studies with phenotypes that can shift in temporal fashion (Sareen et al., 2013, Wainger et al., 2014, Devlin et al., 2015, Selvaraj et al., 2018, Burley et al., 2022, Harley et al., 2023a). The phenotypic variations reported in these studies likely stems from variations in differentiation protocols as well as the generation of mixed MN/glia populations. Excitability in enriched populations of iPSC-derived MNs from different protocols remains to be explored in the context of C9 disease.

A key pathogenic driver of disease progression in ALS is the selective vulnerability of LMNs to glutamate-induced excitotoxicity, that in turn, leads to LMN dysfunction and degeneration towards the latter stages of disease (Van Den Bosch et al., 2006). Glutamate is the major excitatory neurotransmitter in the CNS and excessive synaptic stimulation can trigger altered excitability and excitotoxicity of these neurons that can lead to muscular denervation and consequently, muscular atrophy and impaired movement (Pradhan and Bellingham, 2021). Dysregulation of Ca^{2+}-permeable AMPAr have been widely implicated as the molecular correlate that underpins this excitotoxicity (Cleveland and Rothstein, 2001), especially in the context of C9ALS (Selvaraj et al., 2018, Shi et al., 2018, Gregory et al., 2020, Mignogna et al., 2021). Interestingly, the role of NMDAr dysregulation, another family of Ca^{2+}-permeable glutamatergic receptors, whilst understudied, is now beginning to emerge in LMN excitotoxicity. Dysregulated NMDAr expression and activity has been shown in C9 models of disease (Shi et al., 2018, Xu and Xu, 2018, Dafinca et al., 2020). This study will help elucidate the functional expression and activity of these receptors in C9 iPSC-derived LMNs.

Furthermore, the work here will focus on the impact of the C9 mutation in the context of inhibitory GABA-ergic signalling in iPSC-derived LMNs. Indeed, reduced cortical GABA levels and deregulation of $GABA_AR$ signalling pathways have been reported in FTD/ALS patients, that can trigger a reduction in inhibitory cortical transmission (Foerster et al., 2012, Murley et al., 2020, Higashihara et al., 2024, Lorenc et al., 2024). Altered composition of $GABA_A$ receptor subunits have also been identified in patient data (Petri et al., 2003, Dangond et al., 2004), in addition to a loss of inhibitory GABA-ergic spinal cord neurons in a transgenic SOD1 mouse model (Hossaini et al., 2011). More recently, downregulation of pathways associated with synaptic signalling at GABAergic synapses has been reported in sALS and C9ALS (Aly et al., 2023).

The inherent advantage of iPSC technology allows us to generate different cell types from the same iPSCs, giving considerable scientific dexterity in being able to address whether specific cell types exhibit cell-specific phenotypic properties. In this regard, the previous chapter has demonstrated hypoexcitability in C9 MSNs. In this chapter, I have generated C9 MNs from the same parental iPSC lines to address whether C9 MSN hypoexcitability is a cell-specific feature or a shared feature with C9 MNs using

an identical electrophysiological characterisation of iPSC-derived MSNs in the previous chapter. Furthermore, characterising the physiological behaviour of C9 LMNs generated in this study will enable comparisons with the wide range of physiological phenotypes that have previously been published using C9 patient-derived LMNs (Pasniceanu et al., 2021), which have either utilised variations of the Du et al protocol (Du et al., 2015, Burley et al., 2022, Harley et al., 2023a), or alternative protocols (Bilican et al., 2012, Amoroso et al., 2013, Selvaraj et al., 2018).

4.2. Aims and Objectives

Previously in chapter 3, neurophysiological behaviour of striatal MSNs relating to excitability and neurotransmission were subject to detailed, electrophysiological investigation. Striatal dysfunction is classically associated with movement disorders like Huntington's disease (Milnerwood and Raymond, 2010). Impairments in the striatal function are not typically associated with FTD/ALS and are an overlooked feature of disease. Instead, there has been a predominant focus on LMN perturbations that are now considered a disease hallmark, with extensive characterisation of iPSC-derived LMNs from the molecular level to electrophysiological, that have been generated from divergent of differentiation protocols (Pasniceanu et al., 2021). Here, I hypothesise LMNs derived from the same iPSC-patient lines display neurophysiological impairments that may overlap with those previously observed in striatal MSNs or, provide evidence of regionally specific disease mechanisms in differing neuronal cell types.

To tackle this, patch-clamp electrophysiology was used to build an electrophysiological profile of motor neurons generated from the same iPSC lines as chapter 3 to compare profiles between different regions of the CNS. Therefore, any neuron specific or iPSC line specific phenotypes could be deciphered.

4.3. Results

4.31 Generation of iPSC-derived Motor Neurons

To address this, motor neurons were derived from the same unaffected control iPSC lines plus an additional control line (Con-3) along with patient lines harbouring the *C9ORF72* G_4C_2 repeat as described in Results 1 (Con-1, Con-2, Con-3, C9-1, C9-2, C9-3). An isogenic line (C9-2Δ) was employed in this chapter which is different to that in chapter 3 because the C9-3Δ line did not efficiently differentiate into motor neuron populations. Similarly, the Con-3 line was discontinued for similar reasons. The Du et al., 2015 protocol was utilised and summarised in Figure 4.1A and detailed in Methods section 2.17.

Briefly, NPCs were differentiated from iPSCs as described in Methods section 2.14 and at this stage identical to the MSN protocol. However, from the NPC stage progenitors were incubated with a variety of different neurotrophic factors to induce specification of young motor neurons and eventually mature motors neurons at day 40 (Figure 4.1A). To note, LMN timepoints are referred to from post iPSC-differentiation. Motor neurons derived from the lines described using the same protocol have previously been characterised in detail (Castelli et al., 2021, Zhang et al., 2022). For all lines examined, cultures contained >90% cells that stained for neuronal marker, MAP2, at DIV40 (Figure 4.1B-C), and were enriched for MN specific markers, ChAT (>80% cells, Figure 4.1B, D) and also SMI-32 (Sances et al., 2016). The cultures generated from each line are highly enriched and comparable in their cellular specification.

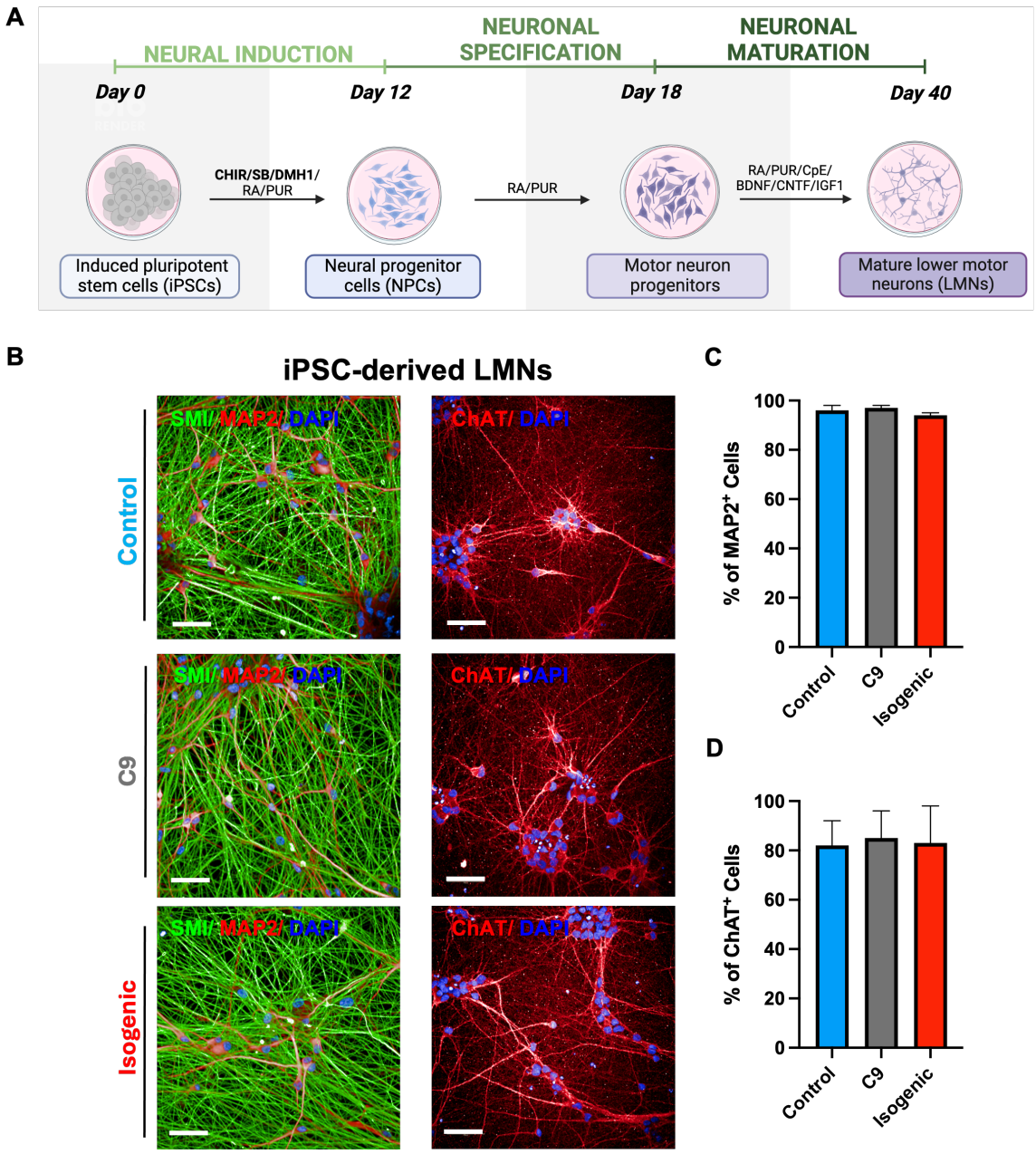

Figure 4.1. Generation of highly enriched LMN cultures from human iPSCs. (A) Fibroblasts were acquired from healthy and C9-patients (Table 2.1) and reprogrammed into iPSCs that underwent neural induction, specification and maturation as detailed in the Methods chapter (Sections 2.1.4- 2.1.5 and 2.1.7). The dual-SMAD inhibition method was used to induce the neuralisation of stem cells. Patterning of NPCs into LMN progenitors was stimulated by RA and PUR treatment. To promote development of motor neuron progenitors, from day 19 to 28 progenitors were treated with a combination of neurotropic factors including RA, PUR, compound-E, BDNF, CNTF and IGF-1. At day 29 to 40 treatment continued with BDNF, CNTF and IGF-1 factors only to promote functional maturation of LMNs. Timepoints cited in this thesis with respect to motor neurons represent the time post iPSC-differentiation (Day 0) to LMN maturation (Day 40) and an extended maturation timepoint at day 50. Figure created in BioRender. **(B)** Representative images of day 40 control, C9 and C9-isogenic LMNs stained for the neuronal markers neurofilament protein (SMI) (green)

and either MAP2 or mature motor neuron marker ChAT (red). Nuclei were counterstained with DAPI (blue). Scale bars: 50 µm. **(C-D)** Bar graphs showing the total number of **(C)** MAP2+ and **(D)** ChAT+ cells expressed as percentage of total number cells counted; Values expressed as mean ± SEM. Highly enriched MAP2+, ChAT+ LMN populations were generated at day 40. Note, images and quantification data were provided by Dr Cleide De Souza. Data, MAP2: Control LMN: N=3; C9-LMN: N=3; Isogenic LMN: N=3; ChAT: Control LMN: N=3; C9-LMN: N=3; Isogenic LMN: N=3. No significant differences between each parameter was determined by means of one-way ANOVA followed by Tukey's multiple comparison test.

4.32 Electrophysiological Characterisation of Motor Neurons

Previously, characterisation of ALS iPSC-derived motor neuron excitability has been reported in a multitude of excitability phenotypes ranging from hypoexcitable (Sareen et al., 2013, Zhao et al., 2020), hyperexcitable (Wainger et al., 2014) or unaltered (Selvaraj et al., 2018). Moreover, use of the same protocol (Du et al., 2015) in the presence of astrocytes was sufficient to alter excitability in C9 iPSC-derived LMNs (Harley et al., 2023a). Importantly, C9-LMNs in the absence of astrocytes using the Du et al., 2015 protocol has not been reported. Further, the ability to cross reference excitability in other neuron types using the same starting iPSCs has rarely been performed, thus the potential for the iPSCs themselves to be driving the altered excitability phenotype has not been addressed.

As a result, day 40 LMNs were evaluated using whole-cell patch-clamp electrophysiology in the current-clamp configuration. Recordings were conducted in the presence of standard extracellular solution (Table 2.14) complemented with blockers of synaptic transmission. From a holding potential of -74mV (LJP corrected), cells were depolarised using sequential 5pA current pulses that ranged from -20 to +50 pA. To help determine the functional maturation of DIV 40 and DIV 50 MNs their capacity to fire action potentials were then examined (Xu et al., 2023). Initially, the output of the individual cell was classified as non-firing, firing single APs or multiple APs (Figure 4.2A). APs were defined by voltage responses above 0 mV. By day 40, LMNs from each control line exhibited robust firing patterns, with at least 85% of all cell lines firing multiple APs (Figure 4.2B). C9-LMNs appeared to show a modest decrease in active cells, with 13-25% of patient lines presenting with single or no AP response from depolarising current stimuli. Nonetheless, robust firing was still

observed overall (Figure 4.2B). The C9-2Δ LMNs also showed comparable firing patterns to its C9-2 counterpart (Figure 4.2B). Firing patterns in C9-LMNs do not appear to be substantially different at 40 days post iPSC differentiation. The robust firing activity observed at day 40, further validates the functional maturity of these neurons at day 40. To test whether the firing patterns of patient-derived LMNs developed impairments with greater culture time, a subset of cultures were taken to day 50. At this timepoint, multiple firing activity was observed uniformly across all lines including those from case lines (Figure 4.2C), comparable with previous reports in an iPSC-derived study from C9 and TDP-43 patients (Harley et al., 2023a). Both C9-1 and C9-2 did demonstrate progressive increases in activity from day 40 to 50 by 13% and 25% respectively (Figure 4.2D). This robust firing activity is evidenced from representative membrane potential recordings presented in Figure 4.3 for each line at day 40, and for select lines, at day 50. These data indicate no clear differences in the firing patterns exhibited by C9-LMNs versus control and isogenic lines. This differs from previous ALS data from iPSC-derived LMN studies (Sareen et al., 2013, Naujock et al., 2016). Hence, even at the most basic level of characterisation, the data provide a strong contrast to the voltage responses of C9-MSNs (Figure 3.2-3.3).

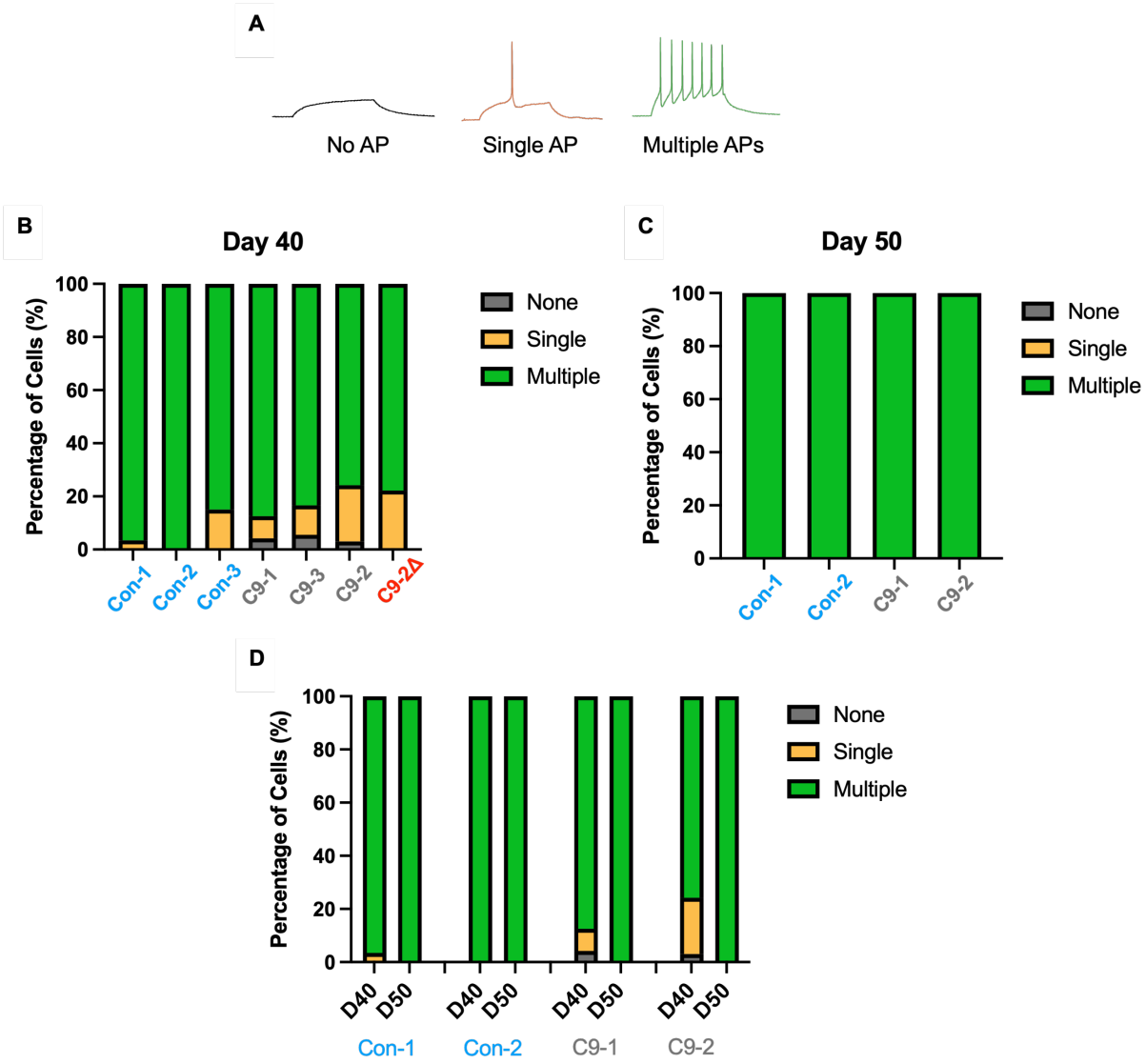

Figure 4.2. Characterisation of voltage responses in day 40 and 50 LMNs. (A) The intensity of AP firing observed following current injections were grouped into three separate categories; no response: where voltage responses failed to surpass 0 mV, firing of a single AP or multiple APs. **(B)** Percentage of Con-1, Con-2, C9-1 and C9-2 LMNs displaying each firing category at days 40 and 50 post iPSC-differentiation. During this period LMNs develop an increased propensity to fire multiple APs from day 40 to 50 with this trend most prominent in both the C9-1 and C9-2 LMNs. **(C-D)** Activity levels remain consistently high across all cell lines at all timepoints. **(D)** All cells exhibit multiple AP firing capacity in response to current stimulation at day 50. Data: Con-1: day 40, n=29, N=7; day 50, n=15, N=3; Con-2: day 40, n=7, N=2; day 50, n=7, N=2; Con-3: day 40, n=20, N=5; C9-1: day 40, n=24, N=7; day 50, n=13, N=3; C9-3: day 40, n=18, N=5; C9-2: day 40, n=33, N=9; day 50, n=11, N=4; C9-2Δ: day 40, n=18, N=4.

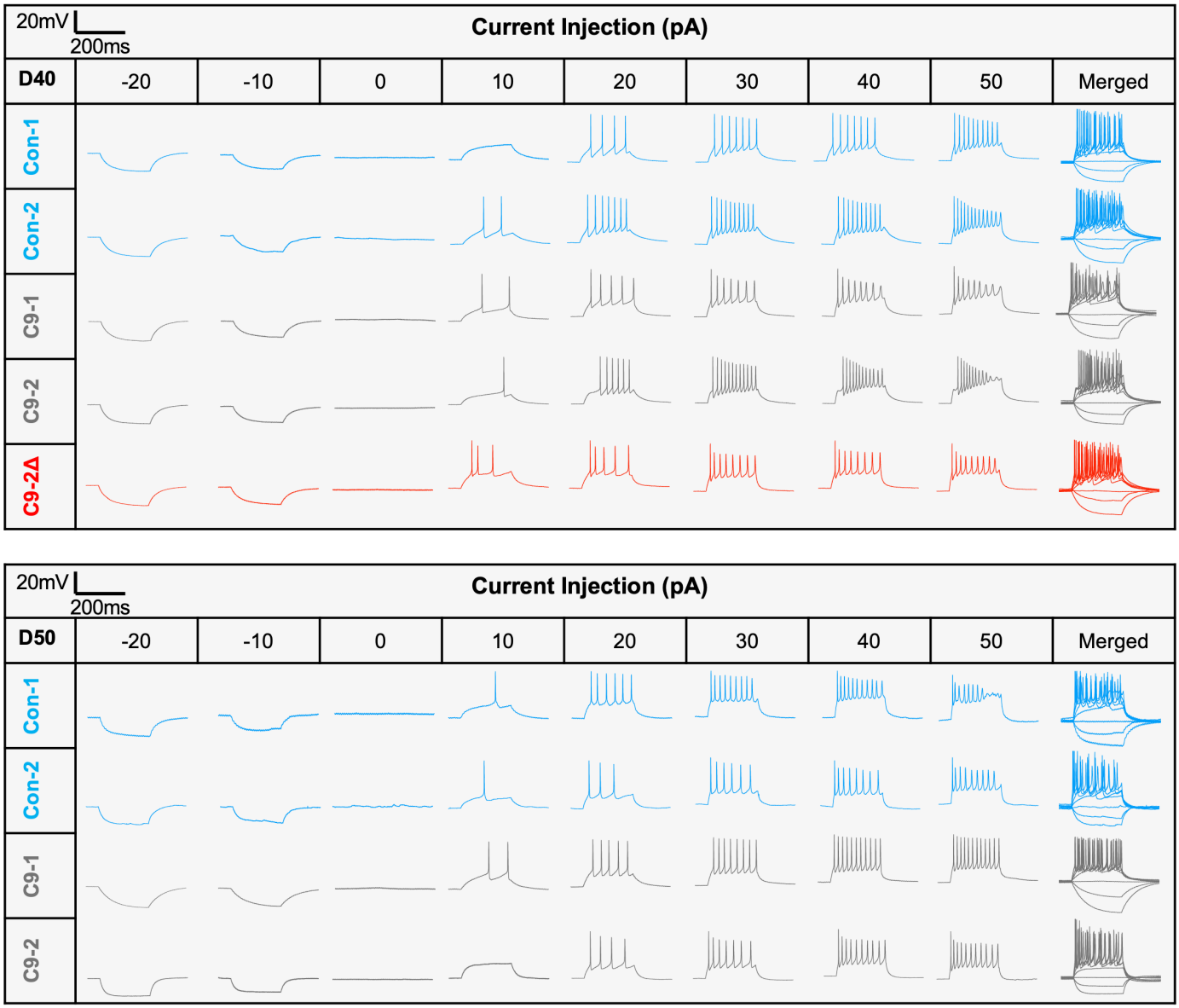

Figure 4.3. C9-LMNs do not display a loss-of-function phenotype. Matrix schematic of illustrative AP traces recorded in the whole-cell current-clamp configuration from individual cells reveal C9-LMNs do not exhibit impairments in excitability. Voltage responses are shown from healthy control lines (blue), C9 patients (grey) and a paired isogenic line C9-2Δ (red) in response to a train of incremental current injections (-20pA to 50pA in 10pA steps) from a LJP corrected resting membrane potential held at -74mV. AP traces were attained from LMNs once full maturation was reached at day 40 and at a later maturation point (day 50).

4.33 Current Stimulus- Action Potential Output Relationships for iPSC-derived LMNs

Firing patterns give an initial overview of excitability properties. However, given that the vast majority of cells for all lines exhibited robust, multiple firing action potential profiles, it is possible that this level of analysis potentially masks altered excitability profiles, i.e., if one MN line fires 3 action potentials on average, whilst another fires 10, they are clearly different, but yet will be classified as multiple APs. Current stimulus input-action potential output (I-O) relationships were therefore constructed for each line investigated at both day 40 and 50 to enable in-depth analysis of motor neuron excitability (Figure 4.4). This involved stimulus protocols previously established for striatal MSNs (0 to +50pA, 5pA steps, 500ms duration).

The I-O data for MNs independent of timepoint or cell line showed an increased intensity in AP output as current stimulation became more depolarised (Figure 4.4), as expected from iPSC-derived motor neurons (Sareen et al., 2013, Cutarelli et al., 2021). Towards higher current depolarisations (35-50pA) this relationship started to plateau in LMNs derived from control iPSC lines and cells demonstrated accommodation of AP firing (Figure 4.4A-B), which was similarly described by Xu et al., 2023. Neuronal cell cultures extended to a day 50 timepoint for Con-1 and Con-2 either demonstrated a significant increase in excitability for (two-way ANOVA: Con-1: $F (10, 410) = 2.485$, $p= 0.0067$) or were comparable to day 40 data (two-way ANOVA: Con-2: $F (10, 100) = 0.2226$, $p= 0.9936$), respectively (Figure 4.4A-B). C9-LMNs behaved similarly to control lines (Figure 4.4C-D) at day 40, with a slight enhancement of AP responsiveness observed in C9-1, though non-significant (two-way ANOVA: $F (10, 350) = 1.202$, $p= 0.288$), but significantly for C9-2 at day 50 with an equivalent protocol (two-way ANOVA: $F (10, 410) = 2.938$, $p= 0.0013$) (Figure 4.4C-D). Comparative analysis for all lines, including isogenic C9-2Δ and female Con-3 at day 40 (Figure 4.4E), yielded insignificant differences in the AP responsiveness (two-way ANOVA: $F (60, 1380) = 1.330$, $p= 0.4328$), indicating that at day 40 LMNs from the lines investigated did not show any notable differences in neuronal excitability. To determine whether a phenotype emerged at a later time point, day 50 LMNs were investigated (Figure 4.4F), but still no significant differences were observed between lines (two-way ANOVA: $F (30, 410) = 1.424$, $p= 0.07$). Full statistical details of day 40 and day 50 post-hoc tests are described in Appendix 6.

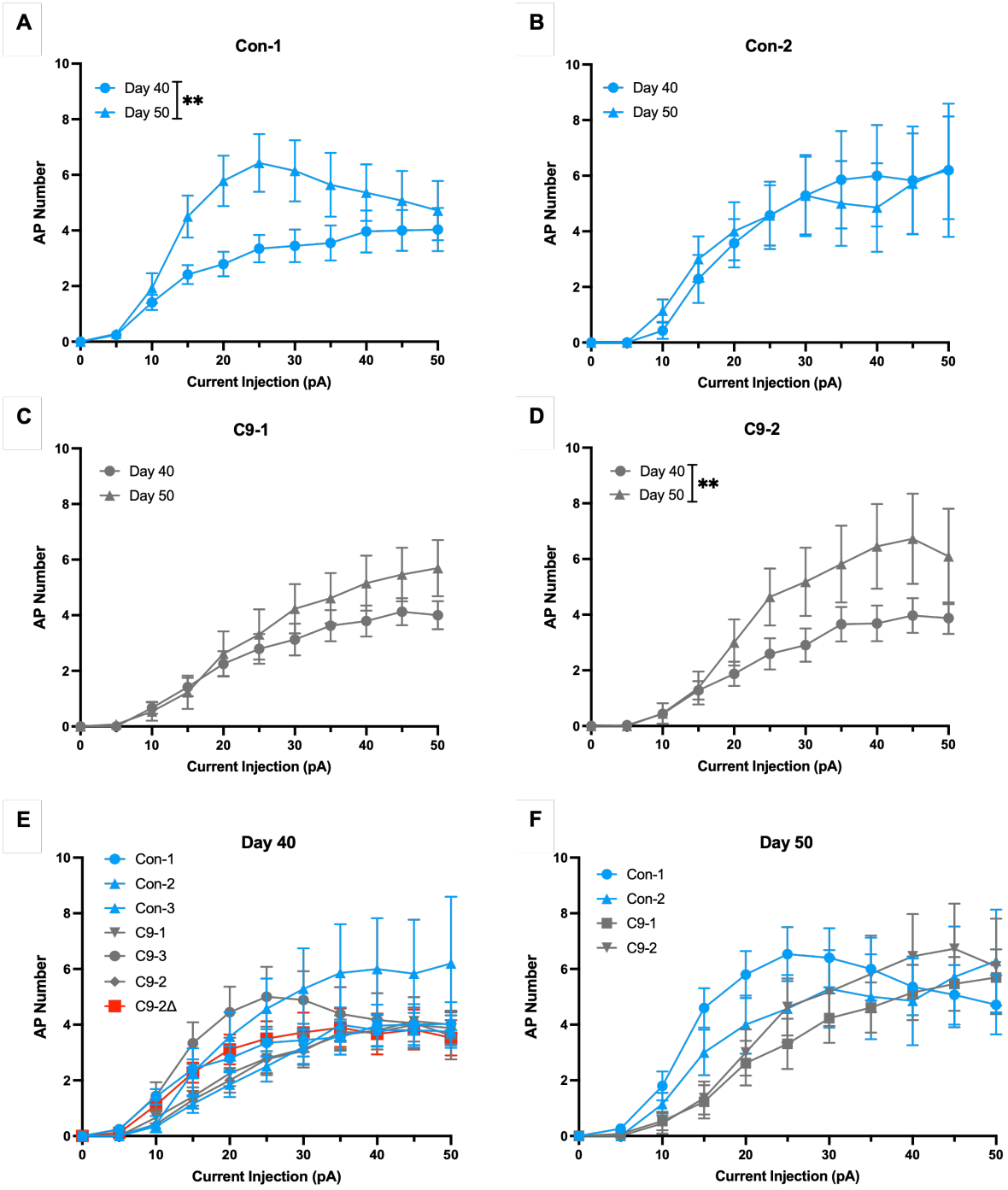

Figure 4.4. Mature LMNs derived from the same C9-patients are not hypoexcitable. (A-D) The number of APs evoked following current stimulation stratified by timepoint (day 40 and 50) for (**A)** Con-1, (**B)** Con-2, (**C)** C9-1 and (**D)** C9-2 LMNs demonstrate trends towards increased excitability between day 40 and 50 for all cell lines bar Con-2. **(E-F)** All C9-LMNs at day 40 and 50 show similar levels of responsiveness to depolarising current injection compared with healthy controls and between the C9-2 vs C9-2Δ LMNs at day 40. Notably, there were no large differences in the AP number of the female Con-3 line versus all other male lines. All data presented as Mean (±SEM). * p<0.05 from repeated measures two-way ANOVA followed by Tukey's multiple comparisons test. Data: Con-1: day 40, n=29, N=7; day

50, n=15, N=3; Con-2: day 40, n=7, N=2; day 50, n=7, N=2; Con-3: day 40, n=20, N=5; C9-1: day 40, n=24, N=7; day 50, n=13, N=3; C9-3: day 40, n=18, N=5; C9-2: day 40, n=33, N=9; day 50, n=11, N=4; C9-2Δ: day 40, n=18, N=4.

This contrasts with previously published iPSC-derived LMN data that have either described no changes in excitability as reported here (Selvaraj et al., 2018), or hyper- (Wainger et al., 2014) and hypoexcitable phenotypes (Sareen et al., 2013, Naujock et al., 2016) in ALS patient lines that can be influenced with maturation time (Devlin et al., 2015, Burley et al., 2022, Harley et al., 2023a). Nevertheless, C9 patient -derived LMNs generated in this study do not show any differences in the I-O relationship. These data place further emphasise that the I-O relationship observed in C9 iPSC-derived MSNs is due to cell type specification, rather than the inherent properties of the iPSC lines.

4.34 Sub-threshold Properties in C9 LMNs

To rule out potential subthreshold differences not observed in the I-O relationship, passive membrane properties relating to the WCC, R_{in} and RMP were investigated from LMNs at both day 40 and 50 timepoints.

The WCC was measured at day 40 in control MNs and found to be consistent with previous reports for iPSC-derived LMNs differentiated using the same Du et al., 2015 based protocol (Burley et al., 2022, Zhang et al., 2022). Data for patient case lines trends toward an increased WCC versus control lines, where the C9-2 MNs show a significant increase in WCC (Kruskal-Wallis test: $p<0.05$) versus Con-1 (Dunn's multiple comparison test: $p=0.04$), Con-3 (Dunn's multiple comparison test: $p=0.019$) and the C9-2Δ MNs (unpaired *t-test*: $p=0.0019$) (Figure 4.5A) and similar to reports from an iPSC-derived MN study (Harley et al., 2023a). Extending the cultures by a further 10 days led to increases in WCC becoming more prominent, significance was demonstrated between each control lines versus C9 lines (Kruskal-Wallis test: $p<0.05$; Dunn's multiple comparison test: Con-1 vs C9-1: $p<0.0001$; Con-1 vs C9-2: $p=0.0097$; Con-2 vs C9-1: $p=0.028$) (Figure 4.5B).

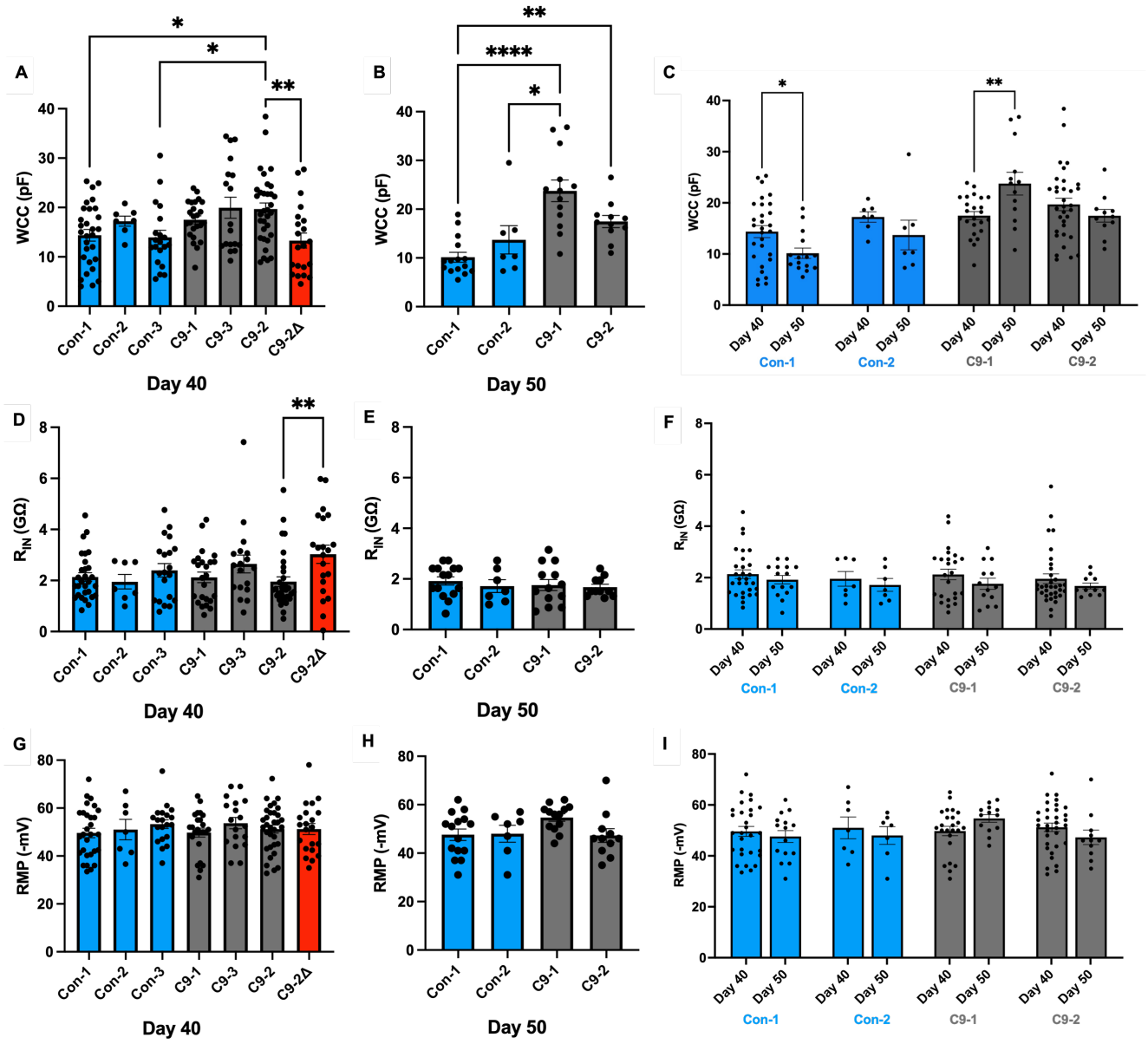

Figure 4.5. Passive membrane properties are not altered in C9-LMNs. (A-I) Intrinsic membrane property data from day 40 is from Con-1, Con-2, Con-3, C9-1, C9-3, C9-2 and C9-2Δ lines and data at day 50 and across both timepoints are from Con-1, Con-2, C9-1 and C9-2 cell lines. Quantification of the mean **(A-C)** whole cell capacitance (WCC) from both days 40 and 50. Individual cells are represented by individual circles superimposed onto the bar graphs. C9-LMNs were generally larger in WCC across this time period versus control and the paired isogenic line. Trends towards a smaller WCC at the later day 50 timepoint were also noted for control and C9-lines. Quantification of the average **(D-F)** membrane input resistance (R_{IN}) at both timepoints was for the most part consistent across all maturation stages. Quantification of the mean **(G-I)** resting membrane potential (RMP) was unaffected with maturation. Of note, no differences in maturation were observed between female Con-3 and all other male cell lines. All data presented as Mean (±SEM). * p<0.05, ** p<0.01, **** p<0.0001 from one-way ANOVA followed by Sidak's multiple comparisons

test or Kruskal-Wallis test followed by Dunn's multiple comparisons test and unpaired t-test (C9-2 vs C9-2Δ). Data: Con-1: day 40, n=29, N=7; day 50, n=15, N=3; Con-2: day 40, n=7, N=2; day 50, n=7, N=2; Con-3: day 40, n=20, N=5; C9-1: day 40, n=24, N=7; day 50, n=13, N=3; C9-3: day 40, n=18, N=5; C9-2: day 40, n=33, N=9; day 50, n=11, N=4; C9-2Δ: day 40, n=18, N=4.

Typically, WCC increases with MN maturation (Devlin et al., 2015, Selvaraj et al., 2018), however the WCC data here, with the exception of C9-1, negatively correlates with maturation time between day 40 and 50 (unpaired *t-test*: day 40 vs 50: Con-1: p=0.02; C9-1: p=0.0028) (Figure 4.5C). Nonetheless, the data are consistent with an increased WCC in C9 LMNs, which is not a feature of C9 MSNs (Results 1, Fig 3.5A-B).

R_{in} was determined in the same manner as described for iPSC-derived MSNs. R_{in} values for control lines were equivalent to those previously reported for LMNs derived from iPSCs using the same protocol (Zhang et al., 2022) or ones different from this study (Zhang et al., 2015). C9 LMNs did not show any significant differences relative to control lines at day 40 or 50 (Kruskal-Wallis test: p>0.05) (Figure 4.5D-E) but statistical differences were noted between C9-2 and its gene-edited control C9-2Δ (unpaired *t-test*: p=0.005). R_{in} is expected to decrease with maturation, reflecting an increased level of subthreshold potassium channel expression, and a trending, but statistically insignificant decrease in R_{in} is observed in all lines from day 40 to day 50 (Figure 4.5F) and complements prior studies by Cutarelli et al., 2021. R_{in} is not impacted in C9 LMNs.

The membrane potential of the cell at rest, without any stimulation (RMP) provides a critical readout of cell health, with healthy cells maintaining a resting potential towards more hyperpolarised membrane potentials (Abdul Kadir et al., 2018). Hence, the RMP of these motor neurons were also characterised. Data values obtained for case lines were consistent with control or isogenic lines at days 40 and 50 (one-way ANOVA: p>0.05) (Figure 4.5G-H), whilst RMP values remained unchanged over time (unpaired *t-test*: p>0.05) (Figure 4.5I). Of note, these insignificant differences were in sync with data from Zhang et al., 2015; Cutarelli et al., 2021, that utilised different MN differentiation protocols. Interestingly, these data deviate from iPSC-derived MN studies that have documented both depolarised (Sareen et al., 2013, Devlin et al.,

2015) and in studies utilising the same MN protocol, hyperpolarised RMPs (Burley et al., 2022, Harley et al., 2023a), though reported values in Burley et al., 2022 were insignificant. Nevertheless, RMP is not impacted in C9 LMNs generated in this study utilising the Du et al., 2015 protocol. These data highlight that MNs lack any C9 dependent shifts in the R_{in} or RMP properties and would therefore indicate no meaningful differences in maturation versus control lines. WCC is however increased, which is different to MSNs, and presents a potential phenotype that is specific to C9 LMNs.

4.35 AP Properties are not Impacted in C9 LMNs

Thus far, C9 iPSC-derived LMNs have produced equivalent I-O relationships relative to control or isogenic lines and with the exception of an enhanced membrane size, have shown inconsequential differences in intrinsic membrane properties. Even so, it is possible AP waveform properties could still be impacted and were therefore investigated next from the first evoked AP (Figure 4.6).

The first property to be investigated was the rheobasic current (Figure 4.6A-C). For analyses of AP parameters, MNs that did not fire any APs were excluded from the analyses. Unlike C9-3 that had a similar rheobase to control lines, the rheobase was drastically altered in day 40 C9-2 LMNs in relation to its paired isogenic line (unpaired *t-test*: $p=0.0018$) and Con-1 (Kruskal-Wallis test: $p<0.05$; Dunn's multiple comparison test: $p=0.0099$) (Figure 4.6A). The rheobase for patient C9-1 line was similar elevated in comparison with Con-1 and Con-2, though insignificant (Dunn's multiple comparison test: $p>0.05$). Statistically insignificant increases in C9 LMN rheobasic current were detected again at the later day 50 timepoint (Kruskal-Wallis test: $p>0.05$) (Figure 4.6B). Overtime there was a slight reduction in recruitment current, with the exception of C9-1 where the rheobase marginally increased (Figure 4.6C). The lack of consistent or meaningful changes in the rheobase of C9 LMNs aligns with I-O relationships previously established in Figure 4.4 as well as earlier reports by Cutarelli et al., 2021. Whilst a greater driving force might have been required in some C9 LMNs to evoke APs, this was not significant enough to influence excitability as once voltage activity of MNs was initiated, they began to fire very actively. AP threshold at day 40 was shown to be very consistent at ~45mV amongst all lines (Figure 4.6D).

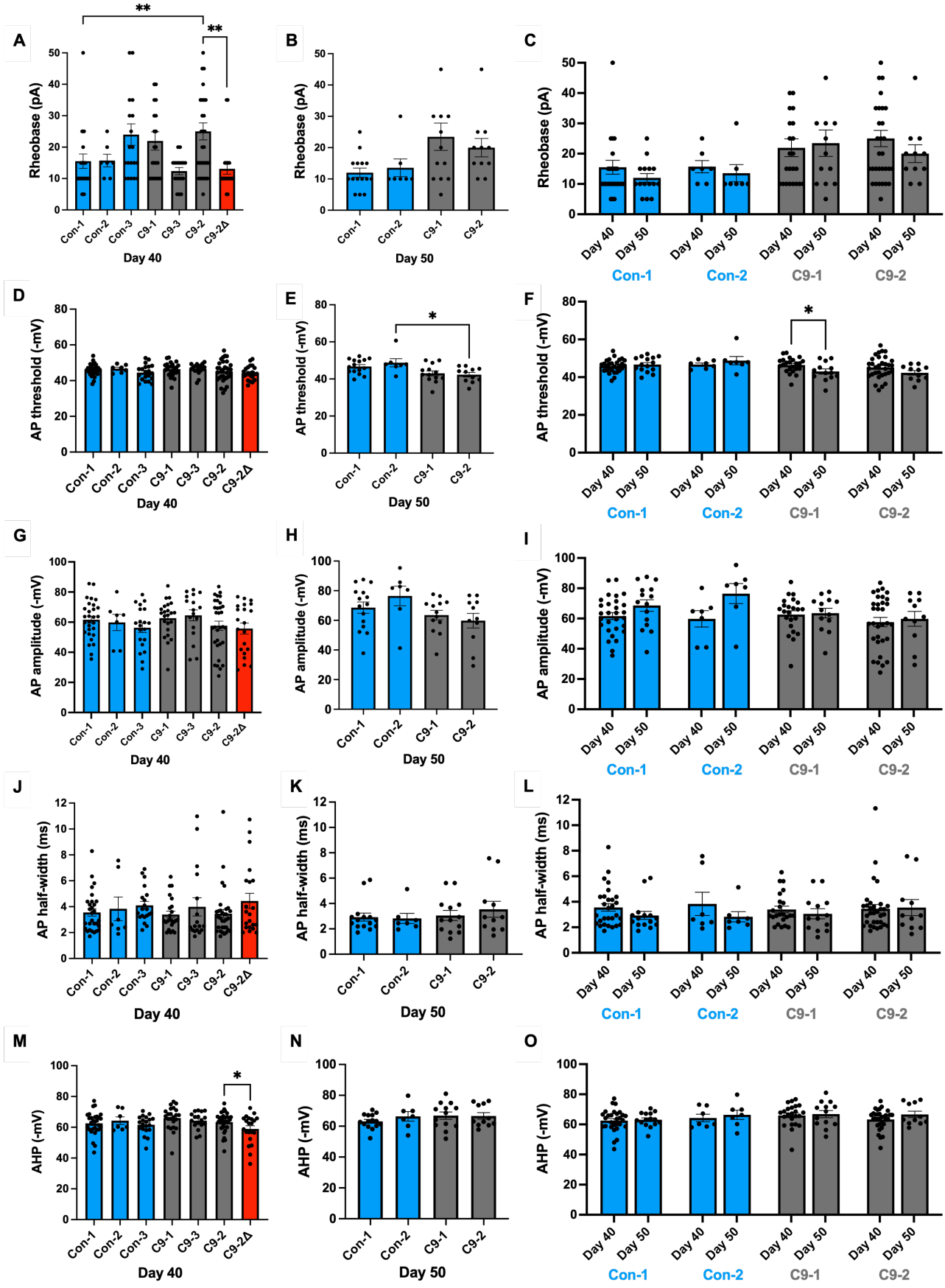
A
B
C
D
E
F
G
H
I
J
K
L
M
N
O
Rheobase (pA)
AP threshold (-mV)
AP amplitude (-mV)
AP half-width (ms)
AHP (-mV)
Con-1
Con-2
Con-3
C9-1
C9-3
C9-2
C9-2Δ
Day 40
Day 50
**
*

Figure 4.6. Key parameters that govern AP structure are unaltered in mature LMNs derived from the same C9 patients. AP parameters were measured and compared from day 40 Con-1, Con-2, Con-3, C9-1, C9-3, C9-2 and C9-2Δ lines and data at day 50 and across both timepoints are from Con-1, Con-2, C9-1 and C9-2 cell lines. Individual cells are represented by individual circles overlaid onto the bar graphs. Measurements of the the recruitment current required to evoke the first AP (rheobase) **(A-C),** threshold potential **(D-F),** AP amplitude **(G-I)**, AP duration **(J-L)** and AHP **(M-O)** were recorded for the first AP evoked by current stimulation at days 40 and 50. All data presented as Mean (±SEM). * $p<0.05$, ** $p<0.01$, from one-way ANOVA followed by Sidak's multiple comparisons test or Kruskal-Wallis test followed by Dunn's multiple comparisons test and unpaired t-test (C9-2 vs C9-2Δ). Data: Con-1: day 40, n=29, N=7; day 50, n=15, N=3; Con-2: day 40, n=7, N=2; day 50, n=7, N=2; Con-3: day 40, n=20, N=5; C9-1: day 40, n=23, N=7; day 50, n=13, N=3; C9-3: day 40, n=17, N=5; C9-2: day 40, n=32, N=9; day 50, n=11, N=4; C9-2Δ: day 40, n=18, N=4.

A slight depolarisation of threshold was noted in day 50 C9 LMNs (Figure 4.6E), especially between Con-2 and C9-2 (Kruskal-Wallis test: $p<0.05$; Dunn's multiple comparison test: $p=0.05$), which corresponds with the trended increases in rheobase currents that were detected in Figure 4.6B. The threshold potential remained unchanged in both control lines (unpaired *t-test*: day 40 vs day 50: Con-1 and Con-2: $p>0.05$) but was depolarised in C9-1 (unpaired *t-test*: $p=0.029$) and ever so slightly in C9-2 overtime (unpaired *t-test*: $p=0.14$) as LMNs were maintained for longer in culture (Figure 4.6F). Like the recruitment current data, any depolarisations of threshold potential were inconsequential in affecting LMN voltage activity.

Comparative analysis of the size of AP evoked was coherent between all lines at day 40 (Figure 4.6G). Extended analysis at day 50 appeared to show a trending enlargement of AP amplitude in control versus patient lines (Figure 4.6H) in line with previous amplitude characterisation at a later timepoint (Harley et al., 2023a). Amplitude has been shown to increase with maturation time (Cutarelli et al., 2021, Xu et al., 2023) and this was supported by longitudinal increases in amplitude observed in Con-1 and Con-2 between recording timepoints that was not seen for patient lines. In line with previous measurement of AP parameters, amplitude deviations were non-significant after statistical comparisons (Kruskal-Wallis test: $p>0.05$) (Figure 4.6G-I).

The next AP parameters to undergo close evaluation was the AP duration (Figure 4.6J-L) and AHP phase of the AP (Figure 4.6M-O). Across all control, isogenic and case

lines studied at day 40 and 50, the AP half-width remained unaltered (Figure 4.6J-K) as characterised in earlier work from iPSC-derived TDP-43 patient lines (Harley et al., 2023a). The absence of any C9-specific or gender-specific phenotypes also extended to the comparative analyses of AHP at these timepoints (Figure 4.6M-N), with AHP remaining unchanged between day 40 to 50 (Figure 4.6O). Although a statistical anomaly, the AHP of day 40 C9-2Δ was significant depolarised with respect to C9-2 LMNs (unpaired *t-test*: p=0.049). Generally, the half-width duration did appear to decrease slightly with maturity which correlates with data from Arama and colleagues, aligning with this parameter being a barometer of functional maturation (Arama et al., 2015) (Figure 4.6L). Overall, the post-threshold properties that govern the AP waveform unlike C9 striatal MSNs are universally undisturbed in C9 LMNs. Thus, the *C9ORF72* repeat expansion would not only appear to induce hypoexcitability but also directly affects waveform-related ion channel activity in striatal neurons. Yet, the same mutation lacks the pathophysiological efficacy to translate these phenotypes in LMNs, a classically associated-ALS neuronal cell type.

4.36 Inhibitory GABA-ergic Responses are Potentiated in C9 LMNs

Until now a lack of phenotypic differences in neuronal excitability or AP waveform has been observed in C9-derived LMNs generated from the Du et al., 2015 protocol. The coordination and balance of both excitatory and inhibitory signalling are key for the regulation of LMN excitability. Accordingly, LMN responses to inhibitory GABA-ergic and excitatory glutamatergic transmission were characterised. Previous studies of inhibitory GABA-ergic signalling in ALS have predominantly focused on signalling within the cortical regions of clinical patients (Kujirai et al., 1993, Menon et al., 2020) or in pre-clinical murine models (Nieto-Gonzalez et al., 2011, Khademullah et al., 2020). Though recent work has begun to converge on inhibitory signalling lower down the motor circuitry (Martin and Chang, 2012, Allodi et al., 2021), GABA-ergic signalling has not been characterised in the context of the *C9ORF72* repeat expansion at the LMN level.

Assessment of functional expression of $GABA_A$Rs was conducted from LMNs at 40 days post iPSC-differentiation using experimental protocols previously described in

results section 3.34. Briefly, GABA-ergic membrane currents were evoked from control, case and the following bath application of GABA (100μM) in the presence of TTX, to inhibit AP generation that could otherwise interfere with recorded membrane currents (Figure 4.7A-B). To confirm expression of $GABA_AR$- mediated currents in day 40 and 50 LMNs, receptor antagonists bicuculine (30μM) was washed on to blocked elicited current responses (Figure 4.7C).

GABA-evoked membrane currents responses were qualitatively assessed into non-responsive or responsive groups. In day 40 voltage-clamp recorded LMNs, 26% and 58% of Con-1 and C9-2Δ LMNs failed to respond to GABA stimulation. This was considerably less in comparison to C9-1 to C9-3 lines whereby the maximum amount of non-responders was in C9-2 LMNs at 16% (Figure 4.7D). By day 50, there was uniform responses to GABA in Con-2 and C9 LMNs with a marked reduction in the number of GABA non-responsive Con-1 LMNs, down from 26% to 7% (Figure 4.7E). Current responses for each cell were than normalised to membrane size for each LMN and the average $GABA_AR$ current densities were compared between lines (Figure 4.7F-G). Measurement of current density rather than raw current amplitudes are critical, as the amplitude of responses are heavily influenced by membrane size. For example, a larger WCC would allow for a greater proportion of ion channels to be localised at the membrane relative to smaller cells with a smaller WCC. However, by normalising the data this is considered and prevents the data from being skewed by cell size. Coherent with qualitative data at day 40 (Figure 4.7D), both C9-1 and C9-2 display drastically augmented responses to GABA relative to Con-1 and C9-2Δ (Figure 4.7F). The average current density for Con-1 was 2.17 pA/pF in comparison to 14.3 and 7.7 pA/pF for C9-1 and C9-2 respectively (Kruskal-Wallis test: $p<0.05$; Con-1 vs C9-1: Dunn's multiple comparison test: $p<0.0001$; Con-1 vs C9-2: Dunn's multiple comparison test: $p=0.0025$). This almost constitutes a 7-fold and 4-fold amplification of GABA transmission in C9 LMNs. In spite of this, the current density of C9-3 was statistically indistinguishable versus Con-1 (Dunn's multiple comparison test: $p= 0.45$). Nonetheless, the C9-2 current density was 88 times the size of C9-2Δ (unpaired *t-test*: $p=0.0013$).

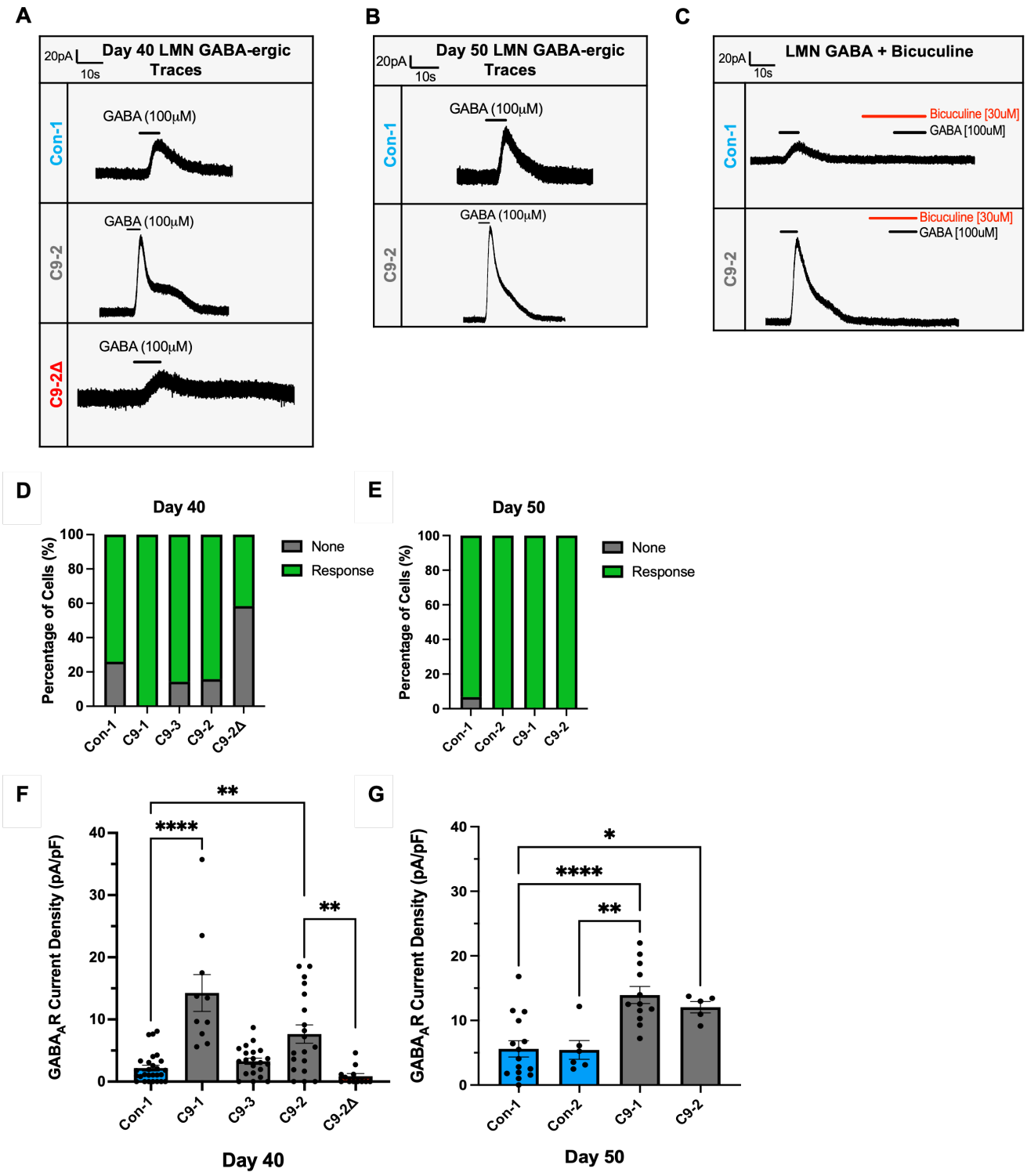

Figure 4.7. Responses to GABA are amplified in C9 LMNs. (A-B) Membrane currents were elicited by bath-applied GABA (100μM) at day 40 **(A)** and day 50 **(B)** and blocked by application of GABA$_A$R antagonist bicuculine (30μM) **(C)** in the whole-cell voltage-clamp configuration from a LJP corrected holding membrane potential of -54mV. **(D-E)** Voltage-clamp recordings from individual LMNs were grouped into either GABA-responsive or GABA non-responsive categories, with a greater proportion of non-responsive control and isogenic cells versus those from C9-patient lines at day 40 and less so at day 50. **(F-G)** The mean whole-cell GABA$_A$R current density was

significantly increased in C9-LMNs versus control and the paired isogenic line (C9-2 and C9-2Δ) at both maturation timepoints. Individual cells are represented by individual data points overlaid onto the bar graph. All data presented as Mean (±SEM). * $p<0.05$, ** $p<0.01$, **** $p<0.0001$ from one-way ANOVA followed by Sidak's multiple comparisons test or Kruskal-Wallis test followed by Dunn's multiple comparisons test and unpaired t-test (C9-2 vs C9-2Δ). Data: Con-1: day 40, n=27, N=5; day 50, n=15, N=3; Con-2: day 50, n=6, N=2; C9-1: day 40, n=10, N=3; day 50, n=12, N=2; C9-3: day 40, n=21, N=5; C9-2: day 40, n=19, N=4; day 50, n=5, N=3; C9-2Δ: day 40, n=12, N=2.

Despite a greater proportion of healthy controls responding to GABA at day 50 that translated with higher current densities in Con-1 and Con-2, enormous differences in GABA-ergic transmission were still detected relative to C9 lines (one-way ANOVA: $p<0.05$; Sidak's multiple comparison test: Con-1 vs C9-1: $p<0.0001$; Con-1 vs C9-2: $p= 0.028$; Con-2 vs C9-1: $p=0.0017$; Con-2 vs C9-2: $p=0.06$) (Figure 4.7G). This data in conjunction with an absence of GABA-evoked current phenotypes in C9-derived striatal neurons provides evidence for an iPSC-derived, LMN specific, impairment in GABA-ergic transmission.

4.37 In C9 LMNs Excitatory NMDA Transmission is Augmented

On the contrary to inhibitory GABA signalling, glutamatergic signalling has been extensively studied in the context of LMNs in ALS. The glutamate-mediate hypothesis of excitotoxicity has long been considered a key pathogenic driver that drives degeneration of LMNs in FTD/ALS (Rothstein et al., 1990, Cleveland and Rothstein, 2001). Motor neurons have been shown to be particularly vulnerable to AMPAr-mediated toxicity in mouse models of ALS (Shaw, 2005), C9 iPSC-derived motor neurons (Selvaraj et al., 2018, Shi et al., 2018) and from post-mortem LMNs (Gregory et al., 2020). The role of NMDAr-mediated excitotoxicity has largely been overlooked especially in the context of the C9 repeat expansion.

To tackle this, day 40 and 50 C9 iPSC-derived LMNs responses to (50μM) AMPA stimulation (Figure 4.8A-B) and NMDA (100μM, in the presence of glycine, 50μM) (Figure 4.9A-B) were analysed in detail. Responses were evoked as previously described in section 3.35.

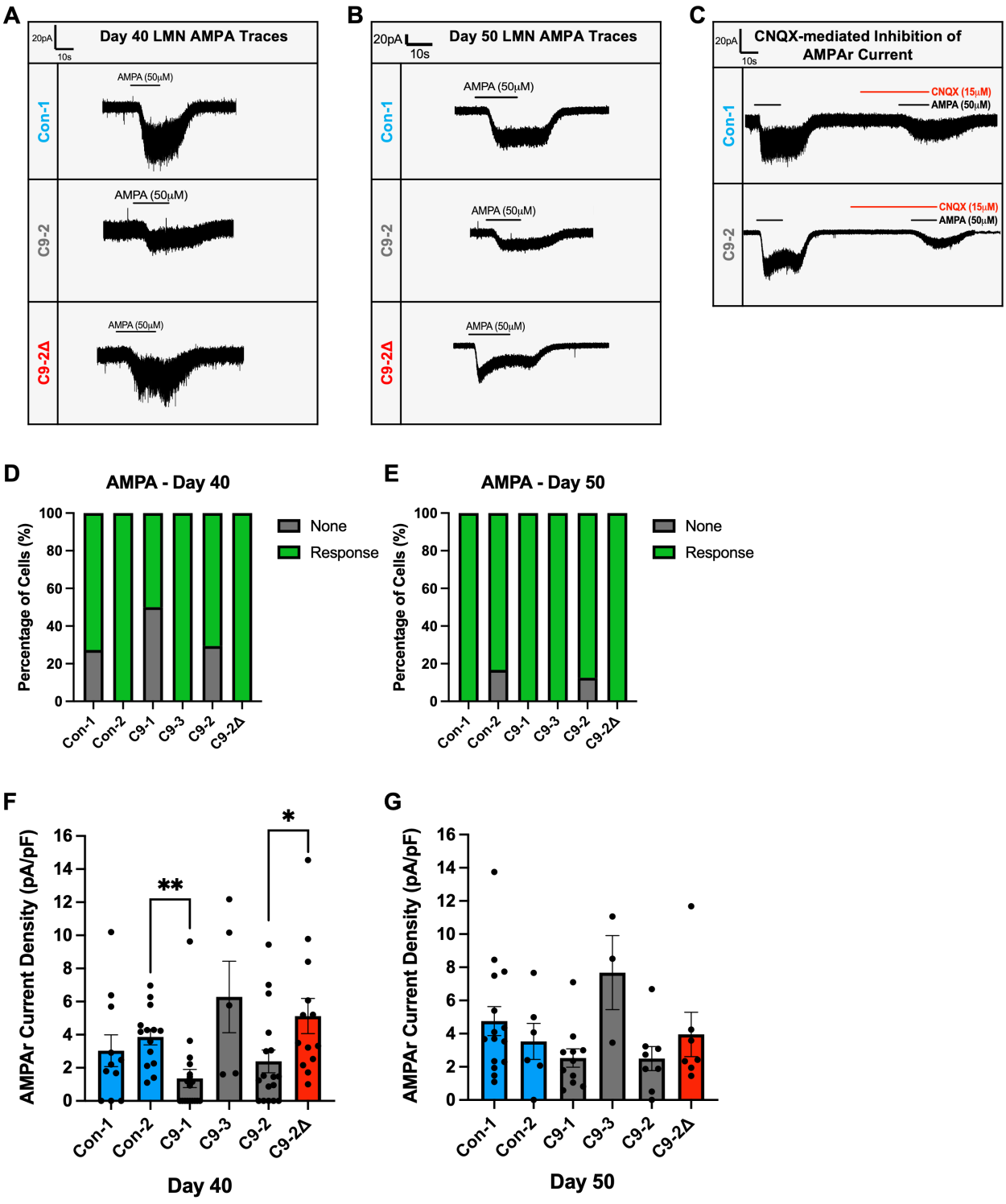

Figure 4.8. C9 LMNs display reduced responses to AMPA-mediated transmission. (A-C) Membrane currents were evoked by bath-applied AMPA (50μM) **(A-B)** and blocked by AMPAr antagonist CNQX (15μM) **(C)** in the whole-cell voltage-clamp configuration from a LJP corrected holding membrane potential of -74mV. **(D-E)** Voltage-clamp recordings from individual LMNs were grouped into either AMPA-responsive or non-responsive categories, with a greater percentage of C9 LMNs at day 40 but not day 50, displaying a reduced ability to respond to AMPA stimulation. **(F-**

G) The mean whole-cell AMPAr current density was markedly reduced in C9 LMNs vs control and isogenic lines at day 40 **(F)** but these differences were non-significant at day 50 **(G)**. Individual cells are represented by individual data points overlaid onto the bar graph. All data presented as Mean (±SEM). * $p<0.05$, ** $p<0.01$ from Kruskal-Wallis test followed by Dunn's multiple comparisons test or unpaired t-test (C9-2 vs C9-2∆). Data: AMPA: Con-1: day 40, n=11, N=4; day 50, n=15, N=5; Con-2: day 40, n=14, N=4; day 50, n=6, N=1; C9-1: day 40, n=18, N=5; day 50, n=11, N=4; C9-3: day 40, n=5, N=3; day 50, n=3, N=1;C9-2: day 40, n=17, N=5; day 50, n=8, N=2; C9-2∆: day 40, n=13, N=3; day 50, n=7, N=1.

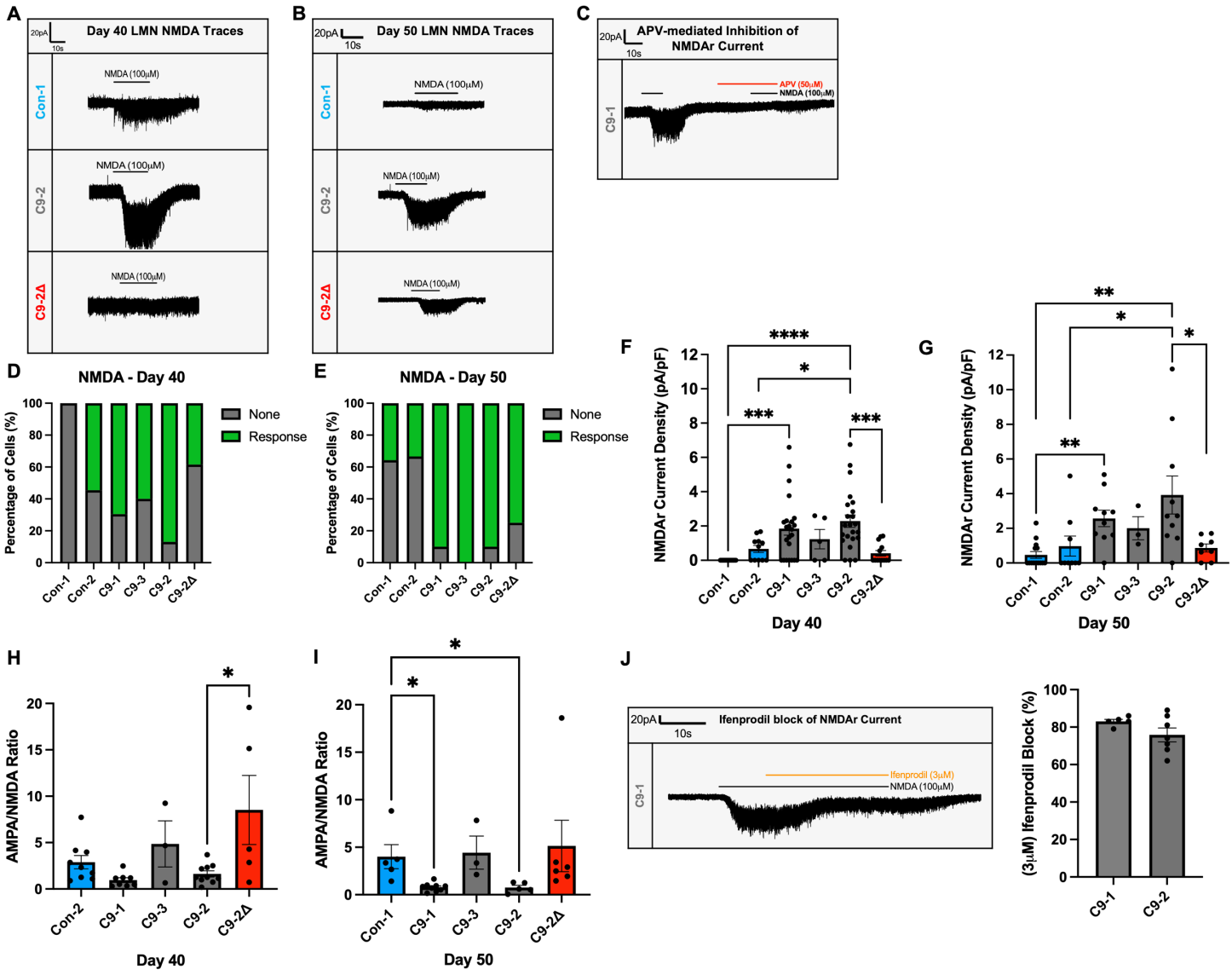

Figure 4.9. C9 LMNs display potentiated responses towards NMDA stimulation. **(A-B)** Membrane currents were evoked by NMDA (100μM, in the presence of glycine, 50μM) **(A-B)** and blocked by NMDAr specific antagonist APV (50μM) **(C)** in the whole-cell voltage-clamp configuration from a LJP corrected holding membrane potential of -74mV. **(D-E)** Voltage-clamp recordings from individual LMNs were grouped into either NMDA-responsive or non-responsive categories, with control and isogenic lines demonstrating a greater incapacity to respond to NMDA stimulation compared with C9-patient lines. **(F-G)** The mean whole-cell NMDAr current density was massively enhanced in C9-patient lineages in comparison to the paired isogenic and control lines. Individual cells are represented by individual data points overlaid onto the bar graph. **(H-I)** C9-LMNs share a reduced AMPA/NMDA ratio indicative of larger proportion of glutamatergic transmission being driven by NMDAr-mediated currents. All data presented as Mean (±SEM). * p<0.05, ** p<0.01, *** p<0.001, **** p<0.0001 from Kruskal-Wallis test followed by Dunn's multiple comparisons test or unpaired t-test (C9-2 vs C9-2Δ). **(J)** Exemplar voltage-clamp recordings of NMDA-evoked membrane currents (100μM, in the presence of glycine, 50μM) and block by ifenprodil (3μM). Quantification of the average percentage block of NMDAr-mediated currents

by ifenprodil. Data: NMDA: Con-1: day 40, n=18, N=7; day 50, n=14, N=5; Con-2: day 40, n=11, N=4; day 50, n=9, N=2; C9-1: day 40, n=23, N=6; day 50, n=10, N=3; C9-3: day 40, n=5, N=3; day 50, n=3, N=1; C9-2: day 40, n=23, N=7; day 50, n=10, N=3; C9-2Δ: day 40, n=13, N=3; day 50, n=8, N=2.

Competitive receptor antagonists CNQX (15μM) and APV (50μM) were transiently applied to block and confirm expression of AMPA (Figure 4.8C) and NMDA receptor mediated currents (Figure 4.9C). Of note, APV-mediated inhibition of NMDA responses in healthy control was not obtained due to the scarcity of NMDA-ergic responses. Across all control, isogenic and C9 patient lines a large majority of cells responded to AMPA stimulation. A greater proportion of patient lines failed to respond to AMPA application, half of C9-1 LMNs and 29% of C9-2 compared with 27% of Con-1 recordings (Figure 4.8D). These differences eroded by day 50 with recordings across all lines displaying AMPA responses with the exception of Con-2 (17%) and C9-2 (13%) (Figure 4.8E). For NMDA responses at day 40, a disproportionate quantity of LMNs failed to respond to NMDA. This was primarily observed in Con-1 which failed to respond to NMDA stimulation whilst 45% of Con-2 and 61% C9-2Δ lacked evoked membrane currents (Figure 4.9D). This was less so in C9-1 and C9-3 lines, and then considerably less in C9-2. By day 50, these same phenotypes were observed between lies albeit to a slightly lesser degree (Figure 4.9E).

The average AMPAr current density was recorded and revealed a general decrease in AMPA-ergic transmission in C9 LMNs in comparison to healthy controls and isogenic line (Figure 4.8F). This was validated by statistical comparisons between Con-2 and C9-1 (Kruskal-Wallis test: $p<0.05$; Dunn's multiple comparison test: $p=0.003$) plus C9-2 and C9-2Δ (unpaired *t-test*: $p=0.03$). Notably, all C9-3 LMNs responded to AMPA, and this is associated with the increased, but insignificant, current densities across both timepoints. Extension of culture times to day 50 resulted in trending but ultimately insignificant reductions in the current density of C9-LMNs (Figure 4.8G). Notably, the statistical power of this dataset is limited, with further work required to deduce any significant differences between cell lines. For instance, a power calculation determined a minimum of twelve recordings per cell line are required to establish statistical significance between C9-2 and C9-2Δ AMPAr current density. Selveraj, Livesey and colleagues previously published AMPAr current densities to be unchanged in C9 LMNs similar to the data presented here at day 50 (Selvaraj et al.,

2018). Contrary to this, C9 LMNs displayed a statistically significant increase in their average NMDAr current densities against healthy control and isogenic lines at day 40 (Kruskal-Wallis test: $p<0.05$; Dunn's multiple comparison test: Con-1 vs C9-1: $p=0.0002$; Con-1 vs C9-2: $p<0.0001$; Con-2 vs C9-2: $p=0.03$) (unpaired *t-test*: C9-2 vs C9-2∆: $p=0.0007$) (Figure 4.9F) and this increase remained consistent at day 50 (Kruskal-Wallis test: $p<0.05$; Dunn's multiple comparison test: Con-1 vs C9-1: $p=0.0056$; Con-1 vs C9-2: $p=0.002$; Con-2 vs C9-2: $p=0.037$) (unpaired *t-test*: C9-2 vs C9-2∆: $p=0.027$) (Figure 4.9G).

The AMPA/NMDA ratios were than calculated from voltage-clamp recordings where both AMPA and NMDA evoked currents were recorded and measured from the same cell (Figure 4.9H-I). Ratio values are useful indicator of the relative strength of AMPAr and NMDAr-mediated currents at glutamatergic excited cells. A value above 1 is indicative of AMPAr dominated currents whilst a value below 1 signify NMDAr mediated currents predominate. Using recorded current densities from Figure 4.8 and 4.9, there were reduced ratio values recorded from DIV40 C9-1 and C9-2 indicating a larger proportion of NMDA currents are evoked in these neurons (Figure 4.9H). At DIV50, the control and isogenic lines continued to exhibit AMPAr dominated-glutamatergic currents, a greater proportion of NMDA currents were evoked in case lines with ratio values below 1 (unpaired *t-test*: day 40: C9-2 vs C9-2∆: $p=0.019$) (one-way ANOVA: $p<0.05$; Sidak's multiple comparison test: day 50: Con-1 vs C9-1: $p=0.01$; Con-1 vs C9-2: $p= 0.023$) (Figure 4.9I). To help determine the subunit composition of NMDAr in C9-LMNs, the GluN2B subunit-selective non-competitive NMDAr antagonist ifenprodil (3µM) was used (Williams, 1993). The negative allosteric modulator was able to block membrane currents evoked by GluN2B-containing NMDARs (Figure 4.9J) in C9-1 and C9-2 by 83% and 76% (Figure 4.9K).

Not only did iPSC-derived LMNs respond to NMDA stimulation but were significantly enhanced in C9 patient-derived LMNs with, a large majority of currents mediated by GluN2B-containing receptors commonly associated with excitotoxicity. These transmission related differences are not reported in MSNs and highlight differing neuropathophysiological profiles in different neuronal cell types generated from the same iPSC lines.

4.4. Discussion

Here, I exploit the ability of iPSC technology to differentiate a population of highly enriched C9 iPSC-derived lower motor neuron cultures from the same parental iPSC lines used to generate C9 iPSC-derived striatal neurons in the previous chapter. Generation of these iPSC-derived LMNs enabled me to ascertain whether the electrophysiological perturbations in C9 MSNs relating to hypoexcitability were a cell-specific or shared phenotypic feature with C9 LMNs. To this end, the electrophysiological characterisation of iPSC-derived LMNs was identical to that in the previous chapter. The combination of human stem cell technology and whole-cell patch-clamp electrophysiology enabled me to evaluate phenotypes between cells of the striatum and LMNs, the site of hallmark dysfunction in FTD/ALS.

The data in this chapter demonstrate functionally mature, patient-derived, C9 LMNs exhibit no alterations in their intrinsic excitability. This is demonstrated by comparable relationships in the current stimulus-AP output that were constructed at MN maturation and an extended maturation timepoint between control, C9 and gene-corrected isogenic LMNs. Consistent with this, AP parameters were not impacted in disease neurons. However, investigation into responses to agonists of key receptor ion channels on LMNs showed potential phenotypic data. Inhibitory GABA-ergic transmission was potentiated in C9 LMNs at both mature timepoints. Similarly, study of excitatory glutamatergic currents revealed NMDAr-mediated transmission, but interestingly not AMPA-ergic transmission, was significantly amplified in C9 LMNs at both timepoints in comparison to healthy control and isogenic lines. In regards to AMPA-ergic responses, transmission was diminished in patient LMNs although significant differences were not consistently upheld across the timepoints studied. These data align with a shift in the composition of glutamatergic currents from AMPAr dominated-glutamatergic currents as observed in control and isogenic lines to a predominance of NMDAr evoked currents in C9 patient lines. Using the NMDAr antagonist ifenprodil (Williams, 1993), I demonstrate a large proportion of NMDAr currents are conducted by GluN2B-containing receptors commonly implicated in excitotoxicity (Liu et al., 2007).

In this chapter and the former I have generated two highly enriched neuronal populations (MSNs and LMNs) from different regions of the CNS. This has allowed me to perform a cross-comparison of electrophysiological function between these divergent cell types which have essentially originated from the same patients. The fact that I observe no differences in the intrinsic excitability of C9 iPSC-derived LMNs, further alludes to the fact that hypoexcitability observed in C9 iPSC-derived MSNs is a specific phenotypic feature of striatal dysfunction in C9 orchestrated disease. These data highlight that such impairments do not arise from patient line related issues otherwise hypoexcitability would have also been a feature of C9 LMNs. Instead, such alterations highlight cell-specific neurophysiological perturbations in neurons that are not directly related to each other and belong to different regions of the CNS. Equally, the potentiation of GABA-ergic and NMDAr evoked currents are a feature of C9 LMNs, but not MSNs. Neuronal function is dependent upon the intrinsic excitability of the neuronal population in addition to the strength and timing of excitatory and inhibitory inputs. In the human *in vitro* cultures utilised in this study, both these determinants of excitability are differentially impacted, which relates to general excitability alterations in FTD/ALS (Pasniceanu et al., 2021). Cell-specific vulnerabilities that give rise to these downstream neurophysiological impairments further highlights the shear complexity of FTD/ALS. Ultimately, this is a key consideration for therapeutic development in appropriately targeting dysfunctional, regionally specific neuronal mechanisms implicated in disease.

Focusing on the electrophysiological excitability of C9 patient-derived LMNs was also conducted to help provide clarity in a field where several reports of LMN excitability in the literature have reported a diverse range of physiological phenotypes. These studies have shown a combination of hyperexcitable, hypoexcitable, transition of phenotypes or no changes in excitability (Sareen et al., 2013, Wainger et al., 2014, Devlin et al., 2015, Naujock et al., 2016, Selvaraj et al., 2018, Zhao et al., 2020, Burley et al., 2022, Harley et al., 2023a). In my highly enriched C9 LMN monocultures I observed equivalent levels of intrinsic excitability between control and case lines at both an early and late maturation timepoint. Concurring with this, AP parameters were largely unchanged in C9 patient lines, nor any were any impairments in the maturation of intrinsic properties detected. Thus, in our C9 iPSC-LMN models at least, changes

in intrinsic excitability are an unlikely contributing factor in the earliest stages of FTD/ALS.

My excitability data provide further rationale for the various phenotypes reported in C9 iPSC-derived MN studies. In mixed C9 iPSC-derived motor neuron and glial cultures, hyperexcitability represents an initial feature (Wainger et al., 2014, Harley et al., 2023a), that transitions towards a non-altered or hypoexcitable state (Sareen et al., 2013, Devlin et al., 2015, Burley et al., 2022). Instead, our excitability data here aligns closely with other studies that report no differences in the intrinsic excitability of C9 patient-derived MNs from highly enriched motor neuron cultures with negligible glial differentiation (Selvaraj et al., 2018, Zhao et al., 2020), analogous to our differentiation protocol. Zhao and colleagues implicated a non-cell autonomous role of contaminant C9ORF72 mutant astrocytes as principal mediators of MN hypoexcitability in previous 'enriched' studies (Sareen et al., 2013, Devlin et al., 2015, Zhao et al., 2020). This is supported by earlier work in primary murine cultures whereby, conditioned media from mutant SOD1 expressing astrocytes induced alterations in ion channel function and excitability of wild-type MNs (Fritz et al., 2013). Thus, the presence of astrocytes in culture can have a significant influence on MN function. However, it is important to note that FTD/ALS is not simply a neuronal disease but there is a non-neuronal component that needs to be considered when generating human *in vitro* disease models, as these can have a profound impact on pathophysiological phenotypes and neuronal viability.

The phenotypic variations in our excitability data and within previous iPSC-derived LMN models may arise from the origin of iPSC lines or due to purity of cultures as discussed above. Equally differences could stem from variations in differentiation protocols that either differ from the ones in this study (Boulting et al., 2011, Bilican et al., 2012, Amoroso et al., 2013, Maury et al., 2015), or are based on the same protocol used here (Du et al., 2015), albeit with modifications (Burley et al., 2022, Harley et al., 2023a). Even so, these studies reported MN hyperexcitability at DIV40 that were crucially not observed in this chapter. These modifications in neuronal media compositions and the timepoints in which neurotrophic reagents were introduced are likely to have contributed to such phenotypes directly or indirectly through generation of neuronal-glial mixed cultures. Another possible source of variation could result from

duration of cultures. Indeed, descriptions of hyperexcitability have been reported at a similar timepoint (approximately between day 38-42 of differentiation) to my earlier DIV40 timepoint where no changes in excitability were displayed (Devlin et al., 2015, Burley et al., 2022, Harley et al., 2023a). Now, extension of culture times that extend beyond the 'later' DIV50 timepoint in this study where again excitability was unaffected in patient lines, showcased a hypoexcitable phenotype in iPSC-derived MNs from C9 patients (7-10 weeks post plating) (Sareen et al., 2013, Devlin et al., 2015) and mTDP-43 patients (day 70 post-iPSC differentiation) (Harley et al., 2023a). Although Burley and colleagues described changes in MN excitability within 7 days using the same differentiation protocol as ours (Burley et al., 2022) and corresponds to similar timepoints in this chapter. The authors suggest a transition in excitability, at similar timepoints as this study, due to varying rates of neurophysiological maturation in their iPSC-derived MNs, which conflicts with the I-O relationships reported here. Together, these variables in iPSC-derived models raise the philosophical issue of the need for consistency and transparency in protocols to help enable replication of results.

Given a lack of changes in the intrinsic excitability of C9 LMNs in this study, I next investigated responses to both excitatory and inhibitory neuromodulatory inputs which are extrinsic factors that contribute to overall neuronal excitability. A substantial increase in the functional expression of $GABA_AR$ was measured in C9-derived LMNs. The data would therefore indicate these patient lines display an increased inhibitory drive in response to GABA-ergic transmission which is likely to dampen down general excitability. Hyperexcitability is not uniformly observed at disease onset in ALS patient spinal MNs (Marchand-Pauvert et al., 2019), and can possibly reflect enhanced inhibitory compensatory mechanisms in surviving MNs as witnessed here. This is of importance in MN survival given that viability correlates closely with MN excitability (Delestree et al., 2014, Leroy et al., 2014, Martinez-Silva et al., 2018). An important consideration of inhibitory drive within spinal MNs needs to consider that glycine, not GABA, is the principal inhibitory neurotransmitter within human spinal cord (Lorenc et al., 2024). Functional abnormalities in glycinergic transmission predominantly in mSOD1 models have previously been implicated in ALS (Martin and Chang, 2012, Allodi et al., 2021, Cavarsan et al., 2023), even in the absence of changes in GABA-ergic transmission (Chang and Martin, 2011). Thus, this needs to be taken into account when assessing the functional implications of increased GABA-ergic current density

on C9 iPSC-derived LMN excitability. The impact of inhibitory transmission within spinal MNs remains scant, but here I begin to provide evidence of dysregulated inhibitory GABA-ergic signalling in the context of the C9 repeat expansion mutation.

Interestingly, in my C9 iPSC-derived LMNs I observed a concurrent but contradictory, increase in the receptor activation of both $GABA_AR$ and NMDAr at the early and later maturation timepoint. These increases are likely to reflect an increase in the receptor expression within patient lines harbouring the C9ORF72 repeat expansion as indicated by increased current amplitudes and current density. These data correlate with previously reported increases in NMDAr subunit expression in C9 iPSC-derived LMNs (Shi et al., 2018, Dafinca et al., 2020). This raises the question of the pathophysiological relevance of increases in both GABA and NMDA transmission in our C9 models of disease, in terms of why this occurs and the contribution of these opposing changes to LMN excitability. The fact that dysfunction in transmission does not occur solely in excitatory (NMDAr) or inhibitory ($GABA_AR$) transmission could relate to a lack of changes in C9 LMNs excitability. Alternatively, these observed alterations in excitatory/inhibitory transmission may be interrelated and represent a compensatory, cause and consequence type relationship, whereby the increased transmission of one leads to a similar phenotype in the other. Nonetheless, LMNs receives excitatory transmission from the UMNs and inhibitory transmission from spinal interneurons. Consequently, alterations in LMN receptor expression could influence responses from these regions and contribute towards dysregulated activity within motor neuron circuitries in FTD/ALS.

Multiple lines of evidence have provided strong links between dysregulated glutamate homeostasis and ALS pathogenesis. Typically, these links have shown selective vulnerability of LMNs to AMPAr-mediated, but not NMDAr mediated excitotoxicity (Rothstein et al., 1992, Rothstein, 1995, Cleveland and Rothstein, 2001). In contrast, this study provides evidence of NMDAr and not AMPAr, dysfunction in C9 patient-derived LMNs that may contribute towards excitotoxicity commonly implicated in ALS. Consistent with previous reports (Selvaraj et al., 2018), I observed trending, but ultimately, non-significant differences in AMPAr-mediated current densities between C9, healthy and isogenic control lines, maintained at both timepoints studied. Yet, amplified current densities were observed in the limited number of C9-3 recordings,

which could point towards individual patient variability in responses and general pathology. Even so, my data indicate a favourable shift towards NMDAr-mediated glutamatergic signalling in C9 patient LMNs but not in healthy control or isogenic lines. Concurrent with this, almost all Con-1 control lines across both timepoints failed to respond to the exogenous application of NMDA. This markedly low NMDAr expression is a universal feature across the other control and isogenic lines and in stark contrast to upregulated NMDAr transmission in C9 LMNs. Importantly, stimulation of overexpressed NMDAr, Ca^{2+} permeable in nature, can give rise to Ca^{2+} dyshomeostasis and in turn lead to an influx of injurious, excitotoxic levels of Ca^{2+} which has been strongly implicated in ALS pathogenesis (Mead et al., 2023). LMNs are particularly susceptible to Ca^{2+} dysregulation due to their low Ca^{2+} buffering capacity intertwined with high Ca^{2+} influxes during neurotransmission. Previous studies have shown upregulated expression of Ca^{2+}-permeable AMPAr (Selvaraj et al., 2018, Gregory et al., 2020), which cannot be excluded here, along with NMDAr-mediated contributions to this pathomechanism (Xu and Xu, 2018, Dafinca et al., 2020). In agreement with these studies, I show a large proportion (~80%) of expressed NMDAr in C9 LMNs are GluN2B-containing receptors that are associated with extrasynaptic localisation and excitotoxicity (Hardingham and Bading, 2010, Huber et al., 2022a). Similar to my findings, Huber and colleagues also demonstrated increased functional expression of GluN2B-containing NMDA receptors in primary hippocampal neurons expressing the C9 repeat expansion mutation (Huber et al., 2022a). Together with my data, this could indicate increased expression of the GluN2B subunit at the protein level. In alignment with this, GluN2B expression was significantly upregulated in FUS and TDP-43^{M337V} iPSC-derived MNs, with a similar non-significant trend observed in C9 iPSC-derived MNs at the RNA level (Bursch et al., 2019, Dafinca et al., 2020). Moreover, GluN2B-NMDAr synaptic expression has been shown in immature neurons (McKay et al., 2012, Zamzow et al., 2013). However, given that no differences in the maturation of control and case lines are observed here at either timepoint along with low-level NMDAr responses in control lines underlines C9 specific dysregulation of functional NMDAr expression likely at extrasynaptic sites.

4.5. Conclusion

In this chapter, regionally specific neurophysiological dysfunction is evident in C9 LMNs that is phenotypically distinct from C9 MSNs investigated in the previous chapter. These cell-specific phenotypes are summarised in Table 4.1. Unlike C9 MSNs, C9 LMNs do not display any changes in excitability or any significant fluctuations in AP parameters. However, divergent from C9 MSNs, pronounced amplification of $GABA_AR$ transmission was observed in LMN patient lines. In addition, alterations in the composition of glutamatergic currents was observed with respect to AMPAr and NMDAr. Indeed, potentiated responses in NMDAr-mediated but not AMPAr-mediated glutamatergic transmission was reported in C9 LMNs at both day 40 and day 50 timepoints, in comparison to healthy control and isogenic lines. The majority of C9 NMDAr transmission was shown to be facilitated by GluN2B-containing receptors commonly associated with excitotoxicity, a major ALS phenotype.

Table 4.1. Summary of the neurophysiological impairments reported in C9 patient-derived striatal MSNs and LMNs. The table compares the neurophysiological properties relating specifically to excitability, AP properties and neurotransmission within C9 MSNs and LMNs generated in this study.

Neurophysiological Properties	C9 Striatal MSNs	C9 LMNs
Intrinsic Excitability	Reduced excitability.	No changes in excitability.
Maturation properties	No impairments in maturation.	No impairments in maturation.
AP Waveform	• Depolarised AP threshold • Reduced AP size • Increased AP duration • Depolarised AHP	No changes in AP waveform properties.
GABA transmission	No changes in transmission.	Potentiated $GABA_AR$ transmission.
Glutamate transmission	No changes in AMPAr or NMDAr transmission.	• Reduced AMPAr transmission. • Potentiated NMDAr responses.

Chapter 5: Homeostatic Responses to Chronic Depolarising Stress are Dysregulated in C9 Patient-derived Lines

5.1. Introduction

Previously in Chapter 4, C9 patient-derived LMNs in response to current stimulation displayed no alterations in their excitability versus control lines. This was determined to be specifically observed in LMNs, as striatal MSNs derived from the same iPSC lines showed intrinsic hypoexcitability (Chapter 3).

I next considered why differences in LMN excitability were not observed in my human *in vitro* cultures, despite considerable evidence for changes in ALS patient LMN excitability as disease progresses (Devlin et al., 2015, Burley et al., 2022, Harley et al., 2023a). Importantly, enriched populations of *in vitro* iPSC-derived neurons are a vital model of disease that recapitulate key physiological components. One of the key considerations here, is that the voltage output of *in vitro* motor neuron monocultures investigated in this study have been recorded in a basal state i.e. in the absence of any cell stressors. Typically, LMNs form part of the corticomotor circuitries receiving inputs from various neuronal and non-neuronal sources. Dysregulation of such inputs or the ability of LMNs to respond appropriately to external stimuli in disease can lead to the aberrant modulation of neuronal activity and therefore function. For instance, *C9ORF72* mutant iPSC-derived astrocytes are sufficient to induce physiological toxicity by way of excitability changes within MNs (Zhao et al., 2020). It is therefore possible that whilst LMNs in this study are in a basal state there are no net changes in excitability, but under specific physiologically challenging conditions, abnormal excitability changes are revealed.

Subsequently, this chapter focuses on an important aspect of disease modelling in studying iPSC-derived LMNs in the presence of acute and chronic stressors to represent *in vivo* conditions where cells are integrated components of large, complex networks. The cells within such networks are constantly subject to both internal and

external activity that can drive alterations in excitability and drive neuronal plasticity. Indeed, the fundamental ability of neurons to adapt and attenuate their responses to stimuli is crucial to maintaining correct neuronal and network function and when this ability to remain 'plastic' becomes impaired (Styr and Slutsky, 2018), maintenance of homeostatic function is lost. Thus, adaptions in neuronal responses to stress is either incorrectly or ineffectively modulated and this is a commonly observed, early feature of neurodegenerative diseases (Milnerwood and Raymond, 2010, Styr and Slutsky, 2018) including FTD and patients with the C9 mutation (Benussi et al., 2016, Beagle et al., 2017).

Plastic changes in neuronal activity in response to stimuli can occur at the synapse or the intrinsic excitability of the neurons themselves (Nelson and Turrigiano, 2008). Multiple studies in *C9ORF72* models have demonstrated shifts in neuronal activity due to functional impairments in plasticity at the synapse (Perry et al., 2017, Ho et al., 2020, Perkins et al., 2021). This concurs with dysregulated gene expression detected in synaptic-plasticity related pathways in *in vitro* human neurons or post-mortem C9 patients (Prudencio et al., 2015, Dafinca et al., 2016, Perkins et al., 2021). Plastic modulation of the intrinsic excitability or AP waveform of neurons can occur in the short-term, seconds to minutes, via changes in ion channel conductances (Shah et al., 2008, Bender and Trussell, 2009, Scott et al., 2014), or by transmitter related neuromodulatory signalling (Bender et al., 2012, Martinello et al., 2015). In addition to these acute modulations of AP generation, activity-dependant structural changes in the AIS are able to modulate excitability in the long-term i.e. take days to weeks to occur (Jamann et al., 2021).

Days of chronic KCl stimulation have routinely been used in *in vitro* neurons to induce these structural forms of plasticity (Grubb and Burrone, 2010, Evans et al., 2013, Sohn et al., 2019). This has served as a useful tool to study homeostatic plasticity-related events linked to both acute and chronic neuronal depolarisation owing to the ease of implementation and manipulation of treatment and thus, downstream depolarisation. Furthermore, this KCl-based model has been crucial in elucidating molecular and structural homeostatic mechanisms of neurons *in vitro,* including in the context of FTD (Sohn et al., 2019).

5.2. Aims and Objectives

The electrophysiological profile of iPSC-derived LMNs in this study has shown patient derived lines in the absence of any stress do not display any changes in excitability. A key feature for any neuron is its ability to remain 'plastic' and attenuate its behaviour in response to internal or external stimuli. This ability to maintain homeostasis in response to neurophysiological challenges is vital to prevent dysfunction that can potentially translate into degeneration at the cellular and network level. Functional impairments in neuronal plasticity are implicated in the early phases of neurodegenerative disease (Milnerwood and Raymond, 2010, Pasniceanu et al., 2021), a study by Benussi and colleagues has shown this occurs 15 years before symptomatic onset in *C9ORF72* patients (Benussi et al., 2016). Here, I wanted to assess the ability of generated C9-iPSC derived LMNs to respond to stressors at an acute (short-term) and (long-term) chronic timepoint to replicate neuronal stress during disease onset and progression.

Using a single healthy control and C9 patient-derived line, I hypothesise homeostatic dysfunction in the excitability of C9-LMNs in response to stressors that are otherwise physiologically managed by the healthy control LMNs.

5.3. Results

5.31 Protocol to Induce Acute and Chronic Stress in Control and C9 Patient-derived LMNs

To explore the neuronal excitability of control and case lines in response to acute and chronic stressors, the Con-1 and C9-2 LMNs were differentiated as described in methods section 2.17 following the motor neuron differentiation protocol set out by Du et al., 2015. At day 40 post-iPSC differentiation the excitability of LMNs were studied using whole-cell current clamp technology under three conditions. The first at day 40 without any additional treatment, with voltage responses recorded following incremental current stimuli as defined in results section 3.32 and 4.32 (Figure 5.1). Then second and third, independent sister cultures of LMNs were incubated for 3 hours with either 15mM of NaCl or KCl before patch-clamp analysis (Figure 5.1).

Hereafter, termed either acute NaCl or KCl treatment. Elevation of the extracellular K^+ concentration by 15mM according to the Nernst potential equation would have been sufficient to depolarise the membrane potential by 33 mV. Therefore, bringing the RMP value closer to the AP threshold and increasing the excitability of cultures. NaCl treatment provided a control for changes in osmotic pressure which can influence excitability. The effective working concentrations of NaCl or KCl is in alignment with similar studies in iPSC-derived neurons (Sohn et al., 2019) *in vitro* murine cultures (Grubb and Burrone, 2010, Evans et al., 2015).

Then to address homeostatic plasticity in response to chronic stimulation, LMNs were cultured as normal until day 40, before culture medium was treated with either NaCl or KCl for 7 days (Figure 5.1), now termed chronic NaCl or KCl. As a baseline comparison for these treatments in the chronic phase, current-clamp recordings were attained from aged-matched untreated LMNs (baseline day 50). Recordings for all LMNs was assessed in standard extracellular solution (Table 2.14) complemented with blockers of synaptic transmission. Moreover, patch-clamp recordings per coverslips of cells was strictly obtained within 1 hour of incubation in extracellular solution to avoid any homeostatic adjustments in excitability of LMNs influencing analysis.

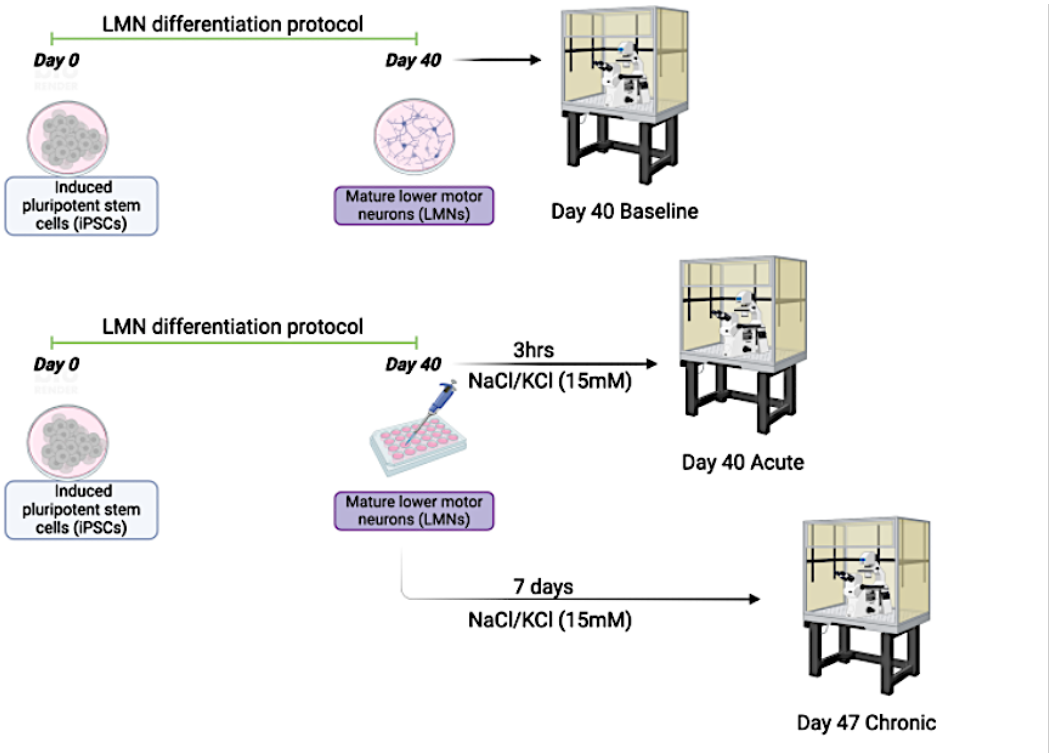

Figure 5.1. Treatment protocol for examining LMN responses to short-term and long-term stressors. LMNs followed the same differentiation protocol as previously described in Sections 2.1.4- 2.1.5 and 2.1.7. At day 40 LMNs without any treatment were taken for patch-clamp recordings and these recordings are detailed as 'day 40 baseline.' Alternatively, culture medium containing day 40 LMNs underwent treatment with either 15mM NaCl or KCl and cells were incubated for 3 hours prior to patch-clamp recording, with these data referred to as 'acute NaCl' or 'acute KCl' respectively. To study LMN responses to long-term stressors, culture medium containing day 40 LMNs were incubated in either 15mM NaCl or KCl for 7 days before being subject to patch-clamp recordings, with these data referred to as 'chronic NaCl' or 'chronic KCl.' Media was changed every 48 hours. As a baseline control for these recordings, patch-clamp analysis of untreated day 50 LMNs was also conducted (not shown) referred to as 'day 50 baseline.'

5.32 The I-O Relationship for C9 LMNs is Differentially Altered in Response to Acute and Chronic Depolarising KCl

Illustrative voltage responses to current stimuli in the various treatment conditions and timepoints are presented for Con-1 and C9-2 LMNs in Figure 5.2. The voltage traces not only show interspecific differences in the firing patterns between lines, but intraspecific changes are also observed within the same line between pharmacological conditions. The traces would indicate Con-1 LMN excitability following acute KCl treatment is similar to baseline, with chronic exposure leading to reduced excitability. Conversely, C9-2 LMN traces would indicate voltage responses following chronic KCl treatment were comparable with baseline output. These data would suggest the neuronal excitability of iPSC-derived LMNs is altered based upon line-specific differences in homeostatic responses to acute or chronic stressors.

To characterise these potential interspecific and intraspecific differences in greater detail, I-O relationships were formed to compare the effect of acute and chronic depolarising stress on AP firing activity between Con-1 and C9-2 (Figure 5.3- 5.4). APs were evoked and recorded in response to previously described current injection stimuli (0 to +50pA, 5pA steps, 500ms duration). This is the same current stimulus protocol used in Results section 4.33, whereby in the absence of any cell stressors, no changes in the excitability of C9 LMNs were described.

Following 3-hour treatment with NaCl and KCl both Con-1 and C9-2 LMNs displayed insignificant changes in their AP output following current stimulation (Figure 5.3A-B). For Con-1, KCl treatment did appear marginally enhanced compared with baseline responses and acute NaCl conditioning, especially between 10-20pA before output reduced towards baseline levels (two-way ANOVA: $F(2, 27) = 2.162$, $p= 0.1347$) (Figure 5.3A). Note, activity of baseline day 40 from both LMNs whilst still comparable, was significantly lower than AP output from separate experiments that were reported in Chapter 4.33. Nonetheless, baseline responses from C9-2 LMNs were similar to the firing activity of LMNs following acute NaCl incubation with acute KCl conditioning, similar to Con-1, led to marginal but non-significant increases in AP output (two-way ANOVA: $F(2, 21) = 1.65$, $p= 0.2159$) (Figure 5.3B). Analogous to a study by Evans and colleagues acute depolarising KCl conditioning failed to impact the neuronal excitability of both Con-1 and C9-2 LMNs (Evans et al., 2015).

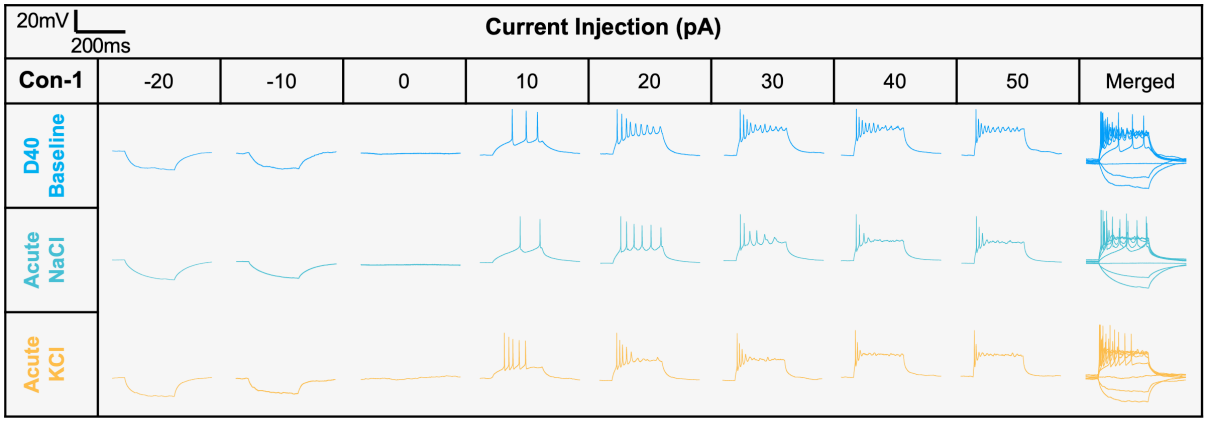
20mV
200ms
Current Injection (pA)
Con-1
-20
-10
0
10
20
30
40
50
Merged
D40 Baseline
Acute NaCl
Acute KCl

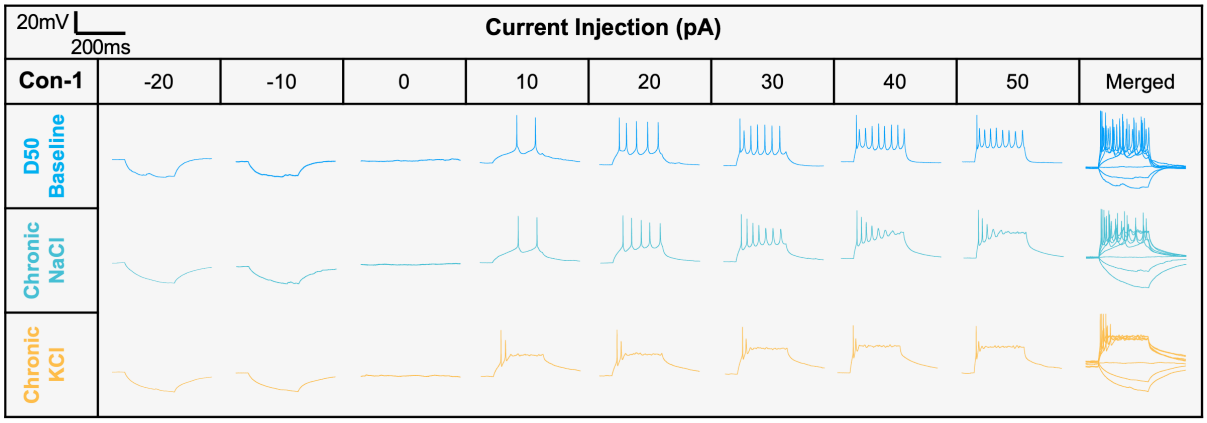
20mV
200ms
Current Injection (pA)
Con-1
-20
-10
0
10
20
30
40
50
Merged
D50 Baseline
Chronic NaCl
Chronic KCl

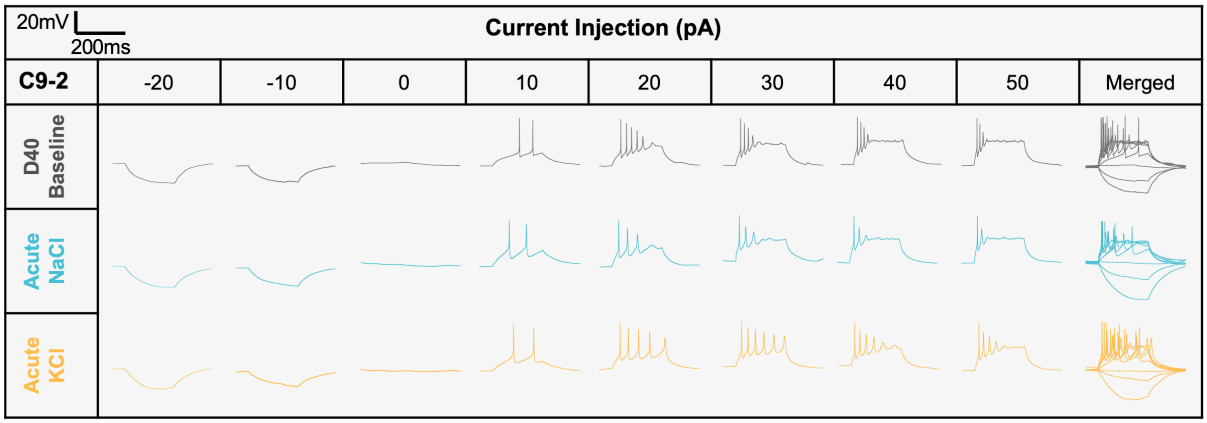
20mV
200ms
Current Injection (pA)
C9-2
-20
-10
0
10
20
30
40
50
Merged
D40 Baseline
Acute NaCl
Acute KCl

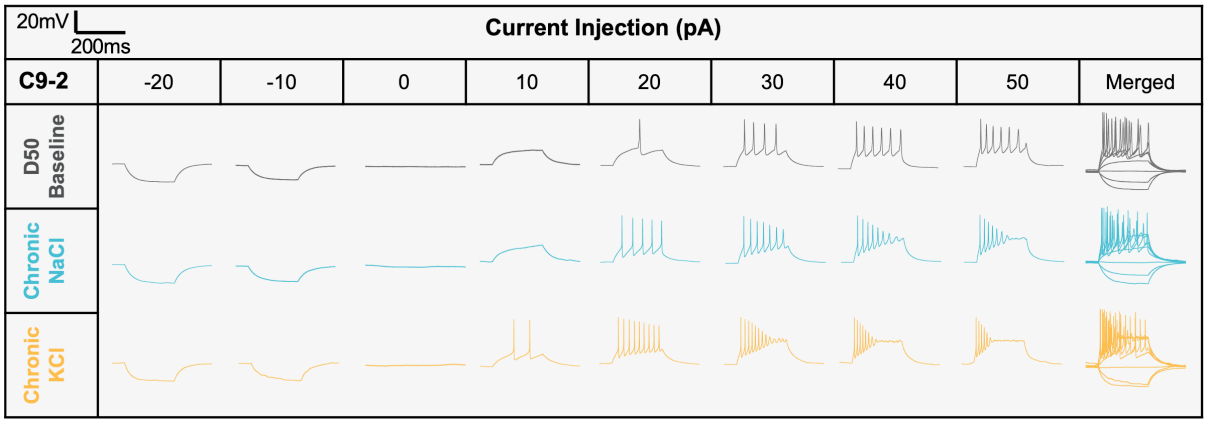
20mV
200ms
Current Injection (pA)
C9-2
-20
-10
0
10
20
30
40
50
Merged
D50 Baseline
Chronic NaCl
Chronic KCl

Figure 5.2. C9 LMNs show differences in their ability to respond to short-term and long-term stressors. Matrix schematic of illustrative AP traces recorded in the whole-cell current-clamp configuration from the healthy Con-1 line (top two panels) and C9-2 patient line (bottom two panels). Voltage responses are shown in response to a train of incremental current injections (-20pA to 50pA in 10pA steps) from a LJP corrected resting membrane potential held at -74mV. Responses shown are from either cells at day 40 or 50, following no treatment or either acute or chronic treatment with NaCl or KCl.

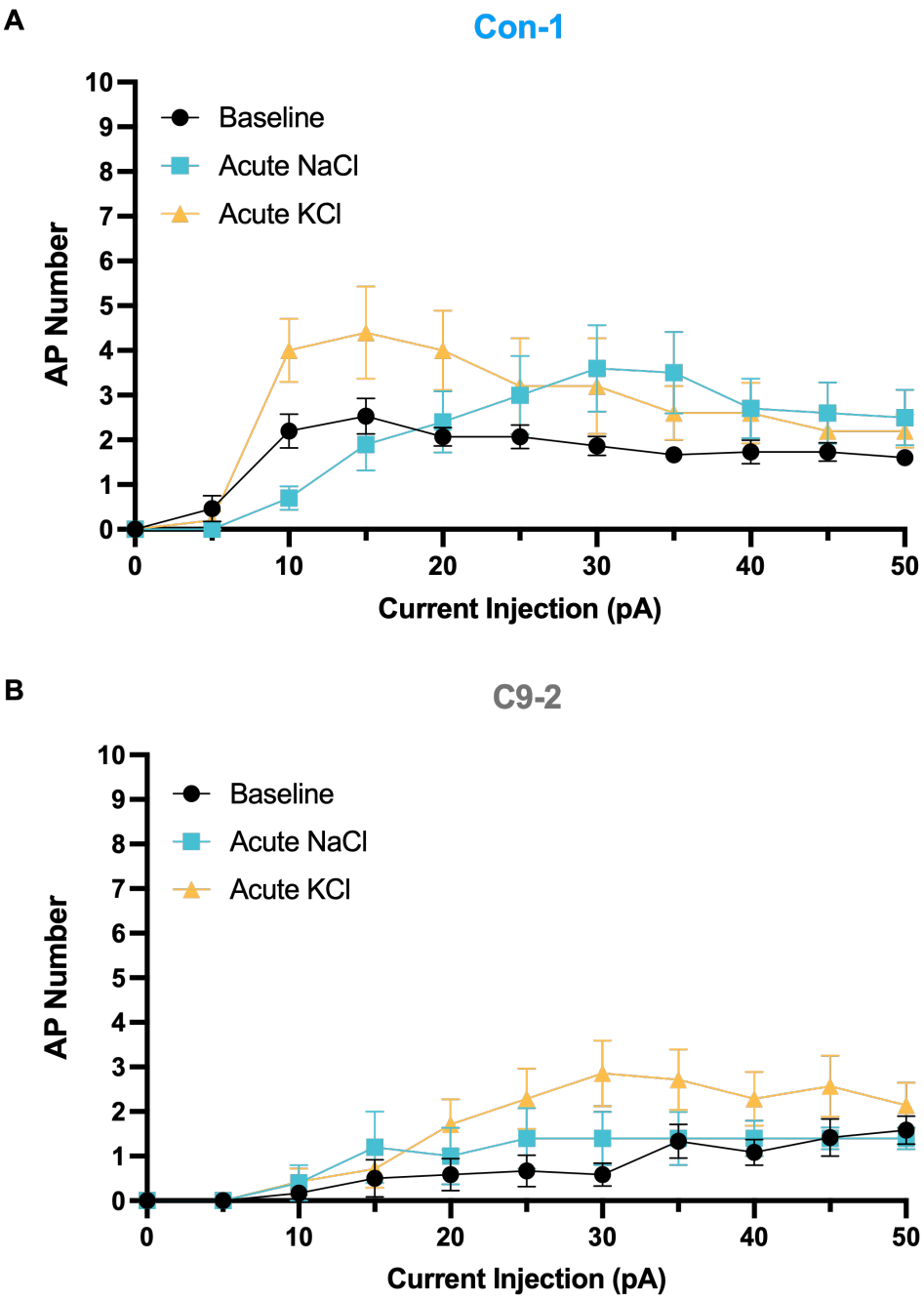

Figure 5.3. Day 40 healthy control and C9-patient LMNs show behave similarly in their response to acute depolarising stress. (A-B) The number of APs evoked following current stimulation stratified by pharmacological treatment (untreated, 3-hour treatment with NaCl or KCl) for **(A)** Con-1 and **(B)** C9-2 LMNs reveals similar voltage responses following acute incubation with NaCl (15 mM, osmotic control) and KCl (15 mM, depolarising stressor) to day 40 baseline voltage responses. All data presented as Mean (±SEM). Data: Con-1: baseline day 40, n=15, N=6; acute NaCl, n=10, N=4; acute KCl, n=5, N=4. C9-2: baseline day 40, n=12, N=5; acute NaCl, n=5, N=2; acute KCl, n=7, N=2. Data determined to be non-significant from repeated measures two-way ANOVA followed by Tukey's multiple comparisons test.

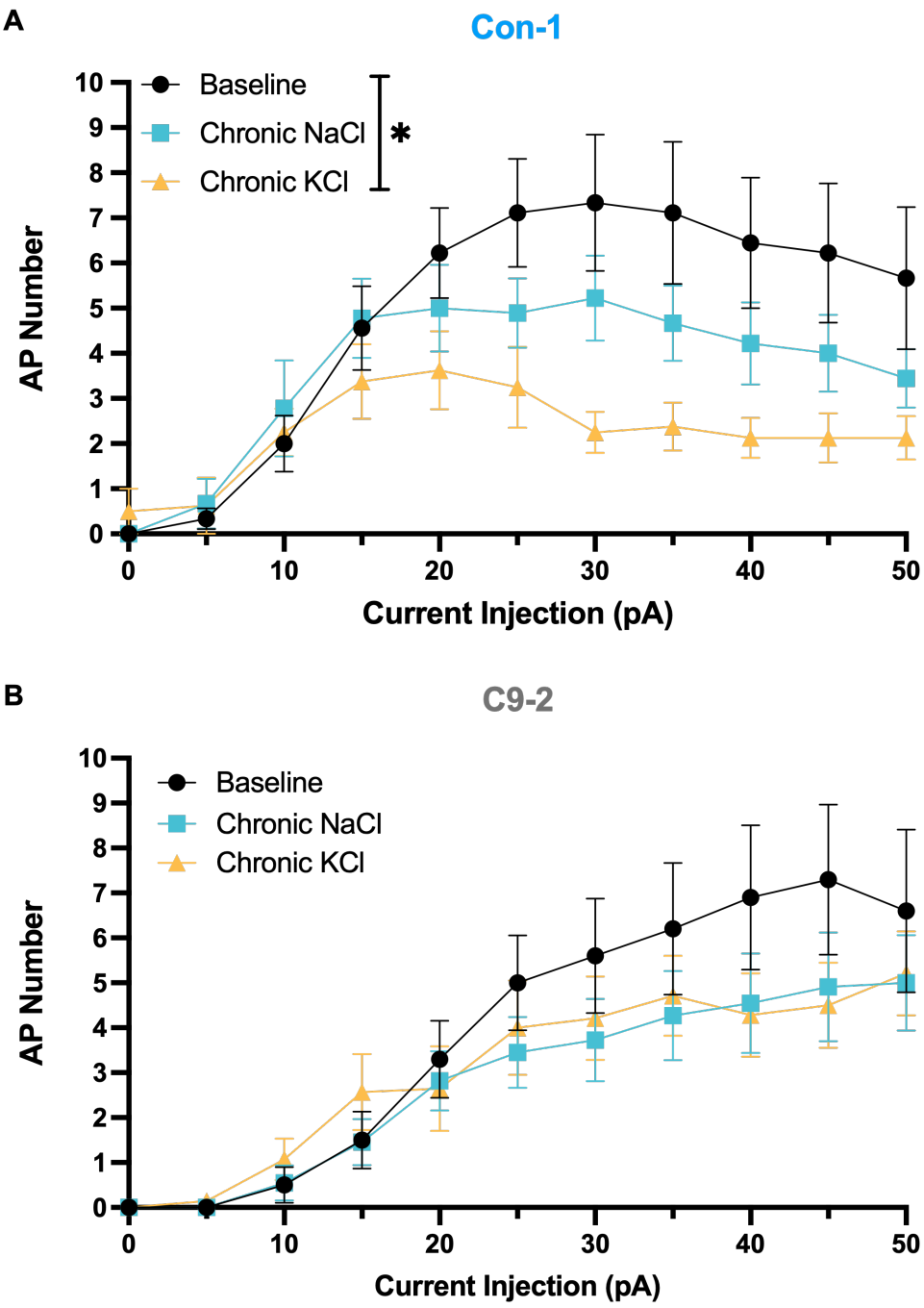

Figure 5.4. Day 50 C9 LMNs have a diminished ability to regulate chronic responses to depolarising stress. (A-B) The number of APs evoked following current stimulation stratified by pharmacological treatment (untreated, 7-day treatment with either NaCl or KCl) for (**A)** Con-1 and (**B)** C9-2 LMNs reveals with respect to the baseline day 50 response, significantly reduced voltage responses to current stimulation after chronic, 7-day KCl treatment in Con-1 but not in C9-2 LMNs. All data presented as Mean (±SEM). * $p<0.05$ from repeated measures two-way ANOVA followed by Tukey's multiple comparisons test. Data: Con-1: baseline day 50, n=9, N=2; chronic NaCl, n=9, N=4; chronic KCl, n=8, N=3. C9-2: baseline day 50, n=10, N=3; chronic NaCl, n=11, N=4; chronic KCl, n=11, N=4.

Accordingly, both cells could maintain homeostatic intrinsic control of excitability in response to short-term stress.

Conversely, chronic depolarising KCl treatment had a substantial impact on neuronal excitability between the different lines as well as the conditions each line was subject to (Figure 5.4A-B). In fact, 7-day incubation with KCl led to a significant decrease in the excitability of Con-1 LMNs compared to baseline and chronic NaCl treated LMNs (two-way ANOVA: $F(2, 23) = 4.96$, $p= 0.0162$) (Figure 5.4A). For example, at 30pA stimulation evoked an average of 7 APs from baseline and 5 from Chronic NaCl Con-1 in contrast with, 2 APs from 7-days KCl treatment. A 3.5- and 2.5-fold difference in the firing activity was seen between these treatment conditions. This was comparable with reduced excitability observed following chronic optogenetic stimulation (Wefelmeyer et al., 2015) or KCl conditioning (Grubb and Burrone, 2010) in *in vitro* rat hippocampal cultures. Even so, the impact of chronic KCl on neuronal excitability was in stark contrast to observations in C9-2. Comparative analysis between baseline, chronic NaCl and KCl in C9-2 showed no significant differences in the firing activity of C9-2 LMNs (two-way ANOVA: $F(2, 32) = 1.015$, $p= 0.374$) (Figure 5.4B). Full details of post-hoc Tukey's multiple comparisons test are detailed in Appendix 7. For instance, at 30pA stimulation an average of 6 APs were evoked in baseline C9-2 compared with 4 spikes following both chronic treatments. Despite a slight decrease in AP output from chronic KCl C9-2 LMNs, this was identical to the output observed in chronic NaCl C9-2. Furthermore, this decrease was modest in comparison to the drop off seen between baseline and chronic KCl in the Con-1 line. The data would indicate whilst homeostatic mechanisms are able to regulate neuronal excitability in the short-term of both Con-1 and C9-2 LMNs, these mechanisms become dysregulated in response to long-term depolarisation in C9 but not healthy controls. Moreover, data from baseline responses at day 40 and 50 (Figure 5.3-5.4) but also from Results section 4.33 suggests, the presence of the repeat expansion itself is not enough to induce excitability changes but required chronic stress to impair excitability homeostasis.

5.33 The AP Waveform is Unaffected in Chronically Treated C9 LMNs

Next, I wanted to determine whether the different treatment conditions affected the AP waveform and complemented the changes or the lack of them in chronic and acute

treated LMNs. Parallel with previous characterisation of the waveform the current threshold for AP spiking, AP amplitude, threshold potential, AP duration and AHP were compared between treatments for both LMNs (Figure 5.5-5.6).

For Con-1, the current threshold for AP output (recruitment current) supports the I-O relationships in Figure 5.3A. Statistical comparisons of the rheobase showed insignificant differences across all treatment types (Kruskal-Wallis test: $p<0.05$; Dunn's multiple comparison test: Con-1: Baseline vs acute NaCl: $p=0.054$; baseline vs acute KCl: $p= >0.99$; acute NaCl vs acute KCl: $p=0.09$) with a slightly higher rheobase for acutely NaCl treated Con-1 LMNs correlating with the reduced output at lower current stimuli (Figure 5.5A). On the other hand, C9-2 LMNs show a sequential but insignificant decrease in the current threshold between baseline, acute NaCl and KCl treatment (one-way ANOVA: $p>0.05$) that has no impact on recorded I-O (Figure 5.5B). Furthermore, treatment conditions had no impact on the current threshold in Con-1 and C9-2 exposed to chronic incubations (Figure 5.6A-B). This opposes findings from previous studies which show amplified current thresholds correlates with reduced excitability following chronic stimulation (Wefelmeyer et al., 2015, Jamann et al., 2021, Harley et al., 2023a). Even so, differences in the I-O relationships are not explained by changes in current threshold in this study.

Study of the AP amplitude, duration and AHP for both motor neurons lines in both acute and chronic conditions yielded only minor differences (Figure 5.5C-D, G-H, I-J) (Figure 5.6C-D, G-H, I-J). Various AP parameters were also unchanged following previous accounts of acute and chronic stimulation in murine models (Grubb and Burrone, 2010, Jamann et al., 2021). Of note, AP duration did show a trending, yet insignificant (~1.2ms) decrease in chronic KCL treated C9 LMNs versus baseline (Sidak's multiple comparison test: $p=0.12$). The speed of the AP half-width was also ~0.5ms faster than the average AP half-width of Con-1 chronic KCl treated LMNs, which corresponds with the differences in excitability between chronic treated lines. Significant differences were observed in the AP threshold of chronic KCl treated C9-2 LMNs but not Con-1 or any acutely treated neurons (Figure 5.5E-F) (Figure 5.6E-F).

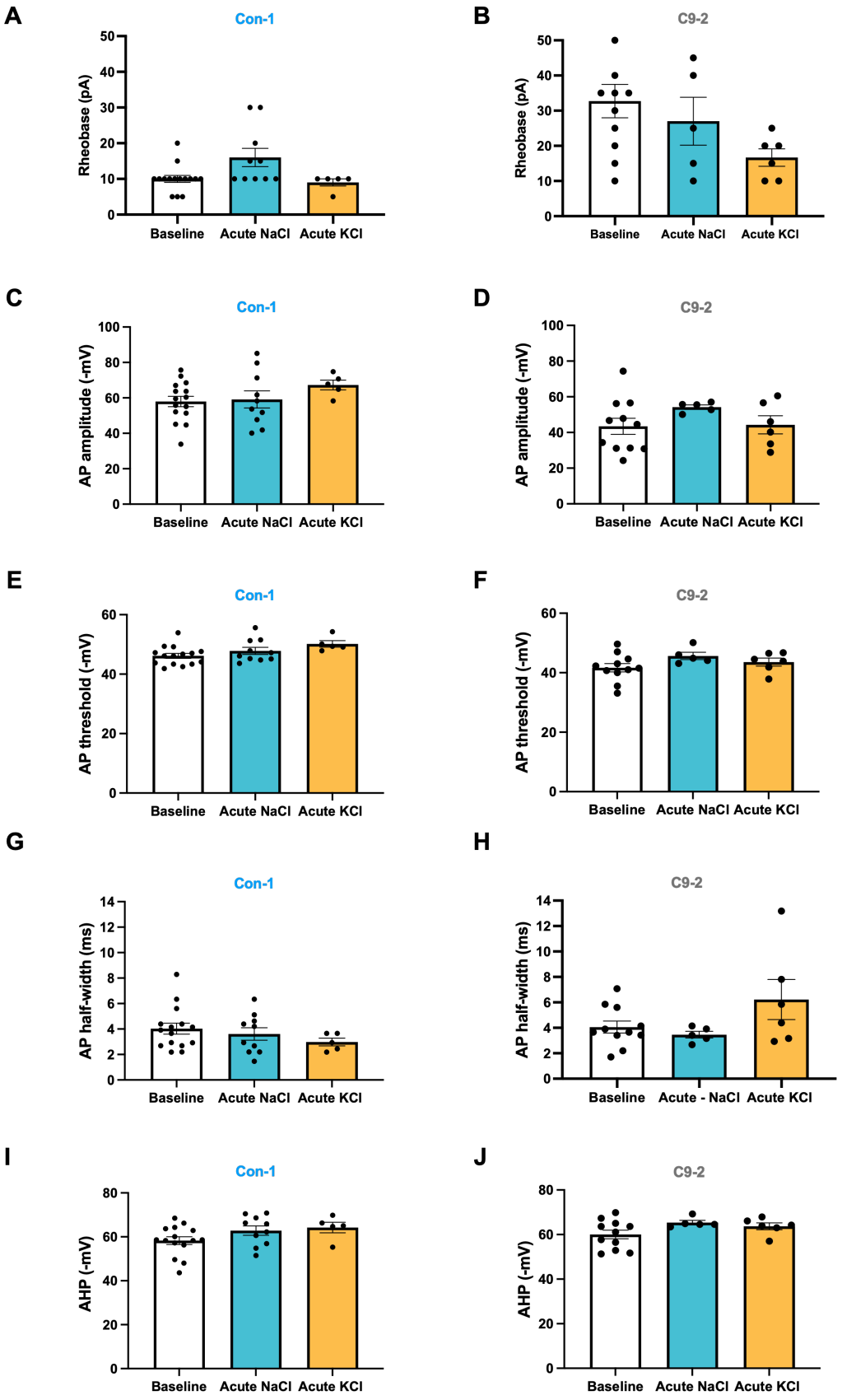
A
Con-1
Rheobase (pA)
Baseline
Acute NaCl
Acute KCl
B
C9-2
Rheobase (pA)
Baseline
Acute NaCl
Acute KCl
C
Con-1
AP amplitude (-mV)
Baseline
Acute NaCl
Acute KCl
D
C9-2
AP amplitude (-mV)
Baseline
Acute NaCl
Acute KCl
E
Con-1
AP threshold (-mV)
Baseline
Acute NaCl
Acute KCl
F
C9-2
AP threshold (-mV)
Baseline
Acute NaCl
Acute KCl
G
Con-1
AP half-width (ms)
Baseline
Acute NaCl
Acute KCl
H
C9-2
AP half-width (ms)
Baseline
Acute - NaCl
Acute KCl
I
Con-1
AHP (-mV)
Baseline
Acute NaCl
Acute KCl
J
C9-2
AHP (-mV)
Baseline
Acute NaCl
Acute KCl

Figure 5.5. Day 40 AP parameters are unaltered following acute treatment with NaCl or KCl. AP parameters were measured from day 40 Con-1 and C9-2 LMNs exposed to different pharmacological conditions. Individual cells are represented by individual circles overlaid onto the bar graphs. Measurements of the recruitment current required to evoke the first AP (rheobase) **(A-B),** AP amplitude **(C-D),** threshold potential **(E-F)**, AP duration **(G-H)** and AHP **(I-J)** were recorded for the first AP evoked by current stimulation. All data presented as Mean (±SEM). Data: Con-1: baseline day 40, n=15, N=6; acute NaCl, n=10, N=4; acute KCl, n=5, N=4. C9-2: baseline day 40, n=11, N=5; acute NaCl, n=5, N=2; acute KCl, n=6, N=2. Data determined to be non-significant from one-way ANOVA followed by Sidak's multiple comparisons test or Kruskal-Wallis test followed by Dunn's multiple comparisons test.

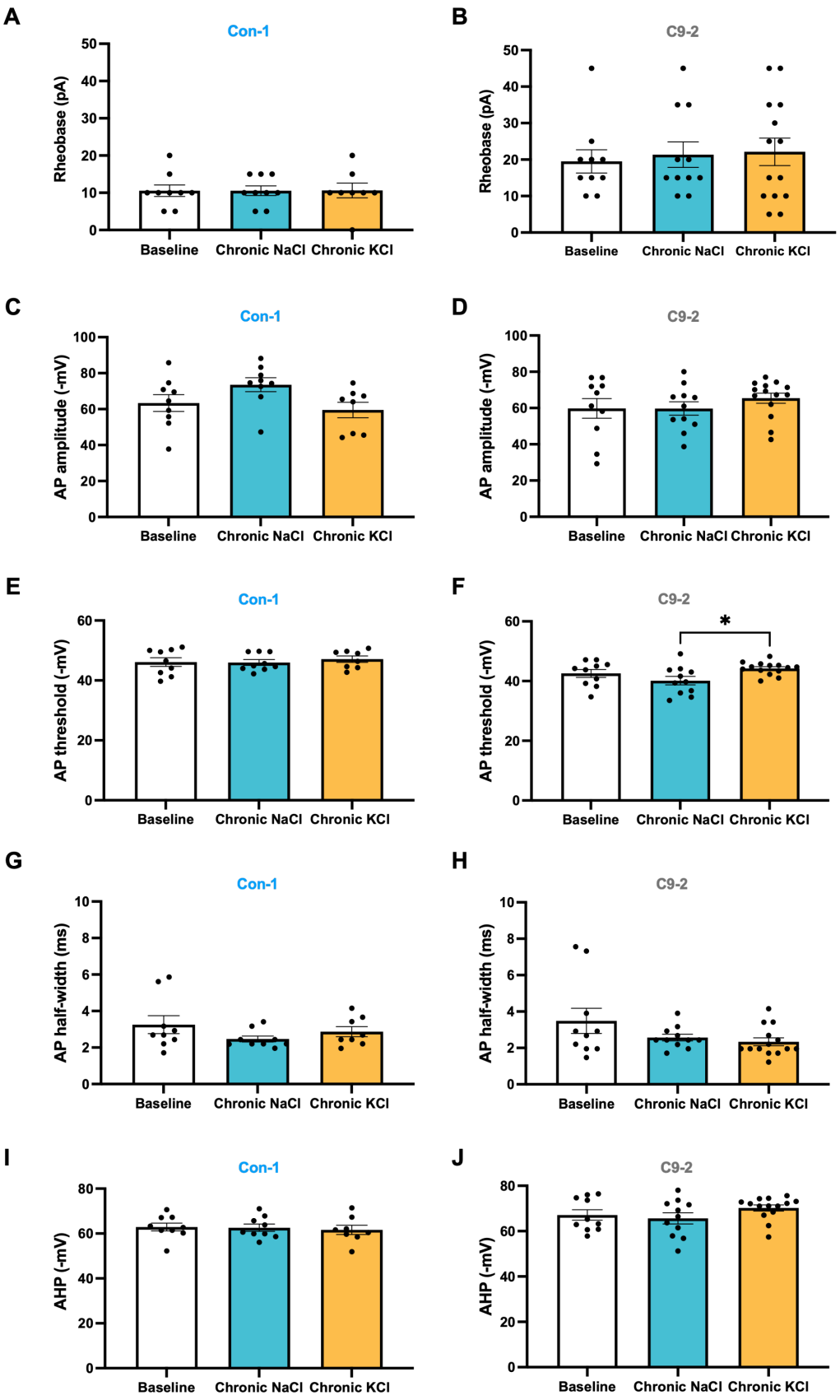
A
Con-1
Rheobase (pA)
50
40
30
20
10
0
Baseline
Chronic NaCl
Chronic KCl
B
C9-2
Rheobase (pA)
C
Con-1
AP amplitude (-mV)
100
80
60
40
20
D
C9-2
AP amplitude (-mV)
E
Con-1
AP threshold (-mV)
F
C9-2
AP threshold (-mV)
*
G
Con-1
AP half-width (ms)
10
8
6
4
2
H
C9-2
AP half-width (ms)
I
Con-1
AHP (-mV)
J
C9-2
AHP (-mV)

Figure 5.6. AP parameters at day 50 are unaltered following chronic treatment with NaCl or KCl. AP parameters were measured from Con-1 and C9-2 LMNs without treatment, or cells exposed to chronic 7-day treatment with either NaCl or KCl. Individual cells are represented by individual circles overlaid onto the bar graphs. Measurements of the recruitment current required to evoke the first AP (rheobase) **(A-B),** AP amplitude **(C-D),** threshold potential **(E-F)**, AP duration **(G-H)** and AHP **(I-J)** were recorded for the first AP evoked by current stimulation. All data presented as Mean (±SEM). * $p<0.05$ from one-way ANOVA followed by Sidak's multiple comparisons test. Data: Con-1: baseline day 50, n=9, N=2; chronic NaCl, n=9, N=4; chronic KCl, n=8, N=3. C9-2: baseline day 50, n=10, N=3; chronic NaCl, n=11, N=4; chronic KCl, n=11, N=4.

Specifically, the threshold potential was hyperpolarised by 4.1mV in C9-2 chronic KCl (-44.2mV) vs chronic NaCl (-40.1mV) (one-way ANOVA: $p<0.05$; Sidak's multiple comparison test: $p=0.029$) but not in regards to the threshold potential in baseline C9-2 neurons (Sidak's multiple comparison test: $p=0.63$). However, this phenotype is not consistent between the baseline and osmotic control which is divergent from depolarised voltage thresholds reported in healthy stimulated iPSC-derived neurons (Harley et al., 2023a). Together with all AP-parameters, altered AP waveform properties do not appear to be the mechanism between impaired I-O relationships in chronically stimulated C9-2 LMNs.

5.34 Changes in Chronic KCl Excitability in C9 LMNs are not Caused by Impaired Passive Membrane Properties

Further comparisons between the intrinsic membrane properties were conducted to determine if these properties were the source behind acute and chronic phenotypes observed in Con-1 and C9-2 LMNs. Ultimately, membrane properties for both cell lines were unchanged in day 40 treated and non-treated LMNs (Figure 5.7A-F) and in LMNs exposed to chronic incubations (Figure 5.7D-L). Similar to AP waveform data in section 5.33, passive membrane properties are not accountable for homeostatic impairments in neuronal excitability.

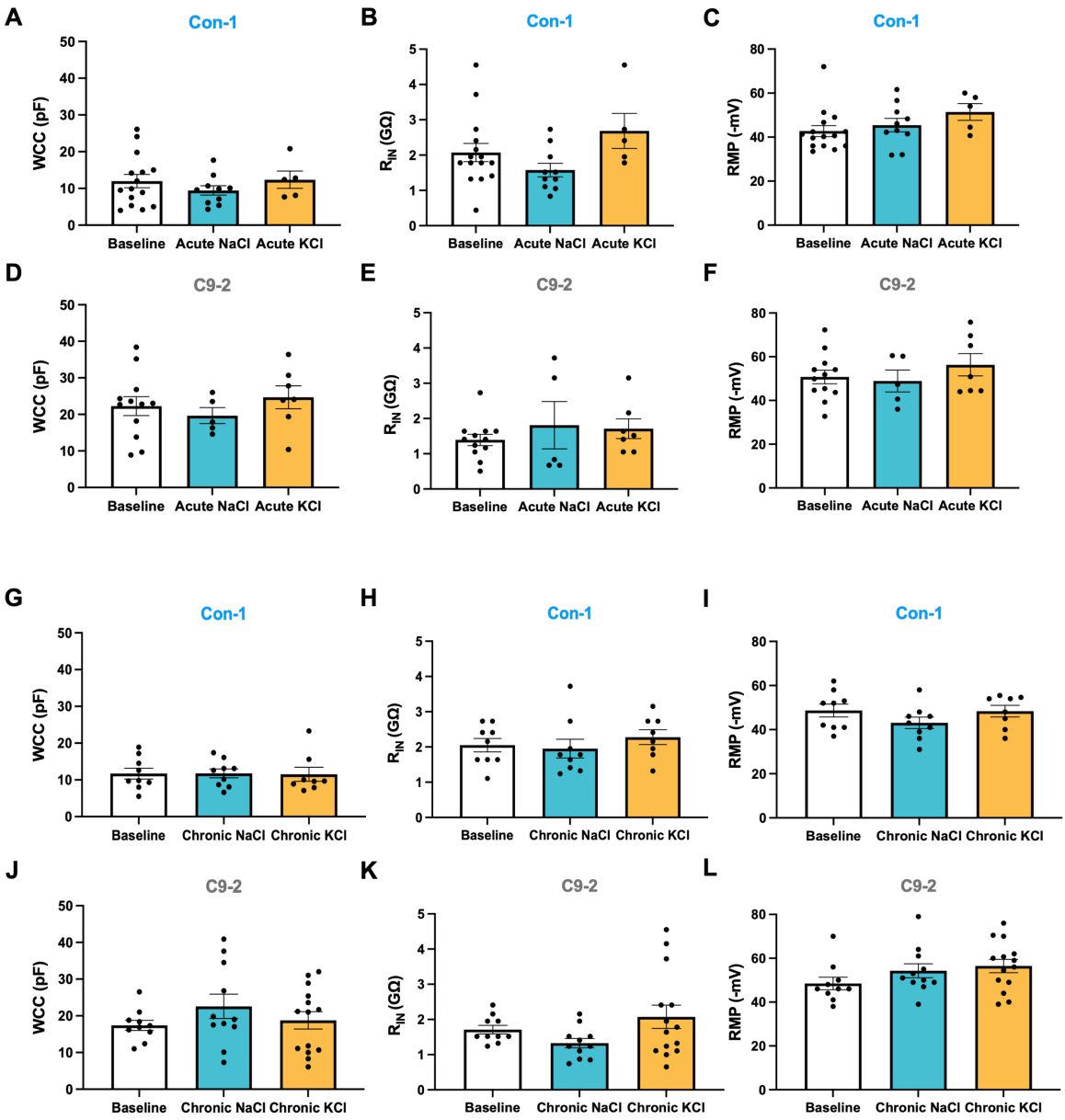

Figure 5.7. Passive membrane properties are not altered by the different acute or chronic treatment conditions. (A-L). Intrinsic membrane property data from Con-1 and C9-2 lines between day 40 to day 50 subjected to the different treatment conditions. Individual cells are represented by individual circles superimposed onto the bar graphs. Quantification of the mean whole cell capacitance (WCC), membrane input resistance (R_{IN}) and resting membrane potential (RMP) from day 40 Con-1 **(A-C)**, day 40 C9-2 **(D-F),** day 47-50 Con-1 **(G-I)** and C9-2 **(J-L)** LMNs. Intrinsic membrane properties were consistent across all treatments. All data presented as Mean (±SEM). Data: Con-1: baseline day 40, n=15, N=6; acute NaCl, n=10, N=4; acute KCl, n=5, N=4; baseline day 50, n=9, N=2; chronic NaCl, n=9, N=4; chronic KCl, n=8, N=3; C9-2: baseline day 40, n=11, N=5; acute NaCl, n=5, N=2; acute KCl, n=6, N=2; baseline day 50, n=10, N=3; chronic NaCl, n=11, N=4; chronic KCl, n=11, N=4. Data determined to be non-significant from one-way ANOVA followed by Sidak's multiple comparisons test or Kruskal-Wallis test followed by Dunn's multiple comparisons test.

5.4. Discussion

In this chapter I have considered a key aspect of disease modelling by recording the ability of C9 iPSC-derived LMNs to appropriately regulate their electrophysiological excitability in response to acute and chronic application of a physiological stressor, elevated extracellular potassium chloride (KCl). Typically, human *in vitro* models, such as C9 iPSC-derived LMNs in the previous chapter are characterised in the absence of any cell stressors, as they are in many other scientific reports (for example, (Selvaraj et al., 2018)). In this basal state, C9 patient LMNs were shown to display no alterations in excitability versus healthy control and isogenic lines (Chapter 4). However, native neurons are exposed to various physiological inputs and stressors in both healthy individuals and neurodegenerative disease. For example, K^+ extrusion from neurons is a major feature of intrinsic potassium conductances during AP firing. This K^+ extrusion requires removal from the vicinity of the neuron (via glia syphoning) since it will cause depolarisation, and potentially depolarisation-mediated excitotoxicity. In ALS it has previously been reported that K^+ syphoning is impaired in SOD1 transgenic animal models (Ding et al., 2024). Importantly, a key protective mechanism of neurons is their ability to downregulate excitability in extended periods of depolarising stress, in order to maintain homeostatic control of neuronal output and function (Gunes et al., 2020). Here, I wanted to determine whether this ability to maintain homeostasis is impaired in C9 patient-derived LMNs in response to physiological stressors that replicate the physiological challenges of LMNs in the corticomotor circuitries they form part of.

To induce acute and chronic depolarising stress, the Con-1 and C9-2 iPSC-derived LMN ‘workhorse’ lines were incubated with 15mM KCl for 3 hours or 7 days, respectively. In accordance with the Nernst potential this would have been sufficient to induce depolarisation of the membrane by 33 mV; from the mean RMP values of these lines (Figure 5.7) this would have caused depolarisation beyond AP threshold (Figure 5.5-5.6) to initiate neuronal activity. Voltage responses were recorded using whole-cell current-clamp mode where neuronal excitability was evaluated under three independent, age-matched conditions: without any additional treatment (baseline) or with either 15mM NaCl or 15mM KCl for 3 hours (acute) or 7 days (chronic). My data indicate that control LMNs present no change in excitability in response to acute

stress, but for chronic stress, a marked reduction in AP numbers elicited versus Con-1 day 50 LMNs at baseline. However, whilst C9 LMNs behave like control LMNs for acute stress, for chronic conditions they demonstrate reduced homeostatic ability to regulate excitability in response to depolarising stress. This is shown by the fact that the number of APs evoked by chronically stimulated C9 LMNs are similar to those evoked by corresponding C9 baseline/osmotic control day 50 LMNs. This is a key outcome that is indicative that C9 neurons do not present with a key neuroprotective mechanism in chronic conditions. I will explore these findings further below.

A key finding from this study is that Con-1 LMNs exhibit robust homeostatic responses to chronic depolarisation. The observed reduction in AP output following chronic KCl exposure is consistent with previous reports demonstrating that neurons downregulate excitability in response to sustained depolarisation (Grubb and Burrone, 2010, Wefelmeyer et al., 2015) . This adaptive mechanism, known as homeostatic plasticity, serves to prevent hyperexcitability and protect neurons from excitotoxicity. The reduction in excitability was interestingly not associated with major changes in AP waveform parameters or significant changes in the passive membrane properties (WCC, R_{IN} or RMP), between baseline or chronic NaCl treatment versus chronic KCl treatment in either iPSC-derived line. Unlike the theoretical Nernst potential value or previous studies that have shown KCl-induced depolarisation of the RMP (Evans et al., 2013, Evans et al., 2015), or hyperpolarising shift in RMP (O'Leary et al., 2010), the data here reveals no such change. One possible explanation may arise from RMP depolarisation during chronic KCl incubation of LMNs which is then reversed once neurons are recorded in physiological extracellular solution with nominal potassium concentration. Alternatively, chronic KCl treatment may influence intrinsic excitability via alternative mechanisms and that both iPSC-derived lines are able to regulate their RMP at 15mM KCl concentration. However, my data present an unclear picture as to the mechanisms that underlie this homeostatic adaptation in control LMNs.

In contrast, C9-2 LMNs failed to exhibit a significant reduction in excitability following chronic KCl treatment. The preservation of baseline-like AP firing suggests a deficit in homeostatic plasticity mechanisms in these neurons. Importantly, this finding aligns with previous studies indicating that homeostatic dysfunction is an early feature of neurodegenerative disease, including C9ORF72-associated FTD/ALS (Milnerwood

and Raymond, 2010, Benussi et al., 2016, Pasniceanu et al., 2021). The inability to regulate excitability under chronic stress conditions may contribute to neuronal vulnerability and degeneration in C9ORF72 patients. In this regard, in the context of chronically elevated, depolarising extracellular KCl, impaired K^+ syphoning and impaired ability to downregulate excitability, presents a plausible mechanism for LMN excitotoxity. Similar to control data, I find no difference in the properties of AP waveform and passive membrane properties. However, the fact that the key phenotype is a reduced responsiveness is perhaps not surprising. In the context of data from other reports, dysregulated ion channel function relating to the AP waveform has previously been associated with excitability changes in ALS patients and C9 models (Kanai et al., 2006, Sareen et al., 2013, Wainger et al., 2014). However, it is unlikely Na^+ or K^+ current dysfunction are significant contributors to compromised excitability homeostasis in C9 LMNs, in fact my data are consistent with an ineffective ability to down tune excitability. This raises the question of what physiological mechanisms are driving impaired excitability homeostasis.

One possibility for phenotypic difference following prolonged KCl treatment may be due to impaired activity-dependant AIS plasticity. Recent work in other model systems has demonstrated a modulation of excitability in response to acute, short-term stimulation, in the form of rapid activity-dependant shortening of the AIS (Evans et al., 2015, Jamann et al., 2021). Evans and colleagues have shown such AIS remodelling to be mediated by Ca^{2+}-dependent process that act in part due to Ca^{2+}-dependent phosphatase calcineurin (Evans et al., 2013, Evans et al., 2015). The AIS, the site of AP initiation, is a specialised microdomain located at the proximal axon that consists of a high density of Na_v and K_v channels anchored to the membrane by a complex arrangement of cytoskeletal scaffolding proteins (Huang and Rasband, 2018). This specialised region is fundamental for setting the intrinsic excitability of the neuron. Thus, the structural changes at the AIS may be the underlying mechanism behind observations here following acute treatment, where dynamic AIS plasticity is able to appropriately regulate neuronal output in response to acute KCl, possibly through Ca^{2+} dependent processes. Interestingly, KCl-induced Ca^{2+} dyshomeostasis leading to increased intracellular Ca^{2+} has been shown previously in C9-iPSC derived MNs (Dafinca et al., 2020, Burley et al., 2022). Consequently, this may impact expression of ion channel genes that contribute to dysregulated I-O observed here in C9 LMNs.

Also, C9 ALS MNs have been shown to exhibit altered CREB activity in addition to downregulated synaptic gene expression or structural synaptic loss that may be relevant for inducing altered homeostatic responses here (Catanese et al., 2021).

Interestingly, a recently published study overlaps significantly with this work (Harley et al., 2023a). The authors demonstrated impaired excitability homeostasis in iPSC-derived MNs from mTDP-43 and C9 patients due to impaired AIS dynamics following external optogenetic stimulation (Harley et al., 2023a). Coinciding with my data here, the study reports similar findings in impaired intrinsic neuronal output in ALS MNs (non-significantly different) that were concurrently decreased in control lines (significantly reduced excitability). Importantly, Harley and colleagues do not report waveform properties to be able to compare with our data sets, it is therefore unknown whether they also observe no shift in these properties (Harley et al., 2023a). Interestingly, iPSC-derived cortical neurons from FTD-Tau patients have been shown to display abnormal increases in neuronal activity in response to chronic KCl depolarisation that are linked to cytoskeletal impairment at the AIS (Sohn et al., 2019), suggesting that responses to extracellular depolarisation could be different depending on brain region.

Multiple lines of evidence have shown the dynamic, plastic ability of the AIS to undergo activity-dependant structural changes to ensure homeostatic regulation of intrinsic excitability (Grubb and Burrone, 2010, Kuba et al., 2010, Evans et al., 2013, Evans et al., 2015, Wefelmeyer et al., 2015, Jamann et al., 2021). Specifically, responses to chronic depolarisation have been shown to induce distal relocation (Grubb and Burrone, 2010, Evans et al., 2013, Wefelmeyer et al., 2015), but chronic deprivation of stimuli leads to increased excitability via increased AIS length (Kuba et al., 2010, Jamann et al., 2021). In line with this, I would hypothesise in response to chronic KCl depolarisation, the AIS in Con-1 LMNs is either shortened or relocated further away from the soma which allows these neurons to dampen intrinsic excitability. Conversely, such AIS activity-dependent plasticity in C9-2 LMNs is impaired (AIS remains same length or does not relocate distally) and leads to aberrant homeostatic regulation of neuronal activity as indicated by modification of the I-O relationship relative to Con-1. Future work should focus on characterising these stress-induced LMNs in greater detail, in terms of excitatory and inhibitory transmission as these are key influences

on neuronal activity and output. In addition, work should address whether the hypothesised structural AIS changes are accompanied with corresponding molecular changes in AIS-specific proteins. These stress-induced changes could result from changes in the phosphorylation status of ion channels, or expression changes in key AIS genes for ankyrin-G and Na_V that have been shown to correlate with changes in AIS length (Evans et al., 2015, Harley et al., 2023a). Key experiments to enhance the characterisation of stress-induced LMNs are discussed in section 6.5.

My data presented here raises an important disease modelling scenario. Crude, long-term treatment with KCl could replicate an early pathophysiological ALS disease state whereby LMNs are constantly depolarised due to UMN hyperexcitability within corticomotor circuits (Pradhan and Bellingham, 2021, Reale et al., 2023) and/or have impaired K^+ extrusion (Ding et al., 2024). Impairments in homeostatic regulation of intrinsic excitability may indeed contribute towards increases in LMN activity that, in turn may contribute towards muscular fasciculations observed at symptomatic onset in ALS patients (Menon et al., 2020), which coincides with a more severe disease prognosis (Shimizu et al., 2014). Furthermore, failure of homeostatic mechanisms may also relate to pathological processes mediated by TDP-43 and C9ORF72. Recent studies have demonstrated elevated LMN activity is sufficient in driving hallmark TDP-43 accumulation and aggregation in addition to the production of toxic DPR species (Westergard et al., 2019, Weskamp et al., 2020). Together, abnormal regulation of neuronal activity and subsequently induced TDP-43 and C9 related pathophysiology could further drive hyperexcitable neuronal dysfunction within LMNs that forms a vicious, degenerative positive feedback cycle in C9FTD/ALS.

5.5. Conclusion

In this chapter and in the previous, I report a lack of alterations in the intrinsic excitability of C9 iPSC-derived LMNs in the absence of cell stressors and in response to acute depolarising stress. Thus, in the short-term C9 LMNs are likely to possess the necessary homeostatic mechanisms to counter acute depolarising stimuli and maintain activity levels accordingly. However, these homeostatic mechanisms appear to become overridden in response to chronic, long-term depolarisation and lead to impairments in excitability homeostasis in C9 LMNs that are not observed in controls. Homeostatic regulation of neuronal activity was not related to perturbations in maturation of chronically treated LMNs or because of AP waveform-related ion channel dysregulation. A possible source of abnormal homeostatic plasticity may occur at the AIS of patient lines. Ultimately, the presence of the repeat expansion itself, alone, is insufficient to induce excitability changes in the absence or following acute exposure of stressors. Instead, the presence of chronic depolarising stress is required in addition to impair excitability homeostasis in C9 patient LMNs in this study.

Chapter 6: Discussion and Future Directions

6.1. Introduction

The primary purpose of this study was to:

A. Investigate the neurophysiological function of C9ORF72 repeat expansion patient-derived medium spiny neurons (MSNs).
B. Investigate the neurophysiological function of iPSC-derived lower motor neurons (LMNs) generated from C9ORF72 repeat expansion patients. Work here was extended to include study of excitability homeostasis.
C. To compare functional electrophysiological properties between patient derived-MSNs and patient-derived LMNs.

These were the overriding aims of my investigations which have been addressed in my work and have been discussed in detail in each of the individual results chapters. In this section I will summarise my results before discussion of my findings in a broader context and address future research directions.

6.2. C9ORF72 Patient-derived MSNs are Hypoexcitable

Data from Chapter 3 provides novel evidence of neurophysiological perturbations in C9FTD/ALS MSNs. Also, the findings here indicate electrophysiological dysfunction extends beyond cortical and motor neurons commonly implicated in disease to other neuronal types that could be significant in disease pathogenesis. A summary of key findings from my investigation into the electrophysiological behaviour of MSNs are as follows:

- Human *in vitro* models of enriched C9 MSNs display reduced intrinsic excitability and are not associated with any impairments in viability or maturation properties including in the expression of transmitter-gated ion channels.
- Consistent with intrinsic hypoexcitability, various components of the AP waveform are heavily impacted including AP amplitude, threshold, duration and AHP.

- Deficits in AP waveform are mediated, at least in part, by reduced functional expression of I_k channels in C9 MSNs. This family of ion channels is a key regulator of the AP repolarisation phase.
- Targeted pharmacological increase of function of specific I_k channels (BK and K_v3 potassium channels) was sufficient to rescue waveform deficits, but importantly, not intrinsic hypoexcitability.
- A possible explanation for these observations in patient MSNs may arise from a dual pathogenic mechanism involving select I_K channel dysfunction that coincides with pathophysiological structural changes linked to AIS function.

6.3. Future Work

What are the implications of MSN hypoexcitability as a pathophysiological feature in the general context of FTD/ALS?

There is an ever-growing amount of evidence that reports striatal dysfunction in FTD/ALS including C9-mediated disease that extends from hallmark TDP-43 pathology to neuronal atrophy or circuitry deficiencies especially in frontostriatal regions (Bede et al., 2013, Brettschneider et al., 2013, Bertoux et al., 2015, Ahmed et al., 2021, Bocchetta et al., 2021). The functional electrophysiological data generated in this study is specific to select patients characterised by the C9ORF72 repeat expansion mutation and adds to this pre-existing body of work. Thus, it will be important to characterise the intrinsic excitability of MSNs derived from sporadic patients in conjunction to those characterised by known mutations in other FTD/ALS genes. This will help establish whether MSN hypoexcitability is indeed a cardinal feature of FTD/ALS in general.

How is MSN hypoexcitability mediated with respect to a possible dual mechanism involving I_K channel dysfunction and structural alterations at the AIS?

In Chapter 3 the electrophysiological data provides supporting evidence of MSN loss-of-function in FTD/ALS, as shown by hypoexcitability of C9 MSNs that coincides with reduced functional expression of I_k channels. As alluded to earlier, my data associates decreased I_k channel expression in MSNs with intrinsic hypoexcitability in contrast to with I_K associated- MN hyperexcitability shown previously (Wainger et al., 2014). The

source of hyperexcitable currents in this study were unknown but hyperexcitability was reduced with the treatment of K_v7 activator, retigabine (Wainger et al., 2014, Huang et al., 2021b). Since K_v7 mediated sub-threshold properties (RMP and R_{IN}) are not impacted in C9 MSNs, I would hypothesise retigabine treatment would exacerbate the hypoexcitable C9 phenotype and instigate hypoexcitability in healthy control and isogenic MSNs. Thus, rendering this pharmacological agent unsuitable for treatment in C9 MSNs.

Pharmacological rescue of AP waveform was demonstrated via targeting BK and K_v channel activity. Of note, AUT1 is reported to target K_v3 channel modulator (Rosato-Siri et al., 2015), and a sister compound is currently in trials for schizophrenia (Angelescu et al., 2022). However, there is limited evidence to suggest K_v3 channel expression in MSNs (Weiser et al., 1994). Thus, AUT1 induced modulation of AP parameters in C9 MSNs may result from: i) non-specific targeting of K_v channels or ii) from MSN expression of K_v3 channels and therefore AUT1 modulation of channel function. Nonetheless, precise gain-of-function in post-threshold I_K channel function noticeably targets the structure of the AP but not the firing tone of C9 MSNs. To confirm whether these ion channels (BK and K_v3) are indeed the principal mediators of dysregulated I_K function, I would propose quantifying channel expression at the protein level primarily via western blot analysis which I would suspect to be downregulated. This could also be supported by proximity ligation assays. If true, findings from iPSC-derived MSNs could be evaluated in post-mortem striatum from C9 patients to determine if such phenotypes are indeed recaptured.

Critically, a combination of both NS11021 and AUT1 were required to rescue all waveform deficits rather than the effects of either compound in isolation. Thus, it would be intriguing to determine the effects of both compounds together on AP waveform and membrane excitability via current-clamp analysis on C9 MSNs. Neurophysiological impairments here are likely to result from dysfunction in more than one I_K channel especially when considering the function role of different ion channels are closely interlinked, as shown previously between BK and K_v2 channels (Kimm et al., 2015).

The AIS is known to regulate neuronal excitability (Kuba et al., 2010, Evans et al., 2015), plus AIS disturbances have been previously reported in multiple studies (Sasaki and Maruyama, 1992, Sohn et al., 2019, Jorgensen et al., 2021, Harley et al., 2023a). Furthermore, rescue of waveform deficits by targeting specific ion channels with concentrated expression at the AIS (Xu et al., 2007, Filipis et al., 2023), does not influence the tone of firing in C9 MSNs. Therefore, it would appear that all roads lead to structural AIS dysfunction in driving hypoexcitability in patients MSNs. To determine whether AIS length is shortened or at a more distal location from the soma in patient MSNs, immunocytochemistry staining for ankyrin-G, a specific AIS marker, in control and C9 MSNs would be paramount. Furthermore, post-mortem ankyrin-G staining could be conducted in post-mortem FTD/ALS patient striatum along with quantification of ankyrin-G expression via western blot or quantitative PCR to evaluate deficits at disease end-stage. A recent study by Harley and colleagues demonstrated late-stage iPSC-derived ALS MNs and ALS post-mortem ALS spinal MNs exhibited reduced AIS length which coincided with neuronal hypoexcitability in their iPSC MN model (Harley et al., 2023a). Moreover, AIS localised I_K channels have been shown to undergo K_v7 induced distal relocation within the AIS that can result in reduced intrinsic excitability (Lezmy et al., 2017). This adds another layer of complexity to AIS plasticity, but is unlikely to occur in our models, at least not via K_v7 orchestrated mechanisms.

Altogether, I hypothesise a double-faced pathomechanism that contributes to C9 MSN hypoexcitability that involves I_k-mediated dysfunction of AP waveform in addition to AIS disturbances that are responsible for reduced excitability.

What type of MSNs are modelled in my human in vitro MSN model?

MSNs are the principal cell type of the dorsal and ventral striatum that comprise up to 95% of the total cellular population (Prager and Plotkin, 2019). The MSNs belonging to these different regions not only have different functions, motor (dorsal) vs cognitive (ventral), but are differentially impacted in disease, FTD/ALS (ventral) vs HD (dorsal). To date, iPSC-derived MSN protocols are yet to define regionally specific MSN striatal differentiation. Although, regional specific markers are beginning to emerge (Chen et al., 2021, Reiner et al., 2024), and will be crucial in the validation of MSN specification here and in future studies. A recent study by Moya and colleagues revealed specific degeneration of Gprin3-expressing cortical neurons in a SOD1 mouse model (Moya et al., 2022). Interestingly, Gprin3 is also expressed with MSNs that form the ‘indirect’

pathway and Gprin3 knockout has to been shown to induce hypoexcitability within these MSNs that was associated with increased motivation (Karadurmus et al., 2019, Moya et al., 2022). MSNs can also be subdivided into two populations based on direct pathway MSN expression of D1-type dopamine receptor or indirect pathway expression of MSN containing D2-type dopamine receptors (Gerfen et al., 1990, Kreitzer, 2009). Previous iPSC-derived striatal protocols report a combination of both dopamine D1-type and D2-type receptor expression (Le Cann et al., 2021, Conforti et al., 2022, Tam and Keung, 2022). Accordingly, future work should focus on characterising dopamine receptor expression and by inference whether iPSC-derived MSNs generated belong to direct or indirect pathways. Linking electrophysiological behaviour to either pathway is of importance given these pathway have separate functions in shaping emotional and motivational behaviours (Wang et al., 2024). Direct pathway MSN projections directly inhibit the output nuclei (substantia nigra pars reticulata and internal globus pallidus). These in turn inhibit glutamatergic thalamus neurons, but becomes disinhibited following D1-MSN activation, subsequently leading to excitatory thalamus inputs into the cortex. Meanwhile, indirect D2-MSNs projects to the substantia nigra pars reticulata indirectly via the external globus pallidus and subthalamic nucleus. Ultimately, activation of D2-MSNs in the indirect pathway leads to increased inhibition of thalamic neurons and subsequently the cortex.

Evaluation of the translational implications of iPSC-derived MSN intrinsic hypoexcitability.

The human *in vitro* neurons generated in this study were enriched, electrophysiologically mature cultures. Subsequently, these iPSC-derived monocultures presented neurophysiological phenotypes that would appear to be initiated by cell autonomous mechanisms, given that these are pure neuronal cultures. Whilst an advantageous feature of this model system it also comes with certain limitations. Importantly, FTD/ALS has a non-cell autonomous component to it that needs to be considered from two different aspects of disease modelling. Firstly, glial cells are particularly crucial for neuronal maturation in terms of synaptic expression and function (Fernandopulle et al., 2018); although it was neurotransmission and the functional expression of ligand-gated channels that were studied, not synaptic transmission. Nonetheless, this links in with the immature nature of iPSC-derived neurons relative to their *in vivo* counterparts in terms of their transcriptomic and fetal-

like epigenetic signatures (Ho et al., 2016). Secondly, astrocytes are known to impact viability and induce LMN hypoexcitability (Zhao et al., 2020), and have also been shown to modulate MSN excitability (Khakh, 2019, Nagai et al., 2019). Consequently, whether expression of glial cells influences the excitability phenotypes here warrants further study. iPSC-derived MSN monocultures are perfect for studying GABA-ergic MSNs in isolation, but they do not articulate the complex neuronal networks (corticostriatal, mesocorticolimbic and nigrostriatal pathways) that MSNs form part off (Figure 1.4). In agreement, interactions between MSNs and for example dopaminergic striatonigral or glutamatergic cortical inputs can influence neuronal function and maturation (Paraskevopoulou et al., 2019). Thus, it is difficult to assess the functional implications of GABA-ergic MSN loss-of-function on downstream targets.

To tackle these limitations, it will be important to study electrophysiological MSN function within models that can replicate mature cellular physiology in conjunction to complex striatal network physiology i.e. striatal inputs and outputs. One approach could involve transgenic FTD/ALS murine models to study neurophysiological MSN properties, whereby striatal dysfunction has already been implicated. Expression of mutant TDP-43^{M337V} in murine models has been shown to induce behavioural and motor phenotypes along with reduced survival that can be partially rescued with tetramethylpyrazine nitrone (Huang et al., 2021a, Yan et al., 2014). Furthermore, expression of TDP-43 with a defective NLS has been shown to result in FTD/ALS phenotypes, along with hallmark TDP-43 deposits within the striatum of transgenic models (Walker et al., 2015a, Walker et al., 2015b). C9FTD/ALS transgenic mouse models display hallmark C9 pathology within the striatum that can be rescued following *in vivo* gene editing, making this a particular model of interest (Meijboom et al., 2022). Morphological abnormalities and alterations in striatal synaptic plasticity and behaviours resulting from degeneration of dopaminergic neurons have also been reported in SOD1^{G93A} models (Geracitano et al., 2003, Fogarty et al., 2017). Collectively these studies support the application of murine models to further investigate striatal dysfunction in FTD/ALS. However no model is perfect, with murine models limited by the inability to fully recapture all elements of disease (Balendra and Isaacs, 2018, Mead et al., 2023).

Alternatively, generation of 3D organoid cultures would allow for study of striatal dysfunction in patient-derived cellular models that recapture the physiological relevance and complexity *in vivo.* Such cultures are already in use in FTD/ALS research (Pereira et al., 2021). Moreover, human striatal organoids and cortico-striatal assembloids have been generated from human iPSCs that produce electrophysiologically mature MSNs (Miura et al., 2020). Although further work is required as this model system is still in its infancy and is limited by the survival time of cultures, incomplete maturation of tissues and high costs associated with cultures (Andrews and Kriegstein, 2022). Another model system that could be of use is the human co-culture system, whereby MSNs are cultured in a controlled environment along with striatal inputs or target neurons.

6.4. Translational Implications of Research Findings

At what stage of disease course is MSN hypoexcitability a feature of?

The data from my C9 iPSC-derived MSNs would indicate patient lines become progressively hypoexcitable with time. Though, its important to note this disease phenotype becomes apparent within the course of 60 days in my human *in vitro* MSN model but in reality FTD/ALS phenotypes appear after decades. Age-associated phenotypes are lost during somatic cell reprogramming and therefore it is difficult to state what stage of the disease course is being modelled in this system (Cerneckis et al., 2024). Inferences from longitudinal neuroimaging studies in C9FTD/ALS patients can be drawn upon to help establish the sequence of striatal dysfunction over the disease course. Evidence of neuronal atrophy within the striatum of post-mortem FTD/ALS patients has been well documented (Kato et al., 1994, Riku et al., 2016). Neuroimaging studies have revealed striatal dysfunction and associated disruption of frontostriatal networks in symptomatic and presymptomatic C9 patients in comparison to healthy controls (Bede et al., 2013, De Vocht et al., 2020, Ahmed et al., 2021, Bocchetta et al., 2023). Deficits in grey matter volume have been shown to progressively worsen over the disease course from presymptomatic to symptomatic stages in FTD/ALS cases including *C9ORF72* cases (Westeneng et al., 2015, Lee et al., 2017a, Bocchetta et al., 2023). This would suggest a loss of striatal network function. Interestingly, Rohrer and colleagues revealed a significant reduction in

striatal volume of FTD/ALS mutant carriers 5 year prior to expected disease onset (Rohrer et al., 2015), that may represent a state whereby striatal dysfunction is prominent prior to TDP-43 pathology (Brettschneider et al., 2013). These and future studies will be crucial in firmly establishing striatal dysfunction in FTD/ALS pathophysiology throughout disease course.

MSN hypoexcitability as a therapeutic target in FTD/ALS.

MSN dysfunction is considered a therapeutic target for multiple neurodegenerative diseases (Soderstrom et al., 2010, Tshilenge et al., 2023) and neurological conditions (Geng et al., 2017, Hong et al., 2019). Similar to GABA-ergic MSNs here, other GABA-ergic interneurons like those in the cortex have also been reported in FTD/ALS to exhibit an hypoexcitable phenotype (Khademullah et al., 2020, Lin et al., 2021). Hence, increasing inhibitory GABA-ergic function is an attractable therapeutic target to rescue loss of GABA-ergic function in the striatum and beyond. Riluzole, the only approved ALS drug licensed in the UK reduces neuronal excitability by inhibition of Na_V channel currents on glutamatergic nerve terminals (Hollingworth et al., 2024). Thus, would be inappropriate in treating hypoexcitable C9 MSNs.

The AP waveform especially in the repolarisation phase was impaired in C9 MSNs and ion channels that regulate this AP phase. These deficits were therefore specifically targeted via pharmacologically available agents in the form of BK channel activator, NS11021, and K_v3 channel modulator, AUT1. Together, both these compounds were adequate in rescuing all aspects of hypoexcitability-associated waveform deficits, but neither were sufficient to increase MSN excitability. Future work could focus on the joint application of both agents to promote increased excitability. Nonetheless, this would suggest rescue of hypoexcitable-related waveform deficits alone are insufficient to rescue MSN excitability deficits and alludes to another neurophysiological mechanism at play here. Interestingly, inhibition of another member of the calcium-activated potassium channels, SK channels, has been shown to increase excitability and exerts a neuroprotective effect in ALS MNs (Castelli et al., 2021, Catanese et al., 2021). Both SK and BK channels contribute to the AHP phase of the AP and have been alternatively modulated to bring about increased excitability (Kshatri et al., 2018). One explanation for this may stem from these channels influencing different downstream pathways that contribute to neuronal excitability and health, as shown by

CREB-dependent rescue following SK inhibition (Catanese et al., 2021). Downstream implications of K^+ conductance that ultimately impact electrophysiological phenotypes may differ based on pathogenic pathways activated in different cell types. This is further exemplified by a lack of functional evidence in C9 MSNs to suggest loss-of-function of sub-threshold K_v7 channels, whereby reduced channel expression has been reported in ALS MNs (Jiang et al., 2005, Harley et al., 2023a), and targeted to reduce LMN hyperexcitability (Wainger et al., 2014, Wainger et al., 2021). This highlights K_v7 channel modulation would be inappropriate in my human *in vitro* MSN model and that future work is required to understand complex, regionally specific K+ disturbances in different cell types. However, modulation of other K_v channels such as K_v3 may be of potential therapeutic value in FTD/ALS. Indeed, AUT1 and its sister compound AUT00206, have been shown to increase parvalbumin-positive GABA-ergic interneuron activity including GABA neurons localised within the basal ganglia by reducing the voltage-dependence of activation in K_v3 channels (Rosato-Siri et al., 2015, Large et al., 2017, Parekh et al., 2018). Augmentation of striatal function via modulation of K_v3 function in GABA-ergic circuits was shown to improve aberrant reward processing in schizophrenia patients (Kaar et al., 2022).

Concurrently, my data also suggests abnormal structural changes linked to length and relocation of the AIS in C9 MSNs that may a constitute a viable target to correct hypoexcitability. Interestingly, hypoexcitability was corrected for following specific excision of the repeat expansion in isogenic lines in addition to reduced I_K channel function. This would indicate such phenotypes are principally mediated by the repeat expansion itself and therefore represents a viable upstream target of these neurophysiological perturbations. Indeed, inhibition of SRSF1-dependent nuclear export of pathological RNA repeat transcripts and subsequent DPR translation may aid in linking C9 pathomechanisms to neurophysiological phenotypes and ultimately rescuing hypoexcitability in C9 MSNs (Hautbergue et al., 2017, Castelli et al., 2021, Castelli et al., 2023).

6.5. C9ORF72 Patient-derived LMNs Display Regional Specific Impairments in Neurophysiological Function

Data from Chapter 4 and 5 provides evidence for regionally specific neurophysiological impairments in the context of C9FTD/ALS. Here, I report pathological phenotypes unique to C9 LMNs that were not simultaneously observed in C9 MSNs from Chapter 3. Furthermore, physiological function of C9 LMNs was assessed in the absence and presence of stressors to determine whether culture environment can alter iPSC-derived neuronal function. A summary of key findings from my investigation into the electrophysiological behaviour of LMNs are as follows:

- No alterations in the intrinsic excitability of C9 iPSC-derived LMNs were identified that was consistent throughout both maturation timepoints studied. These data highlight intrinsic hypoexcitability in C9 MSNs reported in Chapter 3 are regionally specific to the striatum as this phenotype is absent in C9 iPSC-derived LMNs generated from the same iPSC lines.
- Similarly, no changes in intrinsic excitability were identified in response to acute depolarising KCl stress. However, elevation in C9 LMN excitability was displayed in response to chronic KCl treatment relative to controls where excitability was significantly reduced.
- C9 LMN excitability in basal conditions or in response to acute or chronic depolarising stress are not impeded by impairments in maturation or by deficits in AP parameters.
- Chronic stressors in the presence of the C9 mutation may be required to evoke alterations in excitability of patient LMNs due to disturbances in homeostatic plasticity at the AIS. Concurrently, a similar mechanism was suggested to mediate C9 MSN hypoexcitability in the previous chapter.
- In stark contrast to C9 MSNs, patient-derived LMNs at early and late maturation timepoints exhibit potentiated responses in inhibitory GABAergic transmission and excitatory glutamatergic transmission, as shown by amplification of NMDAr- but not AMPAr-mediated currents. This was supported by a favourable shift in evoked glutamatergic signalling towards NMDA-evoked currents in C9 LMNs.

- A large proportion (~80%) of NMDAr expression in C9 LMNs are GluN2B-containing receptors that are associated with extrasynaptic localisation and excitotoxicity.
- Collectively, these data provides evidence for regionally specific electrophysiological dysfunction in FTD/ALS. This is evident by a lack of mutual pathophysiological phenotypes in C9 MSNs and LMNs that would indicate such dysfunction does not arise from iPSC-line specific issues. This has wider implications in future design of disease therapeutics that will need to target specific dysfunction in specific regions of interest.

How to address mechanisms mediating impairments in homeostatic plasticity and downstream implications?

As stated in Chapter 5, I hypothesise aberrant activity-dependant AIS plasticity to be at the centre of dysregulated excitability homeostasis. Similar, to my AIS hypothesis in GABA-ergic MSNs, immunotcytochemistry and western blots would be useful in establishing any abnormal structural changes at the AIS induced from chronic KCl depolarisation. Regulation of AIS plasticity has been tightly linked with Ca^{2+}-dependant signalling (Grubb and Burrone, 2010, O'Leary et al., 2010, Evans et al., 2013, Evans et al., 2015), thus measuring Ca^{2+} homeostasis via live cell imaging of Ca^{2+} dyes may be a key consideration for chronically treated LMNs. Indeed, previous reports have shown elevated Ca^{2+} levels following KCl stimulation in C9 primary hippocampal cultures and iPSC-derived MNs (Dafinca et al., 2020, Huber et al., 2022a).

My findings reveal dysregulated homeostatic regulation of intrinsic neuronal activity in enriched LMN cultures that have undergone chronic KCl treatment. Importantly, there is both a cell and non-cell autonomous component to FTD/ALS that needs to be factored into physiological models to articulate the complexity of disease and address the influences of external stimuli or downstream influences on neuronal activity. Accordingly, it would be of interest to determine whether dysregulated excitability homeostasis is upheld in human *in vitro* neuromuscular co-cultures generated within 3D compartmentalised microdevices and the subsequent impacts on motor unit function (Harley et al., 2023b). Interestingly, a recent study has shown impaired neuromuscular junctions in ALS patient-derived organoids (Pereira et al., 2021).

The physiological relevance of chronic KCl stimulation.

Enhanced concentrations of extracellular potassium provides researchers with an easy, manipulable *in vitro* research tool that induces neuronal depolarisation and recruitment of multiple depolarisation-induced mechanisms. KCl treatment activates Ca^{2+}-related signalling pathways and plasticity-related events, making it a productive research tool that helps replicate *in vivo* physiology. Though, sustained KCl depolarisation is unlikely to recapitulate physiologically relevant timescales or magnitude of LMN excitation. This raises the pathophysiological relevance of using crude KCl treatment to study homeostatic regulation of neuronal activity in FTD/ALS or whether this has greater relevance as a pure model of chronic cellular stress. Alternative, more sophisticated approaches to study homeostatic plasticity in FTD/ALS could be adopted via optogenetic stimulation that can be delivered in intermittent bursts. Even so, this system would require the artificial expression of channel proteins. Nevertheless, my data does demonstrate homeostatic disturbances in C9 LMNs that are unable to cope with chronic depolarising KCl treatment. Importantly, LMNs are likely to be under (intermittent) chronic stress on a longer timescale, spanning decades, that gives rise to neuronal dysfunction and degeneration in FTD/ALS.

What are the functional implications of increased NMDA receptor transmission?

Glutamate receptor-mediated excitotoxicity is a well-established pathophysiological mechanism implicated in ALS LMNs (Cleveland and Rothstein, 2001). Excessive stimulation of Ca^{2+} permeable glutamate receptors can give rise to Ca^{2+} dyshomeostasis and in turn lead to an influx of injurious, excitotoxic levels of Ca^{2+} (Mead et al., 2023). In this study I report increased functional expression of NMDAr in C9 LMNs, with a substantial proportion of NMDAr currents mediated by GluN2B-containing receptors that have been linked with excitotoxicity (Huber et al., 2022a). Yet, further work is required to confirm whether these increases in NMDAr expression do indeed instigate excitotoxicity. This could be investigated by conducting excitotoxicity assays involving immunocytochemistry stains for caspase-3 as a marker of apoptotic cell death. To induce toxicity, it would be important for chronic incubation of LMNs with glycine (co-agonist) and NMDA for at least 12 hours. Simultaneous to this, it would be important to measure cell death in the presence of NMDA with use-dependant antagonists such as MK-801 (Huettner and Bean, 1988), as a control, to determine the specific effect of NMDAr overstimulation. I would anticipate elevated

caspase-3 expression in NMDA incubated C9 LMNs relative to MK801-controls, or isogenic/control lines treated under identical conditions. Additionally, it would be important to confirm increased NMDAr functional expression at the protein level with western blots to quantify NMDAr subunit expression especially GluN2B. Dafinca and colleagues have previously identified significant upregulation of GluN2B in TDP-43^{M337V} iPSC-derived MNs, and a similar non-significant trend was observed in C9 iPSC-derived MNs in RNA sequencing screens (Dafinca et al., 2020). This contrasts with a study by Bursch and colleagues that demonstrated no differences in NMDA responsiveness between iPSC-derived fALS and control MNs, with upregulation of NMDAr expression observed in MNs derived from FUS but crucially not C9 patients (Bursch et al., 2019). It would therefore be important to determine whether this expression is significantly increased in C9 LMNs here. Thus, to support potential findings, quantitative PCR or post-mortem staining of FTD/ALS patient spinal cord for NMDA receptor subunits could be conducted to discern whether subunit expression is augmented at disease end-stage.

Contribution of NMDAr-mediated toxicity in C9FTD/ALS is understudied but data is beginning to emerge to suggest involvement of NMDAr in neurodegeneration. Expression of NMDAr subunit GluN1 and GluN2A have been shown to be amplified in C9 iPSC-derived MNs (Shi et al., 2018, Dafinca et al., 2020) and our data is in accordance with these findings. However, there is a lack of functional studies exploring the implications of NMDAr-induced toxicity. Upregulated expression of both Ca^{2+} permeable AMPAr and NMDAr was linked to aberrant Ca^{2+} dyshomeostasis and increased susceptibility to glutamate-induced cell death (Dafinca et al., 2020). Impaired Ca^{2+} handling of MNs which are known to have low Ca^{2+} buffering capacity, may activate the intrinsic cell stress response and contribute to RAN translation in C9 models (Westergard et al., 2019). In *Drosophila* glutamatergic neurons including MNs, were shown to selectively degenerate due to increased NMDAr-mediating signalling induced by arginine-rich DPR expression (Xu and Xu, 2018). Thus, targeting of DPR-mediated toxicity via SRSF1 inhibition may be of interest here (Hautbergue et al., 2017, Castelli et al., 2021, Castelli et al., 2023). Even so, more work is needed to address pathophysiological abnormalities in NMDAr expression and function in FTD/ALS, in what could be a significant pathomechanism in familial and sporadic forms of disease.

My data indicates a lack of significant change in the functional expression of AMPAr in C9 LMNs which converges with previous reports (Selvaraj et al., 2018, Bursch et al., 2019). Although, this does not necessarily rule out AMPAr-induced excitotoxicity in my C9 LMNs. Indeed, specific upregulation of GluA1 subunit containing, Ca^{2+}-permeable AMPAr has been shown in previous C9-patient dervied MNs and in post-mortem sALS and C9 patient spinal cord (Selvaraj et al., 2018, Shi et al., 2018, Dafinca et al., 2020, Gregory et al., 2020). Dysregulation of AMPAr subunits have also been shown in other ALS genetic background (Udagawa et al., 2015, Bursch et al., 2019, Gregory et al., 2020), that may trigger Ca^{2+} related excitotoxic mechanisms in ALS. Future work could focus on quantification of AMPAr subunit composition via immunoblots or quantitative PCR to measure mRNA and protein subunit levels. Physiological consequences of AMPAr subunit expression could also be measured via voltage-clamp analysis in the presence of NASPM, a selective blocker of Ca^{2+} permeable AMPAr. In addition, single-channel conductance could be measured via non-stationary fluctuation analysis to provide further physiological support for dysregulated Ca^{2+} permeable AMPAr expression.

Downstream consequences of pronounced expression of GluN2B-containing NMDA receptors.

Functional increases in NMDAr expression is likely to promote increased vulnerability in neuronal survival. This vulnerability is further amplified by substantial expression of the NMDA GluN2B receptor subunit. Increased activity of GluN2B-NMDAr has already been implicated in excitotoxic mechanisms in primary C9 hippocampal cultures (Huber et al., 2022a). One possible explanation of increased NMDAr function in C9 LMNs here may result from dysregulated expression of receptors at extrasynaptic locations that are simply not localised there in healthy LMNs. Importantly, activation of these GluN2B receptors have been linked with activation of pro-apoptotic cell-death pathways via downregulation of CREB signalling pathways that can block BDNF expression (Hardingham et al., 2002, Liu et al., 2007). Loss of CREB activity has been associated with hypoexcitable C9 iPSC-derived MN cultures (Catanese et al., 2021).

Therapeutic relevance of regionally specific FTD/ALS mechanisms.

Investigation into the electrophysiological properties of C9 derived- MSNs and LMNs has revealed divergent pathophysiological phenotypes. These pathological

differences between cells of the striatum and spinal cord perhaps alludes to the fact that a diverse range of disease mechanisms are likely to be present in a multitude of disease-relevant cell types. In turn, this not only highlights the need for cell-specific disease therapeutic but perhaps helps explain the difficulty in generating disease-modifying therapies. This difficulty is further extended by the clinical heterogeneity that exists between patients, which not only applies exclusively to FTD/ALS but neurodegenerative diseases in general.

For instance, in my human *in vitro* models I have identified increased functional expression of NMDAr activity that is specific to patient LMNs and not MSNs. Subsequently, if this increased expression was to be associated with excitotoxicity, NMDAr would constitute a viable therapeutic target for receptor antagonists in C9 LMNs. Accordingly, treatment with memantine for example, which is currently approved in Alzheimer's (McShane et al., 2019), has been shown to rescue motor deficits and shortened lifespan by targeting glutamatergic motor neurons in *Drosophila* (Xu and Xu, 2018). However, this would be inappropriate in C9 MSNs where glutamatergic NMDAr function is not impaired. Similarly, block of glutamatergic transmission via riluzole would also be inappropriate in MSNs as discussed previously, but may be of use to reduce excitability in chronically stimulated C9 LMNs. In this regard, it may be of interest to apply retigabine onto chronically treated C9 LMNs to determine whether excitability can be reduced similar to control levels.

The data here perhaps highlights the difficulty in a multi-drug approach to tackle these regional specific disease mechanisms. One possible solution may be to target upstream of pathogenic mechanisms at mutual disease features that are universally implicated across all cell types. This is exemplified by the FDA-approval of tofersen, an antisense oligonucleotide therapy that lowers mutant SOD1 protein (Ludolph and Wiesenfarth, 2025). This argument is strengthened by the amelioration of neurophysiological perturbations in C9 patient-derived MSNs and LMNs in isogenic controls throughout this study. An emerging theme within the field of C9ORF72 disease biology relates to the exacerbation of repeat-dependent gain-of-function phenotypes by C9ORF72 haploinsufficiency in iPSC-derived neurons and murine models (Dong et al., 2020, Zhu et al., 2020, Dane et al., 2023). Indeed, reduced C9ORF72 expression has been shown to not only enhance DPR accumulation (Boivin

et al., 2020, Zhu et al., 2020), but also increases glutamate receptor expression leading to excitotoxicity in human motor neurons (Shi et al., 2018). Furthermore, arginine-rich DPR expression in *Drosophila* motor neurons has been shown to induce NMDAr-mediated excitotoxicity (Xu and Xu, 2018). Thus, in the context of C9 LMNs in this study, enhanced NMDAr expression at the functional level could arise from the cooperative, interlinked contributions of C9ORF72 haploinsufficiency with DPR-mediated toxicity. The excitability phenotypes identified in both MSNs and LMNs could occur downstream from any of the three major C9 pathomechanisms, and future work should look to address the pathogenic framework by which these phenotypes arise. For instance, excitability phenotypes which arise either in basal or stress-related conditions could arise from impaired membrane trafficking of K^+ ion channels linked to haploinsufficiency, RNA foci-induced misprocessing of RNA transcripts or DPR-mediated NCT disruption of ion channel or AIS components (Zhang et al., 2015). Together in equal measure or independently, these pathogenic frameworks could lead to reduced ion channel expression at the membrane in addition to compromising the integrity of the AIS or its ability to remain plastic. In accordance with this, treatments could target TDP-43 pathology or directly target C9-associated pathomechanisms via restoration of C9ORF72 function with small biological compounds (Shi et al., 2018), SRSF1 inhibition of C9-repeat RNA nuclear export (Castelli et al., 2023), or antisense oligonucleotide therapies (Rothstein et al., 2023). However, the recent failures of two independent oligonucleotide therapies would indicate further work is needed before this becomes a viable therapy in C9FTD/ALS (Cammack et al., 2024, van den Berg et al., 2024).

6.6. Concluding Remarks

This study provides novel insights into the neurophysiological dysfunction associated with the C9ORF72 repeat expansion in patient-derived MSNs and LMNs. By systematically investigating intrinsic excitability, AP waveform properties, and synaptic function across neuronal subtypes, I have uncovered distinct, regionally specific impairments that contribute to our understanding of C9FTD/ALS pathophysiology.

C9 MSNs exhibit intrinsic hypoexcitability, driven by deficits in AP waveform components and I_K channel dysfunction. While pharmacological restoration of I_K channel function rescued AP deficits, intrinsic hypoexcitability remained, suggesting an interplay between ion channel dysfunction and structural AIS abnormalities. In contrast, C9 LMNs displayed stable excitability under basal and acute stress conditions but exhibited excitability changes upon chronic depolarising stress, implicating homeostatic plasticity mechanisms. Additionally, C9 LMNs showed potentiated excitatory and inhibitory synaptic transmission, with a shift toward NMDAr-mediated signalling, highlighting a potential excitotoxic vulnerability.

These findings underscore the complexity of C9FTD/ALS-related dysfunction, demonstrating that pathophysiological phenotypes vary between neuronal populations. The regional specificity of these impairments has significant implications for targeted therapeutic strategies, emphasising the need for treatments tailored to distinct neuronal vulnerabilities rather than a one-size-fits-all approach. Future research should explore these mechanisms further and assess how they contribute to disease progression *in vivo*.

7. References

ABDUL KADIR, L., STACEY, M. & BARRETT-JOLLEY, R. 2018. Emerging Roles of the Membrane Potential: Action Beyond the Action Potential. *Front Physiol,* 9**,** 1661.

AGARWAL, S., HIGHTON-WILLIAMSON, E., CAGA, J., HOWELLS, J., DHARMADASA, T., MATAMALA, J. M., MA, Y., SHIBUYA, K., HODGES, J. R., AHMED, R. M., VUCIC, S. & KIERNAN, M. C. 2021. Motor cortical excitability predicts cognitive phenotypes in amyotrophic lateral sclerosis. *Sci Rep,* 11**,** 2172.

AGOSTA, F., FERRARO, P. M., RIVA, N., SPINELLI, E. G., CHIO, A., CANU, E., VALSASINA, P., LUNETTA, C., IANNACCONE, S., COPETTI, M., PRUDENTE, E., COMI, G., FALINI, A. & FILIPPI, M. 2016. Structural brain correlates of cognitive and behavioral impairment in MND. *Hum Brain Mapp,* 37**,** 1614-26.

AHMED, R. M., BOCCHETTA, M., TODD, E. G., TSE, N. Y., DEVENNEY, E. M., TU, S., CAGA, J., HODGES, J. R., HALLIDAY, G. M., IRISH, M., KIERNAN, M. C., PIGUET, O. & ROHRER, J. D. 2021. Tackling clinical heterogeneity across the amyotrophic lateral sclerosis-frontotemporal dementia spectrum using a transdiagnostic approach. *Brain Commun,* 3**,** fcab257.

AL-CHALABI, A., FANG, F., HANBY, M. F., LEIGH, P. N., SHAW, C. E., YE, W. & RIJSDIJK, F. 2010. An estimate of amyotrophic lateral sclerosis heritability using twin data. *J Neurol Neurosurg Psychiatry,* 81**,** 1324-6.

AL-CHALABI, A. & HARDIMAN, O. 2013. The epidemiology of ALS: a conspiracy of genes, environment and time. *Nat Rev Neurol,* 9**,** 617-28.

AL-SARRAJ, S., KING, A., TROAKES, C., SMITH, B., MAEKAWA, S., BODI, I., ROGELJ, B., AL-CHALABI, A., HORTOBAGYI, T. & SHAW, C. E. 2011. p62 positive, TDP-43 negative, neuronal cytoplasmic and intranuclear inclusions in the cerebellum and hippocampus define the pathology of C9orf72-linked FTLD and MND/ALS. *Acta Neuropathol,* 122**,** 691-702.

ALEXANDER, G. E., DELONG, M. R. & STRICK, P. L. 1986. Parallel organization of functionally segregated circuits linking basal ganglia and cortex. *Annu Rev Neurosci,* 9**,** 357-81.

ALLEN, S. P., HALL, B., WOOF, R., FRANCIS, L., GATTO, N., SHAW, A. C., MYSZCZYNSKA, M., HEMINGWAY, J., COLDICOTT, I., WILLCOCK, A., JOB, L., HUGHES, R. M., BOSCHIAN, C., BAYATTI, N., HEATH, P. R., BANDMANN, O., MORTIBOYS, H., FERRAIUOLO, L. & SHAW, P. J. 2019. C9orf72 expansion within astrocytes reduces metabolic flexibility in amyotrophic lateral sclerosis. *Brain,* 142**,** 3771-3790.

ALLODI, I., MONTANANA-ROSELL, R., SELVAN, R., LOW, P. & KIEHN, O. 2021. Locomotor deficits in a mouse model of ALS are paralleled by loss of V1-interneuron connections onto fast motor neurons. *Nat Commun,* 12**,** 3251.

ALONSO, A., LOGROSCINO, G., JICK, S. S. & HERNAN, M. A. 2009. Incidence and lifetime risk of motor neuron disease in the United Kingdom: a population-based study. *Eur J Neurol,* 16**,** 745-51.

ALY, A., LASZLO, Z. I., RAJKUMAR, S., DEMIR, T., HINDLEY, N., LAMONT, D. J., LEHMANN, J., SEIDEL, M., SOMMER, D., FRANZ-WACHTEL, M.,

BARLETTA, F., HEUMOS, S., CZEMMEL, S., KABASHI, E., LUDOLPH, A., BOECKERS, T. M., HENSTRIDGE, C. M. & CATANESE, A. 2023. Integrative proteomics highlight presynaptic alterations and c-Jun misactivation as convergent pathomechanisms in ALS. *Acta Neuropathol,* 146**,** 451-475.
AMALYAN, S., TAMBOLI, S., LAZAREVICH, I., TOPOLNIK, D., BOUMAN, L. H. & TOPOLNIK, L. 2022. Enhanced motor cortex output and disinhibition in asymptomatic female mice with C9orf72 genetic expansion. *Cell Rep,* 40**,** 111043.
AMOROSO, M. W., CROFT, G. F., WILLIAMS, D. J., O'KEEFFE, S., CARRASCO, M. A., DAVIS, A. R., ROYBON, L., OAKLEY, D. H., MANIATIS, T., HENDERSON, C. E. & WICHTERLE, H. 2013. Accelerated high-yield generation of limb-innervating motor neurons from human stem cells. *J Neurosci,* 33**,** 574-86.
ANDREWS, M. G. & KRIEGSTEIN, A. R. 2022. Challenges of Organoid Research. *Annu Rev Neurosci,* 45**,** 23-39.
ANGELESCU, I., KAAR, S. J., MARQUES, T. R., BORGAN, F., VERONESSE, M., SHARMAN, A., SAJJALA, A., DEAKIN, B., HUTCHISON, J., LARGE, C. & HOWES, O. D. 2022. The effect of AUT00206, a Kv3 potassium channel modulator, on dopamine synthesis capacity and the reliability of [(18)F]-FDOPA imaging in schizophrenia. *J Psychopharmacol,* 36**,** 1061-1069.
ANTONIONI, A., RAHO, E. M., LOPRIORE, P., PACE, A. P., LATINO, R. R., ASSOGNA, M., MANCUSO, M., GRAGNANIELLO, D., GRANIERI, E., PUGLIATTI, M., DI LORENZO, F. & KOCH, G. 2023. Frontotemporal Dementia, Where Do We Stand? A Narrative Review. *Int J Mol Sci,* 24.
APPEL, S. H., BEERS, D. R. & ZHAO, W. 2021. Amyotrophic lateral sclerosis is a systemic disease: peripheral contributions to inflammation-mediated neurodegeneration. *Curr Opin Neurol,* 34**,** 765-772.
ARAI, T., HASEGAWA, M., AKIYAMA, H., IKEDA, K., NONAKA, T., MORI, H., MANN, D., TSUCHIYA, K., YOSHIDA, M., HASHIZUME, Y. & ODA, T. 2006. TDP-43 is a component of ubiquitin-positive tau-negative inclusions in frontotemporal lobar degeneration and amyotrophic lateral sclerosis. *Biochem Biophys Res Commun,* 351**,** 602-11.
ARAMA, J., ABITBOL, K., GOFFIN, D., FUCHS, C., SIHRA, T. S., THOMSON, A. M. & JOVANOVIC, J. N. 2015. GABAA receptor activity shapes the formation of inhibitory synapses between developing medium spiny neurons. *Front Cell Neurosci,* 9**,** 290.
ARBER, C., PRECIOUS, S. V., CAMBRAY, S., RISNER-JANICZEK, J. R., KELLY, C., NOAKES, Z., FJODOROVA, M., HEUER, A., UNGLESS, M. A., RODRIGUEZ, T. A., ROSSER, A. E., DUNNETT, S. B. & LI, M. 2015. Activin A directs striatal projection neuron differentiation of human pluripotent stem cells. *Development,* 142**,** 1375-86.
ARMON, C. 2009. Smoking may be considered an established risk factor for sporadic ALS. *Neurology,* 73**,** 1693-8.
ARTHUR, K. C., CALVO, A., PRICE, T. R., GEIGER, J. T., CHIO, A. & TRAYNOR, B. J. 2016. Projected increase in amyotrophic lateral sclerosis from 2015 to 2040. *Nat Commun,* 7**,** 12408.
ASH, P. E., BIENIEK, K. F., GENDRON, T. F., CAULFIELD, T., LIN, W. L., DEJESUS-HERNANDEZ, M., VAN BLITTERSWIJK, M. M., JANSEN-WEST, K., PAUL, J. W., 3RD, RADEMAKERS, R., BOYLAN, K. B., DICKSON, D. W. & PETRUCELLI, L. 2013. Unconventional translation of C9ORF72 GGGGCC

expansion generates insoluble polypeptides specific to c9FTD/ALS. *Neuron,* 77**,** 639-46.
ATANASIO, A., DECMAN, V., WHITE, D., RAMOS, M., IKIZ, B., LEE, H. C., SIAO, C. J., BRYDGES, S., LAROSA, E., BAI, Y., FURY, W., BURFEIND, P., ZAMFIROVA, R., WARSHAW, G., ORENGO, J., OYEJIDE, A., FRALISH, M., AUERBACH, W., POUEYMIROU, W., FREUDENBERG, J., GONG, G., ZAMBROWICZ, B., VALENZUELA, D., YANCOPOULOS, G., MURPHY, A., THURSTON, G. & LAI, K. M. 2016. C9orf72 ablation causes immune dysregulation characterized by leukocyte expansion, autoantibody production, and glomerulonephropathy in mice. *Sci Rep,* 6**,** 23204.
ATWAL, M. S., NIMAC, J., CERCEK, U., GOESCH, S. R., GOESCH, H. R., TZIORTZOUDA, P., ERCOLANI, T., ZATORSKA, A., PASHA, T., CARRE, I., MITCHELL, J., TROAKES, C., TUMMERS, B., ZUPUNSKI, V., ROGELJ, B., HORTOBAGYI, T. & HIRTH, F. 2025. Accumulation of TDP-43 causes karyopherin-alpha4 pathology that characterises amyotrophic lateral sclerosis. *Front Neurosci,* 19**,** 1558227.
BABORIE, A., GRIFFITHS, T. D., JAROS, E., PERRY, R., MCKEITH, I. G., BURN, D. J., MASUDA-SUZUKAKE, M., HASEGAWA, M., ROLLINSON, S., PICKERING-BROWN, S., ROBINSON, A. C., DAVIDSON, Y. S. & MANN, D. M. 2015. Accumulation of dipeptide repeat proteins predates that of TDP-43 in frontotemporal lobar degeneration associated with hexanucleotide repeat expansions in C9ORF72 gene. *Neuropathol Appl Neurobiol,* 41**,** 601-12.
BAE, J. R. & KIM, S. H. 2017. Synapses in neurodegenerative diseases. *BMB Rep,* 50**,** 237-246.
BALDWIN, K. R., GODENA, V. K., HEWITT, V. L. & WHITWORTH, A. J. 2016. Axonal transport defects are a common phenotype in Drosophila models of ALS. *Hum Mol Genet,* 25**,** 2378-2392.
BALENDRA, R. & ISAACS, A. M. 2018. C9orf72-mediated ALS and FTD: multiple pathways to disease. *Nat Rev Neurol,* 14**,** 544-558.
BAMFORD, I. J. & BAMFORD, N. S. 2019. The Striatum's Role in Executing Rational and Irrational Economic Behaviors. *Neuroscientist,* 25**,** 475-490.
BARBER, S. C. & SHAW, P. J. 2010. Oxidative stress in ALS: key role in motor neuron injury and therapeutic target. *Free Radic Biol Med,* 48**,** 629-41.
BARBIER, M., CAMUZAT, A., HACHIMI, K. E., GUEGAN, J., RINALDI, D., LATTANTE, S., HOUOT, M., SANCHEZ-VALLE, R., SABATELLI, M., ANTONELL, A., MOLINA-PORCEL, L., CLOT, F., COURATIER, P., VAN DER ENDE, E., VAN DER ZEE, J., MANZONI, C., CAMU, W., CAZENEUVE, C., SELLAL, F., DIDIC, M., GOLFIER, V., PASQUIER, F., DUYCKAERTS, C., ROSSI, G., BRUNI, A. C., ALVAREZ, V., GOMEZ-TORTOSA, E., DE MENDONCA, A., GRAFF, C., MASELLIS, M., NACMIAS, B., OUMOUSSA, B. M., JORNEA, L., FORLANI, S., FRENCH, C., GENETIC RESEARCH NETWORK ON, F. F.-A., PREVDEMALS, T. I. F. D. G. C. T. E. E. O. D. C. B. N.-C. E. B. N. N. N. T. B. O. T. B. H. C.-I., VAN DEERLIN, V., ROHRER, J. D., GELPI, E., RADEMAKERS, R., VAN SWIETEN, J., LE GUERN, E., VAN BROECKHOVEN, C., FERRARI, R., GENIN, E., BRICE, A. & LE BER, I. 2021. SLITRK2, an X-linked modifier of the age at onset in C9orf72 frontotemporal lobar degeneration. *Brain,* 144**,** 2798-2811.
BARSCHKE, P., OECKL, P., STEINACKER, P., AL SHWEIKI, M. R., WEISHAUPT, J. H., LANDWEHRMEYER, G. B., ANDERL-STRAUB, S., WEYDT, P., DIEHL-SCHMID, J., DANEK, A., KORNHUBER, J., SCHROETER, M. L.,

PRUDLO, J., JAHN, H., FASSBENDER, K., LAUER, M., VAN DER ENDE, E. L., VAN SWIETEN, J. C., VOLK, A. E., LUDOLPH, A. C., OTTO, M. & GERMAN, F. C. 2020. Different CSF protein profiles in amyotrophic lateral sclerosis and frontotemporal dementia with C9orf72 hexanucleotide repeat expansion. *J Neurol Neurosurg Psychiatry,* 91**,** 503-511.

BASHFORD, J., WICKHAM, A., INIESTA, R., DRAKAKIS, E., BOUTELLE, M., MILLS, K. & SHAW, C. 2019. SPiQE: An automated analytical tool for detecting and characterising fasciculations in amyotrophic lateral sclerosis. *Clin Neurophysiol,* 130**,** 1083-1090.

BAUER, C. S., COHEN, R. N., SIRONI, F., LIVESEY, M. R., GILLINGWATER, T. H., HIGHLEY, J. R., FILLINGHAM, D. J., COLDICOTT, I., SMITH, E. F., GIBSON, Y. B., WEBSTER, C. P., GRIERSON, A. J., BENDOTTI, C. & DE VOS, K. J. 2022. An interaction between synapsin and C9orf72 regulates excitatory synapses and is impaired in ALS/FTD. *Acta Neuropathol,* 144**,** 437-464.

BEAGLE, A. J., DARWISH, S. M., RANASINGHE, K. G., LA, A. L., KARAGEORGIOU, E. & VOSSEL, K. A. 2017. Relative Incidence of Seizures and Myoclonus in Alzheimer's Disease, Dementia with Lewy Bodies, and Frontotemporal Dementia. *J Alzheimers Dis,* 60**,** 211-223.

BEDE, P., ELAMIN, M., BYRNE, S., MCLAUGHLIN, R. L., KENNA, K., VAJDA, A., PENDER, N., BRADLEY, D. G. & HARDIMAN, O. 2013. Basal ganglia involvement in amyotrophic lateral sclerosis. *Neurology,* 81**,** 2107-15.

BEDE, P., IYER, P. M., SCHUSTER, C., ELAMIN, M., MCLAUGHLIN, R. L., KENNA, K. & HARDIMAN, O. 2016. The selective anatomical vulnerability of ALS: 'disease-defining' and 'disease-defying' brain regions. *Amyotroph Lateral Scler Frontotemporal Degener,* 17**,** 561-570.

BEDE, P., OMER, T., FINEGAN, E., CHIPIKA, R. H., IYER, P. M., DOHERTY, M. A., VAJDA, A., PENDER, N., MCLAUGHLIN, R. L., HUTCHINSON, S. & HARDIMAN, O. 2018. Connectivity-based characterisation of subcortical grey matter pathology in frontotemporal dementia and ALS: a multimodal neuroimaging study. *Brain Imaging Behav,* 12**,** 1696-1707.

BENDER, K. J. & TRUSSELL, L. O. 2009. Axon initial segment Ca2+ channels influence action potential generation and timing. *Neuron,* 61**,** 259-71.

BENDER, K. J., UEBELE, V. N., RENGER, J. J. & TRUSSELL, L. O. 2012. Control of firing patterns through modulation of axon initial segment T-type calcium channels. *J Physiol,* 590**,** 109-18.

BENTZEN, B. H., NARDI, A., CALLOE, K., MADSEN, L. S., OLESEN, S. P. & GRUNNET, M. 2007. The small molecule NS11021 is a potent and specific activator of Ca2+-activated big-conductance K+ channels. *Mol Pharmacol,* 72**,** 1033-44.

BENUSSI, A., COSSEDDU, M., FILARETO, I., DELL'ERA, V., ARCHETTI, S., SOFIA COTELLI, M., MICHELI, A., PADOVANI, A. & BORRONI, B. 2016. Impaired long-term potentiation-like cortical plasticity in presymptomatic genetic frontotemporal dementia. *Ann Neurol,* 80**,** 472-6.

BENUSSI, A., DI LORENZO, F., DELL'ERA, V., COSSEDDU, M., ALBERICI, A., CARATOZZOLO, S., COTELLI, M. S., MICHELI, A., ROZZINI, L., DEPARI, A., FLAMMINI, A., PONZO, V., MARTORANA, A., CALTAGIRONE, C., PADOVANI, A., KOCH, G. & BORRONI, B. 2017. Transcranial magnetic stimulation distinguishes Alzheimer disease from frontotemporal dementia. *Neurology,* 89**,** 665-672.

BERTOUX, M., FLANAGAN, E. C., HOBBS, M., RUIZ-TAGLE, A., DELGADO, C., MIRANDA, M., IBANEZ, A., SLACHEVSKY, A. & HORNBERGER, M. 2018. Structural Anatomical Investigation of Long-Term Memory Deficit in Behavioral Frontotemporal Dementia. *J Alzheimers Dis,* 62**,** 1887-1900.
BERTOUX, M., O'CALLAGHAN, C., FLANAGAN, E., HODGES, J. R. & HORNBERGER, M. 2015. Fronto-Striatal Atrophy in Behavioral Variant Frontotemporal Dementia and Alzheimer's Disease. *Front Neurol,* 6**,** 147.
BEUTLER, L. R., ELDRED, K. C., QUINTANA, A., KEENE, C. D., ROSE, S. E., POSTUPNA, N., MONTINE, T. J. & PALMITER, R. D. 2011. Severely impaired learning and altered neuronal morphology in mice lacking NMDA receptors in medium spiny neurons. *PLoS One,* 6**,** e28168.
BICANIC, I., HLADNIK, A. & PETANJEK, Z. 2017. A Quantitative Golgi Study of Dendritic Morphology in the Mice Striatal Medium Spiny Neurons. *Front Neuroanat,* 11**,** 37.
BILICAN, B., SERIO, A., BARMADA, S. J., NISHIMURA, A. L., SULLIVAN, G. J., CARRASCO, M., PHATNANI, H. P., PUDDIFOOT, C. A., STORY, D., FLETCHER, J., PARK, I. H., FRIEDMAN, B. A., DALEY, G. Q., WYLLIE, D. J., HARDINGHAM, G. E., WILMUT, I., FINKBEINER, S., MANIATIS, T., SHAW, C. E. & CHANDRAN, S. 2012. Mutant induced pluripotent stem cell lines recapitulate aspects of TDP-43 proteinopathies and reveal cell-specific vulnerability. *Proc Natl Acad Sci U S A,* 109**,** 5803-8.
BIUNDO, F., DEL PRETE, D., ZHANG, H., ARANCIO, O. & D'ADAMIO, L. 2018. A role for tau in learning, memory and synaptic plasticity. *Sci Rep,* 8**,** 3184.
BLOM, H., RONNLUND, D., SCOTT, L., WESTIN, L., WIDENGREN, J., APERIA, A. & BRISMAR, H. 2013. Spatial distribution of DARPP-32 in dendritic spines. *PLoS One,* 8**,** e75155.
BLUMENSTOCK, S. & DUDANOVA, I. 2020. Cortical and Striatal Circuits in Huntington's Disease. *Front Neurosci,* 14**,** 82.
BOCCHETTA, M., MALPETTI, M., TODD, E. G., ROWE, J. B. & ROHRER, J. D. 2021. Looking beneath the surface: the importance of subcortical structures in frontotemporal dementia. *Brain Commun,* 3**,** fcab158.
BOCCHETTA, M., TODD, E. G., BOUZIGUES, A., CASH, D. M., NICHOLAS, J. M., CONVERY, R. S., RUSSELL, L. L., THOMAS, D. L., MALONE, I. B., IGLESIAS, J. E., VAN SWIETEN, J. C., JISKOOT, L. C., SEELAAR, H., BORRONI, B., GALIMBERTI, D., SANCHEZ-VALLE, R., LAFORCE, R., MORENO, F., SYNOFZIK, M., GRAFF, C., MASELLIS, M., TARTAGLIA, M. C., ROWE, J. B., VANDENBERGHE, R., FINGER, E., TAGLIAVINI, F., DE MENDONCA, A., SANTANA, I., BUTLER, C. R., DUCHARME, S., GERHARD, A., DANEK, A., LEVIN, J., OTTO, M., SORBI, S., LE BER, I., PASQUIER, F., ROHRER, J. D. & GENETIC FRONTOTEMPORAL DEMENTIA, I. 2023. Structural MRI predicts clinical progression in presymptomatic genetic frontotemporal dementia: findings from the GENetic Frontotemporal dementia Initiative cohort. *Brain Commun,* 5**,** fcad061.
BOCK, T. & STUART, G. J. 2016. The Impact of BK Channels on Cellular Excitability Depends on their Subcellular Location. *Front Cell Neurosci,* 10**,** 206.
BOETTGER, M. K., TILL, S., CHEN, M. X., ANAND, U., OTTO, W. R., PLUMPTON, C., TREZISE, D. J., TATE, S. N., BOUNTRA, C., COWARD, K., BIRCH, R. & ANAND, P. 2002. Calcium-activated potassium channel SK1- and IK1-like immunoreactivity in injured human sensory neurones and its regulation by neurotrophic factors. *Brain,* 125**,** 252-63.

BOEVE, B. F., BOYLAN, K. B., GRAFF-RADFORD, N. R., DEJESUS-HERNANDEZ, M., KNOPMAN, D. S., PEDRAZA, O., VEMURI, P., JONES, D., LOWE, V., MURRAY, M. E., DICKSON, D. W., JOSEPHS, K. A., RUSH, B. K., MACHULDA, M. M., FIELDS, J. A., FERMAN, T. J., BAKER, M., RUTHERFORD, N. J., ADAMSON, J., WSZOLEK, Z. K., ADELI, A., SAVICA, R., BOOT, B., KUNTZ, K. M., GAVRILOVA, R., REEVES, A., WHITWELL, J., KANTARCI, K., JACK, C. R., JR., PARISI, J. E., LUCAS, J. A., PETERSEN, R. C. & RADEMAKERS, R. 2012. Characterization of frontotemporal dementia and/or amyotrophic lateral sclerosis associated with the GGGGCC repeat expansion in C9ORF72. *Brain,* 135**,** 765-83.

BOEYNAEMS, S., BOGAERT, E., KOVACS, D., KONIJNENBERG, A., TIMMERMAN, E., VOLKOV, A., GUHAROY, M., DE DECKER, M., JASPERS, T., RYAN, V. H., JANKE, A. M., BAATSEN, P., VERCRUYSSE, T., KOLAITIS, R. M., DAELEMANS, D., TAYLOR, J. P., KEDERSHA, N., ANDERSON, P., IMPENS, F., SOBOTT, F., SCHYMKOWITZ, J., ROUSSEAU, F., FAWZI, N. L., ROBBERECHT, W., VAN DAMME, P., TOMPA, P. & VAN DEN BOSCH, L. 2017. Phase Separation of C9orf72 Dipeptide Repeats Perturbs Stress Granule Dynamics. *Mol Cell,* 65**,** 1044-1055 e5.

BOEYNAEMS, S., BOGAERT, E., MICHIELS, E., GIJSELINCK, I., SIEBEN, A., JOVICIC, A., DE BAETS, G., SCHEVENEELS, W., STEYAERT, J., CUIJT, I., VERSTREPEN, K. J., CALLAERTS, P., ROUSSEAU, F., SCHYMKOWITZ, J., CRUTS, M., VAN BROECKHOVEN, C., VAN DAMME, P., GITLER, A. D., ROBBERECHT, W. & VAN DEN BOSCH, L. 2016. Drosophila screen connects nuclear transport genes to DPR pathology in c9ALS/FTD. *Sci Rep,* 6**,** 20877.

BOIVIN, M., PFISTER, V., GAUCHEROT, A., RUFFENACH, F., NEGRONI, L., SELLIER, C. & CHARLET-BERGUERAND, N. 2020. Reduced autophagy upon C9ORF72 loss synergizes with dipeptide repeat protein toxicity in G4C2 repeat expansion disorders. *EMBO J,* 39**,** e100574.

BONAFEDE, R. & MARIOTTI, R. 2017. ALS Pathogenesis and Therapeutic Approaches: The Role of Mesenchymal Stem Cells and Extracellular Vesicles. *Front Cell Neurosci,* 11**,** 80.

BONNEVIE, V. S., DIMINTIYANOVA, K. P., HEDEGAARD, A., LEHNHOFF, J., GRONDAHL, L., MOLDOVAN, M. & MEEHAN, C. F. 2020. Shorter axon initial segments do not cause repetitive firing impairments in the adult presymptomatic G127X SOD-1 Amyotrophic Lateral Sclerosis mouse. *Sci Rep,* 10**,** 1280.

BOOKER, S. A., SIMOES DE OLIVEIRA, L., ANSTEY, N. J., KOZIC, Z., DANDO, O. R., JACKSON, A. D., BAXTER, P. S., ISOM, L. L., SHERMAN, D. L., HARDINGHAM, G. E., BROPHY, P. J., WYLLIE, D. J. A. & KIND, P. C. 2020. Input-Output Relationship of CA1 Pyramidal Neurons Reveals Intact Homeostatic Mechanisms in a Mouse Model of Fragile X Syndrome. *Cell Rep,* 32**,** 107988.

BOULTING, G. L., KISKINIS, E., CROFT, G. F., AMOROSO, M. W., OAKLEY, D. H., WAINGER, B. J., WILLIAMS, D. J., KAHLER, D. J., YAMAKI, M., DAVIDOW, L., RODOLFA, C. T., DIMOS, J. T., MIKKILINENI, S., MACDERMOTT, A. B., WOOLF, C. J., HENDERSON, C. E., WICHTERLE, H. & EGGAN, K. 2011. A functionally characterized test set of human induced pluripotent stem cells. *Nat Biotechnol,* 29**,** 279-86.

BOWEN, D. M., PROCTER, A. W., MANN, D. M., SNOWDEN, J. S., ESIRI, M. M., NEARY, D. & FRANCIS, P. T. 2008. Imbalance of a serotonergic system in frontotemporal dementia: implication for pharmacotherapy. *Psychopharmacology (Berl),* 196**,** 603-10.
BOYLAN, K. 2015. Familial Amyotrophic Lateral Sclerosis. *Neurol Clin,* 33**,** 807-30.
BRENNER, R., CHEN, Q. H., VILAYTHONG, A., TONEY, G. M., NOEBELS, J. L. & ALDRICH, R. W. 2005. BK channel beta4 subunit reduces dentate gyrus excitability and protects against temporal lobe seizures. *Nat Neurosci,* 8**,** 1752-9.
BRETTSCHNEIDER, J., DEL TREDICI, K., TOLEDO, J. B., ROBINSON, J. L., IRWIN, D. J., GROSSMAN, M., SUH, E., VAN DEERLIN, V. M., WOOD, E. M., BAEK, Y., KWONG, L., LEE, E. B., ELMAN, L., MCCLUSKEY, L., FANG, L., FELDENGUT, S., LUDOLPH, A. C., LEE, V. M., BRAAK, H. & TROJANOWSKI, J. Q. 2013. Stages of pTDP-43 pathology in amyotrophic lateral sclerosis. *Ann Neurol,* 74**,** 20-38.
BROWN, C. A., LALLY, C., KUPELIAN, V. & FLANDERS, W. D. 2021. Estimated Prevalence and Incidence of Amyotrophic Lateral Sclerosis and SOD1 and C9orf72 Genetic Variants. *Neuroepidemiology,* 55**,** 342-353.
BROWN, D. A. & PASSMORE, G. M. 2009. Neural KCNQ (Kv7) channels. *Br J Pharmacol,* 156**,** 1185-95.
BROWN, R. H. & AL-CHALABI, A. 2017. Amyotrophic Lateral Sclerosis. *N Engl J Med,* 377**,** 162-172.
BULLMANN, T., KAAS, T., RITZAU-JOST, A., WOHNER, A., KIRMANN, T., RIZALAR, F. S., HOLZER, M., NERLICH, J., PUCHKOV, D., GEIS, C., EILERS, J., KITTEL, R. J., ARENDT, T., HAUCKE, V. & HALLERMANN, S. 2024. Human iPSC-Derived Neurons with Reliable Synapses and Large Presynaptic Action Potentials. *J Neurosci,* 44.
BURATTI, E. & BARALLE, F. E. 2001. Characterization and functional implications of the RNA binding properties of nuclear factor TDP-43, a novel splicing regulator of CFTR exon 9. *J Biol Chem,* 276**,** 36337-43.
BURBERRY, A., SUZUKI, N., WANG, J. Y., MOCCIA, R., MORDES, D. A., STEWART, M. H., SUZUKI-UEMATSU, S., GHOSH, S., SINGH, A., MERKLE, F. T., KOSZKA, K., LI, Q. Z., ZON, L., ROSSI, D. J., TROWBRIDGE, J. J., NOTARANGELO, L. D. & EGGAN, K. 2016. Loss-of-function mutations in the C9ORF72 mouse ortholog cause fatal autoimmune disease. *Sci Transl Med,* 8**,** 347ra93.
BURCHARDT, J. M., MEI, X. W., RANGER, T., MCDERMOTT, C. J., RADUNOVIC, A., COUPLAND, C. & HIPPISLEY-COX, J. 2022. Analysis of incidence of motor neuron disease in England 1998-2019: use of three linked datasets. *Amyotroph Lateral Scler Frontotemporal Degener,* 23**,** 363-371.
BURLEY, S., BECCANO-KELLY, D. A., TALBOT, K., LLANA, O. C. & WADE-MARTINS, R. 2022. Hyperexcitability in young iPSC-derived C9ORF72 mutant motor neurons is associated with increased intracellular calcium release. *Sci Rep,* 12**,** 7378.
BURSCH, F., KALMBACH, N., NAUJOCK, M., STAEGE, S., EGGENSCHWILER, R., ABO-RADY, M., JAPTOK, J., GUO, W., HENSEL, N., REINHARDT, P., BOECKERS, T. M., CANTZ, T., STERNECKERT, J., VAN DEN BOSCH, L., HERMANN, A., PETRI, S. & WEGNER, F. 2019. Altered calcium dynamics and glutamate receptor properties in iPSC-derived motor neurons from ALS

patients with C9orf72, FUS, SOD1 or TDP43 mutations. *Hum Mol Genet,* 28**,** 2835-2850.
BUTTI, Z., PAN, Y. E., GIACOMOTTO, J. & PATTEN, S. A. 2021. Reduced C9orf72 function leads to defective synaptic vesicle release and neuromuscular dysfunction in zebrafish. *Commun Biol,* 4**,** 792.
BUTTI, Z. & PATTEN, S. A. 2018. RNA Dysregulation in Amyotrophic Lateral Sclerosis. *Front Genet,* 9**,** 712.
CAMMACK, A. J., BALENDRA, R. & ISAACS, A. M. 2024. Failure of C9orf72 sense repeat-targeting antisense oligonucleotides: lessons learned and the path forward. *Brain,* 147**,** 2607-2609.
CAPPELLO, V. & FRANCOLINI, M. 2017. Neuromuscular Junction Dismantling in Amyotrophic Lateral Sclerosis. *Int J Mol Sci,* 18.
CASH, D. M., BOCCHETTA, M., THOMAS, D. L., DICK, K. M., VAN SWIETEN, J. C., BORRONI, B., GALIMBERTI, D., MASELLIS, M., TARTAGLIA, M. C., ROWE, J. B., GRAFF, C., TAGLIAVINI, F., FRISONI, G. B., LAFORCE, R., JR., FINGER, E., DE MENDONCA, A., SORBI, S., ROSSOR, M. N., OURSELIN, S., ROHRER, J. D. & GENETIC FTD INITIATIVE, G. 2018. Patterns of gray matter atrophy in genetic frontotemporal dementia: results from the GENFI study. *Neurobiol Aging,* 62**,** 191-196.
CASTELLI, L. M., CUTILLO, L., SOUZA, C. D. S., SANCHEZ-MARTINEZ, A., GRANATA, I., LIN, Y. H., MYSZCZYNSKA, M. A., HEATH, P. R., LIVESEY, M. R., NING, K., AZZOUZ, M., SHAW, P. J., GUARRACINO, M. R., WHITWORTH, A. J., FERRAIUOLO, L., MILO, M. & HAUTBERGUE, G. M. 2021. SRSF1-dependent inhibition of C9ORF72-repeat RNA nuclear export: genome-wide mechanisms for neuroprotection in amyotrophic lateral sclerosis. *Mol Neurodegener,* 16**,** 53.
CASTELLI, L. M., LIN, Y. H., SANCHEZ-MARTINEZ, A., GUL, A., MOHD IMRAN, K., HIGGINBOTTOM, A., UPADHYAY, S. K., MARKUS, N. M., RUA MARTINS, R., COOPER-KNOCK, J., MONTMASSON, C., COHEN, R., WALTON, A., BAUER, C. S., DE VOS, K. J., MEAD, R. J., AZZOUZ, M., DOMINGUEZ, C., FERRAIUOLO, L., SHAW, P. J., WHITWORTH, A. J. & HAUTBERGUE, G. M. 2023. A cell-penetrant peptide blocking C9ORF72-repeat RNA nuclear export reduces the neurotoxic effects of dipeptide repeat proteins. *Sci Transl Med,* 15**,** eabo3823.
CATANESE, A., RAJKUMAR, S., SOMMER, D., FREISEM, D., WIRTH, A., ALY, A., MASSA-LOPEZ, D., OLIVIERI, A., TORELLI, F., IOANNIDIS, V., LIPECKA, J., GUERRERA, I. C., ZYTNICKI, D., LUDOLPH, A., KABASHI, E., MULAW, M. A., ROSELLI, F. & BOCKERS, T. M. 2021. Synaptic disruption and CREB-regulated transcription are restored by K(+) channel blockers in ALS. *EMBO Mol Med,* 13**,** e13131.
CAVARSAN, C. F., STEELE, P. R., GENRY, L. T., REEDICH, E. J., MCCANE, L. M., LAPRE, K. J., PURITZ, A. C., MANUEL, M., KATENKA, N. & QUINLAN, K. A. 2023. Inhibitory interneurons show early dysfunction in a SOD1 mouse model of amyotrophic lateral sclerosis. *J Physiol,* 601**,** 647-667.
CERNECKIS, J., CAI, H. & SHI, Y. 2024. Induced pluripotent stem cells (iPSCs): molecular mechanisms of induction and applications. *Signal Transduct Target Ther,* 9**,** 112.
CHAND, K. K., LEE, K. M., LEE, J. D., QIU, H., WILLIS, E. F., LAVIDIS, N. A., HILLIARD, M. A. & NOAKES, P. G. 2018. Defects in synaptic transmission at the neuromuscular junction precede motor deficits in a TDP-43(Q331K)

transgenic mouse model of amyotrophic lateral sclerosis. *FASEB J,* 32**,** 2676-2689.
CHANG, Q. & MARTIN, L. J. 2011. Glycine receptor channels in spinal motoneurons are abnormal in a transgenic mouse model of amyotrophic lateral sclerosis. *J Neurosci,* 31**,** 2815-27.
CHEN, N., CHEN, X., YU, J. & WANG, J. 2006. Afterhyperpolarization improves spike programming through lowering threshold potentials and refractory periods mediated by voltage-gated sodium channels. *Biochem Biophys Res Commun,* 346**,** 938-45.
CHEN, R., BLOSSER, T. R., DJEKIDEL, M. N., HAO, J., BHATTACHERJEE, A., CHEN, W., TUESTA, L. M., ZHUANG, X. & ZHANG, Y. 2021. Decoding molecular and cellular heterogeneity of mouse nucleus accumbens. *Nat Neurosci,* 24**,** 1757-1771.
CHEW, J., COOK, C., GENDRON, T. F., JANSEN-WEST, K., DEL ROSSO, G., DAUGHRITY, L. M., CASTANEDES-CASEY, M., KURTI, A., STANKOWSKI, J. N., DISNEY, M. D., ROTHSTEIN, J. D., DICKSON, D. W., FRYER, J. D., ZHANG, Y. J. & PETRUCELLI, L. 2019. Aberrant deposition of stress granule-resident proteins linked to C9orf72-associated TDP-43 proteinopathy. *Mol Neurodegener,* 14**,** 9.
CHIO, A., BATTISTINI, S., CALVO, A., CAPONNETTO, C., CONFORTI, F. L., CORBO, M., GIANNINI, F., MANDRIOLI, J., MORA, G., SABATELLI, M., CONSORTIUM, I., AJMONE, C., MASTRO, E., PAIN, D., MANDICH, P., PENCO, S., RESTAGNO, G., ZOLLINO, M. & SURBONE, A. 2014. Genetic counselling in ALS: facts, uncertainties and clinical suggestions. *J Neurol Neurosurg Psychiatry,* 85**,** 478-85.
CHIO, A., LOGROSCINO, G., TRAYNOR, B. J., COLLINS, J., SIMEONE, J. C., GOLDSTEIN, L. A. & WHITE, L. A. 2013. Global epidemiology of amyotrophic lateral sclerosis: a systematic review of the published literature. *Neuroepidemiology,* 41**,** 118-30.
CHIO, A., MAZZINI, L. & MORA, G. 2020. Disease-modifying therapies in amyotrophic lateral sclerosis. *Neuropharmacology,* 167**,** 107986.
CHOI, S. Y., LOPEZ-GONZALEZ, R., KRISHNAN, G., PHILLIPS, H. L., LI, A. N., SEELEY, W. W., YAO, W. D., ALMEIDA, S. & GAO, F. B. 2019. C9ORF72-ALS/FTD-associated poly(GR) binds Atp5a1 and compromises mitochondrial function in vivo. *Nat Neurosci,* 22**,** 851-862.
CHOU, C. C., ZHANG, Y., UMOH, M. E., VAUGHAN, S. W., LORENZINI, I., LIU, F., SAYEGH, M., DONLIN-ASP, P. G., CHEN, Y. H., DUONG, D. M., SEYFRIED, N. T., POWERS, M. A., KUKAR, T., HALES, C. M., GEARING, M., CAIRNS, N. J., BOYLAN, K. B., DICKSON, D. W., RADEMAKERS, R., ZHANG, Y. J., PETRUCELLI, L., SATTLER, R., ZARNESCU, D. C., GLASS, J. D. & ROSSOLL, W. 2018. TDP-43 pathology disrupts nuclear pore complexes and nucleocytoplasmic transport in ALS/FTD. *Nat Neurosci,* 21**,** 228-239.
CIURA, S., LATTANTE, S., LE BER, I., LATOUCHE, M., TOSTIVINT, H., BRICE, A. & KABASHI, E. 2013. Loss of function of C9orf72 causes motor deficits in a zebrafish model of amyotrophic lateral sclerosis. *Ann Neurol,* 74**,** 180-7.
CLARK, R. M., BRIZUELA, M., BLIZZARD, C. A. & DICKSON, T. C. 2018. Reduced Excitability and Increased Neurite Complexity of Cortical Interneurons in a Familial Mouse Model of Amyotrophic Lateral Sclerosis. *Front Cell Neurosci,* 12**,** 328.

CLEVELAND, D. W., LAING, N., HURSE, P. V. & BROWN, R. H., JR. 1995. Toxic mutants in Charcot's sclerosis. *Nature,* 378**,** 342-3.
CLEVELAND, D. W. & ROTHSTEIN, J. D. 2001. From Charcot to Lou Gehrig: deciphering selective motor neuron death in ALS. *Nat Rev Neurosci,* 2**,** 806-19.
COHEN, T. J., HWANG, A. W., RESTREPO, C. R., YUAN, C. X., TROJANOWSKI, J. Q. & LEE, V. M. 2015. An acetylation switch controls TDP-43 function and aggregation propensity. *Nat Commun,* 6**,** 5845.
CONFORTI, P., BOCCHI, V. D., CAMPUS, I., SCARAMUZZA, L., GALIMBERTI, M., LISCHETTI, T., TALPO, F., PEDRAZZOLI, M., MURGIA, A., FERRARI, I., CORDIGLIERI, C., FASCIANI, A., ARENAS, E., FELSENFELD, D., BIELLA, G., BESUSSO, D. & CATTANEO, E. 2022. In vitro-derived medium spiny neurons recapitulate human striatal development and complexity at single-cell resolution. *Cell Rep Methods,* 2**,** 100367.
CONSONNI, M., CONTARINO, V. E., CATRICALA, E., DALLA BELLA, E., PENSATO, V., GELLERA, C., LAURIA, G. & CAPPA, S. F. 2018. Cortical markers of cognitive syndromes in amyotrophic lateral sclerosis. *Neuroimage Clin,* 19**,** 675-682.
CONTET, C., GOULDING, S. P., KULJIS, D. A. & BARTH, A. L. 2016. BK Channels in the Central Nervous System. *Int Rev Neurobiol,* 128**,** 281-342.
COOPER-KNOCK, J., HEWITT, C., HIGHLEY, J. R., BROCKINGTON, A., MILANO, A., MAN, S., MARTINDALE, J., HARTLEY, J., WALSH, T., GELSTHORPE, C., BAXTER, L., FORSTER, G., FOX, M., BURY, J., MOK, K., MCDERMOTT, C. J., TRAYNOR, B. J., KIRBY, J., WHARTON, S. B., INCE, P. G., HARDY, J. & SHAW, P. J. 2012. Clinico-pathological features in amyotrophic lateral sclerosis with expansions in C9ORF72. *Brain,* 135**,** 751-64.
COOPER-KNOCK, J., WALSH, M. J., HIGGINBOTTOM, A., ROBIN HIGHLEY, J., DICKMAN, M. J., EDBAUER, D., INCE, P. G., WHARTON, S. B., WILSON, S. A., KIRBY, J., HAUTBERGUE, G. M. & SHAW, P. J. 2014. Sequestration of multiple RNA recognition motif-containing proteins by C9orf72 repeat expansions. *Brain,* 137**,** 2040-51.
CORNACCHIA, D. & STUDER, L. 2017. Back and forth in time: Directing age in iPSC-derived lineages. *Brain Res,* 1656**,** 14-26.
COX, J. & WITTEN, I. B. 2019. Striatal circuits for reward learning and decision-making. *Nat Rev Neurosci,* 20**,** 482-494.
COYLE-GILCHRIST, I. T., DICK, K. M., PATTERSON, K., VAZQUEZ RODRIQUEZ, P., WEHMANN, E., WILCOX, A., LANSDALL, C. J., DAWSON, K. E., WIGGINS, J., MEAD, S., BRAYNE, C. & ROWE, J. B. 2016. Prevalence, characteristics, and survival of frontotemporal lobar degeneration syndromes. *Neurology,* 86**,** 1736-43.
COYNE, A. N., LORENZINI, I., CHOU, C. C., TORVUND, M., ROGERS, R. S., STARR, A., ZAEPFEL, B. L., LEVY, J., JOHANNESMEYER, J., SCHWARTZ, J. C., NISHIMUNE, H., ZINSMAIER, K., ROSSOLL, W., SATTLER, R. & ZARNESCU, D. C. 2017. Post-transcriptional Inhibition of Hsc70-4/HSPA8 Expression Leads to Synaptic Vesicle Cycling Defects in Multiple Models of ALS. *Cell Rep,* 21**,** 110-125.
COZZOLINO, M. & CARRI, M. T. 2012. Mitochondrial dysfunction in ALS. *Prog Neurobiol,* 97**,** 54-66.
CRUTS, M., GIJSELINCK, I., VAN DER ZEE, J., ENGELBORGHS, S., WILS, H., PIRICI, D., RADEMAKERS, R., VANDENBERGHE, R., DERMAUT, B.,

MARTIN, J. J., VAN DUIJN, C., PEETERS, K., SCIOT, R., SANTENS, P., DE POOTER, T., MATTHEIJSSENS, M., VAN DEN BROECK, M., CUIJT, I., VENNEKENS, K., DE DEYN, P. P., KUMAR-SINGH, S. & VAN BROECKHOVEN, C. 2006. Null mutations in progranulin cause ubiquitin-positive frontotemporal dementia linked to chromosome 17q21. *Nature,* 442**,** 920-4.

CUTARELLI, A., MARTINEZ-ROJAS, V. A., TATA, A., BATTISTELLA, I., ROSSI, D., AROSIO, D., MUSIO, C. & CONTI, L. 2021. A Monolayer System for the Efficient Generation of Motor Neuron Progenitors and Functional Motor Neurons from Human Pluripotent Stem Cells. *Cells,* 10.

CYKOWSKI, M. D., POWELL, S. Z., PETERSON, L. E., APPEL, J. W., RIVERA, A. L., TAKEI, H., CHANG, E. & APPEL, S. H. 2017. Clinical Significance of TDP-43 Neuropathology in Amyotrophic Lateral Sclerosis. *J Neuropathol Exp Neurol,* 76**,** 402-413.

DAFINCA, R., BARBAGALLO, P., FARRIMOND, L., CANDALIJA, A., SCABER, J., ABABNEH, N. A., SATHYAPRAKASH, C., VOWLES, J., COWLEY, S. A. & TALBOT, K. 2020. Impairment of Mitochondrial Calcium Buffering Links Mutations in C9ORF72 and TARDBP in iPS-Derived Motor Neurons from Patients with ALS/FTD. *Stem Cell Reports,* 14**,** 892-908.

DAFINCA, R., SCABER, J., ABABNEH, N., LALIC, T., WEIR, G., CHRISTIAN, H., VOWLES, J., DOUGLAS, A. G., FLETCHER-JONES, A., BROWNE, C., NAKANISHI, M., TURNER, M. R., WADE-MARTINS, R., COWLEY, S. A. & TALBOT, K. 2016. C9orf72 Hexanucleotide Expansions Are Associated with Altered Endoplasmic Reticulum Calcium Homeostasis and Stress Granule Formation in Induced Pluripotent Stem Cell-Derived Neurons from Patients with Amyotrophic Lateral Sclerosis and Frontotemporal Dementia. *Stem Cells,* 34**,** 2063-78.

DANE, T. L., GILL, A. L., VIEIRA, F. G. & DENTON, K. R. 2023. Reduced C9orf72 expression exacerbates polyGR toxicity in patient iPSC-derived motor neurons and a Type I protein arginine methyltransferase inhibitor reduces that toxicity. *Front Cell Neurosci,* 17**,** 1134090.

DANGOND, F., HWANG, D., CAMELO, S., PASINELLI, P., FROSCH, M. P., STEPHANOPOULOS, G., STEPHANOPOULOS, G., BROWN, R. H., JR. & GULLANS, S. R. 2004. Molecular signature of late-stage human ALS revealed by expression profiling of postmortem spinal cord gray matter. *Physiol Genomics,* 16**,** 229-39.

DAVIDSON, Y., ROBINSON, A. C., LIU, X., WU, D., TROAKES, C., ROLLINSON, S., MASUDA-SUZUKAKE, M., SUZUKI, G., NONAKA, T., SHI, J., TIAN, J., HAMDALLA, H., EALING, J., RICHARDSON, A., JONES, M., PICKERING-BROWN, S., SNOWDEN, J. S., HASEGAWA, M. & MANN, D. M. 2016. Neurodegeneration in frontotemporal lobar degeneration and motor neurone disease associated with expansions in C9orf72 is linked to TDP-43 pathology and not associated with aggregated forms of dipeptide repeat proteins. *Neuropathol Appl Neurobiol,* 42**,** 242-54.

DAVIDSON, Y. S., BARKER, H., ROBINSON, A. C., THOMPSON, J. C., HARRIS, J., TROAKES, C., SMITH, B., AL-SARAJ, S., SHAW, C., ROLLINSON, S., MASUDA-SUZUKAKE, M., HASEGAWA, M., PICKERING-BROWN, S., SNOWDEN, J. S. & MANN, D. M. 2014. Brain distribution of dipeptide repeat proteins in frontotemporal lobar degeneration and motor neurone disease associated with expansions in C9ORF72. *Acta Neuropathol Commun,* 2**,** 70.

DE VOCHT, J., BLOMMAERT, J., DEVROME, M., RADWAN, A., VAN WEEHAEGHE, D., DE SCHAEPDRYVER, M., CECCARINI, J., REZAEI, A., SCHRAMM, G., VAN AALST, J., CHIO, A., PAGANI, M., STAM, D., VAN ESCH, H., LAMAIRE, N., VERHAEGEN, M., MERTENS, N., POESEN, K., VAN DEN BERG, L. H., VAN ES, M. A., VANDENBERGHE, R., VANDENBULCKE, M., VAN DEN STOCK, J., KOOLE, M., DUPONT, P., VAN LAERE, K. & VAN DAMME, P. 2020. Use of Multimodal Imaging and Clinical Biomarkers in Presymptomatic Carriers of C9orf72 Repeat Expansion. *JAMA Neurol,* 77**,** 1008-1017.

DEBSKA-VIELHABER, G., MILLER, I., PEEVA, V., ZUSCHRATTER, W., WALCZAK, J., SCHREIBER, S., PETRI, S., MACHTS, J., VOGT, S., SZCZEPANOWSKA, J., GELLERICH, F. N., HERMANN, A., VIELHABER, S. & KUNZ, W. S. 2021. Impairment of mitochondrial oxidative phosphorylation in skin fibroblasts of SALS and FALS patients is rescued by in vitro treatment with ROS scavengers. *Exp Neurol,* 339**,** 113620.

DEJESUS-HERNANDEZ, M., FINCH, N. A., WANG, X., GENDRON, T. F., BIENIEK, K. F., HECKMAN, M. G., VASILEVICH, A., MURRAY, M. E., ROUSSEAU, L., WEESNER, R., LUCIDO, A., PARSONS, M., CHEW, J., JOSEPHS, K. A., PARISI, J. E., KNOPMAN, D. S., PETERSEN, R. C., BOEVE, B. F., GRAFF-RADFORD, N. R., DE BOER, J., ASMANN, Y. W., PETRUCELLI, L., BOYLAN, K. B., DICKSON, D. W., VAN BLITTERSWIJK, M. & RADEMAKERS, R. 2017. In-depth clinico-pathological examination of RNA foci in a large cohort of C9ORF72 expansion carriers. *Acta Neuropathol,* 134**,** 255-269.

DEJESUS-HERNANDEZ, M., MACKENZIE, I. R., BOEVE, B. F., BOXER, A. L., BAKER, M., RUTHERFORD, N. J., NICHOLSON, A. M., FINCH, N. A., FLYNN, H., ADAMSON, J., KOURI, N., WOJTAS, A., SENGDY, P., HSIUNG, G. Y., KARYDAS, A., SEELEY, W. W., JOSEPHS, K. A., COPPOLA, G., GESCHWIND, D. H., WSZOLEK, Z. K., FELDMAN, H., KNOPMAN, D. S., PETERSEN, R. C., MILLER, B. L., DICKSON, D. W., BOYLAN, K. B., GRAFF-RADFORD, N. R. & RADEMAKERS, R. 2011. Expanded GGGGCC hexanucleotide repeat in noncoding region of C9ORF72 causes chromosome 9p-linked FTD and ALS. *Neuron,* 72**,** 245-56.

DELEON, J. & MILLER, B. L. 2018. Frontotemporal dementia. *Handb Clin Neurol,* 148**,** 409-430.

DELESTREE, N., MANUEL, M., IGLESIAS, C., ELBASIOUNY, S. M., HECKMAN, C. J. & ZYTNICKI, D. 2014. Adult spinal motoneurones are not hyperexcitable in a mouse model of inherited amyotrophic lateral sclerosis. *J Physiol,* 592**,** 1687-703.

DESMARAIS, J. A., UNGER, C., DAMJANOV, I., MEUTH, M. & ANDREWS, P. 2016. Apoptosis and failure of checkpoint kinase 1 activation in human induced pluripotent stem cells under replication stress. *Stem Cell Res Ther,* 7**,** 17.

DEVENNEY, E. M., AHMED, R. M. & HODGES, J. R. 2019. Frontotemporal dementia. *Handb Clin Neurol,* 167**,** 279-299.

DEVLIN, A. C., BURR, K., BOROOAH, S., FOSTER, J. D., CLEARY, E. M., GETI, I., VALLIER, L., SHAW, C. E., CHANDRAN, S. & MILES, G. B. 2015. Human iPSC-derived motoneurons harbouring TARDBP or C9ORF72 ALS mutations are dysfunctional despite maintaining viability. *Nat Commun,* 6**,** 5999.

DI GIORGIO, F. P., CARRASCO, M. A., SIAO, M. C., MANIATIS, T. & EGGAN, K. 2007. Non-cell autonomous effect of glia on motor neurons in an embryonic stem cell-based ALS model. *Nat Neurosci,* 10**,** 608-14.
DIAPER, D. C., ADACHI, Y., SUTCLIFFE, B., HUMPHREY, D. M., ELLIOTT, C. J., STEPTO, A., LUDLOW, Z. N., VANDEN BROECK, L., CALLAERTS, P., DERMAUT, B., AL-CHALABI, A., SHAW, C. E., ROBINSON, I. M. & HIRTH, F. 2013. Loss and gain of Drosophila TDP-43 impair synaptic efficacy and motor control leading to age-related neurodegeneration by loss-of-function phenotypes. *Hum Mol Genet,* 22**,** 1539-57.
DIMOS, J. T., RODOLFA, K. T., NIAKAN, K. K., WEISENTHAL, L. M., MITSUMOTO, H., CHUNG, W., CROFT, G. F., SAPHIER, G., LEIBEL, R., GOLAND, R., WICHTERLE, H., HENDERSON, C. E. & EGGAN, K. 2008. Induced pluripotent stem cells generated from patients with ALS can be differentiated into motor neurons. *Science,* 321**,** 1218-21.
DING, F., SUN, Q., LONG, C., RASMUSSEN, R. N., PENG, S., XU, Q., KANG, N., SONG, W., WEIKOP, P., GOLDMAN, S. A. & NEDERGAARD, M. 2024. Dysregulation of extracellular potassium distinguishes healthy ageing from neurodegeneration. *Brain,* 147**,** 1726-1739.
DING, J., PETERSON, J. D. & SURMEIER, D. J. 2008. Corticostriatal and thalamostriatal synapses have distinctive properties. *J Neurosci,* 28**,** 6483-92.
DONG, W., MA, Y., GUAN, F., ZHANG, X., CHEN, W., ZHANG, L. & ZHANG, L. 2021. Ablation of C9orf72 together with excitotoxicity induces ALS in rats. *FEBS J,* 288**,** 1712-1723.
DONG, W., ZHANG, L., SUN, C., GAO, X., GUAN, F., LI, J., CHEN, W., MA, Y. & ZHANG, L. 2020. Knock in of a hexanucleotide repeat expansion in the C9orf72 gene induces ALS in rats. *Animal Model Exp Med,* 3**,** 237-244.
DONNELLY, C. J., ZHANG, P. W., PHAM, J. T., HAEUSLER, A. R., MISTRY, N. A., VIDENSKY, S., DALEY, E. L., POTH, E. M., HOOVER, B., FINES, D. M., MARAGAKIS, N., TIENARI, P. J., PETRUCELLI, L., TRAYNOR, B. J., WANG, J., RIGO, F., BENNETT, C. F., BLACKSHAW, S., SATTLER, R. & ROTHSTEIN, J. D. 2013. RNA toxicity from the ALS/FTD C9ORF72 expansion is mitigated by antisense intervention. *Neuron,* 80**,** 415-28.
DU, Z. W., CHEN, H., LIU, H., LU, J., QIAN, K., HUANG, C. L., ZHONG, X., FAN, F. & ZHANG, S. C. 2015. Generation and expansion of highly pure motor neuron progenitors from human pluripotent stem cells. *Nat Commun,* 6**,** 6626.
DYER, M. S., WOODHOUSE, A. & BLIZZARD, C. A. 2021. Cytoplasmic Human TDP-43 Mislocalization Induces Widespread Dendritic Spine Loss in Mouse Upper Motor Neurons. *Brain Sci,* 11.
EDWARDS, G. & WESTON, A. H. 1995. The role of potassium channels in excitable cells. *Diabetes Res Clin Pract,* 28 Suppl**,** S57-66.
EISEN, A., BRAAK, H., DEL TREDICI, K., LEMON, R., LUDOLPH, A. C. & KIERNAN, M. C. 2017. Cortical influences drive amyotrophic lateral sclerosis. *J Neurol Neurosurg Psychiatry,* 88**,** 917-924.
EISEN, A., KIM, S. & PANT, B. 1992. Amyotrophic lateral sclerosis (ALS): a phylogenetic disease of the corticomotoneuron? *Muscle Nerve,* 15**,** 219-24.
ESPINOSA, F., MARKS, G., HEINTZ, N. & JOHO, R. H. 2004. Increased motor drive and sleep loss in mice lacking Kv3-type potassium channels. *Genes Brain Behav,* 3**,** 90-100.

EVANS, M. D., DUMITRESCU, A. S., KRUIJSSEN, D. L. H., TAYLOR, S. E. & GRUBB, M. S. 2015. Rapid Modulation of Axon Initial Segment Length Influences Repetitive Spike Firing. *Cell Rep,* 13**,** 1233-1245.
EVANS, M. D., SAMMONS, R. P., LEBRON, S., DUMITRESCU, A. S., WATKINS, T. B., UEBELE, V. N., RENGER, J. J. & GRUBB, M. S. 2013. Calcineurin signaling mediates activity-dependent relocation of the axon initial segment. *J Neurosci,* 33**,** 6950-63.
EVANS, M. J. & KAUFMAN, M. H. 1981. Establishment in culture of pluripotential cells from mouse embryos. *Nature,* 292**,** 154-6.
FARG, M. A., KONOPKA, A., SOO, K. Y., ITO, D. & ATKIN, J. D. 2017. The DNA damage response (DDR) is induced by the C9orf72 repeat expansion in amyotrophic lateral sclerosis. *Hum Mol Genet,* 26**,** 2882-2896.
FARG, M. A., SUNDARAMOORTHY, V., SULTANA, J. M., YANG, S., ATKINSON, R. A., LEVINA, V., HALLORAN, M. A., GLEESON, P. A., BLAIR, I. P., SOO, K. Y., KING, A. E. & ATKIN, J. D. 2014. C9ORF72, implicated in amytrophic lateral sclerosis and frontotemporal dementia, regulates endosomal trafficking. *Hum Mol Genet,* 23**,** 3579-95.
FAY, M. M., ANDERSON, P. J. & IVANOV, P. 2017. ALS/FTD-Associated C9ORF72 Repeat RNA Promotes Phase Transitions In Vitro and in Cells. *Cell Rep,* 21**,** 3573-3584.
FENOGLIO, C., SCARPINI, E., SERPENTE, M. & GALIMBERTI, D. 2018. Role of Genetics and Epigenetics in the Pathogenesis of Alzheimer's Disease and Frontotemporal Dementia. *J Alzheimers Dis,* 62**,** 913-932.
FERNANDEZ-PEREZ, E. J., GALLEGOS, S., ARMIJO-WEINGART, L., ARAYA, A., RIFFO-LEPE, N. O., CAYUMAN, F. & AGUAYO, L. G. 2020. Changes in neuronal excitability and synaptic transmission in nucleus accumbens in a transgenic Alzheimer's disease mouse model. *Sci Rep,* 10**,** 19606.
FERNANDOPULLE, M. S., PRESTIL, R., GRUNSEICH, C., WANG, C., GAN, L. & WARD, M. E. 2018. Transcription Factor-Mediated Differentiation of Human iPSCs into Neurons. *Curr Protoc Cell Biol,* 79**,** e51.
FERRAIUOLO, L. & MARAGAKIS, N. J. 2021. Mini-Review: Induced pluripotent stem cells and the search for new cell-specific ALS therapeutic targets. *Neurosci Lett,* 755**,** 135911.
FERRANTE, R. J., BROWNE, S. E., SHINOBU, L. A., BOWLING, A. C., BAIK, M. J., MACGARVEY, U., KOWALL, N. W., BROWN, R. H., JR. & BEAL, M. F. 1997. Evidence of increased oxidative damage in both sporadic and familial amyotrophic lateral sclerosis. *J Neurochem,* 69**,** 2064-74.
FERRER, I. 1999. Neurons and their dendrites in frontotemporal dementia. *Dement Geriatr Cogn Disord,* 10 Suppl 1**,** 55-60.
FILIPIS, L., BLOMER, L. A., MONTNACH, J., LOUSSOUARN, G., DE WAARD, M. & CANEPARI, M. 2023. Nav1.2 and BK channel interaction shapes the action potential in the axon initial segment. *J Physiol,* 601**,** 1957-1979.
FILIPPI, M., BASAIA, S., CANU, E., IMPERIALE, F., MEANI, A., CASO, F., MAGNANI, G., FALAUTANO, M., COMI, G., FALINI, A. & AGOSTA, F. 2017. Brain network connectivity differs in early-onset neurodegenerative dementia. *Neurology,* 89**,** 1764-1772.
FLORESCO, S. B. 2007. Dopaminergic regulation of limbic-striatal interplay. *J Psychiatry Neurosci,* 32**,** 400-11.
FOERSTER, B. R., CALLAGHAN, B. C., PETROU, M., EDDEN, R. A., CHENEVERT, T. L. & FELDMAN, E. L. 2012. Decreased motor cortex

gamma-aminobutyric acid in amyotrophic lateral sclerosis. *Neurology,* 78**,** 1596-600.
FOGARTY, M. J., KLENOWSKI, P. M., LEE, J. D., DRIEBERG-THOMPSON, J. R., BARTLETT, S. E., NGO, S. T., HILLIARD, M. A., BELLINGHAM, M. C. & NOAKES, P. G. 2016. Cortical synaptic and dendritic spine abnormalities in a presymptomatic TDP-43 model of amyotrophic lateral sclerosis. *Sci Rep,* 6**,** 37968.
FOGARTY, M. J., MU, E. W. H., LAVIDIS, N. A., NOAKES, P. G. & BELLINGHAM, M. C. 2017. Motor Areas Show Altered Dendritic Structure in an Amyotrophic Lateral Sclerosis Mouse Model. *Front Neurosci,* 11**,** 609.
FOGARTY, M. J., NOAKES, P. G. & BELLINGHAM, M. C. 2015. Motor cortex layer V pyramidal neurons exhibit dendritic regression, spine loss, and increased synaptic excitation in the presymptomatic hSOD1(G93A) mouse model of amyotrophic lateral sclerosis. *J Neurosci,* 35**,** 643-7.
FRATTA, P., POULTER, M., LASHLEY, T., ROHRER, J. D., POLKE, J. M., BECK, J., RYAN, N., HENSMAN, D., MIZIELINSKA, S., WAITE, A. J., LAI, M. C., GENDRON, T. F., PETRUCELLI, L., FISHER, E. M., REVESZ, T., WARREN, J. D., COLLINGE, J., ISAACS, A. M. & MEAD, S. 2013. Homozygosity for the C9orf72 GGGGCC repeat expansion in frontotemporal dementia. *Acta Neuropathol,* 126**,** 401-9.
FREIBAUM, B. D., LU, Y., LOPEZ-GONZALEZ, R., KIM, N. C., ALMEIDA, S., LEE, K. H., BADDERS, N., VALENTINE, M., MILLER, B. L., WONG, P. C., PETRUCELLI, L., KIM, H. J., GAO, F. B. & TAYLOR, J. P. 2015. GGGGCC repeat expansion in C9orf72 compromises nucleocytoplasmic transport. *Nature,* 525**,** 129-33.
FREIBAUM, B. D. & TAYLOR, J. P. 2017. The Role of Dipeptide Repeats in C9ORF72-Related ALS-FTD. *Front Mol Neurosci,* 10**,** 35.
FRITZ, E., IZAURIETA, P., WEISS, A., MIR, F. R., ROJAS, P., GONZALEZ, D., ROJAS, F., BROWN, R. H., JR., MADRID, R. & VAN ZUNDERT, B. 2013. Mutant SOD1-expressing astrocytes release toxic factors that trigger motoneuron death by inducing hyperexcitability. *J Neurophysiol,* 109**,** 2803-14.
FURNESS, J. B., KEARNEY, K., ROBBINS, H. L., HUNNE, B., SELMER, I. S., NEYLON, C. B., CHEN, M. X. & TJANDRA, J. J. 2004. Intermediate conductance potassium (IK) channels occur in human enteric neurons. *Auton Neurosci,* 112**,** 93-7.
GALLIANO, E., HAHN, C., BROWNE, L. P., P, R. V., TUFO, C., CRESPO, A. & GRUBB, M. S. 2021. Brief Sensory Deprivation Triggers Cell Type-Specific Structural and Functional Plasticity in Olfactory Bulb Neurons. *J Neurosci,* 41**,** 2135-2151.
GAO, K., LIN, Z., WEN, S. & JIANG, Y. 2022. Potassium channels and epilepsy. *Acta Neurol Scand,* 146**,** 699-707.
GARIBOTTO, V., BORRONI, B., AGOSTI, C., PREMI, E., ALBERICI, A., EICKHOFF, S. B., BRAMBATI, S. M., BELLELLI, G., GASPAROTTI, R., PERANI, D. & PADOVANI, A. 2011. Subcortical and deep cortical atrophy in Frontotemporal Lobar Degeneration. *Neurobiol Aging,* 32**,** 875-84.
GASCON, E., LYNCH, K., RUAN, H., ALMEIDA, S., VERHEYDEN, J. M., SEELEY, W. W., DICKSON, D. W., PETRUCELLI, L., SUN, D., JIAO, J., ZHOU, H., JAKOVCEVSKI, M., AKBARIAN, S., YAO, W. D. & GAO, F. B. 2014.

Alterations in microRNA-124 and AMPA receptors contribute to social behavioral deficits in frontotemporal dementia. *Nat Med,* 20**,** 1444-51.
GASSET-ROSA, F., LU, S., YU, H., CHEN, C., MELAMED, Z., GUO, L., SHORTER, J., DA CRUZ, S. & CLEVELAND, D. W. 2019. Cytoplasmic TDP-43 De-mixing Independent of Stress Granules Drives Inhibition of Nuclear Import, Loss of Nuclear TDP-43, and Cell Death. *Neuron,* 102**,** 339-357 e7.
GATTO, N., DOS SANTOS SOUZA, C., SHAW, A. C., BELL, S. M., MYSZCZYNSKA, M. A., POWERS, S., MEYER, K., CASTELLI, L. M., KARYKA, E., MORTIBOYS, H., AZZOUZ, M., HAUTBERGUE, G. M., MARKUS, N. M., SHAW, P. J. & FERRAIUOLO, L. 2021. Directly converted astrocytes retain the ageing features of the donor fibroblasts and elucidate the astrocytic contribution to human CNS health and disease. *Aging Cell,* 20**,** e13281.
GEEVASINGA, N., MENON, P., HOWELLS, J., NICHOLSON, G. A., KIERNAN, M. C. & VUCIC, S. 2015. Axonal ion channel dysfunction in c9orf72 familial amyotrophic lateral sclerosis. *JAMA Neurol,* 72**,** 49-57.
GEEVASINGA, N., MENON, P., OZDINLER, P. H., KIERNAN, M. C. & VUCIC, S. 2016. Pathophysiological and diagnostic implications of cortical dysfunction in ALS. *Nat Rev Neurol,* 12**,** 651-661.
GEEVASINGA, N., VAN DEN BOS, M., MENON, P. & VUCIC, S. 2021. Utility of Transcranial Magnetic Simulation in Studying Upper Motor Neuron Dysfunction in Amyotrophic Lateral Sclerosis. *Brain Sci,* 11.
GELON, P. A., DUTCHAK, P. A. & SEPHTON, C. F. 2022. Synaptic dysfunction in ALS and FTD: anatomical and molecular changes provide insights into mechanisms of disease. *Front Mol Neurosci,* 15**,** 1000183.
GENC, B., JARA, J. H., LAGRIMAS, A. K., PYTEL, P., ROOS, R. P., MESULAM, M. M., GEULA, C., BIGIO, E. H. & OZDINLER, P. H. 2017. Apical dendrite degeneration, a novel cellular pathology for Betz cells in ALS. *Sci Rep,* 7**,** 41765.
GENG, H. Y., ZHANG, J., YANG, J. M., LI, Y., WANG, N., YE, M., CHEN, X. J., LIAN, H. & LI, X. M. 2017. Erbb4 Deletion from Medium Spiny Neurons of the Nucleus Accumbens Core Induces Schizophrenia-Like Behaviors via Elevated GABA(A) Receptor alpha1 Subunit Expression. *J Neurosci,* 37**,** 7450-7464.
GERACITANO, R., PAOLUCCI, E., PRISCO, S., GUATTEO, E., ZONA, C., LONGONE, P., AMMASSARI-TEULE, M., BERNARDI, G., BERRETTA, N. & MERCURI, N. B. 2003. Altered long-term corticostriatal synaptic plasticity in transgenic mice overexpressing human CU/ZN superoxide dismutase (GLY(93)-->ALA) mutation. *Neuroscience,* 118**,** 399-408.
GERFEN, C. R., ENGBER, T. M., MAHAN, L. C., SUSEL, Z., CHASE, T. N., MONSMA, F. J., JR. & SIBLEY, D. R. 1990. D1 and D2 dopamine receptor-regulated gene expression of striatonigral and striatopallidal neurons. *Science,* 250**,** 1429-32.
GERTLER, T. S., CHAN, C. S. & SURMEIER, D. J. 2008. Dichotomous anatomical properties of adult striatal medium spiny neurons. *J Neurosci,* 28**,** 10814-24.
GITTIS, A. H., MOGHADAM, S. H. & DU LAC, S. 2010. Mechanisms of sustained high firing rates in two classes of vestibular nucleus neurons: differential contributions of resurgent Na, Kv3, and BK currents. *J Neurophysiol,* 104**,** 1625-34.
GOETZL, E. J., KAPOGIANNIS, D., SCHWARTZ, J. B., LOBACH, I. V., GOETZL, L., ABNER, E. L., JICHA, G. A., KARYDAS, A. M., BOXER, A. & MILLER, B. L.

2016. Decreased synaptic proteins in neuronal exosomes of frontotemporal dementia and Alzheimer's disease. *FASEB J,* 30**,** 4141-4148.
GOH, C. W., LEE, I. C., SUNDARAM, J. R., GEORGE, S. E., YUSOFF, P., BRUSH, M. H., SZE, N. S. K. & SHENOLIKAR, S. 2018. Chronic oxidative stress promotes GADD34-mediated phosphorylation of the TAR DNA-binding protein TDP-43, a modification linked to neurodegeneration. *J Biol Chem,* 293**,** 163-176.
GOMEZ-DEZA, J., LEE, Y. B., TROAKES, C., NOLAN, M., AL-SARRAJ, S., GALLO, J. M. & SHAW, C. E. 2015. Dipeptide repeat protein inclusions are rare in the spinal cord and almost absent from motor neurons in C9ORF72 mutant amyotrophic lateral sclerosis and are unlikely to cause their degeneration. *Acta Neuropathol Commun,* 3**,** 38.
GORDON, P. H. 2013. Amyotrophic Lateral Sclerosis: An update for 2013 Clinical Features, Pathophysiology, Management and Therapeutic Trials. *Aging Dis,* 4**,** 295-310.
GOVAARTS, R., BEELDMAN, E., FRASCHINI, M., GRIFFA, A., ENGELS, M. M. A., VAN ES, M. A., VELDINK, J. H., VAN DEN BERG, L. H., VAN DER KOOI, A. J., PIJNENBURG, Y. A. L., DE VISSER, M., STAM, C. J., RAAPHORST, J. & HILLEBRAND, A. 2022. Cortical and subcortical changes in resting-state neuronal activity and connectivity in early symptomatic ALS and advanced frontotemporal dementia. *Neuroimage Clin,* 34**,** 102965.
GREAVES, C. V. & ROHRER, J. D. 2019. An update on genetic frontotemporal dementia. *J Neurol,* 266**,** 2075-2086.
GREGORY, J. M., LIVESEY, M. R., MCDADE, K., SELVARAJ, B. T., BARTON, S. K., CHANDRAN, S. & SMITH, C. 2020. Dysregulation of AMPA receptor subunit expression in sporadic ALS post-mortem brain. *J Pathol,* 250**,** 67-78.
GRUBB, M. S. & BURRONE, J. 2010. Activity-dependent relocation of the axon initial segment fine-tunes neuronal excitability. *Nature,* 465**,** 1070-4.
GRUBB, M. S., SHU, Y., KUBA, H., RASBAND, M. N., WIMMER, V. C. & BENDER, K. J. 2011. Short- and long-term plasticity at the axon initial segment. *J Neurosci,* 31**,** 16049-55.
GRUNNET, M. & KAUFMANN, W. A. 2004. Coassembly of big conductance Ca2+-activated K+ channels and L-type voltage-gated Ca2+ channels in rat brain. *J Biol Chem,* 279**,** 36445-53.
GU, N., VERVAEKE, K. & STORM, J. F. 2007. BK potassium channels facilitate high-frequency firing and cause early spike frequency adaptation in rat CA1 hippocampal pyramidal cells. *J Physiol,* 580**,** 859-82.
GUILLOT, S. J., LANG, C., SIMONOT, M., BECKETT, D., LULE, D., BALZ, L. T., KNEHR, A., STUART-LOPEZ, G., VERCRUYSSE, P., DIETERLE, S., WEYDT, P., DORST, J., KANDLER, K., KASSUBEK, J., WASSERMANN, L., ROUAUX, C., ARTHAUD, S., DA CRUZ, S., LUPPI, P. H., ROSELLI, F., LUDOLPH, A. C., DUPUIS, L. & BOLBOREA, M. 2025. Early-onset sleep alterations found in patients with amyotrophic lateral sclerosis are ameliorated by orexin antagonist in mouse models. *Sci Transl Med,* 17**,** eadm7580.
GUNES, Z. I., KAN, V. W. Y., YE, X. & LIEBSCHER, S. 2020. Exciting Complexity: The Role of Motor Circuit Elements in ALS Pathophysiology. *Front Neurosci,* 14**,** 573.
GUO, W., NAUJOCK, M., FUMAGALLI, L., VANDOORNE, T., BAATSEN, P., BOON, R., ORDOVAS, L., PATEL, A., WELTERS, M., VANWELDEN, T., GEENS, N., TRICOT, T., BENOY, V., STEYAERT, J., LEFEBVRE-OMAR, C.,

BOESMANS, W., JARPE, M., STERNECKERT, J., WEGNER, F., PETRI, S., BOHL, D., VANDEN BERGHE, P., ROBBERECHT, W., VAN DAMME, P., VERFAILLIE, C. & VAN DEN BOSCH, L. 2017. HDAC6 inhibition reverses axonal transport defects in motor neurons derived from FUS-ALS patients. *Nat Commun,* 8**,** 861.

GURDON, J. B. 1962. The developmental capacity of nuclei taken from intestinal epithelium cells of feeding tadpoles. *J Embryol Exp Morphol,* 10**,** 622-40.

GURNEY, M. E., FLECK, T. J., HIMES, C. S. & HALL, E. D. 1998. Riluzole preserves motor function in a transgenic model of familial amyotrophic lateral sclerosis. *Neurology,* 50**,** 62-6.

GURNEY, M. E., PU, H., CHIU, A. Y., DAL CANTO, M. C., POLCHOW, C. Y., ALEXANDER, D. D., CALIENDO, J., HENTATI, A., KWON, Y. W., DENG, H. X. & ET AL. 1994. Motor neuron degeneration in mice that express a human Cu,Zn superoxide dismutase mutation. *Science,* 264**,** 1772-5.

HABER, S. N. 2016. Corticostriatal circuitry. *Dialogues Clin Neurosci,* 18**,** 7-21.

HAEUSLER, A. R., DONNELLY, C. J., PERIZ, G., SIMKO, E. A., SHAW, P. G., KIM, M. S., MARAGAKIS, N. J., TRONCOSO, J. C., PANDEY, A., SATTLER, R., ROTHSTEIN, J. D. & WANG, J. 2014. C9orf72 nucleotide repeat structures initiate molecular cascades of disease. *Nature,* 507**,** 195-200.

HAEUSLER, A. R., DONNELLY, C. J. & ROTHSTEIN, J. D. 2016. The expanding biology of the C9orf72 nucleotide repeat expansion in neurodegenerative disease. *Nat Rev Neurosci,* 17**,** 383-95.

HAIDAR, M., VIDEN, A., CUIC, B., WANG, T., ROSIER, M., TOMAS, D., MILLS, S. A., GOVIER-COLE, A., DJOUMA, E., LUIKINGA, S., RYTOVA, V., BARTON, S. K., GONSALVEZ, D. G., PALMER, L. M., MCLEAN, C., KIERNAN, M. C., VUCIC, S. & TURNER, B. J 2021. Cortical hyperexcitability drives dying forward ALS symptoms and pathology in mice
. *bioRxiv*.

HAIDET-PHILLIPS, A. M., HESTER, M. E., MIRANDA, C. J., MEYER, K., BRAUN, L., FRAKES, A., SONG, S., LIKHITE, S., MURTHA, M. J., FOUST, K. D., RAO, M., EAGLE, A., KAMMESHEIDT, A., CHRISTENSEN, A., MENDELL, J. R., BURGHES, A. H. & KASPAR, B. K. 2011. Astrocytes from familial and sporadic ALS patients are toxic to motor neurons. *Nat Biotechnol,* 29**,** 824-8.

HALABI, C., HALABI, A., DEAN, D. L., WANG, P. N., BOXER, A. L., TROJANOWSKI, J. Q., DEARMOND, S. J., MILLER, B. L., KRAMER, J. H. & SEELEY, W. W. 2013. Patterns of striatal degeneration in frontotemporal dementia. *Alzheimer Dis Assoc Disord,* 27**,** 74-83.

HAMILL, O. P., MARTY, A., NEHER, E., SAKMANN, B. & SIGWORTH, F. J. 1981. Improved patch-clamp techniques for high-resolution current recording from cells and cell-free membrane patches. *Pflugers Arch,* 391**,** 85-100.

HAN, X., JING, M. Y., ZHAO, T. Y., WU, N., SONG, R. & LI, J. 2017. Role of dopamine projections from ventral tegmental area to nucleus accumbens and medial prefrontal cortex in reinforcement behaviors assessed using optogenetic manipulation. *Metab Brain Dis,* 32**,** 1491-1502.

HANBY, M. F., SCOTT, K. M., SCOTTON, W., WIJESEKERA, L., MOLE, T., ELLIS, C. E., LEIGH, P. N., SHAW, C. E. & AL-CHALABI, A. 2011. The risk to relatives of patients with sporadic amyotrophic lateral sclerosis. *Brain,* 134**,** 3454-7.

HANDLEY, E. E., PITMAN, K. A., DAWKINS, E., YOUNG, K. M., CLARK, R. M., JIANG, T. C., TURNER, B. J., DICKSON, T. C. & BLIZZARD, C. A. 2017.

Synapse Dysfunction of Layer V Pyramidal Neurons Precedes Neurodegeneration in a Mouse Model of TDP-43 Proteinopathies. *Cereb Cortex,* 27**,** 3630-3647.
HANDLEY, E. E., REALE, L. A., CHUCKOWREE, J. A., DYER, M. S., BARNETT, G. L., CLARK, C. M., BENNETT, W., DICKSON, T. C. & BLIZZARD, C. A. 2022. Estrogen Enhances Dendrite Spine Function and Recovers Deficits in Neuroplasticity in the prpTDP-43(A315T) Mouse Model of Amyotrophic Lateral Sclerosis. *Mol Neurobiol,* 59**,** 2962-2976.
HARDIMAN, O., AL-CHALABI, A., CHIO, A., CORR, E. M., LOGROSCINO, G., ROBBERECHT, W., SHAW, P. J., SIMMONS, Z. & VAN DEN BERG, L. H. 2017. Amyotrophic lateral sclerosis. *Nat Rev Dis Primers,* 3**,** 17085.
HARDIMAN, O. & VAN DEN BERG, L. H. 2017. Edaravone: a new treatment for ALS on the horizon? *Lancet Neurol,* 16**,** 490-491.
HARDINGHAM, G. E. & BADING, H. 2010. Synaptic versus extrasynaptic NMDA receptor signalling: implications for neurodegenerative disorders. *Nat Rev Neurosci,* 11**,** 682-96.
HARDINGHAM, G. E., FUKUNAGA, Y. & BADING, H. 2002. Extrasynaptic NMDARs oppose synaptic NMDARs by triggering CREB shut-off and cell death pathways. *Nat Neurosci,* 5**,** 405-14.
HARLEY, P., KERINS, C., GATT, A., NEVES, G., RICCIO, F., MACHADO, C. B., CHEESBROUGH, A., R'BIBO, L., BURRONE, J. & LIEBERAM, I. 2023a. Aberrant axon initial segment plasticity and intrinsic excitability of ALS hiPSC motor neurons. *Cell Rep,* 42**,** 113509.
HARLEY, P., PAREDES-REDONDO, A., GRENCI, G., VIASNOFF, V., LIN, Y. Y. & LIEBERAM, I. 2023b. 3D Compartmentalised Human Pluripotent Stem Cell-derived Neuromuscular Co-cultures. *Bio Protoc,* 13**,** e4624.
HARWOOD, C. A., MCDERMOTT, C. J. & SHAW, P. J. 2009. Physical activity as an exogenous risk factor in motor neuron disease (MND): a review of the evidence. *Amyotroph Lateral Scler,* 10**,** 191-204.
HAUTBERGUE, G. M., CASTELLI, L. M., FERRAIUOLO, L., SANCHEZ-MARTINEZ, A., COOPER-KNOCK, J., HIGGINBOTTOM, A., LIN, Y. H., BAUER, C. S., DODD, J. E., MYSZCZYNSKA, M. A., ALAM, S. M., GARNERET, P., CHANDRAN, J. S., KARYKA, E., STOPFORD, M. J., SMITH, E. F., KIRBY, J., MEYER, K., KASPAR, B. K., ISAACS, A. M., EL-KHAMISY, S. F., DE VOS, K. J., NING, K., AZZOUZ, M., WHITWORTH, A. J. & SHAW, P. J. 2017. SRSF1-dependent nuclear export inhibition of C9ORF72 repeat transcripts prevents neurodegeneration and associated motor deficits. *Nat Commun,* 8**,** 16063.
HENKEL, L. M., KANKOWSKI, S., MOELLENKAMP, T. M., SMANDZICH, N. J., SCHWARZ, S., DI FONZO, A., GOHRING, G., HOGLINGER, G. & WEGNER, F. 2023. iPSC-Derived Striatal Medium Spiny Neurons from Patients with Multiple System Atrophy Show Hypoexcitability and Elevated alpha-Synuclein Release. *Cells,* 12.
HENSTRIDGE, C. M., SIDERIS, D. I., CARROLL, E., ROTARIU, S., SALOMONSSON, S., TZIORAS, M., MCKENZIE, C. A., SMITH, C., VON ARNIM, C. A. F., LUDOLPH, A. C., LULE, D., LEIGHTON, D., WARNER, J., CLEARY, E., NEWTON, J., SWINGLER, R., CHANDRAN, S., GILLINGWATER, T. H., ABRAHAMS, S. & SPIRES-JONES, T. L. 2018. Synapse loss in the prefrontal cortex is associated with cognitive decline in amyotrophic lateral sclerosis. *Acta Neuropathol,* 135**,** 213-226.

HIDEYAMA, T., YAMASHITA, T., SUZUKI, T., TSUJI, S., HIGUCHI, M., SEEBURG, P. H., TAKAHASHI, R., MISAWA, H. & KWAK, S. 2010. Induced loss of ADAR2 engenders slow death of motor neurons from Q/R site-unedited GluR2. *J Neurosci,* 30**,** 11917-25.

HIGASHIHARA, M., PAVEY, N., MENON, P., VAN DEN BOS, M., SHIBUYA, K., KUWABARA, S., KIERNAN, M. C., KOINUMA, M. & VUCIC, S. 2024. Reduction in short interval intracortical inhibition from the early stage reflects the pathophysiology in amyotrophic lateral sclerosis: A meta-analysis study. *Eur J Neurol,* 31**,** e16281.

HIGASHIHARA, M., PAVEY, N., VAN DEN BOS, M., MENON, P., KIERNAN, M. C. & VUCIC, S. 2021. Association of Cortical Hyperexcitability and Cognitive Impairment in Patients With Amyotrophic Lateral Sclerosis. *Neurology,* 96**,** e2090-e2097.

HIGHLEY, J. R., KIRBY, J., JANSWEIJER, J. A., WEBB, P. S., HEWAMADDUMA, C. A., HEATH, P. R., HIGGINBOTTOM, A., RAMAN, R., FERRAIUOLO, L., COOPER-KNOCK, J., MCDERMOTT, C. J., WHARTON, S. B., SHAW, P. J. & INCE, P. G. 2014. Loss of nuclear TDP-43 in amyotrophic lateral sclerosis (ALS) causes altered expression of splicing machinery and widespread dysregulation of RNA splicing in motor neurones. *Neuropathol Appl Neurobiol,* 40**,** 670-85.

HILL, C. L. & STEPHENS, G. J. 2021. An Introduction to Patch Clamp Recording. *Methods Mol Biol,* 2188**,** 1-19.

HO, R., SANCES, S., GOWING, G., AMOROSO, M. W., O'ROURKE, J. G., SAHABIAN, A., WICHTERLE, H., BALOH, R. H., SAREEN, D. & SVENDSEN, C. N. 2016. ALS disrupts spinal motor neuron maturation and aging pathways within gene co-expression networks. *Nat Neurosci,* 19**,** 1256-67.

HO, W. Y., AGRAWAL, I., TYAN, S. H., SANFORD, E., CHANG, W. T., LIM, K., ONG, J., TAN, B. S. Y., MOE, A. A. K., YU, R., WONG, P., TUCKER-KELLOGG, G., KOO, E., CHUANG, K. H. & LING, S. C. 2021. Dysfunction in nonsense-mediated decay, protein homeostasis, mitochondrial function, and brain connectivity in ALS-FUS mice with cognitive deficits. *Acta Neuropathol Commun,* 9**,** 9.

HO, W. Y., NAVAKKODE, S., LIU, F., SOONG, T. W. & LING, S. C. 2020. Deregulated expression of a longevity gene, Klotho, in the C9orf72 deletion mice with impaired synaptic plasticity and adult hippocampal neurogenesis. *Acta Neuropathol Commun,* 8**,** 155.

HO, W. Y., TAI, Y. K., CHANG, J. C., LIANG, J., TYAN, S. H., CHEN, S., GUAN, J. L., ZHOU, H., SHEN, H. M., KOO, E. & LING, S. C. 2019. The ALS-FTD-linked gene product, C9orf72, regulates neuronal morphogenesis via autophagy. *Autophagy,* 15**,** 827-842.

HOLLINGWORTH, D., THOMAS, F., PAGE, D. A., FOUDA, M. A., DE CASTRO, R. L., SULA, A., MYKHAYLYK, V. B., KELLY, G., ULMSCHNEIDER, M. B., RUBEN, P. C. & WALLACE, B. A. 2024. Structural basis for the rescue of hyperexcitable cells by the amyotrophic lateral sclerosis drug Riluzole. *Nat Commun,* 15**,** 8426.

HONG, S. I., KANG, S., CHEN, J. F. & CHOI, D. S. 2019. Indirect Medium Spiny Neurons in the Dorsomedial Striatum Regulate Ethanol-Containing Conditioned Reward Seeking. *J Neurosci,* 39**,** 7206-7217.

HOSSAINI, M., CARDONA CANO, S., VAN DIS, V., HAASDIJK, E. D., HOOGENRAAD, C. C., HOLSTEGE, J. C. & JAARSMA, D. 2011. Spinal

inhibitory interneuron pathology follows motor neuron degeneration independent of glial mutant superoxide dismutase 1 expression in SOD1-ALS mice. *J Neuropathol Exp Neurol,* 70**,** 662-77.
HOWLAND, D. S., LIU, J., SHE, Y., GOAD, B., MARAGAKIS, N. J., KIM, B., ERICKSON, J., KULIK, J., DEVITO, L., PSALTIS, G., DEGENNARO, L. J., CLEVELAND, D. W. & ROTHSTEIN, J. D. 2002. Focal loss of the glutamate transporter EAAT2 in a transgenic rat model of SOD1 mutant-mediated amyotrophic lateral sclerosis (ALS). *Proc Natl Acad Sci U S A,* 99**,** 1604-9.
HSIUNG, G. Y., DEJESUS-HERNANDEZ, M., FELDMAN, H. H., SENGDY, P., BOUCHARD-KERR, P., DWOSH, E., BUTLER, R., LEUNG, B., FOK, A., RUTHERFORD, N. J., BAKER, M., RADEMAKERS, R. & MACKENZIE, I. R. 2012. Clinical and pathological features of familial frontotemporal dementia caused by C9ORF72 mutation on chromosome 9p. *Brain,* 135**,** 709-22.
HUANG, C., LI, J., ZHANG, G., LIN, Y., LI, C., ZHENG, X., SONG, X., HAN, B., GUO, B., TU, Z., ZHANG, J., SUN, Y., WANG, Y., ZHANG, Z. & YAN, S. 2021a. TBN improves motor function and prolongs survival in a TDP-43M337V mouse model of ALS. *Hum Mol Genet,* 30**,** 1484-1496.
HUANG, C. Y. & RASBAND, M. N. 2018. Axon initial segments: structure, function, and disease. *Ann N Y Acad Sci,* 1420**,** 46-61.
HUANG, X., ROET, K. C. D., ZHANG, L., BRAULT, A., BERG, A. P., JEFFERSON, A. B., KLUG-MCLEOD, J., LEACH, K. L., VINCENT, F., YANG, H., COYLE, A. J., JONES, L. H., FROST, D., WISKOW, O., CHEN, K., MAEDA, R., GRANTHAM, A., DORNON, M. K., KLIM, J. R., SIEKMANN, M. T., ZHAO, D., LEE, S., EGGAN, K. & WOOLF, C. J. 2021b. Human amyotrophic lateral sclerosis excitability phenotype screen: Target discovery and validation. *Cell Rep,* 35**,** 109224.
HUBER, N., HOFFMANN, D., GINIATULLINA, R., ROSTALSKI, H., LESKELA, S., TAKALO, M., NATUNEN, T., SOLJE, E., REMES, A. M., GINIATULLIN, R., HILTUNEN, M. & HAAPASALO, A. 2022a. C9orf72 hexanucleotide repeat expansion leads to altered neuronal and dendritic spine morphology and synaptic dysfunction. *Neurobiol Dis,* 162**,** 105584.
HUBER, N., KORHONEN, S., HOFFMANN, D., LESKELA, S., ROSTALSKI, H., REMES, A. M., HONKAKOSKI, P., SOLJE, E. & HAAPASALO, A. 2022b. Deficient neurotransmitter systems and synaptic function in frontotemporal lobar degeneration-Insights into disease mechanisms and current therapeutic approaches. *Mol Psychiatry,* 27**,** 1300-1309.
HUETTNER, J. E. & BEAN, B. P. 1988. Block of N-methyl-D-aspartate-activated current by the anticonvulsant MK-801: selective binding to open channels. *Proc Natl Acad Sci U S A,* 85**,** 1307-11.
HULL, C. A., CHU, Y., THANAWALA, M. & REGEHR, W. G. 2013. Hyperpolarization induces a long-term increase in the spontaneous firing rate of cerebellar Golgi cells. *J Neurosci,* 33**,** 5895-902.
IGAZ, L. M., KWONG, L. K., LEE, E. B., CHEN-PLOTKIN, A., SWANSON, E., UNGER, T., MALUNDA, J., XU, Y., WINTON, M. J., TROJANOWSKI, J. Q. & LEE, V. M. 2011. Dysregulation of the ALS-associated gene TDP-43 leads to neuronal death and degeneration in mice. *J Clin Invest,* 121**,** 726-38.
IRWIN, D. J., MCMILLAN, C. T., BRETTSCHNEIDER, J., LIBON, D. J., POWERS, J., RASCOVSKY, K., TOLEDO, J. B., BOLLER, A., BEKISZ, J., CHANDRASEKARAN, K., WOOD, E. M., SHAW, L. M., WOO, J. H., COOK, P. A., WOLK, D. A., ARNOLD, S. E., VAN DEERLIN, V. M., MCCLUSKEY, L.

F., ELMAN, L., LEE, V. M., TROJANOWSKI, J. Q. & GROSSMAN, M. 2013. Cognitive decline and reduced survival in C9orf72 expansion frontotemporal degeneration and amyotrophic lateral sclerosis. *J Neurol Neurosurg Psychiatry,* 84**,** 163-9.

ITO, H., WATE, R., ZHANG, J., OHNISHI, S., KANEKO, S., ITO, H., NAKANO, S. & KUSAKA, H. 2008. Treatment with edaravone, initiated at symptom onset, slows motor decline and decreases SOD1 deposition in ALS mice. *Exp Neurol,* 213**,** 448-55.

IWAI, Y., SHIBUYA, K., MISAWA, S., SEKIGUCHI, Y., WATANABE, K., AMINO, H. & KUWABARA, S. 2016. Axonal Dysfunction Precedes Motor Neuronal Death in Amyotrophic Lateral Sclerosis. *PLoS One,* 11**,** e0158596.

JAIN, A. & VALE, R. D. 2017. RNA phase transitions in repeat expansion disorders. *Nature,* 546**,** 243-247.

JAKABEK, D., POWER, B. D., MACFARLANE, M. D., WALTERFANG, M., VELAKOULIS, D., VAN WESTEN, D., LATT, J., NILSSON, M., LOOI, J. C. L. & SANTILLO, A. F. 2018. Regional structural hypo- and hyperconnectivity of frontal-striatal and frontal-thalamic pathways in behavioral variant frontotemporal dementia. *Hum Brain Mapp,* 39**,** 4083-4093.

JAMANN, N., DANNEHL, D., LEHMANN, N., WAGENER, R., THIELEMANN, C., SCHULTZ, C., STAIGER, J., KOLE, M. H. P. & ENGELHARDT, M. 2021. Sensory input drives rapid homeostatic scaling of the axon initial segment in mouse barrel cortex. *Nat Commun,* 12**,** 23.

JENSEN, B. K., SCHULDI, M. H., MCAVOY, K., RUSSELL, K. A., BOEHRINGER, A., CURRAN, B. M., KRISHNAMURTHY, K., WEN, X., WESTERGARD, T., MA, L., HAEUSLER, A. R., EDBAUER, D., PASINELLI, P. & TROTTI, D. 2020. Synaptic dysfunction induced by glycine-alanine dipeptides in C9orf72-ALS/FTD is rescued by SV2 replenishment. *EMBO Mol Med,* 12**,** e10722.

JHANJI, R., BEHL, T., SEHGAL, A. & BUNGAU, S. 2021. Mitochondrial dysfunction and traffic jams in amyotrophic lateral sclerosis. *Mitochondrion,* 58**,** 102-110.

JIANG, Y. M., YAMAMOTO, M., KOBAYASHI, Y., YOSHIHARA, T., LIANG, Y., TERAO, S., TAKEUCHI, H., ISHIGAKI, S., KATSUNO, M., ADACHI, H., NIWA, J., TANAKA, F., DOYU, M., YOSHIDA, M., HASHIZUME, Y. & SOBUE, G. 2005. Gene expression profile of spinal motor neurons in sporadic amyotrophic lateral sclerosis. *Ann Neurol,* 57**,** 236-51.

JIMENEZ-BALADO, J. & EICH, T. S. 2021. GABAergic dysfunction, neural network hyperactivity and memory impairments in human aging and Alzheimer's disease. *Semin Cell Dev Biol,* 116**,** 146-159.

JO, Y., LEE, J., LEE, S. Y., KWON, I. & CHO, H. 2022. Poly-dipeptides produced from C9orf72 hexanucleotide repeats cause selective motor neuron hyperexcitability in ALS. *Proc Natl Acad Sci U S A,* 119**,** e2113813119.

JOHNSTON, J., FORSYTHE, I. D. & KOPP-SCHEINPFLUG, C. 2010. Going native: voltage-gated potassium channels controlling neuronal excitability. *J Physiol,* 588**,** 3187-200.

JORGENSEN, H. S., JENSEN, D. B., DIMINTIYANOVA, K. P., BONNEVIE, V. S., HEDEGAARD, A., LEHNHOFF, J., MOLDOVAN, M., GRONDAHL, L. & MEEHAN, C. F. 2021. Increased Axon Initial Segment Length Results in Increased Na(+) Currents in Spinal Motoneurones at Symptom Onset in the G127X SOD1 Mouse Model of Amyotrophic Lateral Sclerosis. *Neuroscience,* 468**,** 247-264.

JOVICIC, A., MERTENS, J., BOEYNAEMS, S., BOGAERT, E., CHAI, N., YAMADA, S. B., PAUL, J. W., 3RD, SUN, S., HERDY, J. R., BIERI, G., KRAMER, N. J., GAGE, F. H., VAN DEN BOSCH, L., ROBBERECHT, W. & GITLER, A. D. 2015. Modifiers of C9orf72 dipeptide repeat toxicity connect nucleocytoplasmic transport defects to FTD/ALS. *Nat Neurosci,* 18**,** 1226-9.
JOYCE, P. I., FRATTA, P., FISHER, E. M. & ACEVEDO-AROZENA, A. 2011. SOD1 and TDP-43 animal models of amyotrophic lateral sclerosis: recent advances in understanding disease toward the development of clinical treatments. *Mamm Genome,* 22**,** 420-48.
KAAR, S. J., ANGELESCU, I., NOUR, M. M., MARQUES, T. R., SHARMAN, A., SAJJALA, A., HUTCHISON, J., MCGUIRE, P., LARGE, C. & HOWES, O. D. 2022. The effects of AUT00206, a novel Kv3.1/3.2 potassium channel modulator, on task-based reward system activation: a test of mechanism in schizophrenia. *Psychopharmacology (Berl),* 239**,** 3313-3323.
KABILJO, R., IACOANGELI, A., AL-CHALABI, A. & ROSENZWEIG, I. 2022. Amyotrophic lateral sclerosis and cerebellum. *Sci Rep,* 12**,** 12586.
KANAI, K., KUWABARA, S., MISAWA, S., TAMURA, N., OGAWARA, K., NAKATA, M., SAWAI, S., HATTORI, T. & BOSTOCK, H. 2006. Altered axonal excitability properties in amyotrophic lateral sclerosis: impaired potassium channel function related to disease stage. *Brain,* 129**,** 953-62.
KARADURMUS, D., RIAL, D., DE BACKER, J. F., COMMUNI, D., DE KERCHOVE D'EXAERDE, A. & SCHIFFMANN, S. N. 2019. GPRIN3 Controls Neuronal Excitability, Morphology, and Striatal-Dependent Behaviors in the Indirect Pathway of the Striatum. *J Neurosci,* 39**,** 7513-7528.
KASARSKIS, E. J., LINDQUIST, J. H., COFFMAN, C. J., GRAMBOW, S. C., FEUSSNER, J. R., ALLEN, K. D., ODDONE, E. Z., KAMINS, K. A., HORNER, R. D. & ALS GULF WAR CLINICAL REVIEW, T. 2009. Clinical aspects of ALS in Gulf War veterans. *Amyotroph Lateral Scler,* 10**,** 35-41.
KATO, S., ODA, M., HAYASHI, H., KAWATA, A. & SHIMIZU, T. 1994. Participation of the limbic system and its associated areas in the dementia of amyotrophic lateral sclerosis. *J Neurol Sci,* 126**,** 62-9.
KAWAHARA, Y., ITO, K., SUN, H., AIZAWA, H., KANAZAWA, I. & KWAK, S. 2004. Glutamate receptors: RNA editing and death of motor neurons. *Nature,* 427**,** 801.
KAWAHARA, Y. & KWAK, S. 2005. Excitotoxicity and ALS: what is unique about the AMPA receptors expressed on spinal motor neurons? *Amyotroph Lateral Scler Other Motor Neuron Disord,* 6**,** 131-44.
KAZAMA, M., KATO, Y., KAKITA, A., NOGUCHI, N., URANO, Y., MASUI, K., NIIDA-KAWAGUCHI, M., YAMAMOTO, T., WATABE, K., KITAGAWA, K. & SHIBATA, N. 2020. Astrocytes release glutamate via cystine/glutamate antiporter upregulated in response to increased oxidative stress related to sporadic amyotrophic lateral sclerosis. *Neuropathology,* 40**,** 587-598.
KEUSS, M. J., HARLEY, P., RYADNOV, E., JACKSON, R. E., ZANOVELLO, M., WILKINS, O. G., BARATTUCCI, S., MEHTA, P. R., OLIVEIRA, M. G., PARKES, J. E., SINHA, A., CORREA-SANCHEZ, A. F., OLIVER, P. L., FISHER, E. M. C., SCHIAVO, G., SHAH, M., BURRONE, J. & FRATTA, P. 2024. Loss of TDP-43 induces synaptic dysfunction that is rescued by UNC13A splice-switching ASOs. *bioRxiv*.
KHADEMULLAH, C. S., AQRABAWI, A. J., PLACE, K. M., DARGAEI, Z., LIANG, X., PRESSEY, J. C., BEDARD, S., YANG, J. W., GARAND, D., KERAMIDIS, I.,

GASECKA, A., COTE, D., DE KONINCK, Y., KEITH, J., ZINMAN, L., ROBERTSON, J., KIM, J. C. & WOODIN, M. A. 2020. Cortical interneuron-mediated inhibition delays the onset of amyotrophic lateral sclerosis. *Brain,* 143**,** 800-810.

KHAKH, B. S. 2019. Astrocyte-Neuron Interactions in the Striatum: Insights on Identity, Form, and Function. *Trends Neurosci,* 42**,** 617-630.

KIM, J., HUGHES, E. G., SHETTY, A. S., ARLOTTA, P., GOFF, L. A., BERGLES, D. E. & BROWN, S. P. 2017. Changes in the Excitability of Neocortical Neurons in a Mouse Model of Amyotrophic Lateral Sclerosis Are Not Specific to Corticospinal Neurons and Are Modulated by Advancing Disease. *J Neurosci,* 37**,** 9037-9053.

KIMM, T., KHALIQ, Z. M. & BEAN, B. P. 2015. Differential Regulation of Action Potential Shape and Burst-Frequency Firing by BK and Kv2 Channels in Substantia Nigra Dopaminergic Neurons. *J Neurosci,* 35**,** 16404-17.

KING, A. E., WOODHOUSE, A., KIRKCALDIE, M. T. & VICKERS, J. C. 2016. Excitotoxicity in ALS: Overstimulation, or overreaction? *Exp Neurol,* 275 Pt 1**,** 162-71.

KLAWONN, A. M., FRITZ, M., CASTANY, S., PIGNATELLI, M., CANAL, C., SIMILA, F., TEJEDA, H. A., LEVINSSON, J., JAAROLA, M., JAKOBSSON, J., HIDALGO, J., HEILIG, M., BONCI, A. & ENGBLOM, D. 2021. Microglial activation elicits a negative affective state through prostaglandin-mediated modulation of striatal neurons. *Immunity,* 54**,** 225-234 e6.

KLIM, J. R., WILLIAMS, L. A., LIMONE, F., GUERRA SAN JUAN, I., DAVIS-DUSENBERY, B. N., MORDES, D. A., BURBERRY, A., STEINBAUGH, M. J., GAMAGE, K. K., KIRCHNER, R., MOCCIA, R., CASSEL, S. H., CHEN, K., WAINGER, B. J., WOOLF, C. J. & EGGAN, K. 2019. ALS-implicated protein TDP-43 sustains levels of STMN2, a mediator of motor neuron growth and repair. *Nat Neurosci,* 22**,** 167-179.

KOHASHI, T. & CARLSON, B. A. 2014. A fast BK-type KCa current acts as a postsynaptic modulator of temporal selectivity for communication signals. *Front Cell Neurosci,* 8**,** 286.

KOPPERS, M., BLOKHUIS, A. M., WESTENENG, H. J., TERPSTRA, M. L., ZUNDEL, C. A., VIEIRA DE SA, R., SCHELLEVIS, R. D., WAITE, A. J., BLAKE, D. J., VELDINK, J. H., VAN DEN BERG, L. H. & PASTERKAMP, R. J. 2015. C9orf72 ablation in mice does not cause motor neuron degeneration or motor deficits. *Ann Neurol,* 78**,** 426-38.

KOZA, P., BEROUN, A., KONOPKA, A., GORKIEWICZ, T., BIJOCH, L., TORRES, J. C., BULSKA, E., KNAPSKA, E., KACZMAREK, L. & KONOPKA, W. 2019. Neuronal TDP-43 depletion affects activity-dependent plasticity. *Neurobiol Dis,* 130**,** 104499.

KREITZER, A. C. 2009. Physiology and pharmacology of striatal neurons. *Annu Rev Neurosci,* 32**,** 127-47.

KRINGELBACH, M. L. 2005. The human orbitofrontal cortex: linking reward to hedonic experience. *Nat Rev Neurosci,* 6**,** 691-702.

KSHATRI, A. S., GONZALEZ-HERNANDEZ, A. & GIRALDEZ, T. 2018. Physiological Roles and Therapeutic Potential of Ca(2+) Activated Potassium Channels in the Nervous System. *Front Mol Neurosci,* 11**,** 258.

KUBA, H., OICHI, Y. & OHMORI, H. 2010. Presynaptic activity regulates Na(+) channel distribution at the axon initial segment. *Nature,* 465**,** 1075-8.

KUJIRAI, T., CARAMIA, M. D., ROTHWELL, J. C., DAY, B. L., THOMPSON, P. D., FERBERT, A., WROE, S., ASSELMAN, P. & MARSDEN, C. D. 1993. Corticocortical inhibition in human motor cortex. *J Physiol,* 471**,** 501-19.
KWIATKOWSKI, T. J., JR., BOSCO, D. A., LECLERC, A. L., TAMRAZIAN, E., VANDERBURG, C. R., RUSS, C., DAVIS, A., GILCHRIST, J., KASARSKIS, E. J., MUNSAT, T., VALDMANIS, P., ROULEAU, G. A., HOSLER, B. A., CORTELLI, P., DE JONG, P. J., YOSHINAGA, Y., HAINES, J. L., PERICAK-VANCE, M. A., YAN, J., TICOZZI, N., SIDDIQUE, T., MCKENNA-YASEK, D., SAPP, P. C., HORVITZ, H. R., LANDERS, J. E. & BROWN, R. H., JR. 2009. Mutations in the FUS/TLS gene on chromosome 16 cause familial amyotrophic lateral sclerosis. *Science,* 323**,** 1205-8.
KWON, I., XIANG, S., KATO, M., WU, L., THEODOROPOULOS, P., WANG, T., KIM, J., YUN, J., XIE, Y. & MCKNIGHT, S. L. 2014. Poly-dipeptides encoded by the C9orf72 repeats bind nucleoli, impede RNA biogenesis, and kill cells. *Science,* 345**,** 1139-45.
LAGIER-TOURENNE, C., BAUGHN, M., RIGO, F., SUN, S., LIU, P., LI, H. R., JIANG, J., WATT, A. T., CHUN, S., KATZ, M., QIU, J., SUN, Y., LING, S. C., ZHU, Q., POLYMENIDOU, M., DRENNER, K., ARTATES, J. W., MCALONIS-DOWNES, M., MARKMILLER, S., HUTT, K. R., PIZZO, D. P., CADY, J., HARMS, M. B., BALOH, R. H., VANDENBERG, S. R., YEO, G. W., FU, X. D., BENNETT, C. F., CLEVELAND, D. W. & RAVITS, J. 2013. Targeted degradation of sense and antisense C9orf72 RNA foci as therapy for ALS and frontotemporal degeneration. *Proc Natl Acad Sci U S A,* 110**,** E4530-9.
LAGIER-TOURENNE, C., POLYMENIDOU, M. & CLEVELAND, D. W. 2010. TDP-43 and FUS/TLS: emerging roles in RNA processing and neurodegeneration. *Hum Mol Genet,* 19**,** R46-64.
LALL, D., LORENZINI, I., MOTA, T. A., BELL, S., MAHAN, T. E., ULRICH, J. D., DAVTYAN, H., REXACH, J. E., MUHAMMAD, A., SHELEST, O., LANDEROS, J., VAZQUEZ, M., KIM, J., GHAFFARI, L., O'ROURKE, J. G., GESCHWIND, D. H., BLURTON-JONES, M., HOLTZMAN, D. M., SATTLER, R. & BALOH, R. H. 2021. C9orf72 deficiency promotes microglial-mediated synaptic loss in aging and amyloid accumulation. *Neuron,* 109**,** 2275-2291 e8.
LANDIN-ROMERO, R., KUMFOR, F., LEYTON, C. E., IRISH, M., HODGES, J. R. & PIGUET, O. 2017. Disease-specific patterns of cortical and subcortical degeneration in a longitudinal study of Alzheimer's disease and behavioural-variant frontotemporal dementia. *Neuroimage,* 151**,** 72-80.
LANSDALL, C. J., COYLE-GILCHRIST, I. T. S., JONES, P. S., VAZQUEZ RODRIGUEZ, P., WILCOX, A., WEHMANN, E., DICK, K. M., ROBBINS, T. W. & ROWE, J. B. 2017. Apathy and impulsivity in frontotemporal lobar degeneration syndromes. *Brain,* 140**,** 1792-1807.
LARGE, C., NEILL, J., HARTE, M., CADINU, D., CUNNINGHAM, M., LEBEAU, F., MODEBADZE, T. & ALVARO, G. 2017. 3.3 Entraining neural networks through parvalbumin-positive interneurons: Can this offer a better way to treat schizophrenia? . *Schizophr Bull,* 43**,** S3.
LASZLO, Z. I., HINDLEY, N., SANCHEZ AVILA, A., KLINE, R. A., EATON, S. L., LAMONT, D. J., SMITH, C., SPIRES-JONES, T. L., WISHART, T. M. & HENSTRIDGE, C. M. 2022. Synaptic proteomics reveal distinct molecular signatures of cognitive change and C9ORF72 repeat expansion in the human ALS cortex. *Acta Neuropathol Commun,* 10**,** 156.

LATTANTE, S., ROULEAU, G. A. & KABASHI, E. 2013. TARDBP and FUS mutations associated with amyotrophic lateral sclerosis: summary and update. *Hum Mutat,* 34**,** 812-26.
LAU, D., VEGA-SAENZ DE MIERA, E. C., CONTRERAS, D., OZAITA, A., HARVEY, M., CHOW, A., NOEBELS, J. L., PAYLOR, R., MORGAN, J. I., LEONARD, C. S. & RUDY, B. 2000. Impaired fast-spiking, suppressed cortical inhibition, and increased susceptibility to seizures in mice lacking Kv3.2 K+ channel proteins. *J Neurosci,* 20**,** 9071-85.
LAYNE, J. J., NAUSCH, B., OLESEN, S. P. & NELSON, M. T. 2010. BK channel activation by NS11021 decreases excitability and contractility of urinary bladder smooth muscle. *Am J Physiol Regul Integr Comp Physiol,* 298**,** R378-84.
LE BOUC, R., BORDERIES, N., CARLE, G., ROBRIQUET, C., VINCKIER, F., DAUNIZEAU, J., AZUAR, C., LEVY, R. & PESSIGLIONE, M. 2023. Effort avoidance as a core mechanism of apathy in frontotemporal dementia. *Brain,* 146**,** 712-726.
LE CANN, K., FOERSTER, A., ROSSELER, C., ERICKSON, A., HAUTVAST, P., GIESSELMANN, S., PENSOLD, D., KURTH, I., ROTHERMEL, M., MATTIS, V. B., ZIMMER-BENSCH, G., VON HORSTEN, S., DENECKE, B., CLARNER, T., MEENTS, J. & LAMPERT, A. 2021. The difficulty to model Huntington's disease in vitro using striatal medium spiny neurons differentiated from human induced pluripotent stem cells. *Sci Rep,* 11**,** 6934.
LEE, K. H., ZHANG, P., KIM, H. J., MITREA, D. M., SARKAR, M., FREIBAUM, B. D., CIKA, J., COUGHLIN, M., MESSING, J., MOLLIEX, A., MAXWELL, B. A., KIM, N. C., TEMIROV, J., MOORE, J., KOLAITIS, R. M., SHAW, T. I., BAI, B., PENG, J., KRIWACKI, R. W. & TAYLOR, J. P. 2016. C9orf72 Dipeptide Repeats Impair the Assembly, Dynamics, and Function of Membrane-Less Organelles. *Cell,* 167**,** 774-788 e17.
LEE, S., CHOI, K., AHN, H., SONG, K., CHOE, J. & LEE, I. 2005. TuJ1 (class III beta-tubulin) expression suggests dynamic redistribution of follicular dendritic cells in lymphoid tissue. *Eur J Cell Biol,* 84**,** 453-9.
LEE, S. E., KHAZENZON, A. M., TRUJILLO, A. J., GUO, C. C., YOKOYAMA, J. S., SHA, S. J., TAKADA, L. T., KARYDAS, A. M., BLOCK, N. R., COPPOLA, G., PRIBADI, M., GESCHWIND, D. H., RADEMAKERS, R., FONG, J. C., WEINER, M. W., BOXER, A. L., KRAMER, J. H., ROSEN, H. J., MILLER, B. L. & SEELEY, W. W. 2014. Altered network connectivity in frontotemporal dementia with C9orf72 hexanucleotide repeat expansion. *Brain,* 137**,** 3047-60.
LEE, S. E., SIAS, A. C., MANDELLI, M. L., BROWN, J. A., BROWN, A. B., KHAZENZON, A. M., VIDOVSZKY, A. A., ZANTO, T. P., KARYDAS, A. M., PRIBADI, M., DOKURU, D., COPPOLA, G., GESCHWIND, D. H., RADEMAKERS, R., GORNO-TEMPINI, M. L., ROSEN, H. J., MILLER, B. L. & SEELEY, W. W. 2017a. Network degeneration and dysfunction in presymptomatic C9ORF72 expansion carriers. *Neuroimage Clin,* 14**,** 286-297.
LEE, Y. B., BASKARAN, P., GOMEZ-DEZA, J., CHEN, H. J., NISHIMURA, A. L., SMITH, B. N., TROAKES, C., ADACHI, Y., STEPTO, A., PETRUCELLI, L., GALLO, J. M., HIRTH, F., ROGELJ, B., GUTHRIE, S. & SHAW, C. E. 2017b. C9orf72 poly GA RAN-translated protein plays a key role in amyotrophic lateral sclerosis via aggregation and toxicity. *Hum Mol Genet,* 26**,** 4765-4777.
LEMON, R. N. 2008. Descending pathways in motor control. *Annu Rev Neurosci,* 31**,** 195-218.

LEPINE, S., NAULEAU-JAVAUDIN, A., DENEAULT, E., CHEN, C. X., ABDIAN, N., FRANCO-FLORES, A. K., HAGHI, G., CASTELLANOS-MONTIEL, M. J., MAUSSION, G., CHAINEAU, M. & DURCAN, T. M. 2024. Homozygous ALS-linked mutations in TARDBP/TDP-43 lead to hypoactivity and synaptic abnormalities in human iPSC-derived motor neurons. *iScience,* 27**,** 109166.
LEROY, F., LAMOTTE D'INCAMPS, B., IMHOFF-MANUEL, R. D. & ZYTNICKI, D. 2014. Early intrinsic hyperexcitability does not contribute to motoneuron degeneration in amyotrophic lateral sclerosis. *Elife,* 3.
LEROY, F. & ZYTNICKI, D. 2015. Is hyperexcitability really guilty in amyotrophic lateral sclerosis? *Neural Regen Res,* 10**,** 1413-5.
LEZMY, J., LIPINSKY, M., KHRAPUNSKY, Y., PATRICH, E., SHALOM, L., PERETZ, A., FLEIDERVISH, I. A. & ATTALI, B. 2017. M-current inhibition rapidly induces a unique CK2-dependent plasticity of the axon initial segment. *Proc Natl Acad Sci U S A,* 114**,** E10234-E10243.
LI, X. J., ZHANG, X., JOHNSON, M. A., WANG, Z. B., LAVAUTE, T. & ZHANG, S. C. 2009. Coordination of sonic hedgehog and Wnt signaling determines ventral and dorsal telencephalic neuron types from human embryonic stem cells. *Development,* 136**,** 4055-63.
LIEN, C. C. & JONAS, P. 2003. Kv3 potassium conductance is necessary and kinetically optimized for high-frequency action potential generation in hippocampal interneurons. *J Neurosci,* 23**,** 2058-68.
LIM, S. A. O. & SURMEIER, D. J. 2020. Enhanced GABAergic Inhibition of Cholinergic Interneurons in the zQ175(+/-) Mouse Model of Huntington's Disease. *Front Syst Neurosci,* 14**,** 626412.
LIN, L., YUAN, J., SANDER, B. & GOLAS, M. M. 2015. In Vitro Differentiation of Human Neural Progenitor Cells Into Striatal GABAergic Neurons. *Stem Cells Transl Med,* 4**,** 775-88.
LIN, Y., MORI, E., KATO, M., XIANG, S., WU, L., KWON, I. & MCKNIGHT, S. L. 2016. Toxic PR Poly-Dipeptides Encoded by the C9orf72 Repeat Expansion Target LC Domain Polymers. *Cell,* 167**,** 789-802 e12.
LIN, Z., KIM, E., AHMED, M., HAN, G., SIMMONS, C., REDHEAD, Y., BARTLETT, J., PENA ALTAMIRA, L. E., CALLAGHAN, I., WHITE, M. A., SINGH, N., SAWIAK, S., SPIRES-JONES, T., VERNON, A. C., COLEMAN, M. P., GREEN, J., HENSTRIDGE, C., DAVIES, J. S., CASH, D. & SREEDHARAN, J. 2021. MRI-guided histology of TDP-43 knock-in mice implicates parvalbumin interneuron loss, impaired neurogenesis and aberrant neurodevelopment in amyotrophic lateral sclerosis-frontotemporal dementia. *Brain Commun,* 3**,** fcab114.
LINDAU, M., JELIC, V., JOHANSSON, S. E., ANDERSEN, C., WAHLUND, L. O. & ALMKVIST, O. 2003. Quantitative EEG abnormalities and cognitive dysfunctions in frontotemporal dementia and Alzheimer's disease. *Dement Geriatr Cogn Disord,* 15**,** 106-14.
LING, S. C., POLYMENIDOU, M. & CLEVELAND, D. W. 2013. Converging mechanisms in ALS and FTD: disrupted RNA and protein homeostasis. *Neuron,* 79**,** 416-38.
LIPTON, A. M., WHITE, C. L., 3RD & BIGIO, E. H. 2004. Frontotemporal lobar degeneration with motor neuron disease-type inclusions predominates in 76 cases of frontotemporal degeneration. *Acta Neuropathol,* 108**,** 379-85.
LIU, J., LILLO, C., JONSSON, P. A., VANDE VELDE, C., WARD, C. M., MILLER, T. M., SUBRAMANIAM, J. R., ROTHSTEIN, J. D., MARKLUND, S.,

ANDERSEN, P. M., BRANNSTROM, T., GREDAL, O., WONG, P. C., WILLIAMS, D. S. & CLEVELAND, D. W. 2004. Toxicity of familial ALS-linked SOD1 mutants from selective recruitment to spinal mitochondria. *Neuron,* 43**,** 5-17.

LIU, L., CHU, M., NIE, B., JIANG, D., XIE, K., CUI, Y., LIU, L., KONG, Y., CHEN, Z., NAN, H., ROSA-NETO, P. & WU, L. 2023. Altered metabolic connectivity within the limbic cortico-striato-thalamo-cortical circuit in presymptomatic and symptomatic behavioral variant frontotemporal dementia. *Alzheimers Res Ther,* 15**,** 3.

LIU, L., LIU, S., CHU, M., WANG, J., XIE, K., CUI, Y., MA, J., NAN, H., CUI, C., QIAO, H., ROSA-NETO, P., CHAN, P. & WU, L. 2022. Involvement of striatal motoric subregions in familial frontotemporal dementia with parkinsonism harboring the C9orf72 repeat expansions. *NPJ Parkinsons Dis,* 8**,** 128.

LIU, Y., WONG, T. P., AARTS, M., ROOYAKKERS, A., LIU, L., LAI, T. W., WU, D. C., LU, J., TYMIANSKI, M., CRAIG, A. M. & WANG, Y. T. 2007. NMDA receptor subunits have differential roles in mediating excitotoxic neuronal death both in vitro and in vivo. *J Neurosci,* 27**,** 2846-57.

LIVESEY, M. R., MAGNANI, D., CLEARY, E. M., VASISTHA, N. A., JAMES, O. T., SELVARAJ, B. T., BURR, K., STORY, D., SHAW, C. E., KIND, P. C., HARDINGHAM, G. E., WYLLIE, D. J. & CHANDRAN, S. 2016. Maturation and electrophysiological properties of human pluripotent stem cell-derived oligodendrocytes. *Stem Cells,* 34**,** 1040-53.

LOGROSCINO, G., TRAYNOR, B. J., HARDIMAN, O., CHIO, A., MITCHELL, D., SWINGLER, R. J., MILLUL, A., BENN, E., BEGHI, E. & EURALS 2010. Incidence of amyotrophic lateral sclerosis in Europe. *J Neurol Neurosurg Psychiatry,* 81**,** 385-90.

LOMEN-HOERTH, C., ANDERSON, T. & MILLER, B. 2002. The overlap of amyotrophic lateral sclerosis and frontotemporal dementia. *Neurology,* 59**,** 1077-9.

LOMEN-HOERTH, C., MURPHY, J., LANGMORE, S., KRAMER, J. H., OLNEY, R. K. & MILLER, B. 2003. Are amyotrophic lateral sclerosis patients cognitively normal? *Neurology,* 60**,** 1094-7.

LONGINETTI, E. & FANG, F. 2019. Epidemiology of amyotrophic lateral sclerosis: an update of recent literature. *Curr Opin Neurol,* 32**,** 771-776.

LOPEZ-GONZALEZ, R., LU, Y., GENDRON, T. F., KARYDAS, A., TRAN, H., YANG, D., PETRUCELLI, L., MILLER, B. L., ALMEIDA, S. & GAO, F. B. 2016. Poly(GR) in C9ORF72-Related ALS/FTD Compromises Mitochondrial Function and Increases Oxidative Stress and DNA Damage in iPSC-Derived Motor Neurons. *Neuron,* 92**,** 383-391.

LORENC, F., DUPUIS, L. & CASSEL, R. 2024. Impairments of inhibitory neurons in amyotrophic lateral sclerosis and frontotemporal dementia. *Neurobiol Dis,* 203**,** 106748.

LUDOLPH, A. & WIESENFARTH, M. 2025. Tofersen and other antisense oligonucleotides in ALS. *Ther Adv Neurol Disord,* 18**,** 17562864251313915.

MACHTS, J., LOEWE, K., KAUFMANN, J., JAKUBICZKA, S., ABDULLA, S., PETRI, S., DENGLER, R., HEINZE, H. J., VIELHABER, S., SCHOENFELD, M. A. & BEDE, P. 2015. Basal ganglia pathology in ALS is associated with neuropsychological deficits. *Neurology,* 85**,** 1301-9.

MACKENZIE, I. R., ARZBERGER, T., KREMMER, E., TROOST, D., LORENZL, S., MORI, K., WENG, S. M., HAASS, C., KRETZSCHMAR, H. A., EDBAUER, D.

& NEUMANN, M. 2013. Dipeptide repeat protein pathology in C9ORF72 mutation cases: clinico-pathological correlations. *Acta Neuropathol,* 126**,** 859-79.
MAHON, S., VAUTRELLE, N., PEZARD, L., SLAGHT, S. J., DENIAU, J. M., CHOUVET, G. & CHARPIER, S. 2006. Distinct patterns of striatal medium spiny neuron activity during the natural sleep-wake cycle. *J Neurosci,* 26**,** 12587-95.
MAHONEY, C. J., BECK, J., ROHRER, J. D., LASHLEY, T., MOK, K., SHAKESPEARE, T., YEATMAN, T., WARRINGTON, E. K., SCHOTT, J. M., FOX, N. C., ROSSOR, M. N., HARDY, J., COLLINGE, J., REVESZ, T., MEAD, S. & WARREN, J. D. 2012. Frontotemporal dementia with the C9ORF72 hexanucleotide repeat expansion: clinical, neuroanatomical and neuropathological features. *Brain,* 135**,** 736-50.
MAJOUNIE, E., RENTON, A. E., MOK, K., DOPPER, E. G., WAITE, A., ROLLINSON, S., CHIO, A., RESTAGNO, G., NICOLAOU, N., SIMON-SANCHEZ, J., VAN SWIETEN, J. C., ABRAMZON, Y., JOHNSON, J. O., SENDTNER, M., PAMPHLETT, R., ORRELL, R. W., MEAD, S., SIDLE, K. C., HOULDEN, H., ROHRER, J. D., MORRISON, K. E., PALL, H., TALBOT, K., ANSORGE, O., CHROMOSOME, A. L. S. F. T. D. C., FRENCH RESEARCH NETWORK ON, F. F. A., CONSORTIUM, I., HERNANDEZ, D. G., AREPALLI, S., SABATELLI, M., MORA, G., CORBO, M., GIANNINI, F., CALVO, A., ENGLUND, E., BORGHERO, G., FLORIS, G. L., REMES, A. M., LAAKSOVIRTA, H., MCCLUSKEY, L., TROJANOWSKI, J. Q., VAN DEERLIN, V. M., SCHELLENBERG, G. D., NALLS, M. A., DRORY, V. E., LU, C. S., YEH, T. H., ISHIURA, H., TAKAHASHI, Y., TSUJI, S., LE BER, I., BRICE, A., DREPPER, C., WILLIAMS, N., KIRBY, J., SHAW, P., HARDY, J., TIENARI, P. J., HEUTINK, P., MORRIS, H. R., PICKERING-BROWN, S. & TRAYNOR, B. J. 2012. Frequency of the C9orf72 hexanucleotide repeat expansion in patients with amyotrophic lateral sclerosis and frontotemporal dementia: a cross-sectional study. *Lancet Neurol,* 11**,** 323-30.
MALPETTI, M., HOLLAND, N., JONES, P. S., YE, R., COPE, T. E., FRYER, T. D., HONG, Y. T., SAVULICH, G., RITTMAN, T., PASSAMONTI, L., MAK, E., AIGBIRHIO, F. I., O'BRIEN, J. T. & ROWE, J. B. 2021. Synaptic density in carriers of C9orf72 mutations: a [(11) C]UCB-J PET study. *Ann Clin Transl Neurol,* 8**,** 1515-1523.
MALPETTI, M., JONES, P. S., COPE, T. E., HOLLAND, N., NAESSENS, M., ROUSE, M. A., RITTMAN, T., SAVULICH, G., WHITESIDE, D. J., STREET, D., FRYER, T. D., HONG, Y. T., MILICEVIC SEPHTON, S., AIGBIRHIO, F. I., JT, O. B. & ROWE, J. B. 2023. Synaptic Loss in Frontotemporal Dementia Revealed by [(11) C]UCB-J Positron Emission Tomography. *Ann Neurol,* 93**,** 142-154.
MANN, D. M. 2015. Dipeptide repeat protein toxicity in frontotemporal lobar degeneration and in motor neurone disease associated with expansions in C9ORF72-a cautionary note. *Neurobiol Aging,* 36**,** 1224-6.
MANN, D. M., ROLLINSON, S., ROBINSON, A., BENNION CALLISTER, J., THOMPSON, J. C., SNOWDEN, J. S., GENDRON, T., PETRUCELLI, L., MASUDA-SUZUKAKE, M., HASEGAWA, M., DAVIDSON, Y. & PICKERING-BROWN, S. 2013. Dipeptide repeat proteins are present in the p62 positive inclusions in patients with frontotemporal lobar degeneration and motor

neurone disease associated with expansions in C9ORF72. *Acta Neuropathol Commun,* 1**,** 68.
MARCHAND-PAUVERT, V., PEYRE, I., LACKMY-VALLEE, A., QUERIN, G., BEDE, P., LACOMBLEZ, L., DEBS, R. & PRADAT, P. F. 2019. Absence of hyperexcitability of spinal motoneurons in patients with amyotrophic lateral sclerosis. *J Physiol,* 597**,** 5445-5467.
MARCHI, P. M., MARRONE, L., BRASSEUR, L., COENS, A., WEBSTER, C. P., BOUSSET, L., DESTRO, M., SMITH, E. F., WALTHER, C. G., ALFRED, V., MARROCCELLA, R., GRAVES, E. J., ROBINSON, D., SHAW, A. C., WAN, L. M., GRIERSON, A. J., EBBENS, S. J., DE VOS, K. J., HAUTBERGUE, G. M., FERRAIUOLO, L., MELKI, R. & AZZOUZ, M. 2022. C9ORF72-derived poly-GA DPRs undergo endocytic uptake in iAstrocytes and spread to motor neurons. *Life Sci Alliance,* 5.
MARQUES, C., BURG, T., SCEKIC-ZAHIROVIC, J., FISCHER, M. & ROUAUX, C. 2021. Upper and Lower Motor Neuron Degenerations Are Somatotopically Related and Temporally Ordered in the Sod1 Mouse Model of Amyotrophic Lateral Sclerosis. *Brain Sci,* 11.
MARTIN, E., CAZENAVE, W., CATTAERT, D. & BRANCHEREAU, P. 2013. Embryonic alteration of motoneuronal morphology induces hyperexcitability in the mouse model of amyotrophic lateral sclerosis. *Neurobiol Dis,* 54**,** 116-26.
MARTIN, L. J. & CHANG, Q. 2012. Inhibitory synaptic regulation of motoneurons: a new target of disease mechanisms in amyotrophic lateral sclerosis. *Mol Neurobiol,* 45**,** 30-42.
MARTINELLO, K., HUANG, Z., LUJAN, R., TRAN, B., WATANABE, M., COOPER, E. C., BROWN, D. A. & SHAH, M. M. 2015. Cholinergic afferent stimulation induces axonal function plasticity in adult hippocampal granule cells. *Neuron,* 85**,** 346-63.
MARTINEZ-SILVA, M. L., IMHOFF-MANUEL, R. D., SHARMA, A., HECKMAN, C. J., SHNEIDER, N. A., ROSELLI, F., ZYTNICKI, D. & MANUEL, M. 2018. Hypoexcitability precedes denervation in the large fast-contracting motor units in two unrelated mouse models of ALS. *Elife,* 7.
MASRORI, P., BIJNENS, B., FUMAGALLI, L., DAVIE, K., POOVATHINGAL, S. K., MEESE, T., STORM, A., HERSMUS, N., FAZAL, R., VAN DEN BIGGELAAR, D., ASSELBERGH, B., GRUEL, R., VAN DEN DAELE, J., DENTON, H., MIQUEL, P. P., MANZELLA, S., DE VOS, W. H., CHANDRAN, S., VAN DEN BOSCH, L., THAL, D. R., MANCUSO, R. & VAN DAMME, P. 2025. C9orf72 hexanucleotide repeat expansions impair microglial response in ALS. *Nat Neurosci,* 28**,** 2217-2230.
MASSIH, B., VEH, A., SCHENKE, M., MUNGWA, S., SEEGER, B., SELVARAJ, B. T., CHANDRAN, S., REINHARDT, P., STERNECKERT, J., HERMANN, A., SENDTNER, M. & LUNINGSCHROR, P. 2023. A 3D cell culture system for bioengineering human neuromuscular junctions to model ALS. *Front Cell Dev Biol,* 11**,** 996952.
MASUDA, M., SENDA, J., WATANABE, H., EPIFANIO, B., TANAKA, Y., IMAI, K., RIKU, Y., LI, Y., NAKAMURA, R., ITO, M., ISHIGAKI, S., ATSUTA, N., KOIKE, H., KATSUNO, M., HATTORI, N., NAGANAWA, S. & SOBUE, G. 2016. Involvement of the caudate nucleus head and its networks in sporadic amyotrophic lateral sclerosis-frontotemporal dementia continuum. *Amyotroph Lateral Scler Frontotemporal Degener,* 17**,** 571-579.

MAURY, Y., COME, J., PISKOROWSKI, R. A., SALAH-MOHELLIBI, N., CHEVALEYRE, V., PESCHANSKI, M., MARTINAT, C. & NEDELEC, S. 2015. Combinatorial analysis of developmental cues efficiently converts human pluripotent stem cells into multiple neuronal subtypes. *Nat Biotechnol,* 33**,** 89-96.

MCGOWN, A., MCDEARMID, J. R., PANAGIOTAKI, N., TONG, H., AL MASHHADI, S., REDHEAD, N., LYON, A. N., BEATTIE, C. E., SHAW, P. J. & RAMESH, T. M. 2013. Early interneuron dysfunction in ALS: insights from a mutant sod1 zebrafish model. *Ann Neurol,* 73**,** 246-58.

MCKAY, S., GRIFFITHS, N. H., BUTTERS, P. A., THUBRON, E. B., HARDINGHAM, G. E. & WYLLIE, D. J. 2012. Direct pharmacological monitoring of the developmental switch in NMDA receptor subunit composition using TCN 213, a GluN2A-selective, glycine-dependent antagonist. *Br J Pharmacol,* 166**,** 924-37.

MCKEE, A. C., STERN, R. A., NOWINSKI, C. J., STEIN, T. D., ALVAREZ, V. E., DANESHVAR, D. H., LEE, H. S., WOJTOWICZ, S. M., HALL, G., BAUGH, C. M., RILEY, D. O., KUBILUS, C. A., CORMIER, K. A., JACOBS, M. A., MARTIN, B. R., ABRAHAM, C. R., IKEZU, T., REICHARD, R. R., WOLOZIN, B. L., BUDSON, A. E., GOLDSTEIN, L. E., KOWALL, N. W. & CANTU, R. C. 2013. The spectrum of disease in chronic traumatic encephalopathy. *Brain,* 136**,** 43-64.

MCSHANE, R., WESTBY, M. J., ROBERTS, E., MINAKARAN, N., SCHNEIDER, L., FARRIMOND, L. E., MAAYAN, N., WARE, J. & DEBARROS, J. 2019. Memantine for dementia. *Cochrane Database Syst Rev,* 3**,** CD003154.

MEAD, R. J., SHAN, N., REISER, H. J., MARSHALL, F. & SHAW, P. J. 2023. Amyotrophic lateral sclerosis: a neurodegenerative disorder poised for successful therapeutic translation. *Nat Rev Drug Discov,* 22**,** 185-212.

MEHTA, A. R., GREGORY, J. M., DANDO, O., CARTER, R. N., BURR, K., NANDA, J., STORY, D., MCDADE, K., SMITH, C., MORTON, N. M., MAHAD, D. J., HARDINGHAM, G. E., CHANDRAN, S. & SELVARAJ, B. T. 2021. Mitochondrial bioenergetic deficits in C9orf72 amyotrophic lateral sclerosis motor neurons cause dysfunctional axonal homeostasis. *Acta Neuropathol,* 141**,** 257-279.

MEIJBOOM, K. E., ABDALLAH, A., FORDHAM, N. P., NAGASE, H., RODRIGUEZ, T., KRAUS, C., GENDRON, T. F., KRISHNAN, G., ESANOV, R., ANDRADE, N. S., RYBIN, M. J., RAMIC, M., STEPHENS, Z. D., EDRAKI, A., BLACKWOOD, M. T., KAHRIMAN, A., HENNINGER, N., KOCHER, J. A., BENATAR, M., BRODSKY, M. H., PETRUCELLI, L., GAO, F. B., SONTHEIMER, E. J., BROWN, R. H., ZEIER, Z. & MUELLER, C. 2022. CRISPR/Cas9-mediated excision of ALS/FTD-causing hexanucleotide repeat expansion in C9ORF72 rescues major disease mechanisms in vivo and in vitro. *Nat Commun,* 13**,** 6286.

MENDEZ, M. F., SHAPIRA, J. S., MCMURTRAY, A., LICHT, E. & MILLER, B. L. 2007. Accuracy of the clinical evaluation for frontotemporal dementia. *Arch Neurol,* 64**,** 830-5.

MENON, P., HIGASHIHARA, M., VAN DEN BOS, M., GEEVASINGA, N., KIERNAN, M. C. & VUCIC, S. 2020. Cortical hyperexcitability evolves with disease progression in ALS. *Ann Clin Transl Neurol,* 7**,** 733-741.

MENON, P., KIERNAN, M. C. & VUCIC, S. 2015. Cortical hyperexcitability precedes lower motor neuron dysfunction in ALS. *Clin Neurophysiol,* 126**,** 803-9.

MENZIES, F. M., COOKSON, M. R., TAYLOR, R. W., TURNBULL, D. M., CHRZANOWSKA-LIGHTOWLERS, Z. M., DONG, L., FIGLEWICZ, D. A. & SHAW, P. J. 2002. Mitochondrial dysfunction in a cell culture model of familial amyotrophic lateral sclerosis. *Brain,* 125**,** 1522-33.

METZGER, M., DUKIC, S., MCMACKIN, R., GIGLIA, E., MITCHELL, M., BISTA, S., COSTELLO, E., PEELO, C., TADJINE, Y., SIRENKO, V., MCMANUS, L., BUXO, T., FASANO, A., CHIPIKA, R., PINTO-GRAU, M., SCHUSTER, C., HEVERIN, M., COFFEY, A., BRODERICK, M., IYER, P. M., MOHR, K., GAVIN, B., PENDER, N., BEDE, P., MUTHURAMAN, M., HARDIMAN, O. & NASSEROLESLAMI, B. 2024. Distinct Longitudinal Changes in EEG Measures Reflecting Functional Network Disruption in ALS Cognitive Phenotypes. *Brain Topogr,* 38**,** 3.

MEYER, K., FERRAIUOLO, L., MIRANDA, C. J., LIKHITE, S., MCELROY, S., RENUSCH, S., DITSWORTH, D., LAGIER-TOURENNE, C., SMITH, R. A., RAVITS, J., BURGHES, A. H., SHAW, P. J., CLEVELAND, D. W., KOLB, S. J. & KASPAR, B. K. 2014. Direct conversion of patient fibroblasts demonstrates non-cell autonomous toxicity of astrocytes to motor neurons in familial and sporadic ALS. *Proc Natl Acad Sci U S A,* 111**,** 829-32.

MEZZAPESA, D. M., D'ERRICO, E., TORTELLI, R., DISTASO, E., CORTESE, R., TURSI, M., FEDERICO, F., ZOCCOLELLA, S., LOGROSCINO, G., DICUONZO, F. & SIMONE, I. L. 2013. Cortical thinning and clinical heterogeneity in amyotrophic lateral sclerosis. *PLoS One,* 8**,** e80748.

MIGNOGNA, M. L., MUSARDO, S., RANIERI, G., GELMINI, S., ESPINOSA, P., MARRA, P., BELLOLI, S., MURTAJ, V., MORESCO, R. M., BELLONE, C. & D'ADAMO, P. 2021. RAB39B-mediated trafficking of the GluA2-AMPAR subunit controls dendritic spine maturation and intellectual disability-related behaviour. *Mol Psychiatry,* 26**,** 6531-6549.

MILIOTO, C., CARCOLE, M., GIBLIN, A., CONEYS, R., ATTREBI, O., AHMED, M., HARRIS, S. S., LEE, B. I., YANG, M., ELLINGFORD, R. A., NIRUJOGI, R. S., BIGGS, D., SALOMONSSON, S., ZANOVELLO, M., DE OLIVEIRA, P., KATONA, E., GLARIA, I., MIKHEENKO, A., GEARY, B., UDINE, E., VAIZOGLU, D., ANOAR, S., JOTANGIYA, K., CROWLEY, G., SMEETH, D. M., ADAMS, M. L., NICCOLI, T., RADEMAKERS, R., VAN BLITTERSWIJK, M., DEVOY, A., HONG, S., PARTRIDGE, L., COYNE, A. N., FRATTA, P., ALESSI, D. R., DAVIES, B., BUSCHE, M. A., GREENSMITH, L., FISHER, E. M. C. & ISAACS, A. M. 2024. PolyGR and polyPR knock-in mice reveal a conserved neuroprotective extracellular matrix signature in C9orf72 ALS/FTD neurons. *Nat Neurosci,* 27**,** 643-655.

MILLER, T., CUDKOWICZ, M., SHAW, P. J., ANDERSEN, P. M., ATASSI, N., BUCELLI, R. C., GENGE, A., GLASS, J., LADHA, S., LUDOLPH, A. L., MARAGAKIS, N. J., MCDERMOTT, C. J., PESTRONK, A., RAVITS, J., SALACHAS, F., TRUDELL, R., VAN DAMME, P., ZINMAN, L., BENNETT, C. F., LANE, R., SANDROCK, A., RUNZ, H., GRAHAM, D., HOUSHYAR, H., MCCAMPBELL, A., NESTOROV, I., CHANG, I., MCNEILL, M., FANNING, L., FRADETTE, S. & FERGUSON, T. A. 2020. Phase 1-2 Trial of Antisense Oligonucleotide Tofersen for SOD1 ALS. *N Engl J Med,* 383**,** 109-119.

MILLER, T. M., CUDKOWICZ, M. E., GENGE, A., SHAW, P. J., SOBUE, G., BUCELLI, R. C., CHIO, A., VAN DAMME, P., LUDOLPH, A. C., GLASS, J. D., ANDREWS, J. A., BABU, S., BENATAR, M., MCDERMOTT, C. J., COCHRANE, T., CHARY, S., CHEW, S., ZHU, H., WU, F., NESTOROV, I.,

GRAHAM, D., SUN, P., MCNEILL, M., FANNING, L., FERGUSON, T. A., FRADETTE, S., VALOR & GROUP, O. L. E. W. 2022. Trial of Antisense Oligonucleotide Tofersen for SOD1 ALS. *N Engl J Med,* 387**,** 1099-1110.
MILNERWOOD, A. J. & RAYMOND, L. A. 2010. Early synaptic pathophysiology in neurodegeneration: insights from Huntington's disease. *Trends Neurosci,* 33**,** 513-23.
MIURA, Y., LI, M. Y., BIREY, F., IKEDA, K., REVAH, O., THETE, M. V., PARK, J. Y., PUNO, A., LEE, S. H., PORTEUS, M. H. & PASCA, S. P. 2020. Generation of human striatal organoids and cortico-striatal assembloids from human pluripotent stem cells. *Nat Biotechnol,* 38**,** 1421-1430.
MIZIELINSKA, S., GRONKE, S., NICCOLI, T., RIDLER, C. E., CLAYTON, E. L., DEVOY, A., MOENS, T., NORONA, F. E., WOOLLACOTT, I. O. C., PIETRZYK, J., CLEVERLEY, K., NICOLL, A. J., PICKERING-BROWN, S., DOLS, J., CABECINHA, M., HENDRICH, O., FRATTA, P., FISHER, E. M. C., PARTRIDGE, L. & ISAACS, A. M. 2014. C9orf72 repeat expansions cause neurodegeneration in Drosophila through arginine-rich proteins. *Science,* 345**,** 1192-1194.
MIZIELINSKA, S., LASHLEY, T., NORONA, F. E., CLAYTON, E. L., RIDLER, C. E., FRATTA, P. & ISAACS, A. M. 2013. C9orf72 frontotemporal lobar degeneration is characterised by frequent neuronal sense and antisense RNA foci. *Acta Neuropathol,* 126**,** 845-57.
MIZIELINSKA, S., RIDLER, C. E., BALENDRA, R., THOENG, A., WOODLING, N. S., GRASSER, F. A., PLAGNOL, V., LASHLEY, T., PARTRIDGE, L. & ISAACS, A. M. 2017. Bidirectional nucleolar dysfunction in C9orf72 frontotemporal lobar degeneration. *Acta Neuropathol Commun,* 5**,** 29.
MOAKLEY, D., KOH, J., PEREIRA, J. D., DUBREUIL, D. M., DEVLIN, A. C., BEREZOVSKI, E., ZHU, K. & WAINGER, B. J. 2019. Pharmacological Profiling of Purified Human Stem Cell-Derived and Primary Mouse Motor Neurons. *Sci Rep,* 9**,** 10835.
MOLLER, C., DIELEMAN, N., VAN DER FLIER, W. M., VERSTEEG, A., PIJNENBURG, Y., SCHELTENS, P., BARKHOF, F. & VRENKEN, H. 2015. More atrophy of deep gray matter structures in frontotemporal dementia compared to Alzheimer's disease. *J Alzheimers Dis,* 44**,** 635-47.
MOLLIEX, A., TEMIROV, J., LEE, J., COUGHLIN, M., KANAGARAJ, A. P., KIM, H. J., MITTAG, T. & TAYLOR, J. P. 2015. Phase separation by low complexity domains promotes stress granule assembly and drives pathological fibrillization. *Cell,* 163**,** 123-33.
MONTGOMERY, J. R. & MEREDITH, A. L. 2012. Genetic activation of BK currents in vivo generates bidirectional effects on neuronal excitability. *Proc Natl Acad Sci U S A,* 109**,** 18997-9002.
MORI, K., ARZBERGER, T., GRASSER, F. A., GIJSELINCK, I., MAY, S., RENTZSCH, K., WENG, S. M., SCHLUDI, M. H., VAN DER ZEE, J., CRUTS, M., VAN BROECKHOVEN, C., KREMMER, E., KRETZSCHMAR, H. A., HAASS, C. & EDBAUER, D. 2013a. Bidirectional transcripts of the expanded C9orf72 hexanucleotide repeat are translated into aggregating dipeptide repeat proteins. *Acta Neuropathol,* 126**,** 881-93.
MORI, K., WENG, S. M., ARZBERGER, T., MAY, S., RENTZSCH, K., KREMMER, E., SCHMID, B., KRETZSCHMAR, H. A., CRUTS, M., VAN BROECKHOVEN, C., HAASS, C. & EDBAUER, D. 2013b. The C9orf72 GGGGCC repeat is

translated into aggregating dipeptide-repeat proteins in FTLD/ALS. *Science,* 339**,** 1335-8.
MOYA, M. V., KIM, R. D., RAO, M. N., COTTO, B. A., PICKETT, S. B., SFERRAZZA, C. E., HEINTZ, N. & SCHMIDT, E. F. 2022. Unique molecular features and cellular responses differentiate two populations of motor cortical layer 5b neurons in a preclinical model of ALS. *Cell Rep,* 38**,** 110556.
MURLEY, A. G., ROUSE, M. A., JONES, P. S., YE, R., HEZEMANS, F. H., O'CALLAGHAN, C., FRANGOU, P., KOURTZI, Z., RUA, C., CARPENTER, T. A., RODGERS, C. T. & ROWE, J. B. 2020. GABA and glutamate deficits from frontotemporal lobar degeneration are associated with disinhibition. *Brain,* 143**,** 3449-3462.
MURLEY, A. G. & ROWE, J. B. 2018. Neurotransmitter deficits from frontotemporal lobar degeneration. *Brain,* 141**,** 1263-1285.
MURRAY, M. E., DEJESUS-HERNANDEZ, M., RUTHERFORD, N. J., BAKER, M., DUARA, R., GRAFF-RADFORD, N. R., WSZOLEK, Z. K., FERMAN, T. J., JOSEPHS, K. A., BOYLAN, K. B., RADEMAKERS, R. & DICKSON, D. W. 2011. Clinical and neuropathologic heterogeneity of c9FTD/ALS associated with hexanucleotide repeat expansion in C9ORF72. *Acta Neuropathol,* 122**,** 673-90.
NAGAI, J., RAJBHANDARI, A. K., GANGWANI, M. R., HACHISUKA, A., COPPOLA, G., MASMANIDIS, S. C., FANSELOW, M. S. & KHAKH, B. S. 2019. Hyperactivity with Disrupted Attention by Activation of an Astrocyte Synaptogenic Cue. *Cell,* 177**,** 1280-1292 e20.
NAGAI, M., RE, D. B., NAGATA, T., CHALAZONITIS, A., JESSELL, T. M., WICHTERLE, H. & PRZEDBORSKI, S. 2007. Astrocytes expressing ALS-linked mutated SOD1 release factors selectively toxic to motor neurons. *Nat Neurosci,* 10**,** 615-22.
NARBOUX-NEME, N., EVRARD, A., FEREZOU, I., ERZURUMLU, R. S., KAESER, P. S., LAINE, J., ROSSIER, J., ROPERT, N., SUDHOF, T. C. & GASPAR, P. 2012. Neurotransmitter release at the thalamocortical synapse instructs barrel formation but not axon patterning in the somatosensory cortex. *J Neurosci,* 32**,** 6183-96.
NASSEROLESLAMI, B., DUKIC, S., BRODERICK, M., MOHR, K., SCHUSTER, C., GAVIN, B., MCLAUGHLIN, R., HEVERIN, M., VAJDA, A., IYER, P. M., PENDER, N., BEDE, P., LALOR, E. C. & HARDIMAN, O. 2019. Characteristic Increases in EEG Connectivity Correlate With Changes of Structural MRI in Amyotrophic Lateral Sclerosis. *Cereb Cortex,* 29**,** 27-41.
NAUJOCK, M., STANSLOWSKY, N., BUFLER, S., NAUMANN, M., REINHARDT, P., STERNECKERT, J., KEFALAKES, E., KASSEBAUM, C., BURSCH, F., LOJEWSKI, X., STORCH, A., FRICKENHAUS, M., BOECKERS, T. M., PUTZ, S., DEMESTRE, M., LIEBAU, S., KLINGENSTEIN, M., LUDOLPH, A. C., DENGLER, R., KIM, K. S., HERMANN, A., WEGNER, F. & PETRI, S. 2016. 4-Aminopyridine Induced Activity Rescues Hypoexcitable Motor Neurons from Amyotrophic Lateral Sclerosis Patient-Derived Induced Pluripotent Stem Cells. *Stem Cells,* 34**,** 1563-75.
NEHER, E. & LUX, H. D. 1969. Voltage clamp on Helix pomatia neuronal membrane; current measurement over a limited area of the soma surface. *Pflugers Arch,* 311**,** 272-7.
NEHER, E. & SAKMANN, B. 1976. Single-channel currents recorded from membrane of denervated frog muscle fibres. *Nature,* 260**,** 799-802.

NEHER, E., SAKMANN, B. & STEINBACH, J. H. 1978. The extracellular patch clamp: a method for resolving currents through individual open channels in biological membranes. *Pflugers Arch,* 375**,** 219-28.
NEKRASOV, E. D., VIGONT, V. A., KLYUSHNIKOV, S. A., LEBEDEVA, O. S., VASSINA, E. M., BOGOMAZOVA, A. N., CHESTKOV, I. V., SEMASHKO, T. A., KISELEVA, E., SULDINA, L. A., BOBROVSKY, P. A., ZIMINA, O. A., RYAZANTSEVA, M. A., SKOPIN, A. Y., ILLARIOSHKIN, S. N., KAZNACHEYEVA, E. V., LAGARKOVA, M. A. & KISELEV, S. L. 2016. Manifestation of Huntington's disease pathology in human induced pluripotent stem cell-derived neurons. *Mol Neurodegener,* 11**,** 27.
NELSON, S. B. & TURRIGIANO, G. G. 2008. Strength through diversity. *Neuron,* 60**,** 477-82.
NEUMANN, M., SAMPATHU, D. M., KWONG, L. K., TRUAX, A. C., MICSENYI, M. C., CHOU, T. T., BRUCE, J., SCHUCK, T., GROSSMAN, M., CLARK, C. M., MCCLUSKEY, L. F., MILLER, B. L., MASLIAH, E., MACKENZIE, I. R., FELDMAN, H., FEIDEN, W., KRETZSCHMAR, H. A., TROJANOWSKI, J. Q. & LEE, V. M. 2006. Ubiquitinated TDP-43 in frontotemporal lobar degeneration and amyotrophic lateral sclerosis. *Science,* 314**,** 130-3.
NIETO-GONZALEZ, J. L., MOSER, J., LAURITZEN, M., SCHMITT-JOHN, T. & JENSEN, K. 2011. Reduced GABAergic inhibition explains cortical hyperexcitability in the wobbler mouse model of ALS. *Cereb Cortex,* 21**,** 625-35.
NIGRI, A., UMBERTO, M., STANZIANO, M., FERRARO, S., FEDELI, D., MEDINA CARRION, J. P., PALERMO, S., LEQUIO, L., DENEGRI, F., AGOSTA, F., FILIPPI, M., VALENTINI, M. C., CANOSA, A., CALVO, A., CHIO, A., BRUZZONE, M. G. & MOGLIA, C. 2023. C9orf72 ALS mutation carriers show extensive cortical and subcortical damage compared to matched wild-type ALS patients. *Neuroimage Clin,* 38**,** 103400.
NIHEI, K., MCKEE, A. C. & KOWALL, N. W. 1993. Patterns of neuronal degeneration in the motor cortex of amyotrophic lateral sclerosis patients. *Acta Neuropathol,* 86**,** 55-64.
NISHIDA, K., YOSHIMURA, M., ISOTANI, T., YOSHIDA, T., KITAURA, Y., SAITO, A., MII, H., KATO, M., TAKEKITA, Y., SUWA, A., MORITA, S. & KINOSHITA, T. 2011. Differences in quantitative EEG between frontotemporal dementia and Alzheimer's disease as revealed by LORETA. *Clin Neurophysiol,* 122**,** 1718-25.
NISHIMURA, A. L., ZUPUNSKI, V., TROAKES, C., KATHE, C., FRATTA, P., HOWELL, M., GALLO, J. M., HORTOBAGYI, T., SHAW, C. E. & ROGELJ, B. 2010. Nuclear import impairment causes cytoplasmic trans-activation response DNA-binding protein accumulation and is associated with frontotemporal lobar degeneration. *Brain,* 133**,** 1763-71.
O'DONOVAN, B., ADELUYI, A., ANDERSON, E. L., COLE, R. D., TURNER, J. R. & ORTINSKI, P. I. 2019. Altered gating of K(v)1.4 in the nucleus accumbens suppresses motivation for reward. *Elife,* 8.
O'LEARY, T., VAN ROSSUM, M. C. & WYLLIE, D. J. 2010. Homeostasis of intrinsic excitability in hippocampal neurones: dynamics and mechanism of the response to chronic depolarization. *J Physiol,* 588**,** 157-70.
OLNEY, N. T., SPINA, S. & MILLER, B. L. 2017. Frontotemporal Dementia. *Neurol Clin,* 35**,** 339-374.

ONYIKE, C. U. & DIEHL-SCHMID, J. 2013. The epidemiology of frontotemporal dementia. *Int Rev Psychiatry,* 25**,** 130-7.
PAGE, S. C., SRIPATHY, S. R., FARINELLI, F., YE, Z., WANG, Y., HILER, D. J., PATTIE, E. A., NGUYEN, C. V., TIPPANI, M., MOSES, R. L., CHEN, H. Y., TRAN, M. N., EAGLES, N. J., STOLZ, J. M., CATALLINI, J. L., 2ND, SOUDRY, O. R., DICKINSON, D., BERMAN, K. F., APUD, J. A., WEINBERGER, D. R., MARTINOWICH, K., JAFFE, A. E., STRAUB, R. E. & MAHER, B. J. 2022. Electrophysiological measures from human iPSC-derived neurons are associated with schizophrenia clinical status and predict individual cognitive performance. *Proc Natl Acad Sci U S A,* 119.
PALESE, F., BONOMI, E., NUZZO, T., BENUSSI, A., MELLONE, M., ZIANNI, E., CISANI, F., CASAMASSA, A., ALBERICI, A., SCHEGGIA, D., PADOVANI, A., MARCELLO, E., DI LUCA, M., PITTALUGA, A., USIELLO, A., BORRONI, B. & GARDONI, F. 2020. Anti-GluA3 antibodies in frontotemporal dementia: effects on glutamatergic neurotransmission and synaptic failure. *Neurobiol Aging,* 86**,** 143-155.
PALMINHA, N. M., DOS SANTOS SOUZA, C., GRIFFIN, J., LIAO, C., FERRAIUOLO, L. & EL-KHAMISY, S. F. 2022. Defective repair of topoisomerase I induced chromosomal damage in Huntington's disease. *Cell Mol Life Sci,* 79**,** 160.
PARASKEVOPOULOU, F., HERMAN, M. A. & ROSENMUND, C. 2019. Glutamatergic Innervation onto Striatal Neurons Potentiates GABAergic Synaptic Output. *J Neurosci,* 39**,** 4448-4460.
PAREKH, P. K., SIDOR, M. M., GILLMAN, A., BECKER-KRAIL, D., BETTELINI, L., ARBAN, R., ALVARO, G. S., ZAMBELLO, E., MUTINELLI, C., HUANG, Y., LARGE, C. H. & MCCLUNG, C. A. 2018. Antimanic Efficacy of a Novel Kv3 Potassium Channel Modulator. *Neuropsychopharmacology,* 43**,** 435-444.
PASNICEANU, I. S., ATWAL, M. S., SOUZA, C. D. S., FERRAIUOLO, L. & LIVESEY, M. R. 2021. Emerging Mechanisms Underpinning Neurophysiological Impairments in C9ORF72 Repeat Expansion-Mediated Amyotrophic Lateral Sclerosis/Frontotemporal Dementia. *Front Cell Neurosci,* 15**,** 784833.
PATTON, M. H., BIZUP, B. T. & GRACE, A. A. 2013. The infralimbic cortex bidirectionally modulates mesolimbic dopamine neuron activity via distinct neural pathways. *J Neurosci,* 33**,** 16865-73.
PAULI, W. M., O'REILLY, R. C., YARKONI, T. & WAGER, T. D. 2016. Regional specialization within the human striatum for diverse psychological functions. *Proc Natl Acad Sci U S A,* 113**,** 1907-12.
PAULSEN, J. S. 2011. Cognitive impairment in Huntington disease: diagnosis and treatment. *Curr Neurol Neurosci Rep,* 11**,** 474-83.
PEREIRA, J. D., DUBREUIL, D. M., DEVLIN, A. C., HELD, A., SAPIR, Y., BEREZOVSKI, E., HAWROT, J., DORFMAN, K., CHANDER, V. & WAINGER, B. J. 2021. Human sensorimotor organoids derived from healthy and amyotrophic lateral sclerosis stem cells form neuromuscular junctions. *Nat Commun,* 12**,** 4744.
PERKINS, E. M., BURR, K., BANERJEE, P., MEHTA, A. R., DANDO, O., SELVARAJ, B. T., SUMINAITE, D., NANDA, J., HENSTRIDGE, C. M., GILLINGWATER, T. H., HARDINGHAM, G. E., WYLLIE, D. J. A., CHANDRAN, S. & LIVESEY, M. R. 2021. Altered network properties in

C9ORF72 repeat expansion cortical neurons are due to synaptic dysfunction. *Mol Neurodegener,* 16**,** 13.
PERRY, D. C., STURM, V. E., SEELEY, W. W., MILLER, B. L., KRAMER, J. H. & ROSEN, H. J. 2014. Anatomical correlates of reward-seeking behaviours in behavioural variant frontotemporal dementia. *Brain,* 137**,** 1621-6.
PERRY, S., HAN, Y., DAS, A. & DICKMAN, D. 2017. Homeostatic plasticity can be induced and expressed to restore synaptic strength at neuromuscular junctions undergoing ALS-related degeneration. *Hum Mol Genet,* 26**,** 4153-4167.
PETKAU, T. L., NEAL, S. J., MILNERWOOD, A., MEW, A., HILL, A. M., ORBAN, P., GREGG, J., LU, G., FELDMAN, H. H., MACKENZIE, I. R., RAYMOND, L. A. & LEAVITT, B. R. 2012. Synaptic dysfunction in progranulin-deficient mice. *Neurobiol Dis,* 45**,** 711-22.
PETRI, S., KRAMPFL, K., HASHEMI, F., GROTHE, C., HORI, A., DENGLER, R. & BUFLER, J. 2003. Distribution of GABAA receptor mRNA in the motor cortex of ALS patients. *J Neuropathol Exp Neurol,* 62**,** 1041-51.
PETROV, D., MANSFIELD, C., MOUSSY, A. & HERMINE, O. 2017. ALS Clinical Trials Review: 20 Years of Failure. Are We Any Closer to Registering a New Treatment? *Front Aging Neurosci,* 9**,** 68.
PHELPS, E. A. & LEDOUX, J. E. 2005. Contributions of the amygdala to emotion processing: from animal models to human behavior. *Neuron,* 48**,** 175-87.
PICCOLINO, M. 1998. Animal electricity and the birth of electrophysiology: the legacy of Luigi Galvani. *Brain Res Bull,* 46**,** 381-407.
PICKLES, S., SEMMLER, S., BROOM, H. R., DESTROISMAISONS, L., LEGROUX, L., ARBOUR, N., MEIERING, E., CASHMAN, N. R. & VANDE VELDE, C. 2016. ALS-linked misfolded SOD1 species have divergent impacts on mitochondria. *Acta Neuropathol Commun,* 4**,** 43.
PIZZINO, G., IRRERA, N., CUCINOTTA, M., PALLIO, G., MANNINO, F., ARCORACI, V., SQUADRITO, F., ALTAVILLA, D. & BITTO, A. 2017. Oxidative Stress: Harms and Benefits for Human Health. *Oxid Med Cell Longev,* 2017**,** 8416763.
POLLARI, E., GOLDSTEINS, G., BART, G., KOISTINAHO, J. & GINIATULLIN, R. 2014. The role of oxidative stress in degeneration of the neuromuscular junction in amyotrophic lateral sclerosis. *Front Cell Neurosci,* 8**,** 131.
PORCELLO, D. M., HO, C. S., JOHO, R. H. & HUGUENARD, J. R. 2002. Resilient RTN fast spiking in Kv3.1 null mice suggests redundancy in the action potential repolarization mechanism. *J Neurophysiol,* 87**,** 1303-10.
PRADHAN, J. & BELLINGHAM, M. C. 2021. Neurophysiological Mechanisms Underlying Cortical Hyper-Excitability in Amyotrophic Lateral Sclerosis: A Review. *Brain Sci,* 11.
PRAGER, E. M. & PLOTKIN, J. L. 2019. Compartmental function and modulation of the striatum. *J Neurosci Res,* 97**,** 1503-1514.
PROUDFOOT, M., ROHENKOHL, G., QUINN, A., COLCLOUGH, G. L., WUU, J., TALBOT, K., WOOLRICH, M. W., BENATAR, M., NOBRE, A. C. & TURNER, M. R. 2017. Altered cortical beta-band oscillations reflect motor system degeneration in amyotrophic lateral sclerosis. *Hum Brain Mapp,* 38**,** 237-254.
PRUDENCIO, M., BELZIL, V. V., BATRA, R., ROSS, C. A., GENDRON, T. F., PREGENT, L. J., MURRAY, M. E., OVERSTREET, K. K., PIAZZA-JOHNSTON, A. E., DESARO, P., BIENIEK, K. F., DETURE, M., LEE, W. C., BIENDARRA, S. M., DAVIS, M. D., BAKER, M. C., PERKERSON, R. B., VAN

BLITTERSWIJK, M., STETLER, C. T., RADEMAKERS, R., LINK, C. D., DICKSON, D. W., BOYLAN, K. B., LI, H. & PETRUCELLI, L. 2015. Distinct brain transcriptome profiles in C9orf72-associated and sporadic ALS. *Nat Neurosci,* 18**,** 1175-82.

QUAEGEBEUR, A., GLARIA, I., LASHLEY, T. & ISAACS, A. M. 2020. Soluble and insoluble dipeptide repeat protein measurements in C9orf72-frontotemporal dementia brains show regional differential solubility and correlation of poly-GR with clinical severity. *Acta Neuropathol Commun,* 8**,** 184.

QUINLAN, K. A., SCHUSTER, J. E., FU, R., SIDDIQUE, T. & HECKMAN, C. J. 2011. Altered postnatal maturation of electrical properties in spinal motoneurons in a mouse model of amyotrophic lateral sclerosis. *J Physiol,* 589**,** 2245-60.

RADAKOVIC, R., PUTHUSSERYPPADY, V., FLANAGAN, E., KIERNAN, M. C., MIOSHI, E. & HORNBERGER, M. 2018. Frontostriatal grey matter atrophy in amyotrophic lateral sclerosis A visual rating study. *Dement Neuropsychol,* 12**,** 388-393.

RASCOVSKY, K., HODGES, J. R., KNOPMAN, D., MENDEZ, M. F., KRAMER, J. H., NEUHAUS, J., VAN SWIETEN, J. C., SEELAAR, H., DOPPER, E. G., ONYIKE, C. U., HILLIS, A. E., JOSEPHS, K. A., BOEVE, B. F., KERTESZ, A., SEELEY, W. W., RANKIN, K. P., JOHNSON, J. K., GORNO-TEMPINI, M. L., ROSEN, H., PRIOLEAU-LATHAM, C. E., LEE, A., KIPPS, C. M., LILLO, P., PIGUET, O., ROHRER, J. D., ROSSOR, M. N., WARREN, J. D., FOX, N. C., GALASKO, D., SALMON, D. P., BLACK, S. E., MESULAM, M., WEINTRAUB, S., DICKERSON, B. C., DIEHL-SCHMID, J., PASQUIER, F., DERAMECOURT, V., LEBERT, F., PIJNENBURG, Y., CHOW, T. W., MANES, F., GRAFMAN, J., CAPPA, S. F., FREEDMAN, M., GROSSMAN, M. & MILLER, B. L. 2011. Sensitivity of revised diagnostic criteria for the behavioural variant of frontotemporal dementia. *Brain,* 134**,** 2456-77.

RATNAVALLI, E., BRAYNE, C., DAWSON, K. & HODGES, J. R. 2002. The prevalence of frontotemporal dementia. *Neurology,* 58**,** 1615-21.

REALE, L. A., DYER, M. S., PERRY, S. E., YOUNG, K. M., DICKSON, T. C., WOODHOUSE, A. & BLIZZARD, C. A. 2023. Pathologically mislocalised TDP-43 in upper motor neurons causes a die-forward spread of ALS-like pathogenic changes throughout the mouse corticomotor system. *Prog Neurobiol,* 226**,** 102449.

REAUME, A. G., ELLIOTT, J. L., HOFFMAN, E. K., KOWALL, N. W., FERRANTE, R. J., SIWEK, D. F., WILCOX, H. M., FLOOD, D. G., BEAL, M. F., BROWN, R. H., JR., SCOTT, R. W. & SNIDER, W. D. 1996. Motor neurons in Cu/Zn superoxide dismutase-deficient mice develop normally but exhibit enhanced cell death after axonal injury. *Nat Genet,* 13**,** 43-7.

REINER, A. & DENG, Y. P. 2018. Disrupted striatal neuron inputs and outputs in Huntington's disease. *CNS Neurosci Ther,* 24**,** 250-280.

REINER, B. C., CHEHIMI, S. N., MERKEL, R., TOIKUMO, S., BERRETTINI, W. H., KRANZLER, H. R., SANCHEZ-ROIGE, S., KEMBER, R. L., SCHMIDT, H. D. & CRIST, R. C. 2024. A single-nucleus transcriptomic atlas of medium spiny neurons in the rat nucleus accumbens. *Sci Rep,* 14**,** 18258.

RENTON, A. E., CHIO, A. & TRAYNOR, B. J. 2014. State of play in amyotrophic lateral sclerosis genetics. *Nat Neurosci,* 17**,** 17-23.

RENTON, A. E., MAJOUNIE, E., WAITE, A., SIMON-SANCHEZ, J., ROLLINSON, S., GIBBS, J. R., SCHYMICK, J. C., LAAKSOVIRTA, H., VAN SWIETEN, J.

C., MYLLYKANGAS, L., KALIMO, H., PAETAU, A., ABRAMZON, Y., REMES, A. M., KAGANOVICH, A., SCHOLZ, S. W., DUCKWORTH, J., DING, J., HARMER, D. W., HERNANDEZ, D. G., JOHNSON, J. O., MOK, K., RYTEN, M., TRABZUNI, D., GUERREIRO, R. J., ORRELL, R. W., NEAL, J., MURRAY, A., PEARSON, J., JANSEN, I. E., SONDERVAN, D., SEELAAR, H., BLAKE, D., YOUNG, K., HALLIWELL, N., CALLISTER, J. B., TOULSON, G., RICHARDSON, A., GERHARD, A., SNOWDEN, J., MANN, D., NEARY, D., NALLS, M. A., PEURALINNA, T., JANSSON, L., ISOVIITA, V. M., KAIVORINNE, A. L., HOLTTA-VUORI, M., IKONEN, E., SULKAVA, R., BENATAR, M., WUU, J., CHIO, A., RESTAGNO, G., BORGHERO, G., SABATELLI, M., CONSORTIUM, I., HECKERMAN, D., ROGAEVA, E., ZINMAN, L., ROTHSTEIN, J. D., SENDTNER, M., DREPPER, C., EICHLER, E. E., ALKAN, C., ABDULLAEV, Z., PACK, S. D., DUTRA, A., PAK, E., HARDY, J., SINGLETON, A., WILLIAMS, N. M., HEUTINK, P., PICKERING-BROWN, S., MORRIS, H. R., TIENARI, P. J. & TRAYNOR, B. J. 2011. A hexanucleotide repeat expansion in C9ORF72 is the cause of chromosome 9p21-linked ALS-FTD. *Neuron,* 72**,** 257-68.

RIKU, Y., WATANABE, H., YOSHIDA, M., MIMURO, M., IWASAKI, Y., MASUDA, M., ISHIGAKI, S., KATSUNO, M. & SOBUE, G. 2016. Marked Involvement of the Striatal Efferent System in TAR DNA-Binding Protein 43 kDa-Related Frontotemporal Lobar Degeneration and Amyotrophic Lateral Sclerosis. *J Neuropathol Exp Neurol,* 75**,** 801-811.

RIKU, Y., WATANABE, H., YOSHIDA, M., MIMURO, M., IWASAKI, Y., MASUDA, M., ISHIGAKI, S., KATSUNO, M. & SOBUE, G. 2017. Pathologic Involvement of Glutamatergic Striatal Inputs From the Cortices in TAR DNA-Binding Protein 43 kDa-Related Frontotemporal Lobar Degeneration and Amyotrophic Lateral Sclerosis. *J Neuropathol Exp Neurol,* 76**,** 759-768.

RINGHOLZ, G. M., APPEL, S. H., BRADSHAW, M., COOKE, N. A., MOSNIK, D. M. & SCHULZ, P. E. 2005. Prevalence and patterns of cognitive impairment in sporadic ALS. *Neurology,* 65**,** 586-90.

RIZZU, P., BLAUWENDRAAT, C., HEETVELD, S., LYNES, E. M., CASTILLO-LIZARDO, M., DHINGRA, A., PYZ, E., HOBERT, M., SYNOFZIK, M., SIMON-SANCHEZ, J., FRANCESCATTO, M. & HEUTINK, P. 2016. C9orf72 is differentially expressed in the central nervous system and myeloid cells and consistently reduced in C9orf72, MAPT and GRN mutation carriers. *Acta Neuropathol Commun,* 4**,** 37.

ROHRER, J. D., NICHOLAS, J. M., CASH, D. M., VAN SWIETEN, J., DOPPER, E., JISKOOT, L., VAN MINKELEN, R., ROMBOUTS, S. A., CARDOSO, M. J., CLEGG, S., ESPAK, M., MEAD, S., THOMAS, D. L., DE VITA, E., MASELLIS, M., BLACK, S. E., FREEDMAN, M., KEREN, R., MACINTOSH, B. J., ROGAEVA, E., TANG-WAI, D., TARTAGLIA, M. C., LAFORCE, R., JR., TAGLIAVINI, F., TIRABOSCHI, P., REDAELLI, V., PRIONI, S., GRISOLI, M., BORRONI, B., PADOVANI, A., GALIMBERTI, D., SCARPINI, E., ARIGHI, A., FUMAGALLI, G., ROWE, J. B., COYLE-GILCHRIST, I., GRAFF, C., FALLSTROM, M., JELIC, V., STAHLBOM, A. K., ANDERSSON, C., THONBERG, H., LILIUS, L., FRISONI, G. B., PIEVANI, M., BOCCHETTA, M., BENUSSI, L., GHIDONI, R., FINGER, E., SORBI, S., NACMIAS, B., LOMBARDI, G., POLITO, C., WARREN, J. D., OURSELIN, S., FOX, N. C., ROSSOR, M. N. & BINETTI, G. 2015. Presymptomatic cognitive and neuroanatomical changes in genetic frontotemporal dementia in the Genetic

Frontotemporal dementia Initiative (GENFI) study: a cross-sectional analysis. *Lancet Neurol,* 14**,** 253-62.
ROSATO-SIRI, M. D., ZAMBELLO, E., MUTINELLI, C., GARBATI, N., BENEDETTI, R., ALDEGHERI, L., GRAZIANI, F., VIRGINIO, C., ALVARO, G. & LARGE, C. H. 2015. A Novel Modulator of Kv3 Potassium Channels Regulates the Firing of Parvalbumin-Positive Cortical Interneurons. *J Pharmacol Exp Ther,* 354**,** 251-60.
ROSEN, D. R., SIDDIQUE, T., PATTERSON, D., FIGLEWICZ, D. A., SAPP, P., HENTATI, A., DONALDSON, D., GOTO, J., O'REGAN, J. P., DENG, H. X. & ET AL. 1993. Mutations in Cu/Zn superoxide dismutase gene are associated with familial amyotrophic lateral sclerosis. *Nature,* 362**,** 59-62.
ROSENBLUM, L. T. & TROTTI, D. 2017. EAAT2 and the Molecular Signature of Amyotrophic Lateral Sclerosis. *Adv Neurobiol,* 16**,** 117-136.
ROSSINI, P. M., BURKE, D., CHEN, R., COHEN, L. G., DASKALAKIS, Z., DI IORIO, R., DI LAZZARO, V., FERRERI, F., FITZGERALD, P. B., GEORGE, M. S., HALLETT, M., LEFAUCHEUR, J. P., LANGGUTH, B., MATSUMOTO, H., MINIUSSI, C., NITSCHE, M. A., PASCUAL-LEONE, A., PAULUS, W., ROSSI, S., ROTHWELL, J. C., SIEBNER, H. R., UGAWA, Y., WALSH, V. & ZIEMANN, U. 2015. Non-invasive electrical and magnetic stimulation of the brain, spinal cord, roots and peripheral nerves: Basic principles and procedures for routine clinical and research application. An updated report from an I.F.C.N. Committee. *Clin Neurophysiol,* 126**,** 1071-1107.
ROTHSTEIN, J. D. 1995. Excitotoxic mechanisms in the pathogenesis of amyotrophic lateral sclerosis. *Adv Neurol,* 68**,** 7-20; discussion 21-7.
ROTHSTEIN, J. D., BASKERVILLE, V., RAPURI, S., MEHLHOP, E., JAFAR-NEJAD, P., RIGO, F., BENNETT, F., MIZIELINSKA, S., ISAACS, A. & COYNE, A. N. 2023. G(2)C(4) targeting antisense oligonucleotides potently mitigate TDP-43 dysfunction in human C9orf72 ALS/FTD induced pluripotent stem cell derived neurons. *Acta Neuropathol,* 147**,** 1.
ROTHSTEIN, J. D., MARTIN, L. J. & KUNCL, R. W. 1992. Decreased glutamate transport by the brain and spinal cord in amyotrophic lateral sclerosis. *N Engl J Med,* 326**,** 1464-8.
ROTHSTEIN, J. D., TSAI, G., KUNCL, R. W., CLAWSON, L., CORNBLATH, D. R., DRACHMAN, D. B., PESTRONK, A., STAUCH, B. L. & COYLE, J. T. 1990. Abnormal excitatory amino acid metabolism in amyotrophic lateral sclerosis. *Ann Neurol,* 28**,** 18-25.
ROWLAND, L. P. & SHNEIDER, N. A. 2001. Amyotrophic lateral sclerosis. *N Engl J Med,* 344**,** 1688-700.
RUDY, B., CHOW, A., LAU, D., AMARILLO, Y., OZAITA, A., SAGANICH, M., MORENO, H., NADAL, M. S., HERNANDEZ-PINEDA, R., HERNANDEZ-CRUZ, A., ERISIR, A., LEONARD, C. & VEGA-SAENZ DE MIERA, E. 1999. Contributions of Kv3 channels to neuronal excitability. *Ann N Y Acad Sci,* 868**,** 304-43.
RUDY, B. & MCBAIN, C. J. 2001. Kv3 channels: voltage-gated K+ channels designed for high-frequency repetitive firing. *Trends Neurosci,* 24**,** 517-26.
RYAN, M., HEVERIN, M., MCLAUGHLIN, R. L. & HARDIMAN, O. 2019. Lifetime Risk and Heritability of Amyotrophic Lateral Sclerosis. *JAMA Neurol,* 76**,** 1367-1374.
SABERI, S., STAUFFER, J. E., JIANG, J., GARCIA, S. D., TAYLOR, A. E., SCHULTE, D., OHKUBO, T., SCHLOFFMAN, C. L., MALDONADO, M.,

BAUGHN, M., RODRIGUEZ, M. J., PIZZO, D., CLEVELAND, D. & RAVITS, J. 2018. Sense-encoded poly-GR dipeptide repeat proteins correlate to neurodegeneration and uniquely co-localize with TDP-43 in dendrites of repeat-expanded C9orf72 amyotrophic lateral sclerosis. *Acta Neuropathol,* 135**,** 459-474.

SAEZ-ATIENZAR, S., SOUZA, C. D. S., CHIA, R., BEAL, S. N., LORENZINI, I., HUANG, R., LEVY, J., BURCIU, C., DING, J., GIBBS, J. R., JONES, A., DEWAN, R., PENSATO, V., PEVERELLI, S., CORRADO, L., VAN VUGT, J., VAN RHEENEN, W., TUNCA, C., BAYRAKTAR, E., XIA, M., INTERNATIONAL, A. L. S. G. C., CONSORTIUM, I., CONSORTIUM, S., PROJECT MIN, E. A. L. S. S. C., IACOANGELI, A., SHATUNOV, A., TILOCA, C., TICOZZI, N., VERDE, F., MAZZINI, L., KENNA, K., AL KHLEIFAT, A., OPIE-MARTIN, S., RAGGI, F., FILOSTO, M., PICCINELLI, S. C., PADOVANI, A., GAGLIARDI, S., INGHILLERI, M., FERLINI, A., VASTA, R., CALVO, A., MOGLIA, C., CANOSA, A., MANERA, U., GRASSANO, M., MANDRIOLI, J., MORA, G., LUNETTA, C., TANEL, R., TROJSI, F., CARDINALI, P., GALLONE, S., BRUNETTI, M., GALIMBERTI, D., SERPENTE, M., FENOGLIO, C., SCARPINI, E., COMI, G. P., CORTI, S., DEL BO, R., CERONI, M., PINTER, G. L., TARONI, F., BELLA, E. D., BERSANO, E., CURTIS, C. J., LEE, S. H., CHUNG, R., PATEL, H., MORRISON, K. E., COOPER-KNOCK, J., SHAW, P. J., BREEN, G., DOBSON, R. J. B., DALGARD, C. L., AMERICAN GENOME, C., SCHOLZ, S. W., AL-CHALABI, A., VAN DEN BERG, L. H., MCLAUGHLIN, R., HARDIMAN, O., CEREDA, C., SORARU, G., D'ALFONSO, S., CHANDRAN, S., PAL, S., RATTI, A., GELLERA, C., JOHNSON, K., DOUCET-O'HARE, T., PASTERNACK, N., WANG, T., NATH, A., SICILIANO, G., SILANI, V., BASAK, A. N., VELDINK, J. H., CAMU, W., GLASS, J. D., et al. 2024. Mechanism-free repurposing of drugs for C9orf72-related ALS/FTD using large-scale genomic data. *Cell Genom,* 4**,** 100679.

SAHADEVAN, S., HEMBACH, K. M., TANTARDINI, E., PEREZ-BERLANGA, M., HRUSKA-PLOCHAN, M., MEGAT, S., WEBER, J., SCHWARZ, P., DUPUIS, L., ROBINSON, M. D., DE ROSSI, P. & POLYMENIDOU, M. 2021. Synaptic FUS accumulation triggers early misregulation of synaptic RNAs in a mouse model of ALS. *Nat Commun,* 12**,** 3027.

SAINI, A. & CHAWLA, P. A. 2024. Breaking barriers with tofersen: Enhancing therapeutic opportunities in amyotrophic lateral sclerosis. *Eur J Neurol,* 31**,** e16140.

SAKAE, N., BIENIEK, K. F., ZHANG, Y. J., ROSS, K., GENDRON, T. F., MURRAY, M. E., RADEMAKERS, R., PETRUCELLI, L. & DICKSON, D. W. 2018. Poly-GR dipeptide repeat polymers correlate with neurodegeneration and Clinicopathological subtypes in C9ORF72-related brain disease. *Acta Neuropathol Commun,* 6**,** 63.

SALMON, E., BAHRI, M. A., PLENEVAUX, A., BECKER, G., SERET, A., DELHAYE, E., DEGUELDRE, C., BALTEAU, E., LEMAIRE, C., LUXEN, A. & BASTIN, C. 2021. In vivo exploration of synaptic projections in frontotemporal dementia. *Sci Rep,* 11**,** 16092.

SALZINGER, A., RAMESH, V., DAS SHARMA, S., CHANDRAN, S. & THANGARAJ SELVARAJ, B. 2024. Neuronal Circuit Dysfunction in Amyotrophic Lateral Sclerosis. *Cells,* 13.

SANCES, S., BRUIJN, L. I., CHANDRAN, S., EGGAN, K., HO, R., KLIM, J. R., LIVESEY, M. R., LOWRY, E., MACKLIS, J. D., RUSHTON, D., SADEGH, C., SAREEN, D., WICHTERLE, H., ZHANG, S. C. & SVENDSEN, C. N. 2016. Modeling ALS with motor neurons derived from human induced pluripotent stem cells. *Nat Neurosci,* 19**,** 542-53.

SARAC, H., ZAGAR, M., VRANJES, D., HENIGSBERG, N., BILIC, E. & PAVLISA, G. 2008. Magnetic resonance imaging and magnetic resonance spectroscopy in a patient with amyotrophic lateral sclerosis and frontotemporal dementia. *Coll Antropol,* 32 Suppl 1**,** 205-10.

SAREEN, D., O'ROURKE, J. G., MEERA, P., MUHAMMAD, A. K., GRANT, S., SIMPKINSON, M., BELL, S., CARMONA, S., ORNELAS, L., SAHABIAN, A., GENDRON, T., PETRUCELLI, L., BAUGHN, M., RAVITS, J., HARMS, M. B., RIGO, F., BENNETT, C. F., OTIS, T. S., SVENDSEN, C. N. & BALOH, R. H. 2013. Targeting RNA foci in iPSC-derived motor neurons from ALS patients with a C9ORF72 repeat expansion. *Sci Transl Med,* 5**,** 208ra149.

SASAKI, S. & MARUYAMA, S. 1992. Increase in diameter of the axonal initial segment is an early change in amyotrophic lateral sclerosis. *J Neurol Sci,* 110**,** 114-20.

SATTLER, R., TRAYNOR, B. J., ROBERTSON, J., VAN DEN BOSCH, L., BARMADA, S. J., SVENDSEN, C. N., DISNEY, M. D., GENDRON, T. F., WONG, P. C., TURNER, M. R., BOXER, A., BABU, S., BENATAR, M., KURNELLAS, M., ROHRER, J. D., DONNELLY, C. J., BUSTOS, L. M., VAN KEUREN-JENSEN, K., DACKS, P. A., SABBAGH, M. N. & ATTENDEES OF THE INAUGURAL, C. O. R. F. F. T. D. A. L. S. S. 2023. Roadmap for C9ORF72 in Frontotemporal Dementia and Amyotrophic Lateral Sclerosis: Report on the C9ORF72 FTD/ALS Summit. *Neurol Ther,* 12**,** 1821-1843.

SCEKIC-ZAHIROVIC, J., SANJUAN-RUIZ, I., KAN, V., MEGAT, S., DE ROSSI, P., DIETERLE, S., CASSEL, R., JAMET, M., KESSLER, P., WIESNER, D., TZEPLAEFF, L., DEMAIS, V., SAHADEVAN, S., HEMBACH, K. M., MULLER, H. P., PICCHIARELLI, G., MISHRA, N., ANTONUCCI, S., DIRRIG-GROSCH, S., KASSUBEK, J., RASCHE, V., LUDOLPH, A., BOUTILLIER, A. L., ROSELLI, F., POLYMENIDOU, M., LAGIER-TOURENNE, C., LIEBSCHER, S. & DUPUIS, L. 2021. Cytoplasmic FUS triggers early behavioral alterations linked to cortical neuronal hyperactivity and inhibitory synaptic defects. *Nat Commun,* 12**,** 3028.

SCHANZ, O., BAGEAC, D., BRAUN, L., TRAYNOR, B. J., LEHKY, T. J. & FLOETER, M. K. 2016. Cortical hyperexcitability in patients with C9ORF72 mutations: Relationship to phenotype. *Muscle Nerve,* 54**,** 264-9.

SCHMIDT-HIEBER, C., JONAS, P. & BISCHOFBERGER, J. 2004. Enhanced synaptic plasticity in newly generated granule cells of the adult hippocampus. *Nature,* 429**,** 184-7.

SCOTT, R. S., HENNEBERGER, C., PADMASHRI, R., ANDERS, S., JENSEN, T. P. & RUSAKOV, D. A. 2014. Neuronal adaptation involves rapid expansion of the action potential initiation site. *Nat Commun,* 5**,** 3817.

SEELAAR, H., KLIJNSMA, K. Y., DE KONING, I., VAN DER LUGT, A., CHIU, W. Z., AZMANI, A., ROZEMULLER, A. J. & VAN SWIETEN, J. C. 2010. Frequency of ubiquitin and FUS-positive, TDP-43-negative frontotemporal lobar degeneration. *J Neurol,* 257**,** 747-53.

SEELEY, W. W. 2019. The Salience Network: A Neural System for Perceiving and Responding to Homeostatic Demands. *J Neurosci,* 39**,** 9878-9882.

SEELEY, W. W., CRAWFORD, R., RASCOVSKY, K., KRAMER, J. H., WEINER, M., MILLER, B. L. & GORNO-TEMPINI, M. L. 2008. Frontal paralimbic network atrophy in very mild behavioral variant frontotemporal dementia. *Arch Neurol,* 65**,** 249-55.

SELLIER, C., CORCIA, P., VOURC'H, P. & DUPUIS, L. 2024. C9ORF72 hexanucleotide repeat expansion: From ALS and FTD to a broader pathogenic role? *Rev Neurol (Paris),* 180**,** 417-428.

SELVARAJ, B. T., LIVESEY, M. R., ZHAO, C., GREGORY, J. M., JAMES, O. T., CLEARY, E. M., CHOUHAN, A. K., GANE, A. B., PERKINS, E. M., DANDO, O., LILLICO, S. G., LEE, Y. B., NISHIMURA, A. L., PORECI, U., THANKAMONY, S., PRAY, M., VASISTHA, N. A., MAGNANI, D., BOROOAH, S., BURR, K., STORY, D., MCCAMPBELL, A., SHAW, C. E., KIND, P. C., AITMAN, T. J., WHITELAW, C. B. A., WILMUT, I., SMITH, C., MILES, G. B., HARDINGHAM, G. E., WYLLIE, D. J. A. & CHANDRAN, S. 2018. C9ORF72 repeat expansion causes vulnerability of motor neurons to Ca(2+)-permeable AMPA receptor-mediated excitotoxicity. *Nat Commun,* 9**,** 347.

SEPHTON, C. F., TANG, A. A., KULKARNI, A., WEST, J., BROOKS, M., STUBBLEFIELD, J. J., LIU, Y., ZHANG, M. Q., GREEN, C. B., HUBER, K. M., HUANG, E. J., HERZ, J. & YU, G. 2014. Activity-dependent FUS dysregulation disrupts synaptic homeostasis. *Proc Natl Acad Sci U S A,* 111**,** E4769-78.

SHAH, M. M., MIGLIORE, M., VALENCIA, I., COOPER, E. C. & BROWN, D. A. 2008. Functional significance of axonal Kv7 channels in hippocampal pyramidal neurons. *Proc Natl Acad Sci U S A,* 105**,** 7869-74.

SHARPE, J. L., HARPER, N. S., GARNER, D. R. & WEST, R. J. H. 2021. Modeling C9orf72-Related Frontotemporal Dementia and Amyotrophic Lateral Sclerosis in Drosophila. *Front Cell Neurosci,* 15**,** 770937.

SHAW, P. J. 2005. Molecular and cellular pathways of neurodegeneration in motor neurone disease. *J Neurol Neurosurg Psychiatry,* 76**,** 1046-57.

SHAW, P. J., INCE, P. G., FALKOUS, G. & MANTLE, D. 1995. Oxidative damage to protein in sporadic motor neuron disease spinal cord. *Ann Neurol,* 38**,** 691-5.

SHEFNER, J. M., AL-CHALABI, A., BAKER, M. R., CUI, L. Y., DE CARVALHO, M., EISEN, A., GROSSKREUTZ, J., HARDIMAN, O., HENDERSON, R., MATAMALA, J. M., MITSUMOTO, H., PAULUS, W., SIMON, N., SWASH, M., TALBOT, K., TURNER, M. R., UGAWA, Y., VAN DEN BERG, L. H., VERDUGO, R., VUCIC, S., KAJI, R., BURKE, D. & KIERNAN, M. C. 2020. A proposal for new diagnostic criteria for ALS. *Clin Neurophysiol,* 131**,** 1975-1978.

SHEPHEARD, S. R., PARKER, M. D., COOPER-KNOCK, J., VERBER, N. S., TUDDENHAM, L., HEATH, P., BEAUCHAMP, N., PLACE, E., SOLLARS, E. S. A., TURNER, M. R., MALASPINA, A., FRATTA, P., HEWAMADDUMA, C., JENKINS, T. M., MCDERMOTT, C. J., WANG, D., KIRBY, J., SHAW, P. J., PROJECT, M. C. & PROJECT MIN, E. 2021. Value of systematic genetic screening of patients with amyotrophic lateral sclerosis. *J Neurol Neurosurg Psychiatry,* 92**,** 510-518.

SHI, Y., LIN, S., STAATS, K. A., LI, Y., CHANG, W. H., HUNG, S. T., HENDRICKS, E., LINARES, G. R., WANG, Y., SON, E. Y., WEN, X., KISLER, K., WILKINSON, B., MENENDEZ, L., SUGAWARA, T., WOOLWINE, P., HUANG, M., COWAN, M. J., GE, B., KOUTSODENDRIS, N., SANDOR, K. P., KOMBERG, J., VANGOOR, V. R., SENTHILKUMAR, K., HENNES, V., SEAH,

C., NELSON, A. R., CHENG, T. Y., LEE, S. J., AUGUST, P. R., CHEN, J. A., WISNIEWSKI, N., HANSON-SMITH, V., BELGARD, T. G., ZHANG, A., COBA, M., GRUNSEICH, C., WARD, M. E., VAN DEN BERG, L. H., PASTERKAMP, R. J., TROTTI, D., ZLOKOVIC, B. V. & ICHIDA, J. K. 2018. Haploinsufficiency leads to neurodegeneration in C9ORF72 ALS/FTD human induced motor neurons. *Nat Med,* 24**,** 313-325.

SHIBUYA, K., MISAWA, S., ARAI, K., NAKATA, M., KANAI, K., YOSHIYAMA, Y., ITO, K., ISOSE, S., NOTO, Y., NASU, S., SEKIGUCHI, Y., FUJIMAKI, Y., OHMORI, S., KITAMURA, H., SATO, Y. & KUWABARA, S. 2011. Markedly reduced axonal potassium channel expression in human sporadic amyotrophic lateral sclerosis: an immunohistochemical study. *Exp Neurol,* 232**,** 149-53.

SHIBUYA, K., PARK, S. B., GEEVASINGA, N., MENON, P., HOWELLS, J., SIMON, N. G., HUYNH, W., NOTO, Y., GOTZ, J., KRIL, J. J., ITTNER, L. M., HODGES, J., HALLIDAY, G., VUCIC, S. & KIERNAN, M. C. 2016. Motor cortical function determines prognosis in sporadic ALS. *Neurology,* 87**,** 513-20.

SHIMIZU, T., FUJIMAKI, Y., NAKATANI-ENOMOTO, S., MATSUBARA, S., WATABE, K., ROSSINI, P. M. & UGAWA, Y. 2014. Complex fasciculation potentials and survival in amyotrophic lateral sclerosis. *Clin Neurophysiol,* 125**,** 1059-64.

SHIMOJO, M., TAKUWA, H., TAKADO, Y., TOKUNAGA, M., TSUKAMOTO, S., MINATOHARA, K., ONO, M., SEKI, C., MAEDA, J., URUSHIHATA, T., MINAMIHISAMATSU, T., AOKI, I., KAWAMURA, K., ZHANG, M. R., SUHARA, T., SAHARA, N. & HIGUCHI, M. 2020. Selective Disruption of Inhibitory Synapses Leading to Neuronal Hyperexcitability at an Early Stage of Tau Pathogenesis in a Mouse Model. *J Neurosci,* 40**,** 3491-3501.

SIGWORTH, F. J. & NEHER, E. 1980. Single Na+ channel currents observed in cultured rat muscle cells. *Nature,* 287**,** 447-9.

SIRKIS, D. W., GEIER, E. G., BONHAM, L. W., KARCH, C. M. & YOKOYAMA, J. S. 2019. Recent advances in the genetics of frontotemporal dementia. *Curr Genet Med Rep,* 7**,** 41-52.

SMEELE, P. H., CESARE, G. & VACCARI, T. 2024. ALS' Perfect Storm: C9orf72-Associated Toxic Dipeptide Repeats as Potential Multipotent Disruptors of Protein Homeostasis. *Cells,* 13.

SMEYERS, J., BANCHI, E. G. & LATOUCHE, M. 2021. C9ORF72: What It Is, What It Does, and Why It Matters. *Front Cell Neurosci,* 15**,** 661447.

SMITH, R. A., MILLER, T. M., YAMANAKA, K., MONIA, B. P., CONDON, T. P., HUNG, G., LOBSIGER, C. S., WARD, C. M., MCALONIS-DOWNES, M., WEI, H., WANCEWICZ, E. V., BENNETT, C. F. & CLEVELAND, D. W. 2006. Antisense oligonucleotide therapy for neurodegenerative disease. *J Clin Invest,* 116**,** 2290-6.

SODERSTROM, K. E., O'MALLEY, J. A., LEVINE, N. D., SORTWELL, C. E., COLLIER, T. J. & STEECE-COLLIER, K. 2010. Impact of dendritic spine preservation in medium spiny neurons on dopamine graft efficacy and the expression of dyskinesias in parkinsonian rats. *Eur J Neurosci,* 31**,** 478-90.

SOHN, P. D., HUANG, C. T., YAN, R., FAN, L., TRACY, T. E., CAMARGO, C. M., MONTGOMERY, K. M., ARHAR, T., MOK, S. A., FREILICH, R., BAIK, J., HE, M., GONG, S., ROBERSON, E. D., KARCH, C. M., GESTWICKI, J. E., XU,

K., KOSIK, K. S. & GAN, L. 2019. Pathogenic Tau Impairs Axon Initial Segment Plasticity and Excitability Homeostasis. *Neuron,* 104**,** 458-470 e5.
SOLOMON, D. A., STEPTO, A., AU, W. H., ADACHI, Y., DIAPER, D. C., HALL, R., REKHI, A., BOUDI, A., TZIORTZOUDA, P., LEE, Y. B., SMITH, B., BRIDI, J. C., SPINELLI, G., DEARLOVE, J., HUMPHREY, D. M., GALLO, J. M., TROAKES, C., FANTO, M., SOLLER, M., ROGELJ, B., PARSONS, R. B., SHAW, C. E., HORTOBAGYI, T. & HIRTH, F. 2018. A feedback loop between dipeptide-repeat protein, TDP-43 and karyopherin-alpha mediates C9orf72-related neurodegeneration. *Brain,* 141**,** 2908-2924.
SOMMER, D., RAJKUMAR, S., SEIDEL, M., ALY, A., LUDOLPH, A., HO, R., BOECKERS, T. M. & CATANESE, A. 2022. Aging-Dependent Altered Transcriptional Programs Underlie Activity Impairments in Human C9orf72-Mutant Motor Neurons. *Front Mol Neurosci,* 15**,** 894230.
SOSA-ORTIZ, A. L., ACOSTA-CASTILLO, I. & PRINCE, M. J. 2012. Epidemiology of dementias and Alzheimer's disease. *Arch Med Res,* 43**,** 600-8.
SPALLONI, A., ORIGLIA, N., SGOBIO, C., TRABALZA, A., NUTINI, M., BERRETTA, N., BERNARDI, G., DOMENICI, L., AMMASSARI-TEULE, M. & LONGONE, P. 2011. Postsynaptic alteration of NR2A subunit and defective autophosphorylation of alphaCaMKII at threonine-286 contribute to abnormal plasticity and morphology of upper motor neurons in presymptomatic SOD1G93A mice, a murine model for amyotrophic lateral sclerosis. *Cereb Cortex,* 21**,** 796-805.
SREEDHARAN, J., BLAIR, I. P., TRIPATHI, V. B., HU, X., VANCE, C., ROGELJ, B., ACKERLEY, S., DURNALL, J. C., WILLIAMS, K. L., BURATTI, E., BARALLE, F., DE BELLEROCHE, J., MITCHELL, J. D., LEIGH, P. N., AL-CHALABI, A., MILLER, C. C., NICHOLSON, G. & SHAW, C. E. 2008. TDP-43 mutations in familial and sporadic amyotrophic lateral sclerosis. *Science,* 319**,** 1668-72.
STANFIELD, P. R. 1973. The onset of the effects of zinc and tetraethylammonium ions on action potential duration and twitch amplitude of single muscle fibres. *J Physiol,* 235**,** 639-54.
STANFORD, P. M., BROOKS, W. S., TEBER, E. T., HALLUPP, M., MCLEAN, C., HALLIDAY, G. M., MARTINS, R. N., KWOK, J. B. & SCHOFIELD, P. R. 2004. Frequency of tau mutations in familial and sporadic frontotemporal dementia and other tauopathies. *J Neurol,* 251**,** 1098-104.
STANSLOWSKY, N., REINHARDT, P., GLASS, H., KALMBACH, N., NAUJOCK, M., HENSEL, N., LUBBEN, V., PAL, A., VENNERI, A., LUPO, F., DE FRANCESCHI, L., CLAUS, P., STERNECKERT, J., STORCH, A., HERMANN, A. & WEGNER, F. 2016. Neuronal Dysfunction in iPSC-Derived Medium Spiny Neurons from Chorea-Acanthocytosis Patients Is Reversed by Src Kinase Inhibition and F-Actin Stabilization. *J Neurosci,* 36**,** 12027-12043.
STARR, A. & SATTLER, R. 2018. Synaptic dysfunction and altered excitability in C9ORF72 ALS/FTD. *Brain Res,* 1693**,** 98-108.
STROPPOLO, A., GUINEA, B., TIAN, C., SOMMER, J. & EHRLICH, M. E. 2001. Role of phosphatidylinositide 3-kinase in brain-derived neurotrophic factor-induced DARPP-32 expression in medium size spiny neurons in vitro. *J Neurochem,* 79**,** 1027-32.
STYR, B. & SLUTSKY, I. 2018. Imbalance between firing homeostasis and synaptic plasticity drives early-phase Alzheimer's disease. *Nat Neurosci,* 21**,** 463-473.
SU, Z., ZHANG, Y., GENDRON, T. F., BAUER, P. O., CHEW, J., YANG, W. Y., FOSTVEDT, E., JANSEN-WEST, K., BELZIL, V. V., DESARO, P.,

JOHNSTON, A., OVERSTREET, K., OH, S. Y., TODD, P. K., BERRY, J. D., CUDKOWICZ, M. E., BOEVE, B. F., DICKSON, D., FLOETER, M. K., TRAYNOR, B. J., MORELLI, C., RATTI, A., SILANI, V., RADEMAKERS, R., BROWN, R. H., ROTHSTEIN, J. D., BOYLAN, K. B., PETRUCELLI, L. & DISNEY, M. D. 2014. Discovery of a biomarker and lead small molecules to target r(GGGGCC)-associated defects in c9FTD/ALS. *Neuron,* 83**,** 1043-50.

SUDRIA-LOPEZ, E., KOPPERS, M., DE WIT, M., VAN DER MEER, C., WESTENENG, H. J., ZUNDEL, C. A., YOUSSEF, S. A., HARKEMA, L., DE BRUIN, A., VELDINK, J. H., VAN DEN BERG, L. H. & PASTERKAMP, R. J. 2016. Full ablation of C9orf72 in mice causes immune system-related pathology and neoplastic events but no motor neuron defects. *Acta Neuropathol,* 132**,** 145-7.

SWAMINATHAN, A., BOUFFARD, M., LIAO, M., RYAN, S., CALLISTER, J. B., PICKERING-BROWN, S. M., ARMSTRONG, G. A. B. & DRAPEAU, P. 2018. Expression of C9orf72-related dipeptides impairs motor function in a vertebrate model. *Hum Mol Genet,* 27**,** 1754-1762.

SWINNEN, B., BENTO-ABREU, A., GENDRON, T. F., BOEYNAEMS, S., BOGAERT, E., NUYTS, R., TIMMERS, M., SCHEVENEELS, W., HERSMUS, N., WANG, J., MIZIELINSKA, S., ISAACS, A. M., PETRUCELLI, L., LEMMENS, R., VAN DAMME, P., VAN DEN BOSCH, L. & ROBBERECHT, W. 2018. A zebrafish model for C9orf72 ALS reveals RNA toxicity as a pathogenic mechanism. *Acta Neuropathol,* 135**,** 427-443.

TAE, W. S., SUNG, J. H., BAEK, S. H., LEE, C. N. & KIM, B. J. 2020. Shape Analysis of the Subcortical Nuclei in Amyotrophic Lateral Sclerosis without Cognitive Impairment. *J Clin Neurol,* 16**,** 592-598.

TAKAHASHI, K., TANABE, K., OHNUKI, M., NARITA, M., ICHISAKA, T., TOMODA, K. & YAMANAKA, S. 2007. Induction of pluripotent stem cells from adult human fibroblasts by defined factors. *Cell,* 131**,** 861-72.

TAKAHASHI, K. & YAMANAKA, S. 2006. Induction of pluripotent stem cells from mouse embryonic and adult fibroblast cultures by defined factors. *Cell,* 126**,** 663-76.

TAM, R. W. & KEUNG, A. J. 2022. Human Pluripotent Stem Cell-Derived Medium Spiny Neuron-like Cells Exhibit Gene Desensitization. *Cells,* 11.

TAO, Z., WANG, H., XIA, Q., LI, K., LI, K., JIANG, X., XU, G., WANG, G. & YING, Z. 2015. Nucleolar stress and impaired stress granule formation contribute to C9orf72 RAN translation-induced cytotoxicity. *Hum Mol Genet,* 24**,** 2426-41.

TAYLOR, J. P., BROWN, R. H., JR. & CLEVELAND, D. W. 2016. Decoding ALS: from genes to mechanism. *Nature,* 539**,** 197-206.

TEPPER, J. M., KOOS, T. & WILSON, C. J. 2004. GABAergic microcircuits in the neostriatum. *Trends Neurosci,* 27**,** 662-9.

THERRIEN, M., ROULEAU, G. A., DION, P. A. & PARKER, J. A. 2013. Deletion of C9ORF72 results in motor neuron degeneration and stress sensitivity in C. elegans. *PLoS One,* 8**,** e83450.

THOMSON, J. A., ITSKOVITZ-ELDOR, J., SHAPIRO, S. S., WAKNITZ, M. A., SWIERGIEL, J. J., MARSHALL, V. S. & JONES, J. M. 1998. Embryonic stem cell lines derived from human blastocysts. *Science,* 282**,** 1145-7.

TILL, J. E. & MC, C. E. 1961. A direct measurement of the radiation sensitivity of normal mouse bone marrow cells. *Radiat Res,* 14**,** 213-22.

TIMMINS, H. C., VUCIC, S. & KIERNAN, M. C. 2023. Cortical hyperexcitability in amyotrophic lateral sclerosis: from pathogenesis to diagnosis. *Curr Opin Neurol,* 36**,** 353-359.
TORTAROLO, M., GRIGNASCHI, G., CALVARESI, N., ZENNARO, E., SPALTRO, G., COLOVIC, M., FRACASSO, C., GUISO, G., ELGER, B., SCHNEIDER, H., SEILHEIMER, B., CACCIA, S. & BENDOTTI, C. 2006. Glutamate AMPA receptors change in motor neurons of SOD1G93A transgenic mice and their inhibition by a noncompetitive antagonist ameliorates the progression of amytrophic lateral sclerosis-like disease. *J Neurosci Res,* 83**,** 134-46.
TRABJERG, B. B., GARTON, F. C., VAN RHEENEN, W., FANG, F., HENDERSON, R. D., MORTENSEN, P. B., AGERBO, E. & WRAY, N. R. 2020. ALS in Danish Registries: Heritability and links to psychiatric and cardiovascular disorders. *Neurol Genet,* 6**,** e398.
TRAN, H., ALMEIDA, S., MOORE, J., GENDRON, T. F., CHALASANI, U., LU, Y., DU, X., NICKERSON, J. A., PETRUCELLI, L., WENG, Z. & GAO, F. B. 2015. Differential Toxicity of Nuclear RNA Foci versus Dipeptide Repeat Proteins in a Drosophila Model of C9ORF72 FTD/ALS. *Neuron,* 87**,** 1207-1214.
TRITSCH, N. X. & SABATINI, B. L. 2012. Dopaminergic modulation of synaptic transmission in cortex and striatum. *Neuron,* 76**,** 33-50.
TROAKES, C., MAEKAWA, S., WIJESEKERA, L., ROGELJ, B., SIKLOS, L., BELL, C., SMITH, B., NEWHOUSE, S., VANCE, C., JOHNSON, L., HORTOBAGYI, T., SHATUNOV, A., AL-CHALABI, A., LEIGH, N., SHAW, C. E., KING, A. & AL-SARRAJ, S. 2012. An MND/ALS phenotype associated with C9orf72 repeat expansion: abundant p62-positive, TDP-43-negative inclusions in cerebral cortex, hippocampus and cerebellum but without associated cognitive decline. *Neuropathology,* 32**,** 505-14.
TRUBSHAW, M., GOHIL, C., YOGANATHAN, K., KOHL, O., EDMOND, E., PROUDFOOT, M., THOMPSON, A. G., TALBOT, K., STAGG, C. J., NOBRE, A. C., WOOLRICH, M. & TURNER, M. R. 2024. The cortical neurophysiological signature of amyotrophic lateral sclerosis. *Brain Commun,* 6**,** fcae164.
TSHILENGE, K. T., AGUIRRE, C. G., BONS, J., GERENCSER, A. A., BASISTY, N., SONG, S., ROSE, J., LOPEZ-RAMIREZ, A., NAPHADE, S., LOUREIRO, A., BATTISTONI, E., MILANI, M., WEHRFRITZ, C., HOLTZ, A., HETZ, C., MOONEY, S. D., SCHILLING, B. & ELLERBY, L. M. 2023. Proteomic Analysis of Huntington's Disease Medium Spiny Neurons Identifies Alterations in Lipid Droplets. *Mol Cell Proteomics,* 22**,** 100534.
TU, W. Y., XU, W., ZHANG, J., QI, S., BAI, L., SHEN, C. & ZHANG, K. 2023. C9orf72 poly-GA proteins impair neuromuscular transmission. *Zool Res,* 44**,** 331-340.
TUNSTALL, M. J., OORSCHOT, D. E., KEAN, A. & WICKENS, J. R. 2002. Inhibitory interactions between spiny projection neurons in the rat striatum. *J Neurophysiol,* 88**,** 1263-9.
TURNER, B. J., BAUMER, D., PARKINSON, N. J., SCABER, J., ANSORGE, O. & TALBOT, K. 2008. TDP-43 expression in mouse models of amyotrophic lateral sclerosis and spinal muscular atrophy. *BMC Neurosci,* 9**,** 104.
TURNER, M. R., BOWSER, R., BRUIJN, L., DUPUIS, L., LUDOLPH, A., MCGRATH, M., MANFREDI, G., MARAGAKIS, N., MILLER, R. G., PULLMAN, S. L., RUTKOVE, S. B., SHAW, P. J., SHEFNER, J. & FISCHBECK, K. H. 2013. Mechanisms, models and biomarkers in

amyotrophic lateral sclerosis. *Amyotroph Lateral Scler Frontotemporal Degener,* 14 Suppl 1**,** 19-32.
TZIORTZOUDA, P., VAN DEN BOSCH, L. & HIRTH, F. 2021. Triad of TDP43 control in neurodegeneration: autoregulation, localization and aggregation. *Nat Rev Neurosci,* 22**,** 197-208.
UDAGAWA, T., FUJIOKA, Y., TANAKA, M., HONDA, D., YOKOI, S., RIKU, Y., IBI, D., NAGAI, T., YAMADA, K., WATANABE, H., KATSUNO, M., INADA, T., OHNO, K., SOKABE, M., OKADO, H., ISHIGAKI, S. & SOBUE, G. 2015. FUS regulates AMPA receptor function and FTLD/ALS-associated behaviour via GluA1 mRNA stabilization. *Nat Commun,* 6**,** 7098.
UPADHYAY, N., SPOTTKE, A., SCHNEIDER, A., HOFFMANN, D. C., FROMMANN, I., BALLARINI, T., FLIESSBACH, K., BENDER, B., HEEKEREN, H. R., HAYNES, J. D., EWERS, M., DUZEL, E., GLANZ, W., DOBISCH, L., BUERGER, K., JANOWITZ, D., LEVIN, J., DANEK, A., TEIPEL, S., KILIMANN, I., SYNOFZIK, M., WILKE, C., PETERS, O., PREIS, L., PRILLER, J., SPRUTH, E. J., JESSEN, F. & BOECKER, H. 2024. Fronto-striatal alterations correlate with apathy severity in behavioral variant frontotemporal dementia. *Brain Imaging Behav,* 18**,** 66-72.
VAN DEN BERG, L. H., ROTHSTEIN, J. D., SHAW, P. J., BABU, S., BENATAR, M., BUCELLI, R. C., GENGE, A., GLASS, J. D., HARDIMAN, O., LIBRI, V., MOBACH, T., OSKARSSON, B., PATTEE, G. L., RAVITS, J., SHAW, C. E., WEBER, M., ZINMAN, L., JAFAR-NEJAD, P., RIGO, F., LIN, L., FERGUSON, T. A., GOTTER, A. L., GRAHAM, D., MONINE, M., INRA, J., SINKS, S., ERALY, S., GARAFALO, S. & FRADETTE, S. 2024. Safety, tolerability, and pharmacokinetics of antisense oligonucleotide BIIB078 in adults with C9orf72-associated amyotrophic lateral sclerosis: a phase 1, randomised, double blinded, placebo-controlled, multiple ascending dose study. *Lancet Neurol,* 23**,** 901-912.
VAN DEN BOS, M. A. J., GEEVASINGA, N., HIGASHIHARA, M., MENON, P. & VUCIC, S. 2019. Pathophysiology and Diagnosis of ALS: Insights from Advances in Neurophysiological Techniques. *Int J Mol Sci,* 20.
VAN DEN BOSCH, L., VAN DAMME, P., BOGAERT, E. & ROBBERECHT, W. 2006. The role of excitotoxicity in the pathogenesis of amyotrophic lateral sclerosis. *Biochim Biophys Acta,* 1762**,** 1068-82.
VAN ES, M. A., HARDIMAN, O., CHIO, A., AL-CHALABI, A., PASTERKAMP, R. J., VELDINK, J. H. & VAN DEN BERG, L. H. 2017. Amyotrophic lateral sclerosis. *Lancet,* 390**,** 2084-2098.
VAN LANGENHOVE, T., VAN DER ZEE, J. & VAN BROECKHOVEN, C. 2012. The molecular basis of the frontotemporal lobar degeneration-amyotrophic lateral sclerosis spectrum. *Ann Med,* 44**,** 817-28.
VAN SWIETEN, J. & SPILLANTINI, M. G. 2007. Hereditary frontotemporal dementia caused by Tau gene mutations. *Brain Pathol,* 17**,** 63-73.
VANCE, C., ROGELJ, B., HORTOBAGYI, T., DE VOS, K. J., NISHIMURA, A. L., SREEDHARAN, J., HU, X., SMITH, B., RUDDY, D., WRIGHT, P., GANESALINGAM, J., WILLIAMS, K. L., TRIPATHI, V., AL-SARAJ, S., AL-CHALABI, A., LEIGH, P. N., BLAIR, I. P., NICHOLSON, G., DE BELLEROCHE, J., GALLO, J. M., MILLER, C. C. & SHAW, C. E. 2009. Mutations in FUS, an RNA processing protein, cause familial amyotrophic lateral sclerosis type 6. *Science,* 323**,** 1208-1211.

VARCIANNA, A., MYSZCZYNSKA, M. A., CASTELLI, L. M., O'NEILL, B., KIM, Y., TALBOT, J., NYBERG, S., NYAMALI, I., HEATH, P. R., STOPFORD, M. J., HAUTBERGUE, G. M. & FERRAIUOLO, L. 2019. Micro-RNAs secreted through astrocyte-derived extracellular vesicles cause neuronal network degeneration in C9orf72 ALS. *EBioMedicine,* 40**,** 626-635.

VATSAVAYAI, S. C., YOON, S. J., GARDNER, R. C., GENDRON, T. F., VARGAS, J. N., TRUJILLO, A., PRIBADI, M., PHILLIPS, J. J., GAUS, S. E., HIXSON, J. D., GARCIA, P. A., RABINOVICI, G. D., COPPOLA, G., GESCHWIND, D. H., PETRUCELLI, L., MILLER, B. L. & SEELEY, W. W. 2016. Timing and significance of pathological features in C9orf72 expansion-associated frontotemporal dementia. *Brain,* 139**,** 3202-3216.

VERKHRATSKY, A., KRISHTAL, O. A. & PETERSEN, O. H. 2006. From Galvani to patch clamp: the development of electrophysiology. *Pflugers Arch,* 453**,** 233-47.

VERSTRAETE, E., VELDINK, J. H., HENDRIKSE, J., SCHELHAAS, H. J., VAN DEN HEUVEL, M. P. & VAN DEN BERG, L. H. 2012. Structural MRI reveals cortical thinning in amyotrophic lateral sclerosis. *J Neurol Neurosurg Psychiatry,* 83**,** 383-8.

VUCIC, S., NICHOLSON, G. A. & KIERNAN, M. C. 2008. Cortical hyperexcitability may precede the onset of familial amyotrophic lateral sclerosis. *Brain,* 131**,** 1540-50.

VUCIC, S., ZIEMANN, U., EISEN, A., HALLETT, M. & KIERNAN, M. C. 2013. Transcranial magnetic stimulation and amyotrophic lateral sclerosis: pathophysiological insights. *J Neurol Neurosurg Psychiatry,* 84**,** 1161-70.

WAINGER, B. J. & CUDKOWICZ, M. E. 2015. Cortical Hyperexcitability in Amyotrophic Lateral Sclerosis: C9orf72 Repeats. *JAMA Neurol,* 72**,** 1235-6.

WAINGER, B. J., KISKINIS, E., MELLIN, C., WISKOW, O., HAN, S. S., SANDOE, J., PEREZ, N. P., WILLIAMS, L. A., LEE, S., BOULTING, G., BERRY, J. D., BROWN, R. H., JR., CUDKOWICZ, M. E., BEAN, B. P., EGGAN, K. & WOOLF, C. J. 2014. Intrinsic membrane hyperexcitability of amyotrophic lateral sclerosis patient-derived motor neurons. *Cell Rep,* 7**,** 1-11.

WAINGER, B. J., MACKLIN, E. A., VUCIC, S., MCILDUFF, C. E., PAGANONI, S., MARAGAKIS, N. J., BEDLACK, R., GOYAL, N. A., RUTKOVE, S. B., LANGE, D. J., RIVNER, M. H., GOUTMAN, S. A., LADHA, S. S., MAURICIO, E. A., BALOH, R. H., SIMMONS, Z., POTHIER, L., KASSIS, S. B., LA, T., HALL, M., EVORA, A., KLEMENTS, D., HURTADO, A., PEREIRA, J. D., KOH, J., CELNIK, P. A., CHAUDHRY, V., GABLE, K., JUEL, V. C., PHIELIPP, N., MAREI, A., ROSENQUIST, P., MEEHAN, S., OSKARSSON, B., LEWIS, R. A., KAUR, D., KISKINIS, E., WOOLF, C. J., EGGAN, K., WEISS, M. D., BERRY, J. D., DAVID, W. S., DAVILA-PEREZ, P., CAMPRODON, J. A., PASCUAL-LEONE, A., KIERNAN, M. C., SHEFNER, J. M., ATASSI, N. & CUDKOWICZ, M. E. 2021. Effect of Ezogabine on Cortical and Spinal Motor Neuron Excitability in Amyotrophic Lateral Sclerosis: A Randomized Clinical Trial. *JAMA Neurol,* 78**,** 186-196.

WAITE, A. J., BAUMER, D., EAST, S., NEAL, J., MORRIS, H. R., ANSORGE, O. & BLAKE, D. J. 2014. Reduced C9orf72 protein levels in frontal cortex of amyotrophic lateral sclerosis and frontotemporal degeneration brain with the C9ORF72 hexanucleotide repeat expansion. *Neurobiol Aging,* 35**,** 1779 e5-1779 e13.

WALKER, A. K., SPILLER, K. J., GE, G., ZHENG, A., XU, Y., ZHOU, M., TRIPATHY, K., KWONG, L. K., TROJANOWSKI, J. Q. & LEE, V. M. 2015a. Functional recovery in new mouse models of ALS/FTLD after clearance of pathological cytoplasmic TDP-43. *Acta Neuropathol,* 130**,** 643-60.

WALKER, A. K., TRIPATHY, K., RESTREPO, C. R., GE, G., XU, Y., KWONG, L. K., TROJANOWSKI, J. Q. & LEE, V. M. 2015b. An insoluble frontotemporal lobar degeneration-associated TDP-43 C-terminal fragment causes neurodegeneration and hippocampus pathology in transgenic mice. *Hum Mol Genet,* 24**,** 7241-54.

WANG, B., JAFFE, D. B. & BRENNER, R. 2014. Current understanding of iberiotoxin-resistant BK channels in the nervous system. *Front Physiol,* 5**,** 382.

WANG, S. J., WANG, K. Y. & WANG, W. C. 2004. Mechanisms underlying the riluzole inhibition of glutamate release from rat cerebral cortex nerve terminals (synaptosomes). *Neuroscience,* 125**,** 191-201.

WANG, W., DEVER, D., LOWE, J., STOREY, G. P., BHANSALI, A., ECK, E. K., NITULESCU, I., WEIMER, J. & BAMFORD, N. S. 2012. Regulation of prefrontal excitatory neurotransmission by dopamine in the nucleus accumbens core. *J Physiol,* 590**,** 3743-69.

WANG, Z. Z., FOLORUNSO, O. O., MORRIS, K., BERRETTA, S. & ENGIN, E. 2024. Early developmental changes in GABAA receptor expression in nucleus accumbens medium spiny neurons. *Front Neurosci,* 18**,** 1445162.

WANNER, S. G., KOCH, R. O., KOSCHAK, A., TRIEB, M., GARCIA, M. L., KACZOROWSKI, G. J. & KNAUS, H. G. 1999. High-conductance calcium-activated potassium channels in rat brain: pharmacology, distribution, and subunit composition. *Biochemistry,* 38**,** 5392-400.

WANNOP, K., BASHFORD, J., WICKHAM, A., INIESTA, R., DRAKAKIS, E., BOUTELLE, M., MILLS, K. & SHAW, C. 2021. Fasciculation analysis reveals a novel parameter that correlates with predicted survival in amyotrophic lateral sclerosis. *Muscle Nerve,* 63**,** 392-396.

WARMUS, B. A., SEKAR, D. R., MCCUTCHEN, E., SCHELLENBERG, G. D., ROBERTS, R. C., MCMAHON, L. L. & ROBERSON, E. D. 2014. Tau-mediated NMDA receptor impairment underlies dysfunction of a selectively vulnerable network in a mouse model of frontotemporal dementia. *J Neurosci,* 34**,** 16482-95.

WEBSTER, C. P., SMITH, E. F., BAUER, C. S., MOLLER, A., HAUTBERGUE, G. M., FERRAIUOLO, L., MYSZCZYNSKA, M. A., HIGGINBOTTOM, A., WALSH, M. J., WHITWORTH, A. J., KASPAR, B. K., MEYER, K., SHAW, P. J., GRIERSON, A. J. & DE VOS, K. J. 2016. The C9orf72 protein interacts with Rab1a and the ULK1 complex to regulate initiation of autophagy. *EMBO J,* 35**,** 1656-76.

WEFELMEYER, W., CATTAERT, D. & BURRONE, J. 2015. Activity-dependent mismatch between axo-axonic synapses and the axon initial segment controls neuronal output. *Proc Natl Acad Sci U S A,* 112**,** 9757-62.

WEISER, M., VEGA-SAENZ DE MIERA, E., KENTROS, C., MORENO, H., FRANZEN, L., HILLMAN, D., BAKER, H. & RUDY, B. 1994. Differential expression of Shaw-related K+ channels in the rat central nervous system. *J Neurosci,* 14**,** 949-72.

WEN, X., TAN, W., WESTERGARD, T., KRISHNAMURTHY, K., MARKANDAIAH, S. S., SHI, Y., LIN, S., SHNEIDER, N. A., MONAGHAN, J., PANDEY, U. B., PASINELLI, P., ICHIDA, J. K. & TROTTI, D. 2014. Antisense proline-arginine

RAN dipeptides linked to C9ORF72-ALS/FTD form toxic nuclear aggregates that initiate in vitro and in vivo neuronal death. *Neuron,* 84**,** 1213-25.
WESKAMP, K., TANK, E. M., MIGUEZ, R., MCBRIDE, J. P., GOMEZ, N. B., WHITE, M., LIN, Z., GONZALEZ, C. M., SERIO, A., SREEDHARAN, J. & BARMADA, S. J. 2020. Shortened TDP43 isoforms upregulated by neuronal hyperactivity drive TDP43 pathology in ALS. *J Clin Invest,* 130**,** 1139-1155.
WEST, R. J. H., SHARPE, J. L., VOELZMANN, A., MUNRO, A. L., HAHN, I., BAINES, R. A. & PICKERING-BROWN, S. 2020. Co-expression of C9orf72 related dipeptide-repeats over 1000 repeat units reveals age- and combination-specific phenotypic profiles in Drosophila. *Acta Neuropathol Commun,* 8**,** 158.
WESTENENG, H. J., VERSTRAETE, E., WALHOUT, R., SCHMIDT, R., HENDRIKSE, J., VELDINK, J. H., VAN DEN HEUVEL, M. P. & VAN DEN BERG, L. H. 2015. Subcortical structures in amyotrophic lateral sclerosis. *Neurobiol Aging,* 36**,** 1075-82.
WESTERGARD, T., JENSEN, B. K., WEN, X., CAI, J., KROPF, E., IACOVITTI, L., PASINELLI, P. & TROTTI, D. 2016. Cell-to-Cell Transmission of Dipeptide Repeat Proteins Linked to C9orf72-ALS/FTD. *Cell Rep,* 17**,** 645-652.
WESTERGARD, T., MCAVOY, K., RUSSELL, K., WEN, X., PANG, Y., MORRIS, B., PASINELLI, P., TROTTI, D. & HAEUSLER, A. 2019. Repeat-associated non-AUG translation in C9orf72-ALS/FTD is driven by neuronal excitation and stress. *EMBO Mol Med,* 11.
WHITE, M. A., KIM, E., DUFFY, A., ADALBERT, R., PHILLIPS, B. U., PETERS, O. M., STEPHENSON, J., YANG, S., MASSENZIO, F., LIN, Z., ANDREWS, S., SEGONDS-PICHON, A., METTERVILLE, J., SAKSIDA, L. M., MEAD, R., RIBCHESTER, R. R., BARHOMI, Y., SERRE, T., COLEMAN, M. P., FALLON, J. R., BUSSEY, T. J., BROWN, R. H., JR. & SREEDHARAN, J. 2018. TDP-43 gains function due to perturbed autoregulation in a Tardbp knock-in mouse model of ALS-FTD. *Nat Neurosci,* 21**,** 552-563.
WICKS, P., ABRAHAMS, S., PAPPS, B., AL-CHALABI, A., SHAW, C. E., LEIGH, P. N. & GOLDSTEIN, L. H. 2009. SOD1 and cognitive dysfunction in familial amyotrophic lateral sclerosis. *J Neurol,* 256**,** 234-41.
WICKS, P., GANESALINGHAM, J., COLLIN, C., PREVETT, M., LEIGH, N. P. & AL-CHALABI, A. 2007. Three soccer playing friends with simultaneous amyotrophic lateral sclerosis. *Amyotroph Lateral Scler,* 8**,** 177-9.
WILHELM, M., SYCH, Y., FOMINS, A., ALATORRE WARREN, J. L., LEWIS, C., SERRATOSA CAPDEVILA, L., BOEHRINGER, R., AMADEI, E. A., GREWE, B., O'CONNOR, E. C., HALL, B. J. & HELMCHEN, F. 2023. Striatum-projecting prefrontal cortex neurons support working memory maintenance. *Nat Commun,* 14**,** 7016.
WILLIAMS, K. 1993. Ifenprodil discriminates subtypes of the N-methyl-D-aspartate receptor: selectivity and mechanisms at recombinant heteromeric receptors. *Mol Pharmacol,* 44**,** 851-9.
WILLIAMS, K. L., FIFITA, J. A., VUCIC, S., DURNALL, J. C., KIERNAN, M. C., BLAIR, I. P. & NICHOLSON, G. A. 2013. Pathophysiological insights into ALS with C9ORF72 expansions. *J Neurol Neurosurg Psychiatry,* 84**,** 931-5.
WILLIS, A., PRATT, J. A. & MORRIS, B. J. 2021. BDNF and JNK Signaling Modulate Cortical Interneuron and Perineuronal Net Development: Implications for Schizophrenia-Linked 16p11.2 Duplication Syndrome. *Schizophr Bull,* 47**,** 812-826.

WILMUT, I., SCHNIEKE, A. E., MCWHIR, J., KIND, A. J. & CAMPBELL, K. H. 1997. Viable offspring derived from fetal and adult mammalian cells. *Nature,* 385**,** 810-3.
WILSON, C. J. & GROVES, P. M. 1981. Spontaneous firing patterns of identified spiny neurons in the rat neostriatum. *Brain Res,* 220**,** 67-80.
WINTON, M. J., IGAZ, L. M., WONG, M. M., KWONG, L. K., TROJANOWSKI, J. Q. & LEE, V. M. 2008. Disturbance of nuclear and cytoplasmic TAR DNA-binding protein (TDP-43) induces disease-like redistribution, sequestration, and aggregate formation. *J Biol Chem,* 283**,** 13302-9.
WISE, R. A. 2004. Dopamine, learning and motivation. *Nat Rev Neurosci,* 5**,** 483-94.
WU, L. S., CHENG, W. C., CHEN, C. Y., WU, M. C., WANG, Y. C., TSENG, Y. H., CHUANG, T. J. & SHEN, C. J. 2019. Transcriptomopathies of pre- and post-symptomatic frontotemporal dementia-like mice with TDP-43 depletion in forebrain neurons. *Acta Neuropathol Commun,* 7**,** 50.
XIAO, S., MCKEEVER, P. M., LAU, A. & ROBERTSON, J. 2019. Synaptic localization of C9orf72 regulates post-synaptic glutamate receptor 1 levels. *Acta Neuropathol Commun,* 7**,** 161.
XIE, M., PALLEGAR, P. N., PARUSEL, S., NGUYEN, A. T. & WU, L. J. 2023. Regulation of cortical hyperexcitability in amyotrophic lateral sclerosis: focusing on glial mechanisms. *Mol Neurodegener,* 18**,** 75.
XU, H. J., YAO, Y., YAO, F., CHEN, J., LI, M., YANG, X., LI, S., LU, F., HU, P., HE, S., PENG, G. & JING, N. 2023. Generation of functional posterior spinal motor neurons from hPSCs-derived human spinal cord neural progenitor cells. *Cell Regen,* 12**,** 15.
XU, L., LIU, T., LIU, L., YAO, X., CHEN, L., FAN, D., ZHAN, S. & WANG, S. 2020. Global variation in prevalence and incidence of amyotrophic lateral sclerosis: a systematic review and meta-analysis. *J Neurol,* 267**,** 944-953.
XU, M., CAO, R., XIAO, R., ZHU, M. X. & GU, C. 2007. The axon-dendrite targeting of Kv3 (Shaw) channels is determined by a targeting motif that associates with the T1 domain and ankyrin G. *J Neurosci,* 27**,** 14158-70.
XU, W. & XU, J. 2018. C9orf72 Dipeptide Repeats Cause Selective Neurodegeneration and Cell-Autonomous Excitotoxicity in Drosophila Glutamatergic Neurons. *J Neurosci,* 38**,** 7741-7752.
XU, Z., POIDEVIN, M., LI, X., LI, Y., SHU, L., NELSON, D. L., LI, H., HALES, C. M., GEARING, M., WINGO, T. S. & JIN, P. 2013. Expanded GGGGCC repeat RNA associated with amyotrophic lateral sclerosis and frontotemporal dementia causes neurodegeneration. *Proc Natl Acad Sci U S A,* 110**,** 7778-83.
YAMAKAWA, M., ITO, D., HONDA, T., KUBO, K., NODA, M., NAKAJIMA, K. & SUZUKI, N. 2015. Characterization of the dipeptide repeat protein in the molecular pathogenesis of c9FTD/ALS. *Hum Mol Genet,* 24**,** 1630-45.
YAN, S., WANG, C. E., WEI, W., GAERTIG, M. A., LAI, L., LI, S. & LI, X. J. 2014. TDP-43 causes differential pathology in neuronal versus glial cells in the mouse brain. *Hum Mol Genet,* 23**,** 2678-93.
ZAMZOW, D. R., ELIAS, V., SHUMAKER, M., LARSON, C. & MAGNUSSON, K. R. 2013. An increase in the association of GluN2B containing NMDA receptors with membrane scaffolding proteins was related to memory declines during aging. *J Neurosci,* 33**,** 12300-5.

ZAREI, S., CARR, K., REILEY, L., DIAZ, K., GUERRA, O., ALTAMIRANO, P. F., PAGANI, W., LODIN, D., OROZCO, G. & CHINEA, A. 2015. A comprehensive review of amyotrophic lateral sclerosis. *Surg Neurol Int,* 6**,** 171.
ZHANG, H., TAN, C. F., MORI, F., TANJI, K., KAKITA, A., TAKAHASHI, H. & WAKABAYASHI, K. 2008. TDP-43-immunoreactive neuronal and glial inclusions in the neostriatum in amyotrophic lateral sclerosis with and without dementia. *Acta Neuropathol,* 115**,** 115-22.
ZHANG, K., DAIGLE, J. G., CUNNINGHAM, K. M., COYNE, A. N., RUAN, K., GRIMA, J. C., BOWEN, K. E., WADHWA, H., YANG, P., RIGO, F., TAYLOR, J. P., GITLER, A. D., ROTHSTEIN, J. D. & LLOYD, T. E. 2018. Stress Granule Assembly Disrupts Nucleocytoplasmic Transport. *Cell,* 173**,** 958-971 e17.
ZHANG, K., DONNELLY, C. J., HAEUSLER, A. R., GRIMA, J. C., MACHAMER, J. B., STEINWALD, P., DALEY, E. L., MILLER, S. J., CUNNINGHAM, K. M., VIDENSKY, S., GUPTA, S., THOMAS, M. A., HONG, I., CHIU, S. L., HUGANIR, R. L., OSTROW, L. W., MATUNIS, M. J., WANG, J., SATTLER, R., LLOYD, T. E. & ROTHSTEIN, J. D. 2015. The C9orf72 repeat expansion disrupts nucleocytoplasmic transport. *Nature,* 525**,** 56-61.
ZHANG, S., COOPER-KNOCK, J., WEIMER, A. K., SHI, M., MOLL, T., MARSHALL, J. N. G., HARVEY, C., NEZHAD, H. G., FRANKLIN, J., SOUZA, C. D. S., NING, K., WANG, C., LI, J., DILLIOTT, A. A., FARHAN, S., ELHAIK, E., PASNICEANU, I., LIVESEY, M. R., EITAN, C., HORNSTEIN, E., KENNA, K. P., PROJECT MIN, E. A. L. S. S. C., VELDINK, J. H., FERRAIUOLO, L., SHAW, P. J. & SNYDER, M. P. 2022. Genome-wide identification of the genetic basis of amyotrophic lateral sclerosis. *Neuron,* 110**,** 992-1008 e11.
ZHANG, W., ZHANG, L., LIANG, B., SCHROEDER, D., ZHANG, Z. W., COX, G. A., LI, Y. & LIN, D. T. 2016. Hyperactive somatostatin interneurons contribute to excitotoxicity in neurodegenerative disorders. *Nat Neurosci,* 19**,** 557-559.
ZHANG, Y. J., JANSEN-WEST, K., XU, Y. F., GENDRON, T. F., BIENIEK, K. F., LIN, W. L., SASAGURI, H., CAULFIELD, T., HUBBARD, J., DAUGHRITY, L., CHEW, J., BELZIL, V. V., PRUDENCIO, M., STANKOWSKI, J. N., CASTANEDES-CASEY, M., WHITELAW, E., ASH, P. E., DETURE, M., RADEMAKERS, R., BOYLAN, K. B., DICKSON, D. W. & PETRUCELLI, L. 2014. Aggregation-prone c9FTD/ALS poly(GA) RAN-translated proteins cause neurotoxicity by inducing ER stress. *Acta Neuropathol,* 128**,** 505-24.
ZHANG, Z., ALMEIDA, S., LU, Y., NISHIMURA, A. L., PENG, L., SUN, D., WU, B., KARYDAS, A. M., TARTAGLIA, M. C., FONG, J. C., MILLER, B. L., FARESE, R. V., JR., MOORE, M. J., SHAW, C. E. & GAO, F. B. 2013. Downregulation of microRNA-9 in iPSC-derived neurons of FTD/ALS patients with TDP-43 mutations. *PLoS One,* 8**,** e76055.
ZHAO, C., DEVLIN, A. C., CHOUHAN, A. K., SELVARAJ, B. T., STAVROU, M., BURR, K., BRIVIO, V., HE, X., MEHTA, A. R., STORY, D., SHAW, C. E., DANDO, O., HARDINGHAM, G. E., MILES, G. B. & CHANDRAN, S. 2020. Mutant C9orf72 human iPSC-derived astrocytes cause non-cell autonomous motor neuron pathophysiology. *Glia,* 68**,** 1046-1064.
ZHAO, X. & MOORE, D. L. 2018. Neural stem cells: developmental mechanisms and disease modeling. *Cell Tissue Res,* 371**,** 1-6.
ZHU, Q., JIANG, J., GENDRON, T. F., MCALONIS-DOWNES, M., JIANG, L., TAYLOR, A., DIAZ GARCIA, S., GHOSH DASTIDAR, S., RODRIGUEZ, M. J., KING, P., ZHANG, Y., LA SPADA, A. R., XU, H., PETRUCELLI, L., RAVITS,

J., DA CRUZ, S., LAGIER-TOURENNE, C. & CLEVELAND, D. W. 2020. Reduced C9ORF72 function exacerbates gain of toxicity from ALS/FTD-causing repeat expansion in C9orf72. *Nat Neurosci,* 23**,** 615-624.
ZUO, X., ZHOU, J., LI, Y., WU, K., CHEN, Z., LUO, Z., ZHANG, X., LIANG, Y., ESTEBAN, M. A., ZHOU, Y. & FU, X. D. 2021. TDP-43 aggregation induced by oxidative stress causes global mitochondrial imbalance in ALS. *Nat Struct Mol Biol,* 28**,** 132-142.

8. Appendix

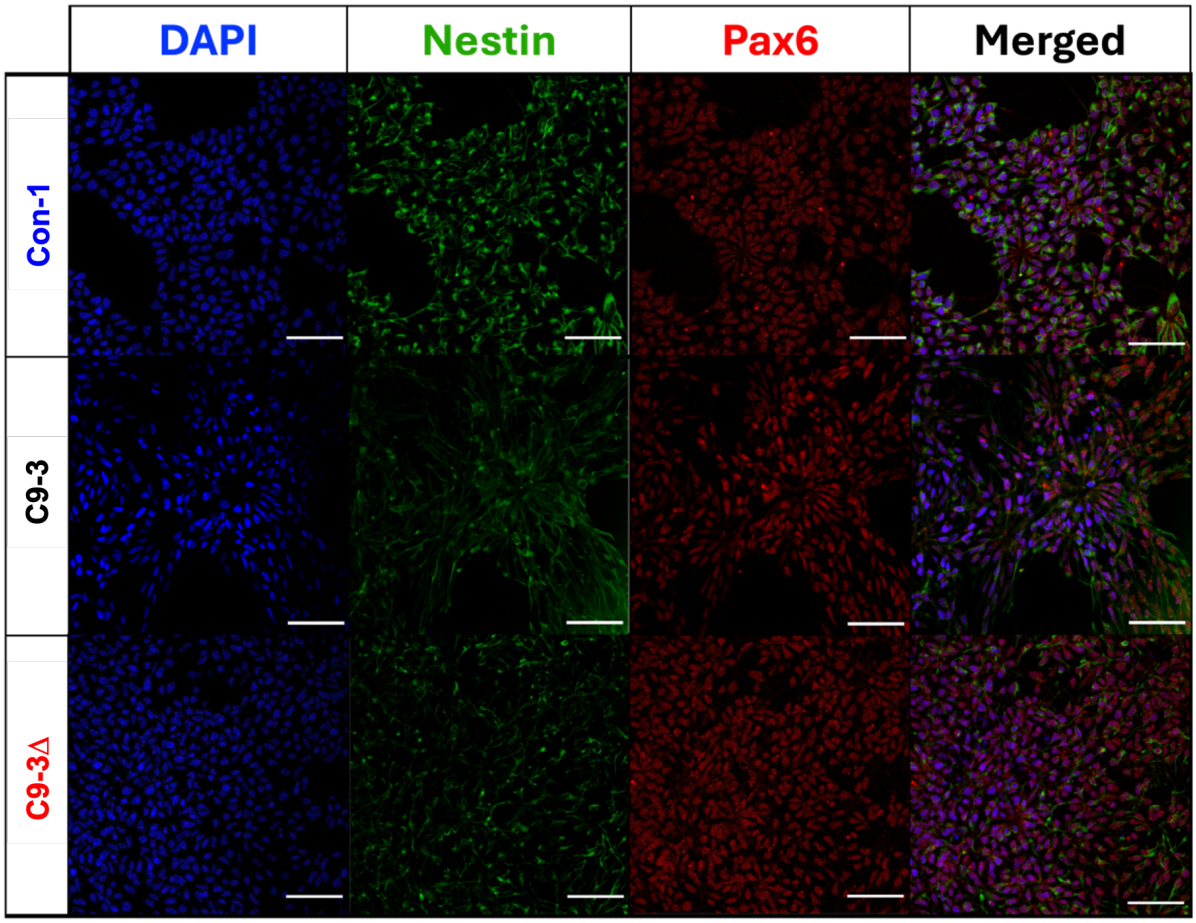

Appendix 1. NPC characterisation. Representative images of NPCs derived from a control, C9 and isogenic iPSCs that have been stained for NPC markers nestin and Pax6. Note, the display of neural rosettes, typically observed at the NPC stage. Scale bar: 50 µm. Data obtained from the Livesey laboratory.

Con-1 TUKEY'S MULTIPLE COMPARISONS TEST

	Significance?	Summary	Adjusted P Value
0 pA current injection			
Day 20 vs. Day 40	No	ns	>0.9999
Day 20 vs. Day 60	No	ns	>0.9999
Day 40 vs. Day 60	No	ns	>0.9999
5 pA current injection			
Day 20 vs. Day 40	No	ns	0.9982
Day 20 vs. Day 60	No	ns	0.9984
Day 40 vs. Day 60	No	ns	>0.9999
10 pA current injection			
Day 20 vs. Day 40	No	ns	0.9977
Day 20 vs. Day 60	No	ns	0.9999
Day 40 vs. Day 60	No	ns	0.9971
15 pA current injection			
Day 20 vs. Day 40	No	ns	0.8209
Day 20 vs. Day 60	No	ns	0.6257
Day 40 vs. Day 60	No	ns	0.934
20 pA current injection			
Day 20 vs. Day 40	No	ns	0.3955
Day 20 vs. Day 60	No	ns	0.1579
Day 40 vs. Day 60	No	ns	0.8177
25 pA current injection			
Day 20 vs. Day 40	No	ns	0.1455
Day 20 vs. Day 60	Yes	**	0.0067
Day 40 vs. Day 60	No	ns	0.4219
30 pA current injection			
Day 20 vs. Day 40	Yes	*	0.0335
Day 20 vs. Day 60	Yes	***	0.0002
Day 40 vs. Day 60	No	ns	0.2289
35 pA current injection			
Day 20 vs. Day 40	Yes	*	0.0197
Day 20 vs. Day 60	Yes	****	<0.0001
Day 40 vs. Day 60	No	ns	0.0959
40 pA current injection			
Day 20 vs. Day 40	Yes	*	0.0173
Day 20 vs. Day 60	Yes	****	<0.0001
Day 40 vs. Day 60	No	ns	0.0565
45 pA current injection			
Day 20 vs. Day 40	Yes	*	0.0193
Day 20 vs. Day 60	Yes	****	<0.0001
Day 40 vs. Day 60	Yes	**	0.0051
50 pA current injection			
Day 20 vs. Day 40	No	ns	0.1257
Day 20 vs. Day 60	Yes	****	<0.0001
Day 40 vs. Day 60	Yes	**	0.0017

Con-2 TUKEY'S MULTIPLE COMPARISONS TEST

	Significance?	Summary	Adjusted P Value
0 pA current injection			
Day 20 vs. Day 40	No	ns	>0.9999
Day 20 vs. Day 60	No	ns	>0.9999
Day 40 vs. Day 60	No	ns	>0.9999
5 pA current injection			
Day 20 vs. Day 40	No	ns	>0.9999
Day 20 vs. Day 60	No	ns	>0.9999
Day 40 vs. Day 60	No	ns	>0.9999
10 pA current injection			
Day 20 vs. Day 40	No	ns	0.8978
Day 20 vs. Day 60	No	ns	0.8633
Day 40 vs. Day 60	No	ns	>0.9999
15 pA current injection			
Day 20 vs. Day 40	No	ns	0.9829
Day 20 vs. Day 60	No	ns	0.853
Day 40 vs. Day 60	No	ns	0.8111
20 pA current injection			
Day 20 vs. Day 40	No	ns	0.4841
Day 20 vs. Day 60	No	ns	0.9186
Day 40 vs. Day 60	No	ns	0.7106
25 pA current injection			
Day 20 vs. Day 40	No	ns	0.153
Day 20 vs. Day 60	No	ns	0.1589
Day 40 vs. Day 60	No	ns	0.9594
30 pA current injection			
Day 20 vs. Day 40	Yes	**	0.0025
Day 20 vs. Day 60	Yes	****	<0.0001
Day 40 vs. Day 60	No	ns	0.9111
35 pA current injection			
Day 20 vs. Day 40	Yes	****	<0.0001
Day 20 vs. Day 60	Yes	****	<0.0001
Day 40 vs. Day 60	No	ns	0.6465
40 pA current injection			
Day 20 vs. Day 40	Yes	****	<0.0001
Day 20 vs. Day 60	Yes	****	<0.0001
Day 40 vs. Day 60	No	ns	0.9974
45 pA current injection			
Day 20 vs. Day 40	Yes	****	<0.0001
Day 20 vs. Day 60	Yes	****	<0.0001
Day 40 vs. Day 60	No	ns	0.9839
50 pA current injection			
Day 20 vs. Day 40	Yes	****	<0.0001
Day 20 vs. Day 60	Yes	****	<0.0001
Day 40 vs. Day 60	No	ns	0.9994

C9-2 TUKEY'S MULTIPLE COMPARISONS TEST

	Significance?	Summary	Adjusted P Value
0 pA current injection			
Day 20 vs. Day 40	No	ns	>0.9999
Day 20 vs. Day 60	No	ns	>0.9999
Day 40 vs. Day 60	No	ns	>0.9999
5 pA current injection			
Day 20 vs. Day 40	No	ns	>0.9999
Day 20 vs. Day 60	No	ns	>0.9999
Day 40 vs. Day 60	No	ns	>0.9999
10 pA current injection			
Day 20 vs. Day 40	No	ns	0.8088
Day 20 vs. Day 60	No	ns	0.8635
Day 40 vs. Day 60	No	ns	0.9947
15 pA current injection			
Day 20 vs. Day 40	No	ns	0.9977
Day 20 vs. Day 60	No	ns	0.983
Day 40 vs. Day 60	No	ns	0.9925
20 pA current injection			
Day 20 vs. Day 40	No	ns	0.7415
Day 20 vs. Day 60	No	ns	0.5143
Day 40 vs. Day 60	No	ns	0.9207
25 pA current injection			
Day 20 vs. Day 40	No	ns	0.5717
Day 20 vs. Day 60	No	ns	0.3747
Day 40 vs. Day 60	No	ns	0.9324
30 pA current injection			
Day 20 vs. Day 40	No	ns	0.6044
Day 20 vs. Day 60	No	ns	0.4166
Day 40 vs. Day 60	No	ns	0.9411
35 pA current injection			
Day 20 vs. Day 40	No	ns	0.3502
Day 20 vs. Day 60	No	ns	0.1226
Day 40 vs. Day 60	No	ns	0.8088
40 pA current injection			
Day 20 vs. Day 40	No	ns	0.3367
Day 20 vs. Day 60	No	ns	0.0969
Day 40 vs. Day 60	No	ns	0.7596
45 pA current injection			
Day 20 vs. Day 40	No	ns	0.1154
Day 20 vs. Day 60	No	ns	0.2018
Day 40 vs. Day 60	No	ns	0.9639
50 pA current injection			
Day 20 vs. Day 40	No	ns	0.0583
Day 20 vs. Day 60	No	ns	0.164
Day 40 vs. Day 60	No	ns	0.895

C9-3 TUKEY'S MULTIPLE COMPARISONS TEST

	Significance?	Summary	Adjusted P Value
0 pA current injection			
Day 20 vs. Day 40	No	ns	>0.9999
Day 20 vs. Day 60	No	ns	>0.9999
Day 40 vs. Day 60	No	ns	>0.9999
5 pA current injection			
Day 20 vs. Day 40	No	ns	0.9783
Day 20 vs. Day 60	No	ns	0.9779
Day 40 vs. Day 60	No	ns	>0.9999
10 pA current injection			
Day 20 vs. Day 40	No	ns	0.7331
Day 20 vs. Day 60	No	ns	0.637
Day 40 vs. Day 60	No	ns	0.9823
15 pA current injection			
Day 20 vs. Day 40	No	ns	>0.9999
Day 20 vs. Day 60	No	ns	0.9146
Day 40 vs. Day 60	No	ns	0.8774
20 pA current injection			
Day 20 vs. Day 40	No	ns	0.6024
Day 20 vs. Day 60	No	ns	0.637
Day 40 vs. Day 60	No	ns	0.0613
25 pA current injection			
Day 20 vs. Day 40	No	ns	0.8873
Day 20 vs. Day 60	No	ns	0.3913
Day 40 vs. Day 60	No	ns	0.0807
30 pA current injection			
Day 20 vs. Day 40	No	ns	0.9992
Day 20 vs. Day 60	No	ns	0.5103
Day 40 vs. Day 60	No	ns	0.3996
35 pA current injection			
Day 20 vs. Day 40	No	ns	0.9968
Day 20 vs. Day 60	No	ns	0.3371
Day 40 vs. Day 60	No	ns	0.1712
40 pA current injection			
Day 20 vs. Day 40	No	ns	0.7726
Day 20 vs. Day 60	No	ns	0.637
Day 40 vs. Day 60	No	ns	0.1309
45 pA current injection			
Day 20 vs. Day 40	No	ns	0.9857
Day 20 vs. Day 60	No	ns	0.5733
Day 40 vs. Day 60	No	ns	0.3338
50 pA current injection			
Day 20 vs. Day 40	No	ns	0.8916
Day 20 vs. Day 60	No	ns	0.951
Day 40 vs. Day 60	No	ns	0.6265

C9-3Δ TUKEY'S MULTIPLE COMPARISONS TEST

	Significance?	Summary	Adjusted P Value
0 pA current injection			
Day 20 vs. Day 40	No	ns	>0.9999
Day 20 vs. Day 60	No	ns	>0.9999
Day 40 vs. Day 60	No	ns	>0.9999
5 pA current injection			
Day 20 vs. Day 40	No	ns	0.9431
Day 20 vs. Day 60	No	ns	0.9895
Day 40 vs. Day 60	No	ns	0.9935
10 pA current injection			
Day 20 vs. Day 40	No	ns	0.9222
Day 20 vs. Day 60	No	ns	0.8848
Day 40 vs. Day 60	No	ns	0.9742
15 pA current injection			
Day 20 vs. Day 40	No	ns	0.7353
Day 20 vs. Day 60	No	ns	0.9895
Day 40 vs. Day 60	No	ns	0.7269
20 pA current injection			
Day 20 vs. Day 40	Yes	*	0.0354
Day 20 vs. Day 60	No	ns	0.9983
Day 40 vs. Day 60	No	ns	0.1247
25 pA current injection			
Day 20 vs. Day 40	Yes	*	0.0102
Day 20 vs. Day 60	No	ns	0.8718
Day 40 vs. Day 60	Yes	*	0.01
30 pA current injection			
Day 20 vs. Day 40	Yes	*	0.0105
Day 20 vs. Day 60	No	ns	0.6138
Day 40 vs. Day 60	Yes	**	0.002
35 pA current injection			
Day 20 vs. Day 40	No	ns	0.0523
Day 20 vs. Day 60	No	ns	0.1709
Day 40 vs. Day 60	Yes	***	0.0003
40 pA current injection			
Day 20 vs. Day 40	No	ns	0.1526
Day 20 vs. Day 60	No	ns	0.0656
Day 40 vs. Day 60	Yes	***	0.0002
45 pA current injection			
Day 20 vs. Day 40	No	ns	0.5915
Day 20 vs. Day 60	Yes	*	0.0207
Day 40 vs. Day 60	Yes	***	0.0005
50 pA current injection			
Day 20 vs. Day 40	No	ns	0.8533
Day 20 vs. Day 60	Yes	*	0.0109
Day 40 vs. Day 60	Yes	***	0.0008

Appendix 2. Post-hoc Tukey's multiple comparisons test between GABA-ergic MSN timepoints. To evaluate statistical significance of evoked AP activity following current stimulation across time points for each MSN cell line (Con-1, Con-2, C9-2, C9-3, C9-3Δ), a two-way ANOVA was employed followed by Tukey's multiple comparisons test. The table above shows significance and adjusted p-values for each current step in the protocol.

TUKEY'S MULTIPLE COMPARISONS TEST

	Significance?	Summary	Adjusted P Value
0 pA current injection			
Con-1 vs. Con-2	No	ns	>0.9999
Con-1 vs. C9-1	No	ns	>0.9999
Con-1 vs. C9-2	No	ns	>0.9999
Con-1 vs. C9-3	No	ns	>0.9999
Con-2 vs. C9-1	No	ns	>0.9999
Con-2 vs. C9-2	No	ns	>0.9999
Con-2 vs. C9-3	No	ns	>0.9999
C9-1 vs. C9-2	No	ns	>0.9999
C9-1 vs. C9-3	No	ns	>0.9999
C9-2 vs. C9-3	No	ns	>0.9999
5 pA current injection			
Con-1 vs. Con-2	No	ns	>0.9999
Con-1 vs. C9-1	No	ns	>0.9999
Con-1 vs. C9-2	No	ns	>0.9999
Con-1 vs. C9-3	No	ns	>0.9999
Con-2 vs. C9-1	No	ns	>0.9999
Con-2 vs. C9-2	No	ns	>0.9999
Con-2 vs. C9-3	No	ns	>0.9999
C9-1 vs. C9-2	No	ns	>0.9999
C9-1 vs. C9-3	No	ns	>0.9999
C9-2 vs. C9-3	No	ns	>0.9999
10 pA current injection			
Con-1 vs. Con-2	No	ns	0.9928
Con-1 vs. C9-1	No	ns	0.6927
Con-1 vs. C9-2	No	ns	0.7468
Con-1 vs. C9-3	No	ns	0.9591
Con-2 vs. C9-1	No	ns	0.9435
Con-2 vs. C9-2	No	ns	0.9642
Con-2 vs. C9-3	No	ns	0.9999
C9-1 vs. C9-2	No	ns	>0.9999
C9-1 vs. C9-3	No	ns	0.9453
C9-2 vs. C9-3	No	ns	0.9687
15 pA current injection			
Con-1 vs. Con-2	No	ns	0.3323
Con-1 vs. C9-1	Yes	***	0.0004
Con-1 vs. C9-2	Yes	*	0.0121
Con-1 vs. C9-3	Yes	**	0.008
Con-2 vs. C9-1	No	ns	0.3206
Con-2 vs. C9-2	No	ns	0.8464
Con-2 vs. C9-3	No	ns	0.8761
C9-1 vs. C9-2	No	ns	0.859
C9-1 vs. C9-3	No	ns	0.732
C9-2 vs. C9-3	No	ns	0.9999
20 pA current injection			
Con-1 vs. Con-2	No	ns	0.3323
Con-1 vs. C9-1	Yes	****	<0.0001
Con-1 vs. C9-2	Yes	****	<0.0001
Con-1 vs. C9-3	Yes	****	<0.0001
Con-2 vs. C9-1	Yes	***	0.0008
Con-2 vs. C9-2	Yes	*	0.012
Con-2 vs. C9-3	Yes	**	0.0048
C9-1 vs. C9-2	No	ns	0.9099
C9-1 vs. C9-3	No	ns	0.9009
C9-2 vs. C9-3	No	ns	>0.9999
25 pA current injection			
Con-1 vs. Con-2	No	ns	0.7352
Con-1 vs. C9-1	Yes	****	<0.0001
Con-1 vs. C9-2	Yes	****	<0.0001
Con-1 vs. C9-3	Yes	****	<0.0001
Con-2 vs. C9-1	Yes	****	<0.0001
Con-2 vs. C9-2	Yes	****	<0.0001
Con-2 vs. C9-3	Yes	****	<0.0001
C9-1 vs. C9-2	No	ns	0.6888
C9-1 vs. C9-3	No	ns	0.8873
C9-2 vs. C9-3	No	ns	0.9871

	Significance?	Summary	Adjusted P Value
30 pA current injection			
Con-1 vs. Con-2	No	ns	0.9999
Con-1 vs. C9-1	Yes	****	<0.0001
Con-1 vs. C9-2	Yes	****	<0.0001
Con-1 vs. C9-3	Yes	****	<0.0001
Con-2 vs. C9-1	Yes	****	<0.0001
Con-2 vs. C9-2	Yes	****	<0.0001
Con-2 vs. C9-3	Yes	****	<0.0001
C9-1 vs. C9-2	No	ns	0.555
C9-1 vs. C9-3	No	ns	0.773
C9-2 vs. C9-3	No	ns	0.9881
35 pA current injection			
Con-1 vs. Con-2	No	ns	0.9489
Con-1 vs. C9-1	Yes	****	<0.0001
Con-1 vs. C9-2	Yes	****	<0.0001
Con-1 vs. C9-3	Yes	****	<0.0001
Con-2 vs. C9-1	Yes	****	<0.0001
Con-2 vs. C9-2	Yes	****	<0.0001
Con-2 vs. C9-3	Yes	****	<0.0001
C9-1 vs. C9-2	No	ns	0.9591
C9-1 vs. C9-3	No	ns	0.9931
C9-2 vs. C9-3	No	ns	0.9975
40 pA current injection			
Con-1 vs. Con-2	No	ns	0.796
Con-1 vs. C9-1	Yes	****	<0.0001
Con-1 vs. C9-2	Yes	****	<0.0001
Con-1 vs. C9-3	Yes	****	<0.0001
Con-2 vs. C9-1	Yes	****	<0.0001
Con-2 vs. C9-2	Yes	****	<0.0001
Con-2 vs. C9-3	Yes	****	<0.0001
C9-1 vs. C9-2	No	ns	0.9306
C9-1 vs. C9-3	No	ns	0.9864
C9-2 vs. C9-3	No	ns	0.9961
45 pA current injection			
Con-1 vs. Con-2	No	ns	>0.9999
Con-1 vs. C9-1	Yes	****	<0.0001
Con-1 vs. C9-2	Yes	****	<0.0001
Con-1 vs. C9-3	Yes	****	<0.0001
Con-2 vs. C9-1	Yes	****	<0.0001
Con-2 vs. C9-2	Yes	****	<0.0001
Con-2 vs. C9-3	Yes	****	<0.0001
C9-1 vs. C9-2	No	ns	0.8045
C9-1 vs. C9-3	No	ns	>0.9999
C9-2 vs. C9-3	No	ns	0.6776
50 pA current injection			
Con-1 vs. Con-2	No	ns	0.9489
Con-1 vs. C9-1	Yes	****	<0.0001
Con-1 vs. C9-2	Yes	****	<0.0001
Con-1 vs. C9-3	Yes	****	<0.0001
Con-2 vs. C9-1	Yes	****	<0.0001
Con-2 vs. C9-2	Yes	****	<0.0001
Con-2 vs. C9-3	Yes	****	<0.0001
C9-1 vs. C9-2	No	ns	0.8661
C9-1 vs. C9-3	No	ns	>0.9999
C9-2 vs. C9-3	No	ns	0.756

Appendix 3. Post-hoc Tukey's multiple comparisons test between day 60 MSNs. To evaluate statistical significance of evoked AP activity following current stimulation between each control and C9 MSN line at day 60 (Con-1, Con-2, C9-1, C9-2, C9-3), a two-way ANOVA was employed followed by Tukey's multiple comparisons test. The table above shows significance and adjusted p-values for each current step in the protocol.

C9-3 VS C9-3Δ SIDAK'S MULTIPLE COMPARISONS TEST

	Significance?	Summary	Adjusted P Value
0 pA current injection	No	ns	>0.9999
5 pA current injection	No	ns	>0.9999
10 pA current injection	No	ns	>0.9999
15 pA current injection	No	ns	0.197
20 pA current injection	Yes	****	<0.0001
25 pA current injection	Yes	****	<0.0001
30 pA current injection	Yes	****	<0.0001
35 pA current injection	Yes	****	<0.0001
40 pA current injection	Yes	****	<0.0001
45 pA current injection	Yes	****	<0.0001
50 pA current injection	Yes	****	<0.0001

Appendix 4. Post-hoc Sidak's multiple comparisons test between day 60 MSNs. To evaluate statistical significance of evoked AP activity following current stimulation between C9-3 and corresponding C9-3Δ MSNs at day 60, a two-way ANOVA was employed followed by Sidak's multiple comparisons test. The table above shows significance and adjusted p-values for each current step in the protocol.

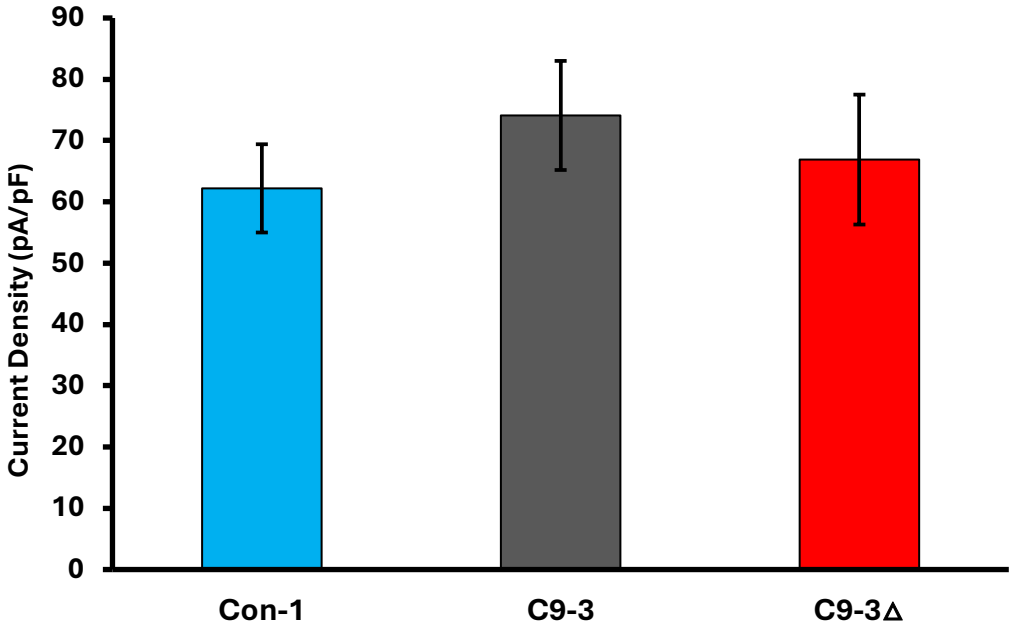

Appendix 5. Functional Na_V expression is consistent in MSNs. The mean current density for Con-1, C9-3 and C9-3Δ MSNs at day 60. All data presented as Mean (±SEM). Data obtained from the Livesey laboratory. Con-1: n=16, C9-3: n=19, C9-3Δ: n=11 from a minimum of 3 de-novo preperations.

CON-1 D40 VS D50 SIDAK'S MULTIPLE COMPARISONS TEST

	Significance?	Summary	Adjusted P Value
0 pA current injection	No	ns	>0.9999
5 pA current injection	No	ns	>0.9999
10 pA current injection	No	ns	>0.9999
15 pA current injection	No	ns	0.3174
20 pA current injection	Yes	*	0.0265
25 pA current injection	Yes	*	0.0196
30 pA current injection	No	ns	0.0671
35 pA current injection	No	ns	0.3142
40 pA current injection	No	ns	0.8472
45 pA current injection	No	ns	0.9712
50 pA current injection	No	ns	0.9994

C9-2 D40 VS D50 SIDAK'S MULTIPLE COMPARISONS TEST

	Significance?	Summary	Adjusted P Value
0 pA current injection	No	ns	>0.9999
5 pA current injection	No	ns	>0.9999
10 pA current injection	No	ns	>0.9999
15 pA current injection	No	ns	>0.9999
20 pA current injection	No	ns	0.9724
25 pA current injection	No	ns	0.4271
30 pA current injection	No	ns	0.2737
35 pA current injection	No	ns	0.3437
40 pA current injection	No	ns	0.0833
45 pA current injection	No	ns	0.0852
50 pA current injection	No	ns	0.3092

Appendix 6. Post-hoc Sidak's multiple comparisons test between early and late LMN timepoints. To evaluate statistical significance of evoked AP activity following current stimulation across time points for each cell line (Con-1, Con-2, C9-1, C9-2), a two-way ANOVA was employed followed by post-hoc comparisons test. The table above shows significance and adjusted p-values for each current step in the protocol for Con-1 and C9-2 LMNs.

CON-1 TUKEY'S MULTIPLE COMPARISONS TEST

	Significance?	Summary	Adjusted P Value
0 pA current injection			
Baseline vs. Chronic NaCl	No	ns	>0.9999
Baseline vs. Chronic KCl	No	ns	0.9245
Chronic NaCl vs. Chronic KCl	No	ns	0.9245
5 pA current injection			
Baseline vs. Chronic NaCl	No	ns	0.9636
Baseline vs. Chronic KCl	No	ns	0.9736
Chronic NaCl vs. Chronic KCl	No	ns	0.9995
10 pA current injection			
Baseline vs. Chronic NaCl	No	ns	0.8173
Baseline vs. Chronic KCl	No	ns	0.9805
Chronic NaCl vs. Chronic KCl	No	ns	0.9162
15 pA current injection			
Baseline vs. Chronic NaCl	No	ns	0.9836
Baseline vs. Chronic KCl	No	ns	0.6462
Chronic NaCl vs. Chronic KCl	No	ns	0.5403
20 pA current injection			
Baseline vs. Chronic NaCl	No	ns	0.6083
Baseline vs. Chronic KCl	No	ns	0.1241
Chronic NaCl vs. Chronic KCl	No	ns	0.5534
25 pA current injection			
Baseline vs. Chronic NaCl	No	ns	0.1961
Baseline vs. Chronic KCl	Yes	*	0.0108
Chronic NaCl vs. Chronic KCl	No	ns	0.4322
30 pA current injection			
Baseline vs. Chronic NaCl	No	ns	0.2295
Baseline vs. Chronic KCl	Yes	***	0.0005
Chronic NaCl vs. Chronic KCl	No	ns	0.0659
35 pA current injection			
Baseline vs. Chronic NaCl	No	ns	0.14
Baseline vs. Chronic KCl	Yes	**	0.0012
Chronic NaCl vs. Chronic KCl	No	ns	0.1959
40 pA current injection			
Baseline vs. Chronic NaCl	No	ns	0.1961
Baseline vs. Chronic KCl	Yes	**	0.0036
Chronic NaCl vs. Chronic KCl	No	ns	0.2546
45 pA current injection			
Baseline vs. Chronic NaCl	No	ns	0.1961
Baseline vs. Chronic KCl	Yes	**	0.0062
Chronic NaCl vs. Chronic KCl	No	ns	0.3343
50 pA current injection			
Baseline vs. Chronic NaCl	No	ns	0.1961
Baseline vs. Chronic KCl	Yes	*	0.0217
Chronic NaCl vs. Chronic KCl	No	ns	0.5799

C9-2 TUKEY'S MULTIPLE COMPARISONS TEST

	Significance?	Summary	Adjusted P Value
0 pA current injection			
Baseline vs. Chronic NaCl	No	ns	>0.9999
Baseline vs. Chronic KCl	No	ns	>0.9999
Chronic NaCl vs. Chronic KCl	No	ns	>0.9999
5 pA current injection			
Baseline vs. Chronic NaCl	No	ns	>0.9999
Baseline vs. Chronic KCl	No	ns	0.9933
Chronic NaCl vs. Chronic KCl	No	ns	0.9929
10 pA current injection			
Baseline vs. Chronic NaCl	No	ns	0.9994
Baseline vs. Chronic KCl	No	ns	0.898
Chronic NaCl vs. Chronic KCl	No	ns	0.9082
15 pA current injection			
Baseline vs. Chronic NaCl	No	ns	0.9994
Baseline vs. Chronic KCl	No	ns	0.6855
Chronic NaCl vs. Chronic KCl	No	ns	0.6485
20 pA current injection			
Baseline vs. Chronic NaCl	No	ns	0.9336
Baseline vs. Chronic KCl	No	ns	0.8674
Chronic NaCl vs. Chronic KCl	No	ns	0.9894
25 pA current injection			
Baseline vs. Chronic NaCl	No	ns	0.4947
Baseline vs. Chronic KCl	No	ns	0.7197
Chronic NaCl vs. Chronic KCl	No	ns	0.9017
30 pA current injection			
Baseline vs. Chronic NaCl	No	ns	0.3566
Baseline vs. Chronic KCl	No	ns	0.5323
Chronic NaCl vs. Chronic KCl	No	ns	0.9208
35 pA current injection			
Baseline vs. Chronic NaCl	No	ns	0.3356
Baseline vs. Chronic KCl	No	ns	0.4847
Chronic NaCl vs. Chronic KCl	No	ns	0.9344
40 pA current injection			
Baseline vs. Chronic NaCl	No	ns	0.1971
Baseline vs. Chronic KCl	No	ns	0.1085
Chronic NaCl vs. Chronic KCl	No	ns	0.9768
45 pA current injection			
Baseline vs. Chronic NaCl	No	ns	0.1875
Baseline vs. Chronic KCl	No	ns	0.0787
Chronic NaCl vs. Chronic KCl	No	ns	0.9434
50 pA current injection			
Baseline vs. Chronic NaCl	No	ns	0.4704
Baseline vs. Chronic KCl	No	ns	0.5323
Chronic NaCl vs. Chronic KCl	No	ns	0.9841

Appendix 7. Post-hoc Tukey's multiple comparisons test between baseline and chronic treatments for Con-1 and C9-2 LMNs. To evaluate statistical significance of evoked AP activity following current stimulation across different treatment conditions for each cell line (Con-1 and C9-2), a two-way ANOVA was employed followed by post-hoc comparisons test. The table above shows significance and adjusted p-values for each current step in the protocol for Con-1 and C9-2 LMNs.